DISSERTATION

New monomer systems for the additive manufacturing of high-performance polymers

ausgeführt zum Zwecke der Erlangung

des akademischen Grades eines Doktors der Naturwissenschaften

unter der Leitung von

Univ.-Prof. Dipl.-Ing. Dr.techn. Robert Liska

and

Univ.Ass. Dipl.-Ing. Dr.techn. Patrick Knaack

E163

Institut für Angewandte Synthesechemie

eingereicht an der Technischen Universität Wien

Fakultät für Technische Chemie

von

Raffael Johannes Bodo Andre Wolff, MA, MSc

11928307

Wien, March 24

Raffael Wolff, MA, MSc

Die approbierte gedruckte Originalversion dieser Dissertation ist an der TU Wien Bibliothek verfügbar.
The approved original version of this doctoral thesis is available in print at TU Wien Bibliothek.

Die approbierte gedruckte Originalversion dieser Dissertation ist an der TU Wien Bibliothek verfügbar.
The approved original version of this doctoral thesis is available in print at TU Wien Bibliothek.

Danksagung

Die approbierte gedruckte Originalversion dieser Dissertation ist an der TU Wien Bibliothek verfügbar.
The approved original version of this doctoral thesis is available in print at TU Wien Bibliothek.

Die approbierte gedruckte Originalversion dieser Dissertation ist an der TU Wien Bibliothek verfügbar.
The approved original version of this doctoral thesis is available in print at TU Wien Bibliothek.

Kurzfassung

Klassische Lithographie basierte additive Fertigungsverfahren (L-AMTs) sind der Maßstab wenn es um hochpräzise Fertigung von Bauteilen geht. Dennoch leidet die Industrie unter der geringen Auswahl an Materialen, die ihnen in diesem Bereich zur Verfügung steht. Die träge Reaktionskinetik vieler Monomersysteme machen sie untauglich für die klassischen L-AMTS. Mit Hot Lithography wurde kürzlich eine hierfür passende Ergänzung auf den Markt gebracht. Durch Erhitzen der relevanten Teile während des additiven Fertigungsprozesses sind plötzlich komplett neue Material im Bereich des 3D Druckes denkbar.

Diese Innovationsmöglichkeit wird in dieser Arbeit genutzt um gänzlich neue Polymer, bevorzugt hochleistungs Polymere, für additive Fertigung zu erforschen. Durch die Auswahl und Analyse passender Katalysatoren sowie Co-Katalysatoren, konnten drei, im Bereich der licht-induzierten Härtung zuvor wenig oder unbekannte Polymere, photo-chemisch hergestellt werden. Es wurden soweit wie möglich die chemischen Aspekte hinter der Reaktion analysiert, die passende Reaktionsparameter evaluiert und das jeweilige System soweit optimiert, dass es, wenn möglich, additiv gefertigt werden kann.

In dieser Arbeit wird neben dem ersten 3D Druck von puren Phenoplasten, auch bekannt als Bakelit, die additive Fertigung von reinen Polycyanuraten mit einer Glasübergangstemperatur von über 330 °C vorgestellt. Desweiteren kann die überhaupt erstmals beschriebene licht-induzierte Härtung von Isocyanaten hinzu Polyisocyanuraten und ihrer Nutzung im Bereich der Beschichtungstechnologie vorgestellt werden.

Generell werden in dieser Arbeit drei verschiedene Proof-of-Concepts vorgestellt, die zum einen das Portfolio der Materialen im Bereich der additiven Fertigung erweitern sollen sowie ein Grundgerüst für die weitere Forschungsarbeiten im Bereich der lichtinduzierten Härtung darstellen sollen.

Die approbierte gedruckte Originalversion dieser Dissertation ist an der TU Wien Bibliothek verfügbar.
The approved original version of this doctoral thesis is available in print at TU Wien Bibliothek.
TU WIEN Bibliothek Your knowledge hub

Die approbierte gedruckte Originalversion dieser Dissertation ist an der TU Wien Bibliothek verfügbar.
The approved original version of this doctoral thesis is available in print at TU Wien Bibliothek.

Abstract

Classic lithography-based additive manufacturing processes (L-AMTs) are the benchmark when it comes to the high-precision production of components. Nevertheless, the industry suffers from the limited choice of materials available to them in this area. The slow reaction kinetics of many monomer systems make them unsuitable for classic L-AMTS. With Hot Lithography, a suitable addition was recently launched on the market. By heating the relevant parts during the additive manufacturing (AM) process, completely new materials are suddenly feasible in the field of 3D printing.

This innovation opportunity is used in this work to research completely new polymers, preferably high-performance polymers, for AM. By selecting and analyzing suitable catalysts and co-catalysts, three polymers, previously little or unknown in the field of light-induced curing, could be produced photo-chemically. The chemical aspects behind the reaction were analyzed as far as possible, the appropriate reaction parameters were evaluated, and the respective system was optimized to the extent that it can be additively manufactured if possible.

In addition to the first 3D printing of pure phenoplasts, also known as Bakelite, the AM of pure polycyanurates with a glass transition temperature of over 330 °C is presented in this work. Furthermore, for the first time ever, the light-induced curing of isocyanates to polyisocyanurates and their use in the field of coating technology can be presented.

In general, three different proof-of-concepts are presented in this work, which are intended to expand the portfolio of materials in the field of AM and further to provide a basic framework for further research work in the field of light-induced curing.

Die approbierte gedruckte Originalversion dieser Dissertation ist an der TU Wien Bibliothek verfügbar.
The approved original version of this doctoral thesis is available in print at TU Wien Bibliothek.
TU WIEN Bibliothek Your knowledge hub

Die approbierte gedruckte Originalversion dieser Dissertation ist an der TU Wien Bibliothek verfügbar.
The approved original version of this doctoral thesis is available in print at TU Wien Bibliothek.

Table of Contents

Introduction	**1**
Objective	**16**
General Part	**18**
Summary	**118**
Experimental Part	**124**

	Gen.	Exp.
1 Photo-chemically induced polycondensation of phenolic resins for additive manufacturing	**18**	**124**
1.1 State of the art	**18**	
1.2 Evaluation of curing agents	**23**	**124**
1.2.1 Hexamethylenetetramine	24	124
1.2.2 Paraformaldehyde	25	124
1.2.3 (Poly-)oxymethylene derivatives	28	125
1.2.3.1 1,3,5-Trioxane	28	125
1.2.3.2 Polyoxymethylene	30	125
1.2.3.3 Polyoxymethylene dimethyl ethers	32	125
1.2.3.4 Trioxymethylene diacetate	33	125
1.2.4 Formals	36	127
1.2.4.1 Glycerol formal	37	127
1.2.4.2 Cyclic trimethylolpropane formal	39	127
1.2.4.3 4-Phenyl-1,3-dioxane	39	127
1.2.4.4 Pentaerythritol diformal	42	127
1.2.5 Miscellaneous curing agents	42	128
1.2.5.1 Furfuryl alcohol	42	128
1.2.5.2 Salicylaldehyde	43	129

Die approbierte gedruckte Originalversion dieser Dissertation ist an der TU Wien Bibliothek verfügbar.
The approved original version of this doctoral thesis is available in print at TU Wien Bibliothek.
TU WIEN Bibliothek Your knowledge hub

1.3 3D printing of the phenolic formulations via Hot Lithography **44** **129**

1.4 Comparative mechanical testing of the 3D printed and bulk cured materials **50** **129**

1.5 Evaluation of additives to prevent bubble formation **53** **129**

1.6 Further tested formaldehyde-based resins **57** **130**

1.6.1 Resole 57 130

1.6.2 Urea resin 58 130

1.6.3 Melamine resin 58 131

1.6.4 Furane resin 59 131

2 Photo-induced catalytic poly-trimerization of cyanate ester to form high-performance polycyanurates for additive manufacturing **64** **132**

2.1 State of the art **64**

2.2 Evaluation of photocatalysts **69** **132**

2.3 Photopolymerization of a phenolic novolak cyanate ester **71** **132**

2.3.1 Theoretical investigation of cyanurates 71 132

2.3.2 Determination of the conversion 72 135

2.3.2.1 Photo-DSC 72 135

2.3.2.2 IR 74 135

2.3.3 Thermal characterization 76 135

2.4 Photopolymerization of a bisphenol based cyanate ester **77** **135**

2.4.1 Photo-DSC & Conversion 78 135

2.4.2 Thermal characterization 81 136

2.5 Photopolymerization of a mixture of PT-15 and BADCy **82** **136**

2.5.1 Photo-DSC 82 136

2.5.2 Thermal characterization 84 136

Die approbierte gedruckte Originalversion dieser Dissertation ist an der TU Wien Bibliothek verfügbar.
The approved original version of this doctoral thesis is available in print at TU Wien Bibliothek.
TU WIEN Bibliothek Your knowledge hub

2.6 3D printing of the PT-30 formulation via Hot Lithography **85** **136**

2.6.1 Stability of the formulation 85 136

2.6.2 Printing & Overpolymerization 86 136

2.7 Comparative mechanical testing of the 3D printed and bulk cured materials **91** **137**

3 Photo-induced catalytic poly-trimerization of isocyanates to form polyisocyanurates **93** **138**

3.1 State of the art **93**

3.2 Basic studies **96** **138**

3.2.1 Screening of photocatalysts 96 138

3.2.2 Screening of bases 99 139

3.2.3 Screening of monomers 100 139

3.2.4 Theoretical investigation of isocyanurates 102 139

3.3 Optimization of the system **103** **141**

3.3.1 Influence of the concentration of the photocatalyst 104 141

3.3.2 Influence of the concentration of the co-catalyst 105 141

3.3.3 Influence of the temperature 107 141

3.3.4 Influence of the intensity 108 141

3.4 Investigation HMDI vs. TMDI **110** **142**

3.4.1 Photo-DSC & Conversion 110 142

3.4.2 Thermal characterization 112 142

3.4.3 Mechanical testing 113 142

3.4.4 Printing & Coating 116 142

Materials and methods **144**

Abbreviations **150**

Bibliography **155**

Die approbierte gedruckte Originalversion dieser Dissertation ist an der TU Wien Bibliothek verfügbar.
The approved original version of this doctoral thesis is available in print at TU Wien Bibliothek.
TU WIEN Bibliothek Your knowledge hub

Die approbierte gedruckte Originalversion dieser Dissertation ist an der TU Wien Bibliothek verfügbar.
The approved original version of this doctoral thesis is available in print at TU Wien Bibliothek.

INTRODUCTION

Additive manufacturing technologies

Additive manufacturing technologies (AMTs) have left their mark more and more on today's manufacturing technology since their introduction in the 1980s. Due to the increased interest in business and science, additive manufacturing (AM) is also sometimes referred to as the '*third industrial revolution*'.[1] In general, AM methods can be defined within two categories. '*Rapid prototyping*' is the AM of models or the name-giving prototypes, while '*rapid manufacturing*' describes the production of finished parts and products. '*Rapid tooling*', the production of tools and the like, despite often being considered as a separate category, can be assigned to one of the previously described categories depending on the tool part. Other terms in literature for AM are '*layer manufacturing*', '*solid free-form manufacturing*' or '*desktop manufacturing*'. All of these refer to a partial aspect resulting from technical conditions of AMTs.[2] Probably the most prevalent name, especially in social and public media, is 3D printing (3DP), due to its ease of understanding.[2,3]

Based on a '*layer-to-layer*' approach, in AMTs objects are initially created in purely virtual steps via computer-aided design (CAD) and usually saved as a standard transformation language (STL) file before being sliced into the processable layer thickness in the final digital step. Building on this data, the various AMTs can then be used to obtain the physical object (Figure 1).[2,4]

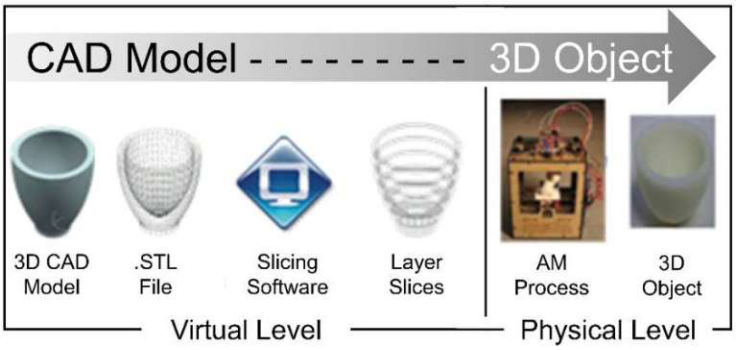

Figure 1: Generic AMT process flow. (adapted from [4])

Die approbierte gedruckte Originalversion dieser Dissertation ist an der TU Wien Bibliothek verfügbar.
The approved original version of this doctoral thesis is available in print at TU Wien Bibliothek.
TU WIEN Bibliothek Your knowledge hub

It is this '*layer-to-layer*' process in particular that distinguishes AMTs from the other two of the generally three existing manufacturing methods.[5] In subtractive manufacturing, defined areas are removed from a bulk material e.g. by milling or turning. The disadvantage of this process is the unnecessary loss of material, as well as the limitation with regard to complex shapes; pure hollow bodies cannot be produced in this way. The third manufacturing method is formative manufacturing, which gives the desired shape by means of changing the geometry of a material. This is achieved, for example, by forging, bending or casting, while at the same time applying an external force or heat.[2] The best known process in polymer technology for this type of manufacturing is injection molding.[3] Here the complexity of the shape of the desired product is just as limited as in the subtractive production. Furthermore, this process is limited to certain classes of materials that can be formed under the given parameters.[2] The disadvantages of the previously described manufacturing techniques do not exist with AMTs. The production of complex shapes in any thinkable geometry and orientation is generally possible, there is no or rarely little unnecessary material loss and the range of materials is much broader. Hence from an ecological point of view, material is saved and the most suitable material for the respective application can be used, which can extend the service life of products. Furthermore, with the elimination of costly and labor-intensive tools, AMTs also offer low initial costs. On the other hand, the output in AMTs is significantly reduced in terms of produced goods per time. If in comparison the costs per piece of e.g., injection molding, are taken into account, then the initial costs per piece are decreasing with a high number of pieces, while the costs in the case of AM are almost the same. Especially in the area of small volume, individualized and highly complex products as well the need of high-performing materials, AM is an interesting solution.[1–3]

That AM has now moved from academia to industry is demonstrated by the double-digit sales growth of the AM industry in 25 years since its start 34 years ago. Industries such as automotive, aerospace, industrial machinery, consumer electronics, and healthcare provided nearly $18 billion in revenue in 2022, corresponding to 18.3 % year-over-year growth for the AM market.[6] In addition, the more utilization of polymer powders over photopolymers for the first time in 2020 and making it the most used material in this segment indicates an increasing use of series production in the AM sector.[7]

Die approbierte gedruckte Originalversion dieser Dissertation ist an der TU Wien Bibliothek verfügbar.
The approved original version of this doctoral thesis is available in print at TU Wien Bibliothek.
TU WIEN Bibliothek Your knowledge hub

In general, materials for AM are divided into three segments. Metals represent about 30-40 % of sales worldwide. Ceramics still play a minor role in terms of economic relevance, but have good prospects for the future. Polymers account for over 50% of AM revenues despite their relatively lower prices compared to metals. Contrary it is the low cost of polymers combined with their versatility and lower initial cost that makes them the leading choice for AMTs.[8] Therefore, it is not surprising that especially in the field of polymer-based AMTs companies have found successful business models and established additive manufactured products on the market. For example, ALIGN TECHNOLOGY, INC. utilizes AM in its process to produce individualized custom aligners to create the personalized molds. This process produces 1 million aligners per day for 14 million patients worldwide.[9] One further example has emerged from a collaboration between ADIDAS AG and CARBON, INC., which used data analysis from professional runners to create a midsole that can only be manufactured cost-effectively using AM methods.[10]

However, especially the technological progress in the field of AMTs has made the actual manufacturing machines more manageable and cheaper, so that the private market for 3D printers is booming. Whether designers, engineers, universities or just hobbyists, with prices under $500, a more elaborate project can quickly be solved with ease.[11] In this context, fused deposition modelling (FDM) is frequently employed as a polymer-based AMT, especially in the home sector. Based on a thermoplastic filament which is extruded from a heated nozzle to a building platform, this technique builds up an object in layer-by-layer fashion. In addition, selective laser sintering (SLS) is considered the second best-known method in the field of melt-based technologies for AM in the polymer sector. In this process, polymer powder, as described above now the most used material in the AM area, is fused by means of a laser beam and thus a three-dimensional object is created.[3]

On the other hand, photopolymers are the second most important material in the AM sector. These are converted into a 3D object employing a fundamentally different principle. By means of radiation, mostly in the ultraviolet (UV) to blue range, the polymer is formed *in situ* from a liquid. Apart from material jetting, in which droplets of the photopolymer are applied selectively and subsequently cured, this area is often

Die approbierte gedruckte Originalversion dieser Dissertation ist an der TU Wien Bibliothek verfügbar.
The approved original version of this doctoral thesis is available in print at TU Wien Bibliothek.
TU WIEN Bibliothek Your knowledge hub

referred to as '*vat photopolymerization*'. In this type of lithography-based AMT (L-AMT), a vat filled with photopolymer and a laser (laser stereolithography, SLA) or a digital light processor (DLP) are used to cure only the irradiated area on a building platform located in the vat. By moving the platform, it can be recoated and the desired object can be created layer by layer. The advantage of L-AMTs is their typically very high precision compared to their melt-based counterparts. Since light radiation utilizing optical devices can usually operate on a nanometer scale, L-AMTs yield unsurpassed accuracy and surface quality.[3] Hence, this is one of the reasons why this work is exclusively focused on L-AMTs exploiting photopolymerization for the AM of high-performance polymers.

Lithography-based additive manufacturing technologies

Photopolymerization

Photopolymerization in the course of vat polymerization is a well-researched field, but remains interesting in the attempt to generate material properties that are inherent to thermoplastics particularly in melt-based AM as well as polymers that have not yet been additively manufacturable.[12,13] Generally, photopolymerization is a technique where liquid organic substances consisting of monomers, oligomers, or polymers, alongside a light-sensitive molecule called a photoinitiator (PI) are cured with the help of electromagnetic radiation.[14] This radiation is mainly part of the UV, visible, or near-IR light spectrum, which activates the PI and sets off the polymerization reaction.[15,16]

The photopolymerization process is widely known for its advantages such as higher spatial resolutions, no need of solvents, low emission of volatile compounds, quick curing also at room temperature, low energy consumption, and cost-effectiveness. Furthermore, LEDs have been implemented to replace traditional mercury lamps, which require even less energy.[14–17]

Mixtures of several components are used in photosensitive formulations to meet particular requirements and various purposes. The primary components of such formulations a polymerizable monomer and a PI. For industrial applications, a variety of components might be necessitated, including stabilizers, inhibitors, fillers,

Die approbierte gedruckte Originalversion dieser Dissertation ist an der TU Wien Bibliothek verfügbar.
The approved original version of this doctoral thesis is available in print at TU Wien Bibliothek.
TU Bibliothek Your knowledge hub WIEN

plasticizers, pigments, surfactants, and regulators, among others, and at times a complex blend of various monomers and initiators.[17,18] Monomers for photopolymerization possess polymerizable functional groups which contain a great amount of latent energy, such as double bonds or strained rings. Consequently, the structure of these molecules has a major influence on the eventual features of the cured polymer. As the direct production of reactive species from the monomer is inefficient, a PI is needed. Upon irradiation, this particular compound produces reactive centers that can then initiate free-radical, ionic or step-growth photopolymerization, with free-radical photopolymerization being the most widely employed in industry.[15]

When it was first introduced in the 1940s, the curing depth was limited to millimeters due to absorption processes of either the monomer, the PI, its by-products or additives, which restricted it to protective and decorative coatings of paper, wood, metals or plastics.[19] However, with substantial research, the curing depths have been enhanced, thus allowing for its use in dental fillings, optical materials, adhesives, biocompatible and biodegradable polymers used in medical applications and lithography-based AM technologies.[14–17,20,21]

Stereolithography

SLA was introduced in the 1980s as the first L-AMT which gained ample use in the domain of rapid prototyping.[22] SLA employs a UV laser to photopolymerize a liquid formulation at exact locations within each layer in three-dimensions (x-y-z) and with a precisely defined layer thickness. In a top-down arrangement, the building platform is then lowered into the formulation in the z-dimension to cover the solidified element with uncured resin before curing the consecutive layer on top (Figure 2). To avoid environmental effects, such as oxygen inhibition, a bottom-up inverted-SLA set up with irradiation via a transparent vat is employed, in which the hardened part is lifted to enable the subsequent layer to solidify.[23]

Die approbierte gedruckte Originalversion dieser Dissertation ist an der TU Wien Bibliothek verfügbar.
The approved original version of this doctoral thesis is available in print at TU Wien Bibliothek.
TU WIEN Bibliothek Your knowledge hub

Figure 2: Schematic setup of upside-down SLA printer.[24]

SLA has a significant edge over other AMT methods in terms of precision and accuracy of geometry, as well as surface quality, due to the laser solidification process. Nevertheless, challenges may arise from the photopolymerization process, such as shrinkage during UV-curing and the weak structural integrity of photopolymer materials.[3,25,26] Furthermore, the high cost of advanced laser systems, and the limited range of suitable formulations, restrict the applicability of SLA to epoxy or (meth)acrylate-based formulations of low viscosity, usually below 1 Pa s, requiring reactive diluents or solvents for optimum printing. In addition, due to the high network density of the cured resins, very brittle parts are usually obtained, which feature poor (thermo)mechanical properties.[1,3,12,21] Despite these difficulties, SLA is a popular and constantly evolving technology for its outstanding resolution and surface quality of printed parts.[27]

Digital light processing

The concept behind DLP is similar to that of SLA. It utilizes a masked LED light source which is modified by a Digital Micromirror device (DMD) chip (Figure 3, Number 2), enabling the irradiation of a whole layer at once. In general, the bottom-up versions are usually more prominent in DLP machines (Figure 3).[28]

Die approbierte gedruckte Originalversion dieser Dissertation ist an der TU Wien Bibliothek verfügbar.
The approved original version of this doctoral thesis is available in print at TU Wien Bibliothek.
TU WIEN Bibliothek Your knowledge hub

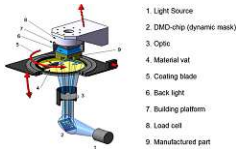

Figure 3: Schematic setup of a bottom-up DLP printer.[14]

This drastically decreases the amount of time needed for the solidification of each layer, making DLP much quicker than SLA. Additionally, DLP is more cost-effective due to the less expensive irradiation system, although its lateral resolution is limited to 10-50 µm, depending on the resolution and size of the DMD chip and corresponding pixel size.[3,25] Low viscosity photopolymerizable formulations are typically used in DLP, although it has been demonstrated that it can also be applied to filled systems such as ceramic slurries, as demonstrated by LITHOZ GMBH, who use it to manufacture individualized high-performance tools.[29] Furthermore, DLP has been used to fabricate complex silicon oxycarbide (SiOC) microstructures with high precision, showing its utility in the production of high-performance ceramics.[30]

High-performance polymers

The development of high-performing polymers (HPPs) originated in the late 1950s. The need for thermally stable polymers in particular in the aircraft and electronics industries and the associated market potential attracted some interested parties into the development of these unusual materials. But it was not until the incorporation of heterocycles into the polymer chain at the end of the 1960s that the first branded products, still very well known today, such as DuPont's polyimide-based Kapton™, became available for commercialization. Subsequently, in the 1970s, other candidates such as the polyamide Kevlar™ or the thermoplastic polyetherimide Utem™ came onto the market. Further developments in the field of microelectronics (such as interlayer dielectrics or photoresist), membrane production and aerospace brought further momentum to the development of HPPs in the 90s. However, the production and processing of these materials was and still is a challenging task. Especially in the field

Die approbierte gedruckte Originalversion dieser Dissertation ist an der TU Wien Bibliothek verfügbar.
The approved original version of this doctoral thesis is available in print at TU Wien Bibliothek.
TU WIEN Bibliothek Your knowledge hub

of microelectronics and the production of membranes, the choices are still limited.[31–33]

In general, HPPs are understood to be polymers that not only withstand harsh conditions but also perform under them. Temperature is often listed as the decisive criterion that makes a polymer an HPP, but in addition to thermal resistance, chemical and mechanical resistance as well as electrical and other physical properties are of significance. Since a polymer often meets several of these criteria but not all of them, there is no clear definition of what HPPs are and what they are not.[32,34] Nevertheless, there is an understanding that unlike standard polymers (produced in large quantities and performing in the range below 100 °C) as well as engineering polymers (small-quantity products with a performance range between 100 and 150 °C), they offer exceptional performance in the ranges from 150 °C upwards (Figure 4).[34]

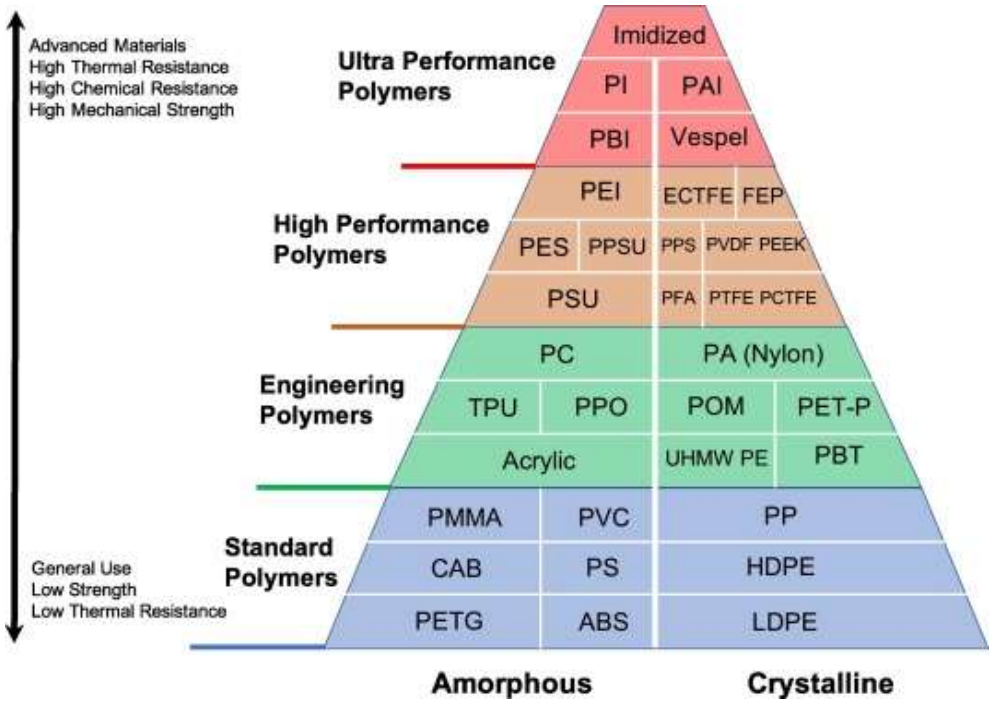

Figure 4: Classification of polymers according to their performance in the areas of temperature, chemical and mechanical stability.[34]

Common criteria often used to classify HPPs are:

- The polymer's resilience must endure for a minimum of 10,000 h at a temperature of 177 °C. During this thermal condition, the polymer ought to uphold its characteristics following both brief and extended periods of

Die approbierte gedruckte Originalversion dieser Dissertation ist an der TU Wien Bibliothek verfügbar.
The approved original version of this doctoral thesis is available in print at TU Wien Bibliothek.
TU Bibliothek Your knowledge hub WIEN

encountering mechanical strain, harsh chemicals, and electrical impacts. Moreover, under these conditions, the polymer must also be resistant to various types of radiation and corrosive environments while exposed to the specified temperature.

- At 450 °C, a maximum weight loss of 5 wt% is desirable, associated with a decomposition temperature above that level. Generally, a moderate weight loss at elevated temperatures is associated with HPPs.
- A deflection of 10 % at a load of 1.52 MPa should occur at a minimum temperature of 177 °C.
- Polymers that contain a significant amount of aromatic structures and relatively inflexible segments should have elevated glass transition temperatures (T_g) along with exceptional mechanical characteristics.[32]

Especially the last point characterizes the structures of HPPs at the molecular level and is required for effective development of them. Through aromatic rings in the polymer backbone and/or mechanical rigid and oxidative stable groups such as carbonyl, ether or fluorine functionalities, in addition to the use of aromatic instead of aliphatic hydrogens, high thermal and chemical stability is achieved. A crucial factor for the thermal stability is the strength of the chemical bonds, which is quantified by the bond dissociation energy. This energy indicates a measure of how much of it is required to break a chemical bond. Breaking a C=C (145 kcal·mol^{-1}) bond requires more energy than breaking a C-C bond (83 kcal·mol^{-1}), which explains the predominance of C=C bonds in the backbones of most HPPs. In parallel, polymers with C-F bonds (123 kcal·mol^{-1}), so-called fluorinated polymers, are expected to exhibit higher thermal stability than their non-fluorinated counterparts (C-H bond 99 kcal·mol^{-1}). The incorporation of resonance-stabilized units through aromatic parts is estimated to increase the bond strength by 40-70 kcal·mol^{-1}.[32,35]

Under elevated temperatures, these polymers resist generating volatile fragments due to the heightened durability of resonance-stabilized bonds against rupture. Beyond elevating thermal stability, the inclusion of resonance-stabilized units enhances the chemical resistance of these polymers. At high temperatures, the initiation of polymer degradation yields radical species. These radicals interact with the polymer chain,

Die approbierte gedruckte Originalversion dieser Dissertation ist an der TU Wien Bibliothek verfügbar.
The approved original version of this doctoral thesis is available in print at TU Wien Bibliothek.
TU Bibliothek Your knowledge hub WIEN

eventually cleaving it. However, radical species originating from resonance-stabilized units exhibit diminished reactivity due to the dispersion of π-electrons within their structure. Therefore, replacing aliphatic units with aromatic ones not only improves the bond strength of the polymer chain, but also heightens its resilience against the attack by radical species.[36]

In a broad sense, HPPs can be categorized into two primary classifications (Figure 4). On the one hand amorphous polymers, including materials like polyetherimides (PEI), polysulphones (PSU), polyphenylenesulphones (PPSU), polyethersulfones (PES), polybenzimidazoles (PBI), and polyimides (PIS). On the other hand semi-crystalline polymers, which encompass polyaryleneetherketones (such as polyetheretherketone (PEEK) and polyetherketoneketone (PEKK)), fluoropolymers like polytetrafluoroethylene (PTFE or Teflon), polyvinylidene difluoride (PVDF), polyamide-imides (PAI), and polyphenylene sulphide (PPS). Occasionally, polymers that undergo imidization (such as PAI, PBI, and PIS) are grouped separately and positioned as ultra-performance polymers, situated beyond the high-performance polymers category. These imidized polymers possess highly distinct combinations of properties, such as notably elevated continuous use temperatures and the absence of a melting point. However, they also exhibit considerable challenges during processing and show diminished chemical resistance towards boiling water, strong alkalis, bases, and amines. In addition to the two categories, there are other HPPSs that cannot be classified quite clearly. Examples are thermoset epoxy resins, polyurethanes (especially rigid ones with high polyisocyanurate content) and phenoplasts.[34,37–40]

Step-growth polymerization

Most of these HPPs are prepared via step-growth polymerizations rather than chain-growth reactions, in contrast to the common photopolymers. The primary contrast among these reaction types lies in the extent of the degree of polymerization (P_n) as the reaction progresses (Figure 5). This means that in chain-growth reactions, elongated polymer chains are present even at very low conversion rates (< 10 %). Conversely, in the scenarios of polycondensations and polyadditions, numerous but short molecules (oligomers) are initially generated. Therefore, to achieve a high P_n and thus high molecular weights, a high conversion is required. A special case is the so-called living polymerization. This type of polymerization can be continued forever

Die approbierte gedruckte Originalversion dieser Dissertation ist an der TU Wien Bibliothek verfügbar.
The approved original version of this doctoral thesis is available in print at TU Wien Bibliothek.
TU Bibliothek Your knowledge hub WIEN

without explicit termination by addition of further monomer, hence also living. This reaction technique is mainly used for block copolymers and polymers with a defined molecular weight.[41]

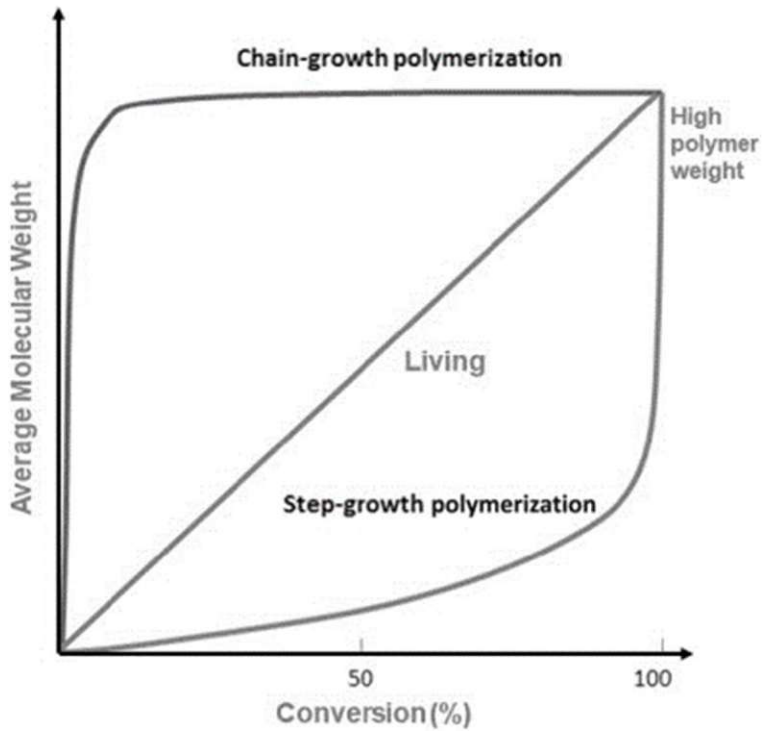

Figure 5: Schematic representation of the course of the degree of polymerization as a function of the conversion rate.[42]

But step-growth polymerization can also be used to tune the molecular weight. For this purpose, Carothers established an equation that explains the relationship between the sample weight (more precisely the ratio of the functional groups = q), the conversion (p) and the P_n:

$$\bar{P}_n = \frac{1+q}{1+q-2qp}$$

Equation 1: Carothers Equation.[43]

If, for example, a conversion of p=1 is assumed here, the dependence of the P_n is reduced exclusively to the ratio of the functional groups in the reaction mixture, which can consequently be adjusted by means of the initial weight. This phenomenon of

Die approbierte gedruckte Originalversion dieser Dissertation ist an der TU Wien Bibliothek verfügbar.
The approved original version of this doctoral thesis is available in print at TU Wien Bibliothek.
TU WIEN Bibliothek Your knowledge hub

oligomerization or prepolymer generation finds utilization in numerous technological contexts. On one side, monomers could exhibit considerable instability, leading to polymerization during storage or transformation into unwanted substances.[44] Conversely, this approach ensures that consumers are not exposed to monomers, which often raise toxicological apprehensions. Instead, they gain access to prepolymers of greater molecular weight, carrying fewer risks, and primed for subsequent processing.[45]

Polycondensation

Generally, condensation is understood to be a reaction in which two molecules react with each other to form small by-products, such as water or carbon dioxide. A large number of these reactions are equilibrium reactions, in which the educts and the products are in equilibrium and a complete conversion of the starting materials is not possible without further effort.[46]

A polycondensation reaction involves a gradual condensation reaction using stable yet still chemically active intermediate compounds. In this process, polymers are created from numerous low-molecular-weight substances by releasing simpler molecules. The resulting products of this reaction are termed polycondensates, which vary depending on the specific reaction involved. Among the notable examples within the polycondensate category are significant technical polymers like polyamides, polyesters, polyimides, polycarbonates, as well as elastomers including silicones, and thermosetting materials like phenolic or melamine resins. Unlike chain-growth polymerization or polyaddition processes, where by-products are not continuously released during the reaction, in polycondensation reactions, by-products are generated and must be consistently removed. This is necessary to ensure that polycondensation can proceed at the highest attainable conversions, resulting in elevated degrees of polymerization and molecular weights.[46–48]

To initiate a polycondensation reaction successfully, a fundamental requirement is that the monomers must possess a minimum of two active functional groups, like hydroxyl (-OH), carboxyl (-COOH), or amino (-NH2) groups. These two functional groups may exist within a single molecule (Scheme 1 top), or they can be found on two separate molecules (Scheme 1, bottom), where more than one of the same groups is existing.[46]

Die approbierte gedruckte Originalversion dieser Dissertation ist an der TU Wien Bibliothek verfügbar.
The approved original version of this doctoral thesis is available in print at TU Wien Bibliothek.
TU WIEN Bibliothek Your knowledge hub

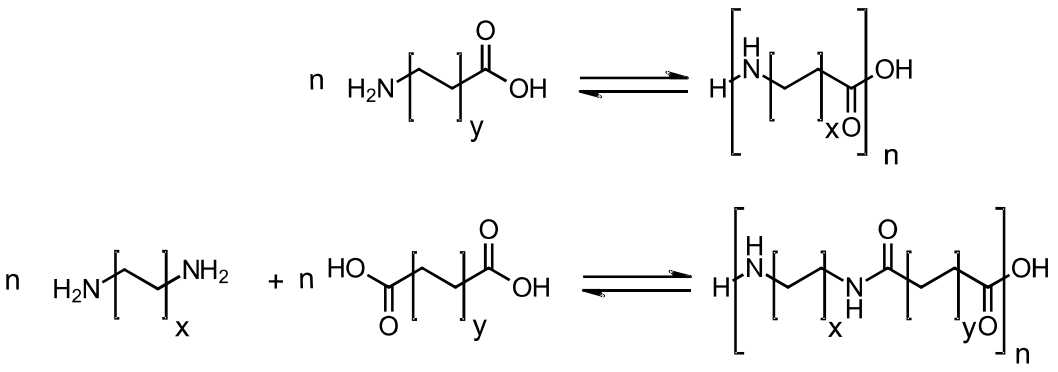

Scheme 1: Example of intra- (top) and intermolecular (bottom) polycondensation of a polyamide.

Polyaddition

In addition to chain-growth polymerization and polycondensation reactions, there exists a third category of polymer formation reactions called polyadditions. In terms of their stepwise progression, they closely resemble polycondensations. However, what sets polyaddition reactions apart from other polymerization processes is that all molecules within the system actively engage with one another via their functional groups, allowing for the construction of the polymer chain. Much like in polycondensation, the functional groups on individual molecules exhibit roughly similar reactivity levels, ensuring that the likelihood of them reacting with each other is uniform across all molecules. However, in contrast to polycondensation reactions, polyaddition doesn't involve the removal of low-molecular-weight groups. Instead, all the atoms and atomic groups present in the starting materials are retained in the final product. Consequently, the products generated through this process are termed polyadducts.[46,47]

The structural prerequisite for a polyaddition reaction is the presence of monomers with at least two functional groups, one of which must have a double bond or a ring structure (Scheme 2). Only very few systems meet these necessary criteria for a successful polyaddition reaction. Among the most important and technologically significant representatives of polyaddition reactions are polyurethanes and epoxy resins, but also polyureas, polysulfides and some polyamides.[46,47,49]

Die approbierte gedruckte Originalversion dieser Dissertation ist an der TU Wien Bibliothek verfügbar.
The approved original version of this doctoral thesis is available in print at TU Wien Bibliothek.
TU WIEN Bibliothek Your knowledge hub

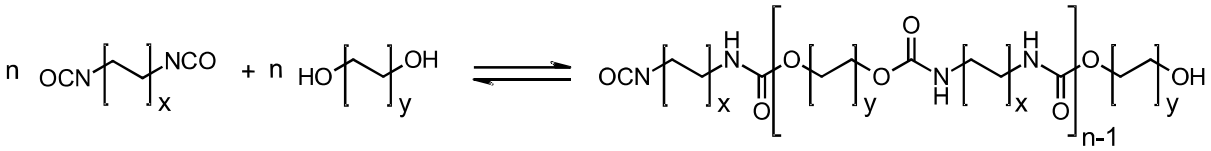

Scheme 2: Example of polyaddition of a polyurethane.

Hot Lithography

The advancement of SLA and DLP technologies is geared towards achieving swift cross-linking of liquid formulations through photopolymerization. The monomers predominantly employed in L-AMTs have been adapted from industrial coating applications, where there's a pressing need for rapid curing, extensive cross-linking, high hardness, and robust adhesion.[16] However, when applied to SLA or DLP, these monomers encounter substantial challenges due to their heightened reactivity and low viscosity. Typically, acrylate and methacrylate monomers are the primary choices for photopolymerization in L-AMTs. This selection leads to shrinkage, with cycloaliphatic and aromatic dimethacrylates exhibiting around 5% shrinkage, while aliphatic dimethacrylates show more than a 10% reduction in volume. Depending on the extent of this shrinkage, printed parts may undergo deformations or exhibit curling effects.[3,50]

Furthermore, when low molecular weight compounds undergo photopolymerization, they yield photopolymers that are distinctly brittle, lacking in toughness, impact resistance, and heat deflection temperatures. To mitigate these issues, structural precursors derived from (meth)acrylated oligomers, such as polyethers, polyesters, epoxy resins, or polyurethanes, are employed. This helps to reduce shrinkage and enhance the mechanical properties of the resulting photopolymers.[51,52] However, it's important to note that these monomers possess high viscosity and cannot be readily processed in conventional L-AMTs at room temperature. To address this, the addition of reactive diluents or solvents becomes necessary.[12]

To overcome these limitations within L-AMT and achieve the desired material properties, a novel L-AMT technique called Hot Lithography has recently emerged.[21,53,54] In Hot Lithography, it incorporates the principles of SLA or DLP but operates within a bottom-up 3D printing configuration, utilizing elevated temperatures, often reaching up to 140 °C. This elevated temperature allows for the processing of

Die approbierte gedruckte Originalversion dieser Dissertation ist an der TU Wien Bibliothek verfügbar.
The approved original version of this doctoral thesis is available in print at TU Wien Bibliothek.
TU WIEN Bibliothek Your knowledge hub

high-viscosity monomers. Consequently, structural monomer resins and oligomeric precursors with viscosities as high as 20 Pa·s can be effectively used at these elevated temperatures, while traditional L-AMTs are typically confined to formulations below 1 Pa·s.[21,55] In the Hot Lithography approach based on SLA, a laser with a specific wavelength is employed to provide high-energy irradiation to the formulation through the transparent vat (Figure 6).[56]

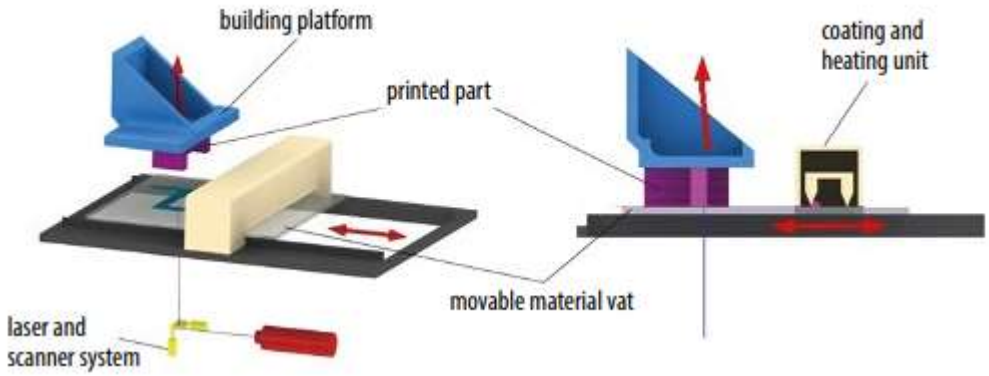

Figure 6: Schematic Hot Lithography SLA setup.[56]

Due to the higher temperatures employed in Hot Lithography, it has become possible to work with polybutadiene-based resins, unsaturated polyester resins, and formulations filled with thermoplastics. This advancement significantly improves the thermomechanical characteristics of the printed items.[57] Essentially, reducing the viscosity of the formulation enhances the mobility of the resins, leading to a noticeable boost in printing speeds.

Moreover, as demonstrated with dimethacrylate-based compositions, the elevated temperature employed in the Hot Lithography printing method results in substantially higher conversions, greater tensile strength, and enhanced storage modulus.[54] Furthermore, the increased temperature makes it possible to use completely new polymer systems for AM, such as oxazolines,[58] lactones[59] or furan-based resins.[60] In a broader context, it's worth noting that Hot Lithography can bring about a general improvement in reactivity during photopolymerization and opens the possibility of applying previously too slow systems, such as step growth polymerizations, in the field of AM.

Die approbierte gedruckte Originalversion dieser Dissertation ist an der TU Wien Bibliothek verfügbar.
The approved original version of this doctoral thesis is available in print at TU Wien Bibliothek.
TU WIEN Bibliothek Your knowledge hub

OBJECTIVE

In recent decades, advancements in lithography-based additive manufacturing technologies (L-AMTs) have led to innovative developments across numerous industrial applications. While L-AMTs match unparalleled precision and surface qualities, they encounter limitations coming from the photopolymerization reaction and the characteristics of the resulting photopolymer products. The introduction of hot lithography, originally intended to reduce the viscosity of higher molecular weight resins, opened up completely new opportunities in the development of materials for additive manufacturing (AM). With the possibility of performing photo-initiated chemistry at > 100 °C, polymerization reactions that were previously unavailable for AM due to insufficient reaction kinetics, let alone the melting point, are now possible. Therefore, this opportunity is to be used to develop material classes known from other manufacturing processes for the exploitation in AM. The focus here is on materials that can either be classified directly as high-performing polymer (HPP) or can be used as matrix, turning it into one with the right fillers.

In the first part of this work, phenolic resins are considered as monomers for Hot Lithography. The specific focus is on novolaks, which are predestined for this type of 3D printing technology due to their long-term stability at high temperatures. By evaluating suitable hardeners, an acid-catalyzed curing towards phenoplastics, also known as Bakelite, is to be achieved by means of a photoacid. Based on a photo-DSC analysis at elevated temperatures and a thermal characterization using simultaneous thermal analysis (STA) and rheology, a formulation suitable for AM is to be found. After successful 3D printing, the material would be compared on its mechanical properties and with its non-additive manufactured counterparts.

In the second part of this work, polycyanurates are considered as material for Hot Lithography. These HPPs consisting of cyanate esters are particularly popular in the field of high-temperature applications in lightweight construction. Similar to the phenolic resins, the basics of photochemical curing are to be analyzed using photo-DSC and STA as well as to find an AM capable formulation. In addition to the search for a suitable photocatalyst, this includes the choice of the right cyanate ester monomer. After 3D printing, these will be then tested for its mechanical and thermal

Die approbierte gedruckte Originalversion dieser Dissertation ist an der TU Wien Bibliothek verfügbar.
The approved original version of this doctoral thesis is available in print at TU Wien Bibliothek.
TU WIEN Bibliothek Your knowledge hub

properties in the same way as previously with non-additive manufactured test specimens.

Finally, polyisocyanurates are being considered as a more cost-effective alternative to polycyanurates. These thermosets, which are formed only from isocyanates, can have very different property profiles depending on the monomer. Therefore, it is possible to adapt these precisely to a desired requirement profile. In addition to the search for the right photocatalyst, the right monomer and potential co-catalysts are a relevant factor. Here, too, the chemical background and the possibility of AM using photo-DSC and STA are to be determined. The mechanical properties of these materials will then be tested to establish what is potentially possible with this type of material class.

In general, these three polymer classes should add a spectrum to AM that is not only thermally exceptional, but also generally has good mechanical properties. Where possible, commercially available starting materials should be used to make adaptation to an industrial process as simple as possible. If in principle the photopolymization of one material is possible, but the system cannot be used in Hot Lithography, an alternative area of application should be pursued.

Die approbierte gedruckte Originalversion dieser Dissertation ist an der TU Wien Bibliothek verfügbar.
The approved original version of this doctoral thesis is available in print at TU Wien Bibliothek.
TU WIEN Bibliothek Your knowledge hub

GENERAL PART

1 Photo-chemically induced polycondensation of phenolic resins for additive manufacturing

1.1 State of the art

Phenolic resins hold the distinction of being the earliest industrially manufactured polymers globally. Baekeland's breakthrough in 1907 marked the inception of the triumph story of industrial plastics, which have remained indispensable ever since and have significantly influenced an entire era.[61] In acknowledgment of its historic significance as the world's first synthetic plastic, Baekeland's polymer earned the title of a National Historic Chemical Landmark from the American Chemical Society in 1993.[62]

The resulting phenoplasts are formidable thermosetting materials, boasting exceptional mechanical strength and outstanding flame-retardant properties. This unique combination of attributes, coupled with their reduced weight compared to metals, paves the way for a wide array of applications spanning electronics, automotive, construction, and various other industries.[63] Especially in the area of automotive applications, there exists a few of industrial successful components, and there's an expectation of their application range expanding further. Fiberglass-reinforced molding compounds have found primary usage in mechanical and structural parts within the automotive industry. These compounds serve as a suitable alternative to metal, presenting both a '*lightweight solution*' and a '*low-cost solution*'. As a result, their adoption in functional components like peripheral engine parts, enclosures for electronic instrumentation, and components related to pumps has experienced continuous growth year after year.[64–66]

Additionally, phenolic resins find utility as binding agents for friction materials, including but not limited to brake linings, disc pads, and clutch facings. The demands placed on

Die approbierte gedruckte Originalversion dieser Dissertation ist an der TU Wien Bibliothek verfügbar.
The approved original version of this doctoral thesis is available in print at TU Wien Bibliothek.
TU WIEN Bibliothek Your knowledge hub

phenolic resins in these applications have increased significantly. Phenolic resins utilized in brake systems must exhibit exceptional qualities as friction materials, including high tensile strength, outstanding heat resistance, exceptional flexibility, effective vibration damping properties, and excellent water repellency. In response to these requirements, novel formulations have emerged in recent years, for example specialized silicone-modified phenolic resins, rubber-enhanced phenolic resins, and aromatic-modified phenolic resins, among others.[63,66]

Extensive research efforts have been devoted to the development of sustainable resources as for most polymers. In the regard to phenoplasts, the focus has been on phenol, often referred to as "green phenol," which is derived from non-edible biomass for example via a growth-independent bioprocess driven by genetic engineering.[66–69] Additionally, significant attention has been given to the development of manufacturing technologies for highly functional resins based on green phenol. Initially, breakthroughs were achieved by converting inedible plant resources, such as rice straws and corn stems, into green phenol using a sugar mixture obtained through saccharification and fermentation. This process not only conserves energy but is also environmentally friendly.[66] Furthermore, ongoing research aims to create resins from lignin extracted from plant-based sources, specifically woody biomass like wood powder and book powder. This is accomplished through a thermochemical process utilizing sub-critical water. The use of environmentally friendly sub-critical hot water enables precise control of the molecular weight of the extracted lignin, resulting in the production of lignin resins with exceptional moldability. These resins can serve as substitutes for traditional phenolic resins.[66,70,71]

Further, ongoing efforts are being made to advance recycling techniques. One promising approach being explored is a novel chemical recycling process that aims to achieve almost complete reclamation of recycled resins with a linear structure. These resins are initially generated using a water-phenol mixture in either a new supercritical or sub-supercritical state as the reactive solvent. Remarkably, the entire decomposition process can be accomplished within a remarkably short reaction time, typically ranging from 10 to 20 minutes. This recycled resin can be employed as a novolak-type phenolic resin. When compared to conventional novolak phenolic resins, these recycled

Die approbierte gedruckte Originalversion dieser Dissertation ist an der TU Wien Bibliothek verfügbar.
The approved original version of this doctoral thesis is available in print at TU Wien Bibliothek.
TU WIEN Bibliothek Your knowledge hub

counterparts have a smaller molecular weight and solidify rapidly. The composite materials produced using this recycled resin as a raw material exhibit mechanical properties, electrical characteristics, and heat resistance that closely approach those of composites derived from virgin novolak phenolic resin.[40,66]

In general, these resins are very often used as composites with fillers to achieve the necessary properties. Within phenolic resin-based filler-reinforced plastics, the phenolic resin serves as the foundational matrix, providing binding capabilities. The filler, on the other hand, functions as a strength-enhancing component, enhancing the material's mechanical properties.[72] It is therefore hardly surprising that research in this field continues to be very active.[72–76] Of particular note, scholars have shown considerable interest in fiber-reinforced plastics that seamlessly combine structural and functional features. Such materials can be engineered to serve multiple purposes, including heat insulation, ablation resistance, electromagnetic shielding, and energy absorption, all while supporting loads.[77] A prime example of this is carbon fiber-reinforced plastic with phenolic resin as the matrix, which exemplifies a typical structure-functional integrated composite material.[78,79] These innovative composites have found extensive applications in the production of pressure vessels and pipelines, including aerospace engine nozzles and high-pressure gas storage cylinders.[80,81]

Composite materials utilizing fibers, are categorized within two categories: long fibers and short fibers. Short fibers offer notable advantages, such as ease of processing and greater design flexibility.[82] Consequently, they represent an ideal choice for enhancing the molding process.[83] The procedures for processing and shaping composite materials encompass various techniques, including winding, molding, pultrusion, manual adhesion, and spraying, among others. Given that components often possess complex designs, they typically undergo rough processing before precise machining. Among these techniques, molding stands out for its significant benefits, characterized by cost-effectiveness and high efficiency, making it a prevalent method for crafting such filler-reinforced phenoplasts.[63,72]

Phenolic resins are synthesized via the polycondensation of phenol and formaldehyde. When operating under alkaline conditions with a phenol-to-formaldehyde molar ratio less than one, resols are generated. These resins possess a low viscosity at room temperature and undergo self-condensation at elevated temperatures. Conversely, novolaks are produced in acidic environments with a phenol-to-formaldehyde molar

Die approbierte gedruckte Originalversion dieser Dissertation ist an der TU Wien Bibliothek verfügbar.
The approved original version of this doctoral thesis is available in print at TU Wien Bibliothek.
TU Bibliothek Your knowledge hub WIEN

ratio exceeding one. Novolaks remain in solid form at room temperature but melt within the range of 50 to 120 °C. Consequently, they exhibit stability at high temperatures and necessitate curing agents (CAs) for complete polymerization.[84] Common CAs include hexamethylenetetramine (Hexa) or paraformaldehyde (PF), which release formaldehyde upon heating, thus facilitating the full polycondensation process into a cured thermosetting material.[85,86] This reaction can be catalyzed with an acid, following a similar approach to novolak production (Scheme 3).

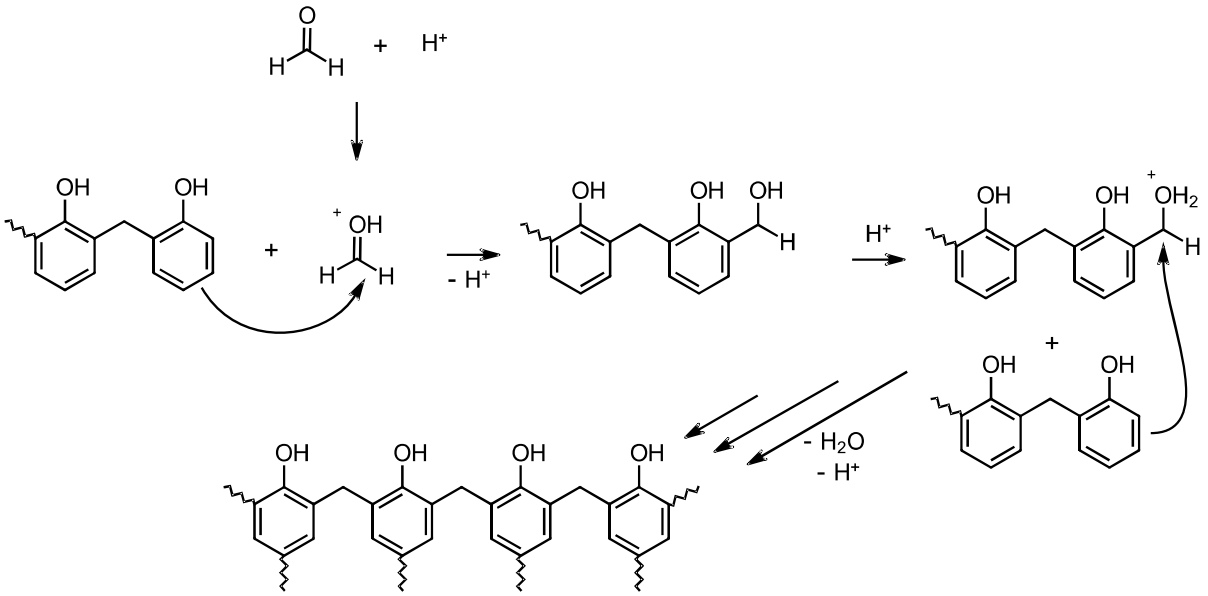

Scheme 3: Acid-catalyzed curing of a novolak (adapted from [84])

In brief, the curing of a novolak necessitates the presence of a CA, elevated temperature, and ideally, an acid. This catalytic curing process of phenolic resins using acid has been exploited for the photopolymerization of these systems via the use of photoacid generators (PAGs).[87,88] Originally derived from cationic polymerization, these PAGs consist of onium-based salts that decompose when exposed to ultraviolet (UV) light, releasing a highly potent acid. This released acid, can in turn, catalyze the curing reaction, as outlined in Scheme 3.[89]

Since the technically relevant research of cationic photopolymerization by Crivello et al. in the 1970s, continuous advancements have significantly enhanced cationic photoinitiation systems. These improvements have been driven by the growing

Die approbierte gedruckte Originalversion dieser Dissertation ist an der TU Wien Bibliothek verfügbar.
The approved original version of this doctoral thesis is available in print at TU Wien Bibliothek.
TU WIEN Bibliothek Your knowledge hub

demands of industrial applications and innovative technologies.[15,90] In the conventional photodecomposition process, the cation becomes excited to a singlet state, leading to subsequent homolytic or heterolytic cleavage events.[91] For instance, in the case of a diphenyliodonium cation, the cleavage of the halogen-carbon bond triggers the formation of radical-cations, radicals, cations, and arylhalides via homolytic and heterolytic cleavage processes (Scheme 4). In the homolytic decomposition pathway, intermediate radicals engage in hydrogen abstraction from either the monomer or potentially present solvent, resulting in the creation of neutral aromatic species and the corresponding Brønsted acid from the counterion present in the system. Conversely, in the heterolytic decomposition pathway, intermediate phenyl cations undergo electrophilic attack on the monomer or solvent, generating neutral photolysis products that include the corresponding Brønsted acid. Through electron transfer mechanisms, the products from homolytic decomposition can be transformed into the corresponding heterolytic products.[92,93]

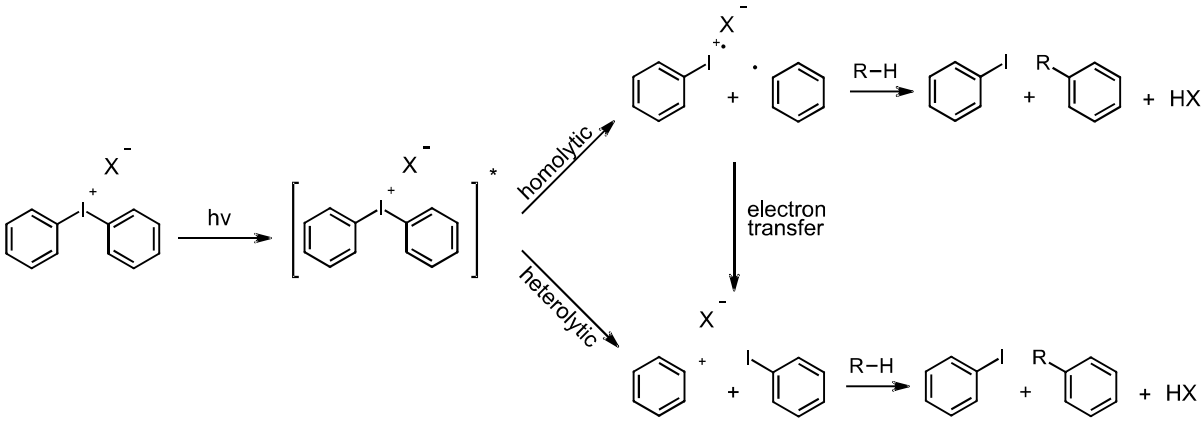

Scheme 4: Photodecomposition pathways of diphenyliodonium salts in homolytic and heterolytic decay.

Very complex shapes of phenoplasts are very difficult to access via existing methodologies, and if so, very costly. Therefore, additive manufacturing (AM) of these resins is a desirable goal in research and industry. However, research to date in this area has been limited to thin-film photoresists, systems that use another polymer as a matrix or phenolic resins which are modified with functional groups to be accessible via stereolithography applications.[94–98] Research is also being conducted on more elaborate AM methods for filler-reinforced phenolic resins, but with moderate resolution to date.[99] The development of Hot Lithography has introduced an innovative shaping

Die approbierte gedruckte Originalversion dieser Dissertation ist an der TU Wien Bibliothek verfügbar.
The approved original version of this doctoral thesis is available in print at TU Wien Bibliothek.
TU WIEN Bibliothek Your knowledge hub

technique, and since high temperatures are essential for processing phenolic resins, this distinctive method opens up the possibility of AM for pure phenoplasts.

1.2 Evaluation of curing agents

A low melting novolak was initially used for AM of phenolic resins, since resols are self-condensing at elevated temperatures and thus would be expected to have a short shelf life during printing. The pure resin (Novo, Figure 7 left) boasts a melting point of approximately 50 °C, as stated by the supplier. Initially, we conducted tests to assess its thermal reactivity both with and without p-(octyloxyphenyl)phenyliodonium hexafluoroantimonate (I-Sb, Figure 7 right) as a PAG (Figure 8).

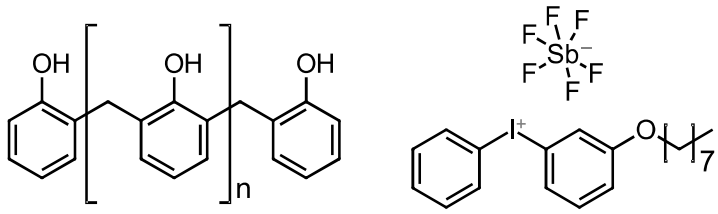

Figure 7: Structure of the novolak resin (Novo, left) and the PAG p-(octyloxyphenyl)phenyliodonium hexafluoroantimonate (I-Sb, right)

Novo itself exhibits stability up to temperatures reaching around 280 °C before it commences thermal degradation. However, it's worth noting that PAGs can also undergo thermal dissociation, yielding super-acids. Consequently, when I-Sb is present, an earlier degradation is observed at roughly 200 °C. Nevertheless, the starting materials, in the absence of a CA, exhibit sufficient stability to facilitate photochemical experiments at temperatures around 100 °C.

Die approbierte gedruckte Originalversion dieser Dissertation ist an der TU Wien Bibliothek verfügbar.
The approved original version of this doctoral thesis is available in print at TU Wien Bibliothek.
TU WIEN Bibliothek Your knowledge hub

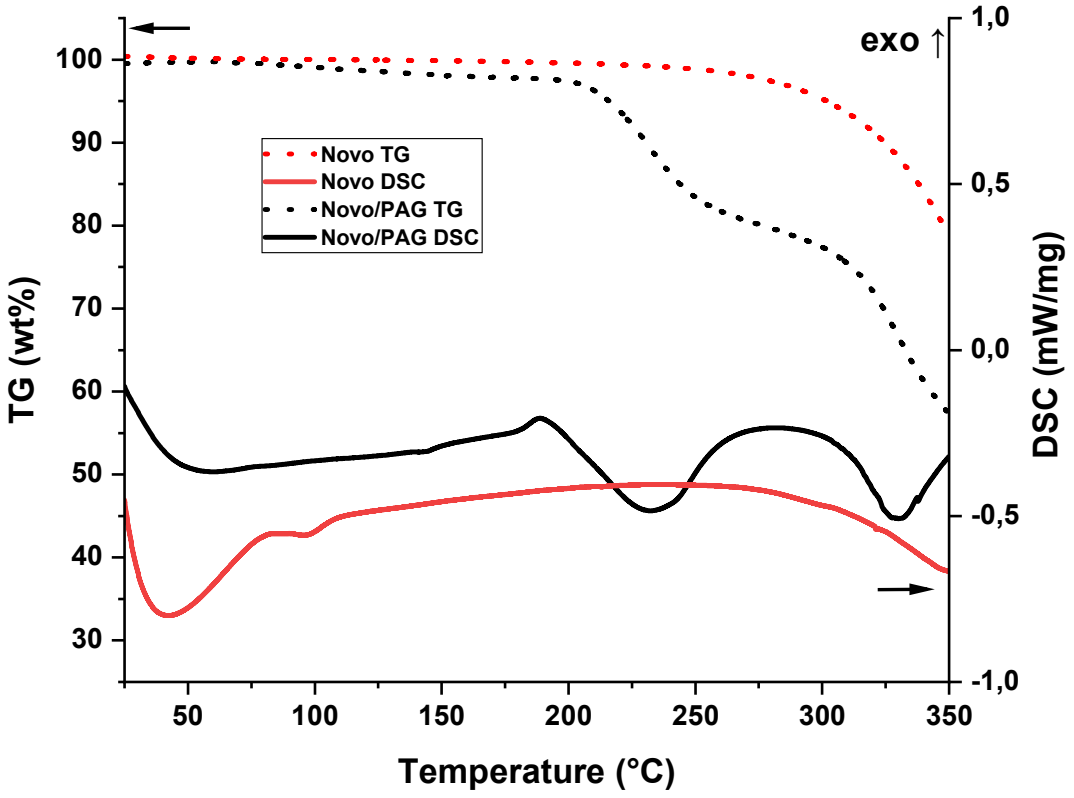

Figure 8: STA of the pure Novo (red; TG: dot; DSC: solid) and Novo/PAG (95/5, w/w, black; TG: dot; DSC: solid).

As described previously, curing agents (CAs) play an essential role in the curing of novolak-based phenolic resins. Therefore, in the subsequent phases of development, we examined both widely recognized CAs found in literature as well as unknown CAs. These were studied in conjunction with I-Sb as potential systems for the curing process.

1.2.1 Hexamethylenetetramine

Photo-DSC experiments at 80 °C with the Novo without CA but with 10 wt% PAG did not result in any curing under illumination with light in the wavelength range of 320-500 nm and an intensity of 60 mW·cm^{-2}.

Therefore Hexa (Figure 9), probably the most conventional hardener for novolaks, was added accordingly to literature[86] at 10 wt% and the experiment was repeated. Nevertheless, this formulation did not lead to any curing, although it is known that Hexa

Die approbierte gedruckte Originalversion dieser Dissertation ist an der TU Wien Bibliothek verfügbar.
The approved original version of this doctoral thesis is available in print at TU Wien Bibliothek.
TU Bibliothek Your knowledge hub WIEN

releases formaldehyde under acidic conditions.[100] Presumably, the release of the photoacid is inhibited by the basic nitrogen of Hexa, thus preventing the release of formaldehyde.

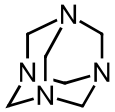

Figure 9: Structure of hexamethylenetetramine (Hexa).

1.2.2 Paraformaldehyde

Paraformaldehyde (PF) is a widely recognized heterogeneous curing agent for novolaks. In line with the research conducted by Adabbo et al., a weight content of 15 wt% was selected for PF.[85] In all the formulations, 5 wt% of I-Sb was employed as PAG. PF typically undergoes a transformation into formaldehyde when subjected to heat. This transformation occurs gradually at room temperature but accelerates considerably at temperatures exceeding 120 °C. However, this process can be accelerated by the presence of an acid and can also take place at temperatures below 120 °C, as illustrated in Scheme 5. In this context, the PAG serves a dual purpose. On one hand, it facilitates the decomposition of the curing agent into formaldehyde following irradiation. On the other hand, it catalyzes the curing process of the novolak, leading to the formation of phenoplast.

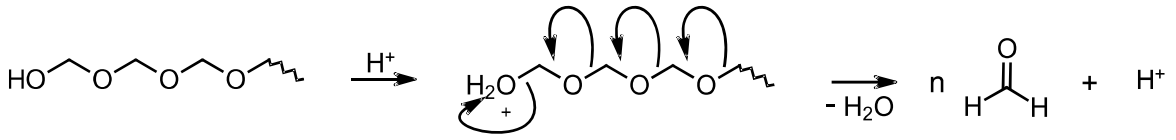

Scheme 5: Acid-catalyzed decomposition of PF to formaldehyde.

The photopolymerization characteristics of the PF formulation were assessed at various elevated temperatures using photo-DSC (Figure 10a and Table 1). At 60 °C, the reaction remained incomplete, but a peak enthalpy within the 80-90 °C range was evident (Figure 10b). Above these temperatures, a reduction in exothermic behavior was observed. This behavior can be attributed to the reaction mechanism: polycondensation results in the generation of one water molecule per

Die approbierte gedruckte Originalversion dieser Dissertation ist an der TU Wien Bibliothek verfügbar.
The approved original version of this doctoral thesis is available in print at TU Wien Bibliothek.
TU Bibliothek Your knowledge hub WIEN

polycondensation step. Consequently, if the reaction temperature exceeds 100 °C, stoichiometric quantities of water vapor accumulate. Since this process is endothermic, it leads to a decrease in the measured enthalpy. As the material solidifies, this evaporation process results in the formation of bubbles in the cured samples, as seen in Figure 10c. However, this phenomenon was not observed within the temperature range below the boiling point of water.

The reaction rate, evaluated based on the curve's maximum (t_{max}), accelerates with higher temperatures, as anticipated. Nevertheless, there was no significant difference in reaction speed between 100 and 120 °C. Despite this, the achieved reaction rates are considered sufficiently rapid to create a functional system for Hot Lithography, especially when employing a laser instead of a broad-spectrum light source.

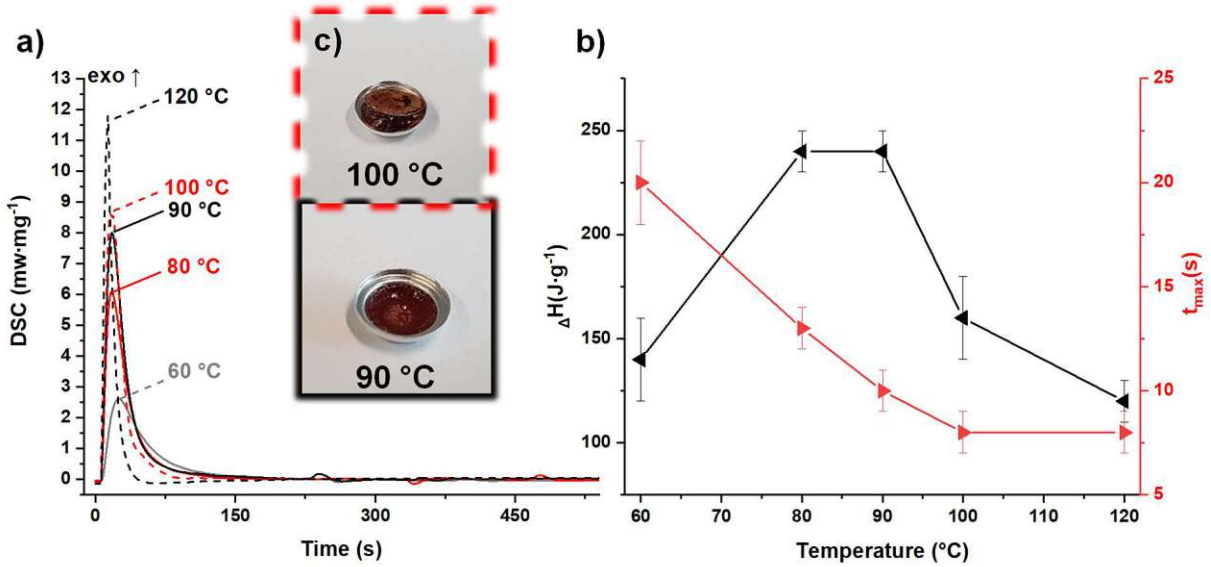

Figure 10: (a) Photo-DSC of the PF (15 wt%) formulation at 60-120 °C, 2 × 900 s, 320-500 nm, 60 mW·cm^{-2}. (b) Temperature dependence of photo-DSC results for the PF formulation: enthalpy change (ΔH black) and time until maximal heat is released (t_{max} red). (c) Cured Samples at 90 & 100 °C.

Table 1: Results of the photo-DSC experiments of the PF (15 wt%) formulation.

Temp. [°C]	ΔH [J·g^{-1}]	t_{max} [s]
60	145 ± 10	20 ± 1
80	240 ± 10	13 ± 1
90	240 ± 10	10 ± 1
100	160 ± 10	8 ± 1
120	120 ± 10	8 ± 1

Die approbierte gedruckte Originalversion dieser Dissertation ist an der TU Wien Bibliothek verfügbar.
The approved original version of this doctoral thesis is available in print at TU Wien Bibliothek.
TU Bibliothek Your knowledge hub WIEN

Additionally, the irradiated samples were subjected to an assessment of stability and the extent of the reaction using simultaneous thermal analysis (STA), with the non-irradiated formulation serving as a reference (Figure 11). It's worth noting that the chosen photoacid can also undergo thermal cleavage, indicating that the reaction can be initiated solely by heating. This is illustrated by the DSC curve along with simultaneous weight loss in the thermogravimetric analysis (TG). In contrast to the pure formulation, the cured sample (cured at 90 °C) did not exhibit exothermic behavior. Only the further evaporation of water led to a slightly endothermic peak and weight loss above 100 °C.

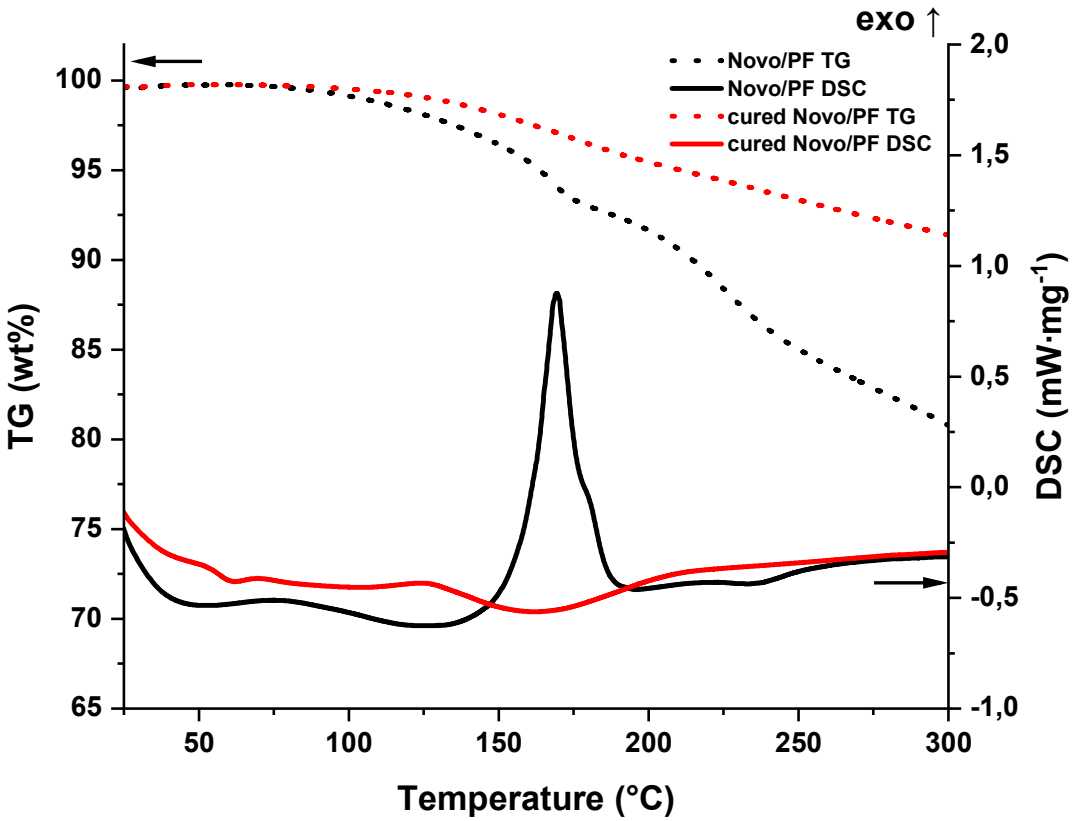

Figure 11: STA of the PF (15 wt%) formulation (black; TG: dot; DSC: solid) and the photo-DSC cured (red; TG: dot; DSC: solid) sample (90 °C).

Die approbierte gedruckte Originalversion dieser Dissertation ist an der TU Wien Bibliothek verfügbar.
The approved original version of this doctoral thesis is available in print at TU Wien Bibliothek.
TU Bibliothek Your knowledge hub WIEN

In summary, optimal curing and bubble-free samples were achieved within the temperature range of 80 to 90 °C. Beyond 100 °C, despite improved reactivity, the formation of bubbles during curing limits its practical use. Moreover, the insolubility of PF in Novo results in a heterogeneous mixture, which could introduce inaccuracies during the 3D printing process. Consequently, consideration was given to further alternative more homogeneous CAs.

1.2.3 (Poly-)oxymethylene derivatives

Due to the fact that paraformaldehyde has left a positive effect as a CA, further components based on the oxymethylene basic structure were investigated, which could in principle be decomposed into formaldehyde with the aid of an acid. In addition to the *'quasi'* ring-shaped paraformaldehyde, the 1,3,5-Trioxane (chapter 1.2.3.1), end-group-protected paraformaldehydes such as polyoxymethylene (POM, chapter 1.2.3.2) were tested as long-chain paraformaldehydes as well as polyoxymethylene dimethyl ether ($PODE_5$,chapter 1.2.3.3) and trioxymethylene diacetate (TOMDA, chapter 1.2.3.4) as low-molecular compounds.

1.2.3.1 1,3,5-Trioxane

Like the two components described above, trioxane (Figure 12) is also known as a CA, among others things also in the field of deep UV lithography.[101]

Figure 12: Structure of 1,3,5-trioxane.

Trioxane is a proven source of formaldehyde, especially when a strong acid acts as a catalyst.[102] Consequently, various formulation compositions were prepared and analyzed using photo-DSC at 80 °C (Table 2).

Die approbierte gedruckte Originalversion dieser Dissertation ist an der TU Wien Bibliothek verfügbar.
The approved original version of this doctoral thesis is available in print at TU Wien Bibliothek.
TU WIEN Bibliothek Your knowledge hub

Table 2: Results of the photo-DSC experiments of the trioxane formulations at 80 °C, 2 × 900 s, 320-500 nm, 60 mW·cm^{-2}.

PAG [wt%]	Trioxane [wt%]	ΔH [J·g^{-1}]	t_{max} [s]
5	10	210 ± 10	19 ± 1
5	20	200 ± 10	19 ± 1
10	10	190 ± 10	25 ± 1

As can be seen from the enthalpy values, the differences in the weight of the PAG and the CA hardly make any difference. In absolute terms, the values are slightly below those of the PF formulation, but still provide satisfactory solid materials. However, the samples with only 10 wt% trioxane were more easily deformed when repeatedly heated to 100 °C, so that a lower network density can be assumed than for those with 20 wt% trioxane. The t_{max} of 20-25 s is significantly higher than that of the PF formulation. This could be due to the higher stability of the trioxane compared to the PF due to the ring enthalpy, which results in a delay in decomposition to formaldehyde.

A theoretically possible cationic polymerization of the trioxane was excluded by means of an experiment between trioxane and PAG at 80°C. This also corresponds to the results of the literature, which describes the ceiling-temperature of this reaction at about 30 °C and consequently a degradation of the polymer above this temperature by means of a back-biting mechanism.[103,104]

For further characterization, the pure formulation with 20 wt% trioxane and a sample cured from this formulation were analyzed using STA (Figure 13).

Die approbierte gedruckte Originalversion dieser Dissertation ist an der TU Wien Bibliothek verfügbar.
The approved original version of this doctoral thesis is available in print at TU Wien Bibliothek.
TU WIEN Bibliothek Your knowledge hub

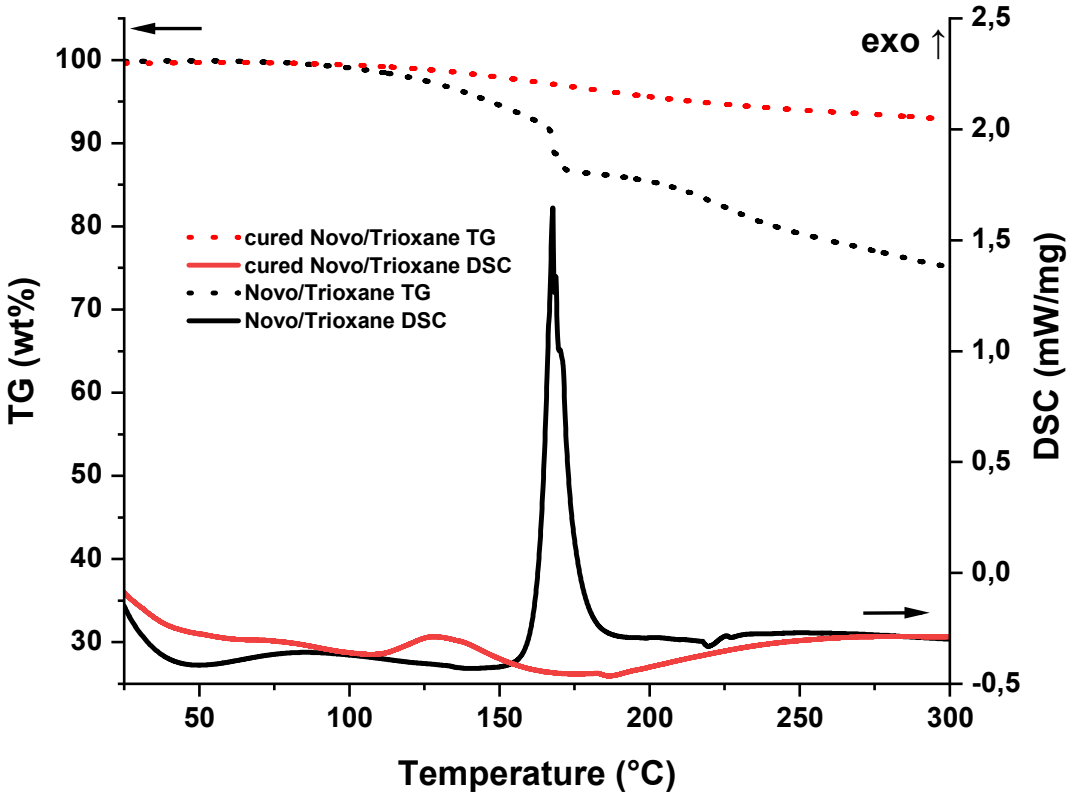

Figure 13: STA of the 20 wt% trioxane formulation (black; TG: dot; DSC: solid) and the photo-DSC cured (red; TG: dot; DSC: solid) sample (80 °C).

The cured sample shows a slight exothermic peak at around 130 °C followed by an endothermic peak between 160 and 200 °C. Consequently, not all trioxane has reacted, meaning that post-curing would still be necessary. As with the PF formulation, the unured formulation shows a strongly exothermic peak at 170 °C, combined with a weight loss in the region of 15 wt%. This is significantly more in comparison to the previous tests and is due to the low boiling point of 116 °C of the trioxane. Together with the known high volatility of trioxane, this attribute makes trioxane rather unsuitable for a suitable CA in the field of Hot Lithography. With constant heating, the CA would gradually evaporate from the formulation and thus lead to an intensified unscented curing.

1.2.3.2 Polyoxymethylene

Lüftl et al. describe the thermo-oxidative decomposition of homo-polyoxymethylene (POM-H) to the main product formaldehyde. This process is considerably accelerated

Die approbierte gedruckte Originalversion dieser Dissertation ist an der TU Wien Bibliothek verfügbar.
The approved original version of this doctoral thesis is available in print at TU Wien Bibliothek.
TU Bibliothek Your knowledge hub WIEN

by the formation of acids, also known as acidolysis.[105,106] Since PF (hydroxy group, Figure 14 right) and POM-H (acetate group, Figure 14 left) differ only in the end group apart from the molecular weight and the main decomposition product of both is proven to be formaldehyde, POM-H seemed to be a suitable candidate.

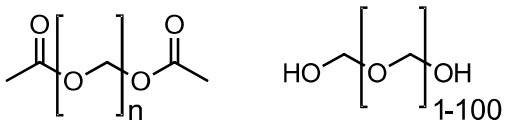

Figure 14: Structure of Polyoxymethylene (POM, left) and Paraformaldehyde (PF, right).

Therefore, different POM granules were finely ground in the cryomill and mixed with the Novo at 160 °C (15 wt% POM). The melting point of all POMs is 178 °C, but at this temperature Novo already reacted as an acid and decomposed the POMs to formaldehydes. A slight increase in viscosity was already observed at the selected temperature. The POMs used and their properties are listed in Table 3.

Table 3: Used POMs as CAs.

Name POM	Type	Mw
Delrin 1700P	Homopolymer	Low
Delrin 500P	Homopolymer	High
Ultraform S2320	Copolymer	High

Only the 1700P formulation gave a clear mixture without a large amount of unmelted POM. The PAG (5 wt%) was added in a second step at 90 °C. Nevertheless, all formulations were tested by photo-DSC (Table 4).

Die approbierte gedruckte Originalversion dieser Dissertation ist an der TU Wien Bibliothek verfügbar.
The approved original version of this doctoral thesis is available in print at TU Wien Bibliothek.
TU Bibliothek Your knowledge hub WIEN

Table 4: Photo-DSC results of the POM (15 wt%) formulations at different temperatures, 2 × 900 s, 320-500 nm, 60 mW·cm^{-2}.

Temp. [°C]	POM	$_{\Delta}H$ [J·g^{-1}]	t_{max} [s]
80	Delrin 500P	300 ± 10	14 ± 1
	Delrin 1700P	315 ± 10	16 ± 2
	Ultraform S2320	310 ± 10	16 ± 2
90	Delrin 500P	330 ± 10	11 ± 1
	Delrin 1700P	330 ± 10	12 ± 1
	Ultraform S2320	340 ± 10	11 ± 1
100	Delrin 500P	200 ± 20	7 ± 1
	Delrin 1700P	240 ± 20	7 ± 1
	Ultraform S2320	165 ± 20	7 ± 1

As can be seen in Table 4, the values for the different formulations are very similar depending on the temperature. At 330 J·g^{-1}, they are even higher than the formulation with 15 wt% PF. The increased energy is presumably due to the increased proportion of formaldehyde. Since no exact molecular weights are known for the POMs, the same weight-percentage was weighed in, which ultimately leads to more formaldehyde in the formulation. Lifting of the lid could be observed at 100 °C as well as with PF. However, as the processability of the formulation is difficult and the various POM CAs are not completely soluble in Novo, additional polyoxymethylene-based CAs were sought.

1.2.3.3 Polyoxymethylene dimethyl ethers

Reuss et al. describe not only pure polyoxymethylenes such as trioxane or PF, but also polyoxymethylene dimethyl ether (PODE) and short-chain polyoxymethylene diacetates (POMDA), which are based on formaldehyde.[107] Both derivatives are liquid depending on the chain length and have a high boiling point. However, only a few chain lengths can be easily produced or are commercially available.

PODEs (Figure 15) are considered as future diesel substitute fuel and are attracting more and more interest. Wang et al. describe the decomposition of PODE with water and acid at elevated temperature.[108] Again, the main product is formaldehyde. Especially the chain lengths with n= 3,4,5 are of industrial interest, therefore $PODE_5$

Die approbierte gedruckte Originalversion dieser Dissertation ist an der TU Wien Bibliothek verfügbar.
The approved original version of this doctoral thesis is available in print at TU Wien Bibliothek.
TU WIEN Bibliothek Your knowledge hub

as the molecule with the most formaldehyde units and a boiling point of 242 °C was considered as another CA.

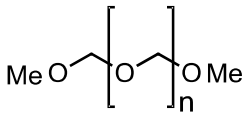

Figure 15: Structure of Polyoxymethylene dimethyl ether (PODE).

Consequently, to obtain approximately the same molar amount of formaldehyde compared to the PF formulations, 20 wt% $PODE_5$ was added to 5 wt% PAG and mixed at 80 °C. This formulation was tested using photo-DSC (Table 5).

Table 5: Photo-DSC results of the $PODE_5$ (20 wt%) formulation at different temperatures, 2 × 900 s, 320-500 nm, 60 mW·cm^{-2}.

Temp. [°C]	ΔH [J·g^{-1}]	t_{max} [s]
70	250 ± 10	35 ± 2
80	280 ± 10	23 ± 1
90	250 ± 10	15 ± 1

The energy values from the photo-DSC are already in the range of the PF formulations at 80-90 °C. The t_{max}, on the other hand, is somewhat lower and implicates a slow reaction. At 70 °C, the surface of the samples is smooth, but as soon as the temperature is increased, bubbles and defects appear. Consequently, higher temperatures to accelerate the reaction are not technically feasible due to the evaporation of the methanol (b.p. 65 °C) and complete curing cannot be guaranteed. However, the formulation offers significantly better processability, with similar reactivity to PF formulations.

1.2.3.4 Trioxymethylene diacetate

POMDAs are considered as liquid POM due its chemical nature, depending on the chain length. Especially within the oligomeric range (consisting of 2 to 6 formaldehyde

Die approbierte gedruckte Originalversion dieser Dissertation ist an der TU Wien Bibliothek verfügbar.
The approved original version of this doctoral thesis is available in print at TU Wien Bibliothek.
TU WIEN Bibliothek Your knowledge hub

units), these substances exhibit a liquid state while remaining non-volatile. Already in 1932 Staudinger described the production and properties of these diacetates.[109]

Hence, one of these low-molecular POMDAs, specifically trioxymethylene diacetate (TOMDA), was explored as a potential homogeneous CA. TOMDA is recognized for its formation as an intermediate during the cationic polymerization of n-trioxane in the initiation step, particularly under cryogenic conditions.[110] Tomiška et al. further established that utilizing zinc chloride as a catalyst, with the equimolar use of n-trioxane and acetic anhydride, yields TOMDA as the primary product in high yield.[111] This colorless liquid possesses a boiling point of 135 °C at 3 mbar.

The decomposition of TOMDA, triggered by the influence of a PAG, is expected to result in the generation of three parts formaldehyde and two parts acetic acid (Scheme 6). The latter is anticipated to catalyze the acid-induced polymerization as a subsequent step.

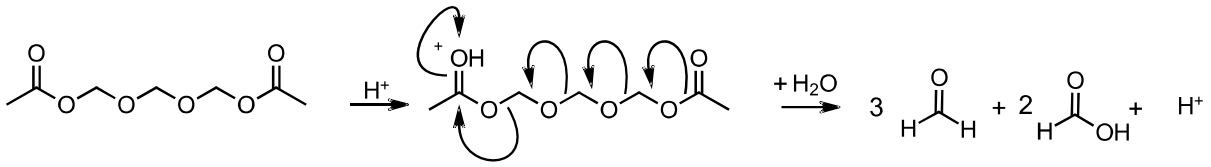

Scheme 6: Acid-catalyzed decomposition of TOMDA to formaldehyde and acetic acid.

To equate the formaldehyde equivalents from the prior formulations, analogous to the PODE formulation, 20 wt% of TOMDA was employed as the CA (5 wt% PAG). In contrast to the PF formulation, the photo-DSC results (Figure 16a, Figure 16b & Table 6) revealed significantly higher energy values, comparable to these from the POM formulations. This suggests a higher degree of reaction conversion and consequently a greater cross-linking density. The improved homogeneity achieved in the formulation, coupled with the elevated enthalpy values, may be attributed not only to TOMDA but also to the introduced acetic acid serving as an additional catalyst. Moreover, the decline in energy values due to water evaporation was notably observed at higher temperatures. The samples obtained at 100 °C exhibited considerably less bubble formation compared to the PF formulation (Figure 16c). This phenomenon can be attributed to the system's production of acetic acid, which, when combined with water, forms an zeotropic mixture with a boiling point higher than that of water, depending on

Die approbierte gedruckte Originalversion dieser Dissertation ist an der TU Wien Bibliothek verfügbar.
The approved original version of this doctoral thesis is available in print at TU Wien Bibliothek.
TU WIEN Bibliothek Your knowledge hub

the mixing ratio.[112] Interestingly, the reaction speed, as indicated by t_{max}, showed no significant difference from the previous formulation.

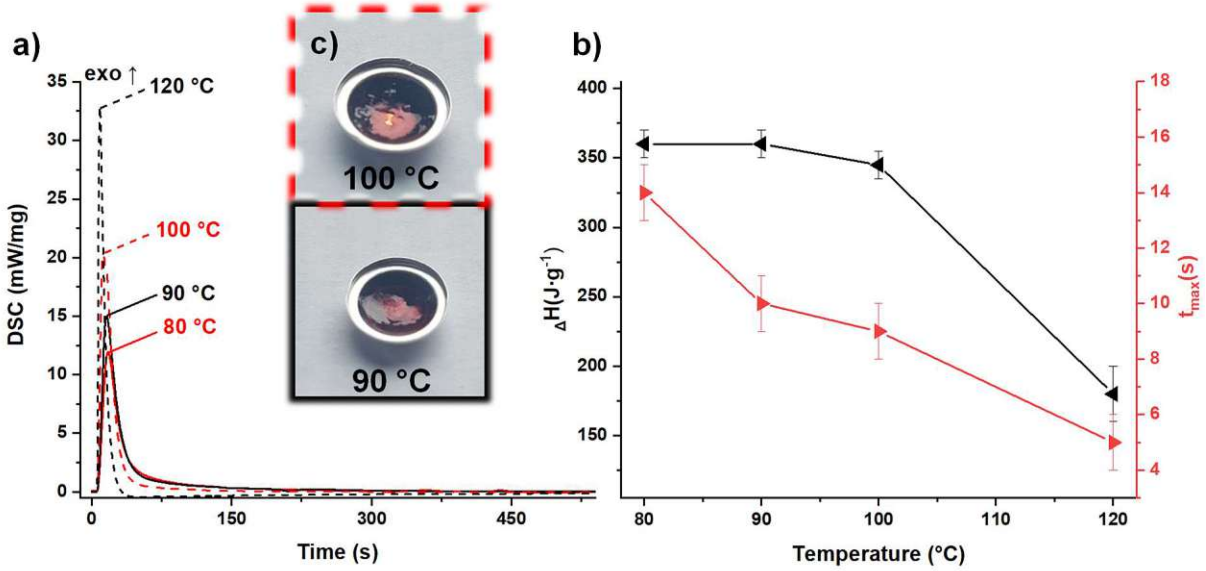

Figure 16: (a) Photo-DSC of the TOMDA (20 wt%) formulation at 80-120 °C, 2 × 900 s, 320-500 nm, 60 mW·cm^{-2}. (b) Temperature dependence of photo-DSC results for the TOMDA formulation: enthalpy change (ΔH black) and time until maximal heat is released (t_{max} red). (c) Cured Samples at 90 & 100 °C.

Table 6: Results of the photo-DSC experiments of the TOMDA (20 wt%) formulation.

Temp. [°C]	ΔH [J·g^{-1}]	t_{max} [s]
80	360 ± 10	14 ± 1
90	360 ± 10	10 ± 1
100	345 ± 10	9 ± 1
120	180 ± 20	5 ± 1

When examining the cured sample at 90 °C in comparison to the pure formulation using STA, the observed trend aligns with the previous findings (Figure 17). The pure formulation displays an exothermic peak around 190 °C, whereas the cured sample exhibits a notable weight loss and an endothermic peak around 125 °C, attributed to the evaporation of water and acetic acid. In contrast, the PF formulation displayed an exothermic peak at approximately 170 °C. This early peak can be explained by the lower stability of PF. Depending on the molecular weight, PF undergoes melting in the

Die approbierte gedruckte Originalversion dieser Dissertation ist an der TU Wien Bibliothek verfügbar.
The approved original version of this doctoral thesis is available in print at TU Wien Bibliothek.
TU Bibliothek Your knowledge hub WIEN

range of 120–170 °C.[113] Once it transitions from a solid to a liquid state, the pure novolak can initiate the decomposition of PF by acting as an acid. The esterification of the short oxymethylene chain, achieved through capping the hydroxyl end groups, enhances stability.[114] Consequently, the mixture with TOMDA reacts at a higher temperature.

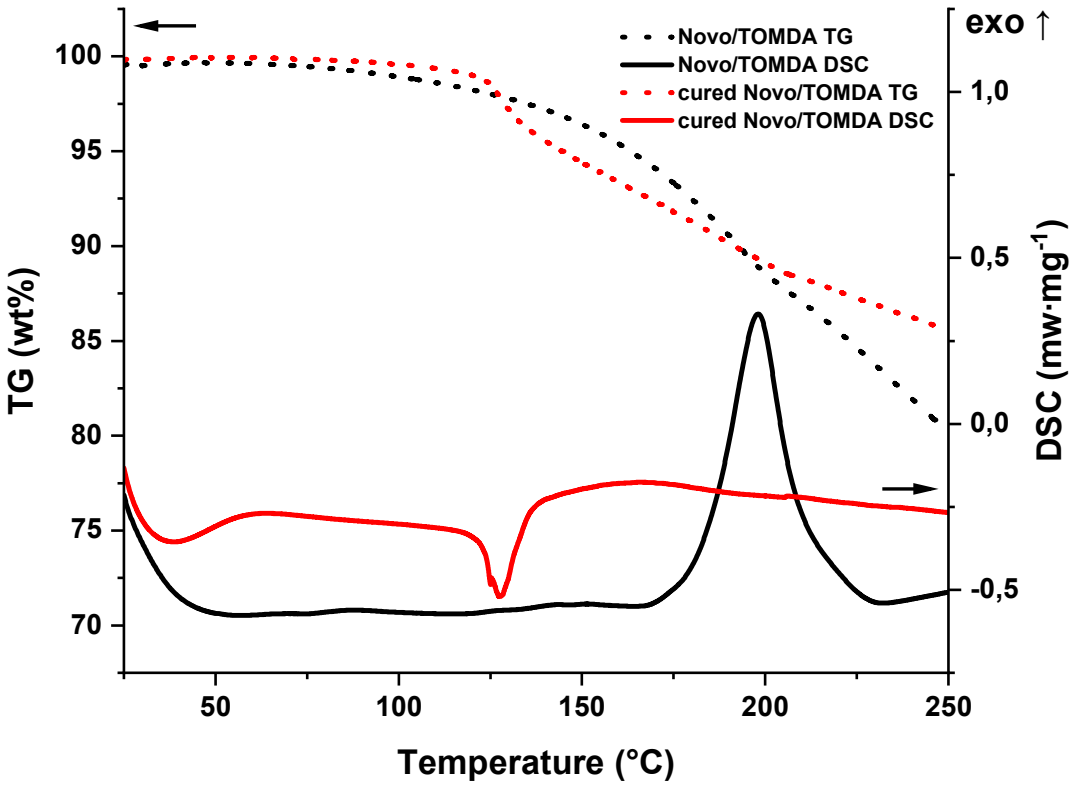

Figure 17: STA of the TOMDA (20 wt%) formulation (black; TG: dot; DSC: solid) and the photo-DSC cured (red; TG: dot; DSC: solid) sample (90 °C).

All in all, the formulation with TOMDA as CA offers very good conditions for further use in the field of AM, especially in the temperature range between 80 and 90 °C. Hot Lithography is therefore the method of choice.

1.2.4 Formals

Heslinga & Schors report the use of various cyclic formals as CA for novolaks in combination with an acid as catalyst.[115] They postulate that the ring is opened by the protonation of the dioxolane to produce an alcohol. In the next step, formaldehyde is

Die approbierte gedruckte Originalversion dieser Dissertation ist an der TU Wien Bibliothek verfügbar.
The approved original version of this doctoral thesis is available in print at TU Wien Bibliothek.
TU Bibliothek Your knowledge hub WIEN

split off and a carbenium ion is generated, which subsequently reacts with the aromatic compound in the phenolic system Scheme 7. This means that both the formaldehyde and the reaction of the residue, if di-functional, contribute to the cross-linking of the novolak.

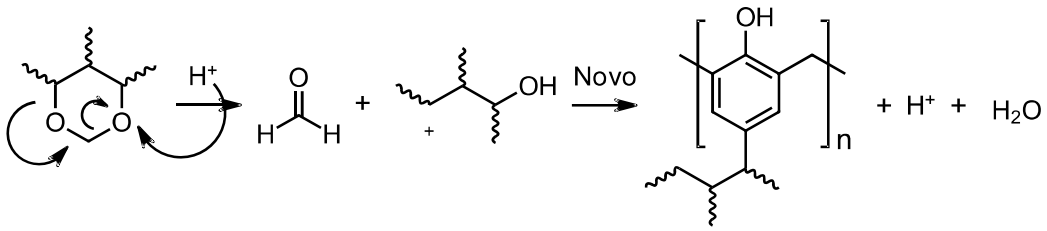

Scheme 7: Postulate reaction mechanism of formals with novolaks by Heslinga & Schors.[115]

Some of these are commercially available, liquid at room temperature and yet have a high boiling point. Consequently, this non-volatile substance class offers a further possibility for curing novolaks in Hot Lithography.

1.2.4.1 Glycerol formal

First, a monofunctional dioxolane was tested with glycerol formal (GF, Figure 18). With a boiling point of 192 °C, this should be sufficiently thermally stable to be present in the formulation for a longer period of time.

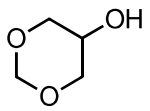

Figure 18: Structure of Glycerol formal (GF).

Several formulations (5 wt% PAG) with different amounts of GF were prepared and analyzed using photo-DSC (100 °C, Table 7) and STA (Figure 19).

Die approbierte gedruckte Originalversion dieser Dissertation ist an der TU Wien Bibliothek verfügbar.
The approved original version of this doctoral thesis is available in print at TU Wien Bibliothek.
TU Bibliothek Your knowledge hub WIEN

Table 7: Photo-DSC results of the GF formulations at 100 °C, 2 × 900 s, 320-500 nm, 60 mW·cm^{-2}.

GF [wt%]	ΔH [J·g^{-1}]	t_{max} [s]
10	20 ± 10	n.a.
20	20 ± 10	n.a.
40	20 ± 10	n.a.

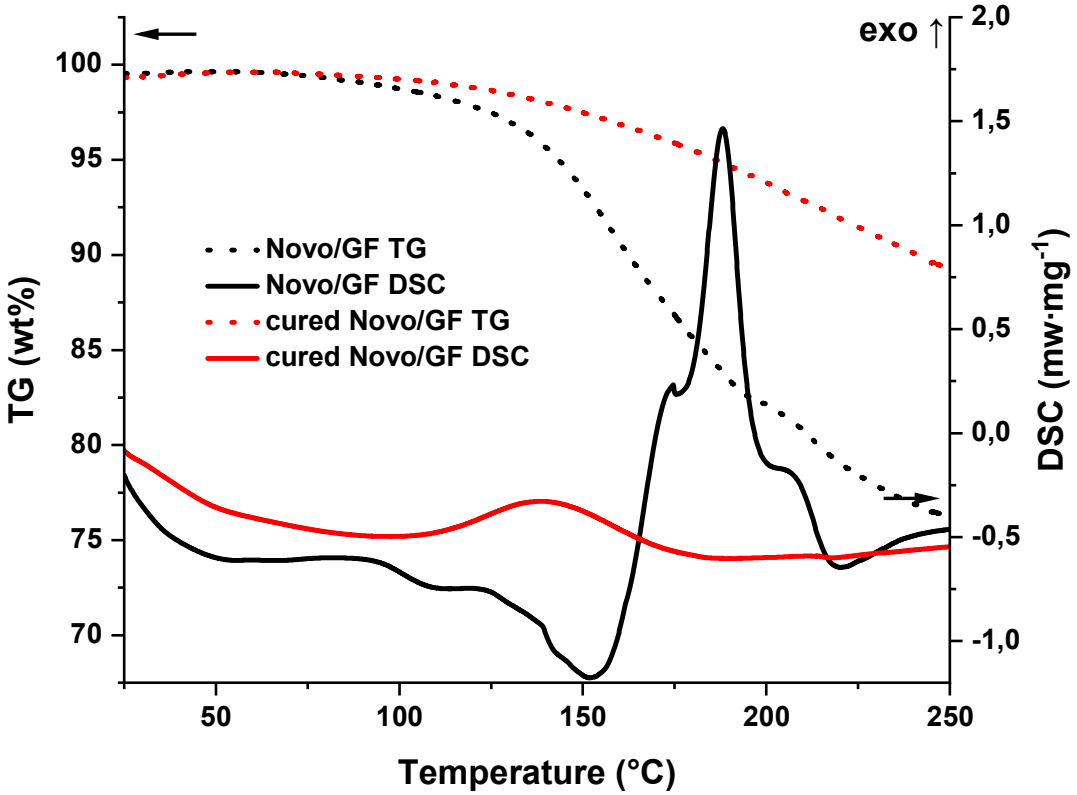

Figure 19: STA of the GF (40 wt%) formulation (black; TG: dot; DSC: solid) and the photo-DSC cured (red; TG: dot; DSC: solid) sample (100 °C).

The photo-DSC does not indicate polymerization during illumination. The samples also melted after treatment with light at 100 °C. Nevertheless, the pure formulation shows in the STA a strongly exothermic peak at almost 190 °C. In comparison to the Novo/PAG formulation (Figure 8), just thermal curing may be present here. No further analyses were carried out as the temperature required for the reaction was considered too high for polycondensation of the Novo.

Die approbierte gedruckte Originalversion dieser Dissertation ist an der TU Wien Bibliothek verfügbar.
The approved original version of this doctoral thesis is available in print at TU Wien Bibliothek.
TU Bibliothek Your knowledge hub WIEN

1.2.4.2 Cyclic trimethylolpropane formal

The next tested formal was the also commercially available cyclic trimethylolpropane formal (CMF, Figure 20).

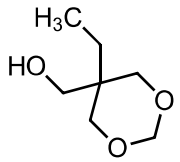

Figure 20: Structure of cyclic trimethylolpropane formal (CMF).

Unfortunately, the pure CMF (5 wt% PAG) as well as the mixture with Novo with 40 wt% CMF did not show any curing reaction in the photo-DSC (100 °C). Therefore, no further testing of this CA was executed.

1.2.4.3 4-Phenyl-1,3-dioxane

As the previous formals did not work as desired, a dioxolane used by Heslinga & Schors was tried next.[115] Since it was the only one commercially available cyclic formal of their work, 4-phenyl-1,3-dioxane (PD, Figure 21) was used as potential CA.

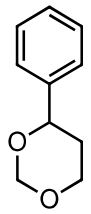

Figure 21: Structure of 4-phenyl-1,3-dioxane (PD).

For the photo-DSC analysis, a formulation (5 wt% PAG) with 40 wt% PD was prepared (comparable molar amount to the PF formulation) and irradiated at different temperatures (Figure 22 & Table 8).

Die approbierte gedruckte Originalversion dieser Dissertation ist an der TU Wien Bibliothek verfügbar.
The approved original version of this doctoral thesis is available in print at TU Wien Bibliothek.
TU WIEN Bibliothek Your knowledge hub

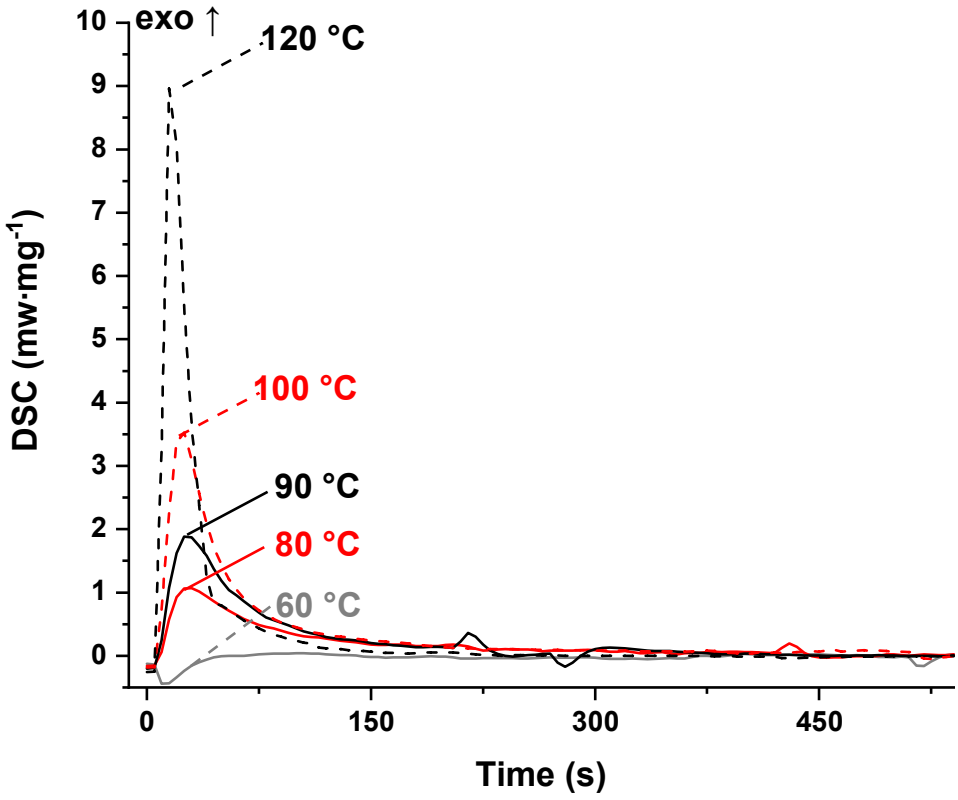

Figure 22: Photo-DSC of the PD (40 wt%) formulation at 80-120 °C, 2 × 900 s, 320-500 nm, 60 mW·cm^{-2}.

Table 8: Results of the photo-DSC experiments of the PD (40 wt%) formulation.

Temp. [°C]	ΔH [J·g^{-1}]	t_{max} [s]
60	-	-
80	90 ± 10	24 ± 2
90	110 ± 10	20 ± 3
100	170 ± 10	17 ± 1
120	210 ± 10	12 ± 1

During the temperature-dependent series of measurements, an acceleration of the curing reaction was observed in addition to increasing exotherm. As with the previous CAs, this led to the evaporation of the water formed during polycondensation as the temperature increased from 100 °C. The enthalpy values are below the range of the

Die approbierte gedruckte Originalversion dieser Dissertation ist an der TU Wien Bibliothek verfügbar.
The approved original version of this doctoral thesis is available in print at TU Wien Bibliothek.
TU WIEN Bibliothek Your knowledge hub

prior formulations and indicate incomplete curing. Therefore, STA measurements were taken of all cured samples and the pure formulation (Figure 23).

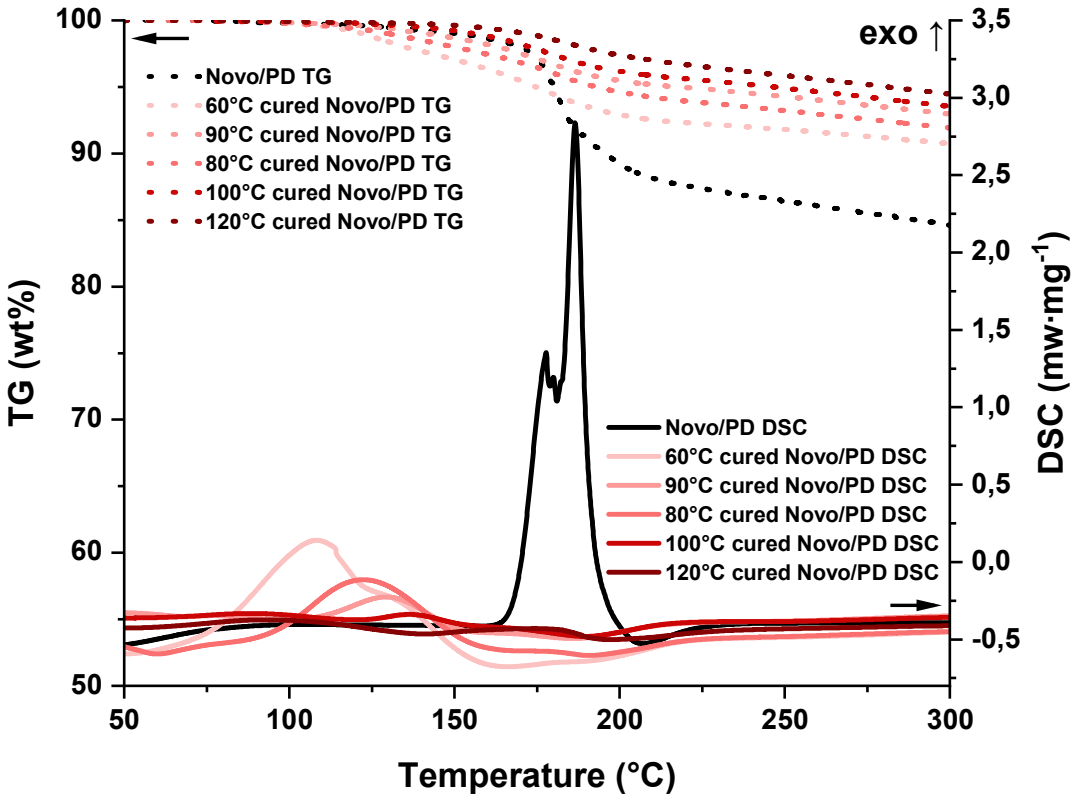

Figure 23: STA of the PD (40 wt%) formulation (black; TG: dot; DSC: solid) and at different temperatures in the photo-DSC cured samples.

A clear decrease in the remaining reactive centers with increasing curing temperature can be seen at the peak between 100 and 150 °C. At higher temperatures, a shift of the peak maximum towards higher temperatures can also be observed. This could be explained by the higher network density. The larger the network, the more immobile the chains are. At higher temperatures, this immobility could be compensated, and further reactions could take place. The peak of the pure formulation is highest at around 175 °C, but here the initiator must first be thermally cleaved. Similar to the reactive centers, the completeness of the reaction can be read from the weight loss. The higher the temperature during the reaction, the lower the weight loss. The resulting water evaporates at temperatures of 100 °C and above. The fact that a constant further

Die approbierte gedruckte Originalversion dieser Dissertation ist an der TU Wien Bibliothek verfügbar.
The approved original version of this doctoral thesis is available in print at TU Wien Bibliothek.
TU WIEN Bibliothek Your knowledge hub

weight loss can be observed for all samples could be explained by the weight proportion of PD and the resulting unreacted PD. This would evaporate from the formulation over time. The results of the STA give the same picture as those of the photo-DSC. The higher the temperature during the curing reaction, the better. A print at 90 °C with PD would therefore be conceivable.

1.2.4.4 Pentaerythritol diformal

The only difunctional formal used by Heslinga and Schors was pentaerythritol diformal (PDF, Figure 24).[115] As this product is difficult to obtain commercially, the CA was prepared according to the information in the literature.[116] By using pentaerythritol as adduct, the formal was formed through reaction with paraformaldehyde under acidic conditions.

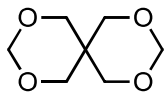

Figure 24: Structure of pentaerythritol diformal (PDF).

This compound (20 wt% half of the PD, as it is difunctional) was then used to prepare a formulation (5 wt% PAG) for analysis using photo-DSC at various temperatures. However, an incomplete enthalpy (compared to the PF or TOMDA formulation) of 120 $J \cdot g^{-1}$ was only observed from a temperature of 120 °C. Due to the temperature being too high for curing with this CA, no further analyses were carried out on this formulation either.

1.2.5 Miscellaneous curing agents

In the course of the work, two further potential CAs were tested, which were considered due to their structure and functional groups.

1.2.5.1 Furfuryl alcohol

The first of the two candidates was furfuryl alcohol (FA). This substance offers an aliphatic OH group in addition to the aromatic system. This structure of FA (Figure 25) is reminiscent of the intermediate stage in the polycondensation of novolak before

Die approbierte gedruckte Originalversion dieser Dissertation ist an der TU Wien Bibliothek verfügbar.
The approved original version of this doctoral thesis is available in print at TU Wien Bibliothek.
TU Bibliothek Your knowledge hub WIEN

water H_2O is split off in a further step. Therefore, the idea was to use FA, with the possibility that the aromatic system of a novolak could attack there with the help of an acid to complete the condensation.

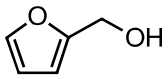

Figure 25: Structure of furfuryl alcohol (FA).

However, the measurement of the formulation (5 wt% PAG, 40 wt% FA) in the photo-DSC did not show any enthalpy. In addition, no condensation of water nor an increase in viscosity could be observed.

1.2.5.2 Salicylaldehyde

The second idea for a CA was salicylaldehyde (SA, Figure 26). Theoretically, the aldehyde functionality could serve as a formaldehyde equivalent and thus serve to cure the novolak.

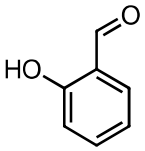

Figure 26: Structure of salicylaldehyde (SA).

However, in the photo-DSC experiments with SA (40 wt%) and PAG (5 wt%), neither enthalpy nor solidification could be detected. Consequently, SA was also classified as unsuitable for further experiments.

Die approbierte gedruckte Originalversion dieser Dissertation ist an der TU Wien Bibliothek verfügbar.
The approved original version of this doctoral thesis is available in print at TU Wien Bibliothek.
TU WIEN Bibliothek Your knowledge hub

1.3 3D printing of the phenolic formulations via Hot Lithography

Since several formulations were found to have potential CAs in Photo-DSC and STA, four different formulations were prepared, each with different Cas (Figure 27), and consequently initial printing tests were performed using Hot Lithography stereolithography.

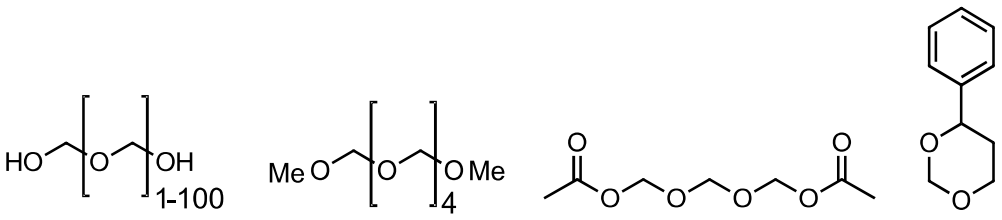

Figure 27: Different used CAs for the pritning tests (from left to right, PF, PODE5, TOMDA and PD)

In this process, the formulation is heated without a build platform and illuminated from below in a disk shape to determine the potential thickness of the layers at the corresponding laser speed (100 mm·s^{-1}). The CAs selected were PF (15 wt%, Figure 28 left), PODE$_5$ (20 wt%, Figure 28 right), TOMDA (20 wt%, Figure 29 left) and PD (40 wt%, Figure 29 right), each with 5 wt% PAG. The selected temperature was 80 °C, except for PODE$_5$ based on the methanol formed (70 °C), as bubble formation due to H_2O can be avoided at this temperature and sufficient reaction speed is still achieved.

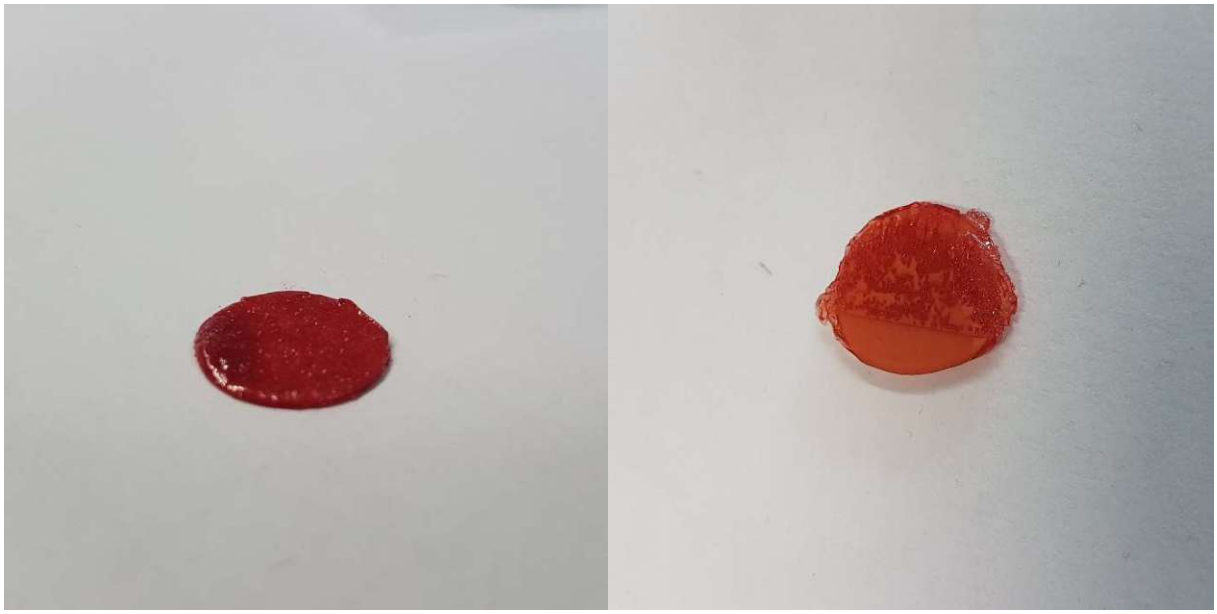

Figure 28: Printing tests (70-80 °C) of PF (15 wt%, left) formulation and PODE$_5$ (20 wt%, right) formulation.

Die approbierte gedruckte Originalversion dieser Dissertation ist an der TU Wien Bibliothek verfügbar.
The approved original version of this doctoral thesis is available in print at TU Wien Bibliothek.
TU WIEN Bibliothek Your knowledge hub

Figure 29: Printing tests (80 °C) of TOMDA (20 wt%, left) formulation and PD (40 wt%, right) formulation.

All four formulations delivered successful printing tests with layer thicknesses of 200-400 µm. In the test with $PODE_5$, the temperature was increased from 70 to 80 °C during the test in order to analyze the effect of evaporation. Clear defects can be seen, which would lead to problems in a proper printing job. The test with PD resulted in a thin layer (200 µm) which was still easily deformable at the selected temperature. Therefore, further print jobs were only carried out with the PF and TOMDA formulations.

The absorption spectrum of I-Sb peaks at 227 nm, extending into a tail-out range up to a wavelength of 360 nm.[117] This spectrum does not align with the wavelength of the laser employed in the 3D printer (375 nm). Despite this, preliminary exposure tests have shown positive results. The assumption of a self-sensitizing effect was made due to the material's coloration. As a result, a UV-Vis spectrum was acquired for both the pure resin and a cured thin film sample (Figure 30a).

Die approbierte gedruckte Originalversion dieser Dissertation ist an der TU Wien Bibliothek verfügbar.
The approved original version of this doctoral thesis is available in print at TU Wien Bibliothek.
TU WIEN Bibliothek Your knowledge hub

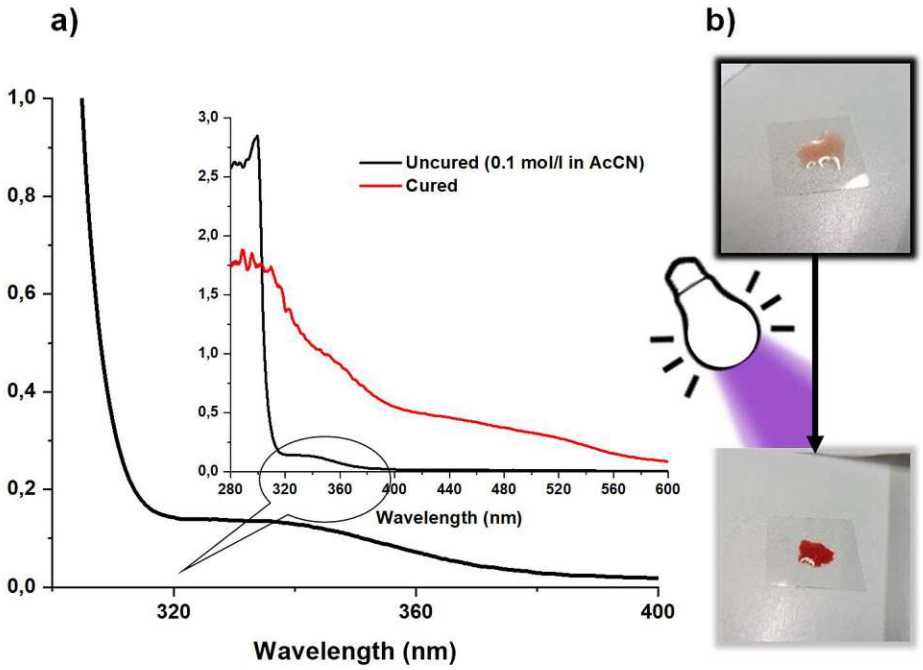

Figure 30: a) UV-Vis of the uncured (0.1 mol·L^{-1} in AcCN, black) and cured (red) PF formulation. b) Color changes during curing.

The spectrum of the pure novolak exhibits absorption extending up to 400 nm. Upon the curing of the thermoset, there is a bathochromic shift in the material. The formation of a distinct conjugated π-system results in the obtained samples appearing bright red (Figure 30b). This further reinforces the assumption of a self-sensitizing system, wherein the I-Sb is decomposed into a super-acid through the absorption of the resin.

Unlike traditional stereolithographic 3D printers, which are constrained to low-viscosity formulations, Hot Lithography can handle highly viscous resins with viscosities of up to 20 Pa·s. The formulations discussed in this study showcase viscosities ranging from 2 Pa·s (PF) to 150 mPa·s (TOMDA, PD, PODE$_5$) at the specified printing temperature of 80 °C. An additional consideration during the printing process is the thermal stability of the CAs. If formulation components evaporate due to prolonged exposure to elevated temperatures, polymerization may become more challenging or remain partially incomplete. To address this, the formulations underwent exposure to 90 °C with a continuous nitrogen flow (no lid on the crucibles) for 1 h, and the weight loss was monitored through thermal gravimetric analysis (TGA, Figure 31). The temperature was set to 90 °C, as this level provided the highest reactivity without inducing bubble formations during the curing process.

Die approbierte gedruckte Originalversion dieser Dissertation ist an der TU Wien Bibliothek verfügbar.
The approved original version of this doctoral thesis is available in print at TU Wien Bibliothek.
TU WIEN Bibliothek Your knowledge hub

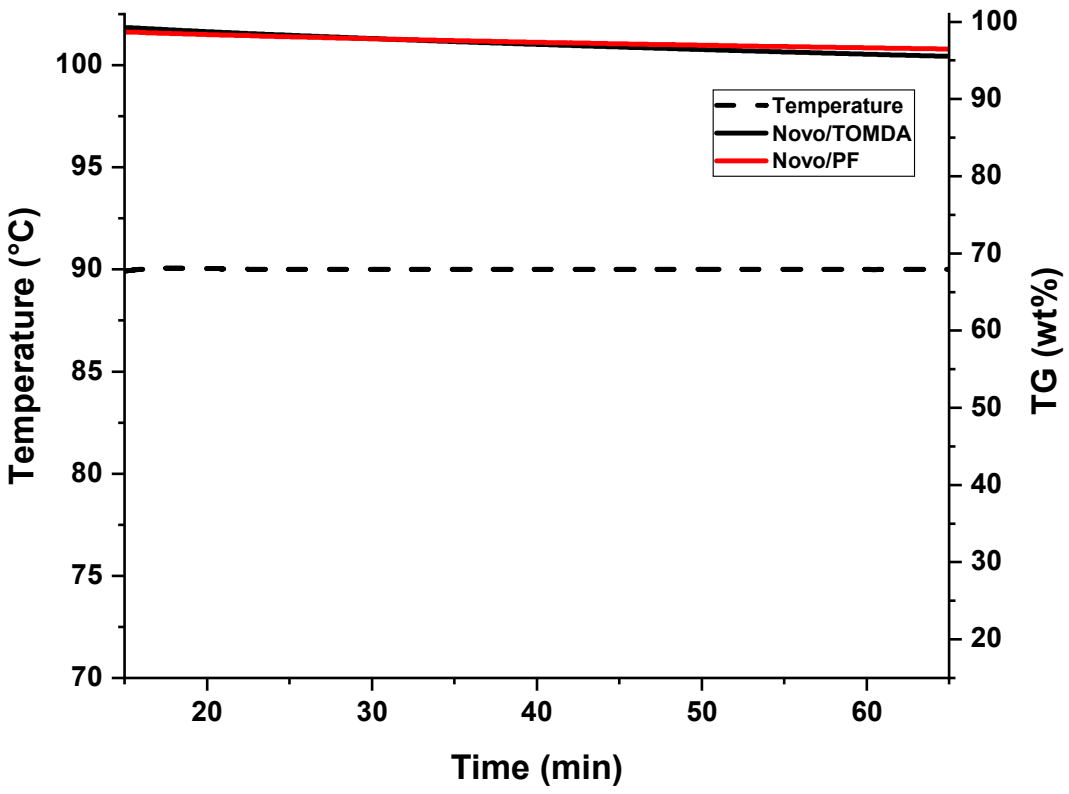

Figure 31: TGA of the TOMDA formulation (black) and PF formulation (red) at 90 °C.

Although there was some observed weight loss in the low weight percentage range for both formulations, it is negligible within the timeframes relevant to the 3D printing process. The TOMDA formulation shows slightly higher weight loss due to its higher CA content (20 wt% TOMDA compared to 15 wt% PF). Following the experiment, the treated formulations remained curable. In this regard, both formulations exhibited adequate thermal stability for application in Hot Lithography.

In subsequent phases of the study, both formulations were effectively employed to manufacture tensile and dynamic mechanical thermal analysis (DMTA) test specimens using molds, in conjunction with a UV oven and Hot Lithography. It's important to note that the irradiation conditions in the curing oven utilized offered higher intensities compared to the conditions for photo-DSC and Hot Lithography. This difference arises because the light sources for photo-DSC had to be coupled into light guides, while Hot Lithography relies on a laser.

Die approbierte gedruckte Originalversion dieser Dissertation ist an der TU Wien Bibliothek verfügbar.
The approved original version of this doctoral thesis is available in print at TU Wien Bibliothek.
TU WIEN Bibliothek Your knowledge hub

Furthermore, to showcase the capabilities of 3D printing, a digital object design was created (Figure 32a) and printed using the TOMDA formulation in a size of 2.5 cm × 1.5 cm (Figure 32b).

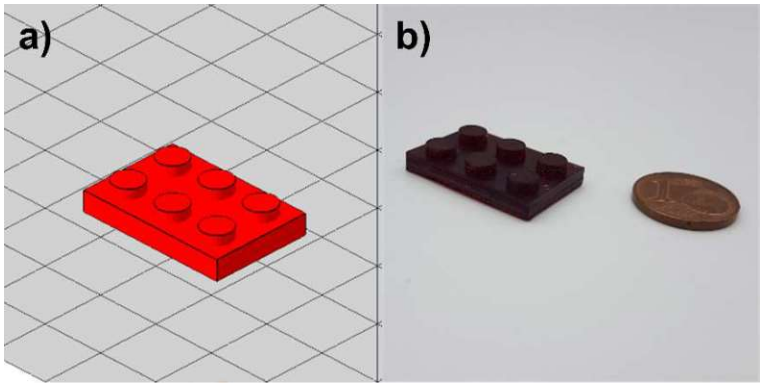

Figure 32: (a Designed object as CAD model. (b 3D printed object of TOMDA formulation via Hot Lithography.

Even without highly specific process optimization, the results are highly promising. The overall shape of the brick is already satisfactory, and microscopic images reveal a dense, well-connected surface in both the details of the edge region (Figure 34a) and the flat regions of the mechanical specimen. For the sake of comparability and to achieve the most thorough curing possible, all samples underwent a thermal post-treatment program (Figure 33). Post-curing did not lead to any significant deformation of the geometry, as evidenced by microscopy (Figure 34b). No thermally induced delamination was observed.

Die approbierte gedruckte Originalversion dieser Dissertation ist an der TU Wien Bibliothek verfügbar.
The approved original version of this doctoral thesis is available in print at TU Wien Bibliothek.
TU WIEN Bibliothek Your knowledge hub

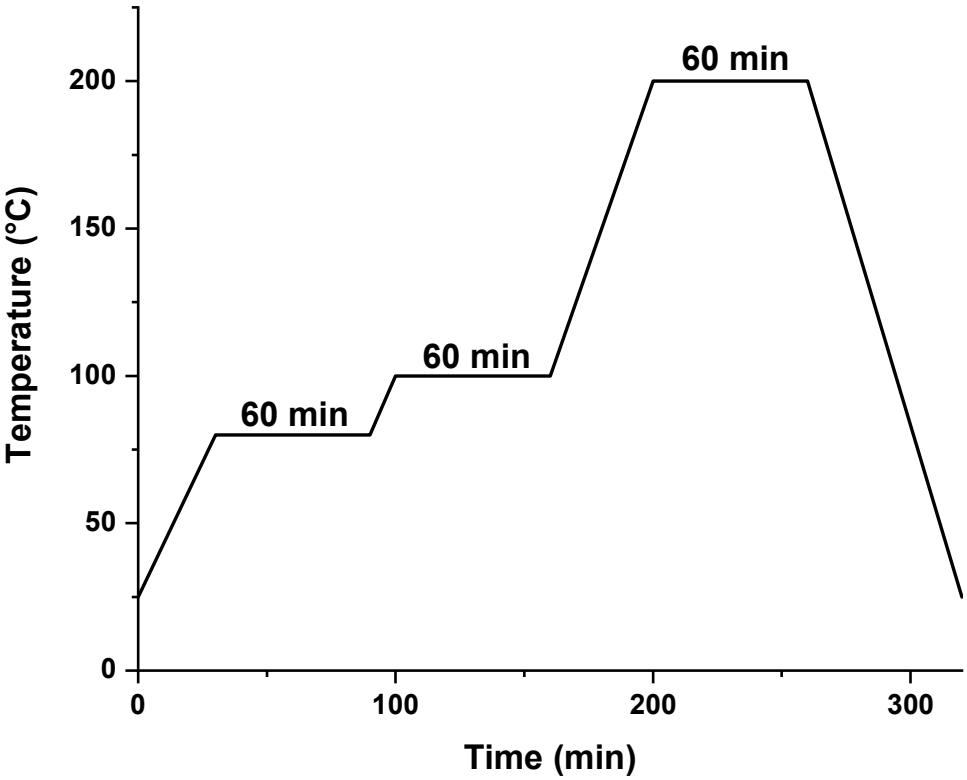

Figure 33: Post-processing program with a heating rate of 2 K·min^{-1}.

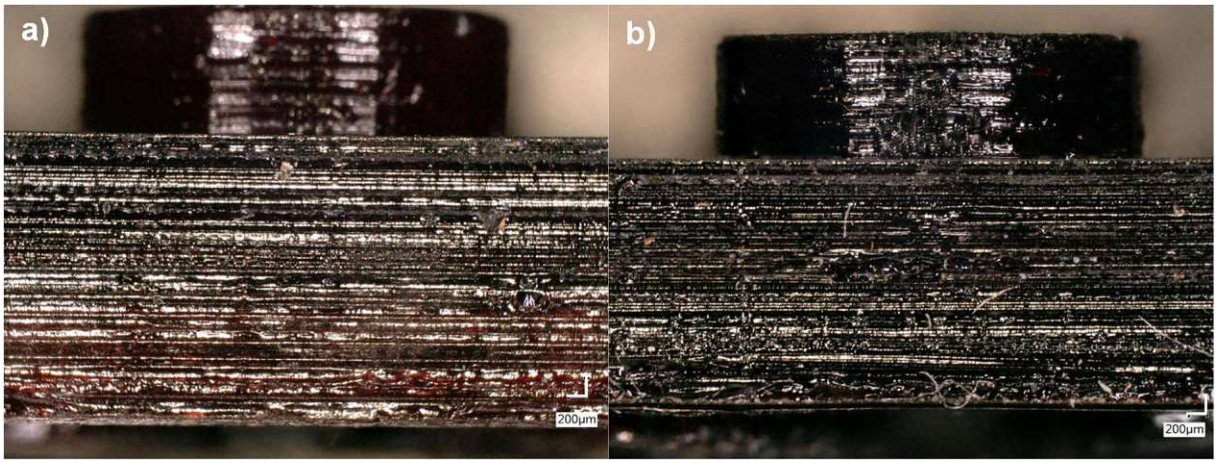

Figure 34: Microscopic image of the 3D printed object (a) before and (b) after the post-curing process.

Die approbierte gedruckte Originalversion dieser Dissertation ist an der TU Wien Bibliothek verfügbar.
The approved original version of this doctoral thesis is available in print at TU Wien Bibliothek.
TU WIEN Bibliothek Your knowledge hub

1.4 Comparative mechanical testing of the 3D printed and bulk cured materials

The thermally post-cured samples (both 3D printed and bulk cured) underwent characterization through tensile tests and DMTA, and a comparative analysis was conducted based on their processing method. Surprisingly, the tensile tests revealed an increase in both elongation at break (Figure 35a) and tensile strength (Figure 35b) for the 3D printed specimens. Higher tensile strength typically indicates a greater cross-linking density in the thermoset, implying a higher conversion during polymerization. This outcome is somewhat unexpected, as higher cross-linking density usually leads to reduced elongation at break. A plausible explanation for this phenomenon is that bulk-produced samples lack the opportunity to release water into the environment during polymerization. In bulk curing, the light source illuminates the material from above, and water becomes trapped in the sample due to the mold. Consequently, voids are formed in the bulk material due to water confinement, even when produced below 100 °C. In contrast, the layer-by-layer approach in Hot Lithography allows the release of water into the remaining resin in the vat, facilitating evaporation during the printing process. As a result, AM of the samples enables nearly void-free processing of the materials, as clearly seen in microscopy images (Figure 36). PF bulk-cured samples exhibit more voids than the TOMDA samples, while 3D printed samples display few to no voids. Ultimately, this leads to higher tensile strength and elongation at break for the 3D printed parts.

Comparing the two formulations, it is evident that TOMDA-prepared specimens exhibit significantly better values in tensile strength and elongation at break. This, coupled with increased enthalpy values from photo-DSC, indicates a superior cross-linking density and higher conversion, as mentioned earlier. A possible explanation, apart from increased acidity due to CA decomposition, is the homogeneity of the formulation. Additionally, the slightly lower viscosity and resulting chain mobility could contribute to a higher reaction conversion.

Die approbierte gedruckte Originalversion dieser Dissertation ist an der TU Wien Bibliothek verfügbar.
The approved original version of this doctoral thesis is available in print at TU Wien Bibliothek.
TU WIEN Bibliothek Your knowledge hub

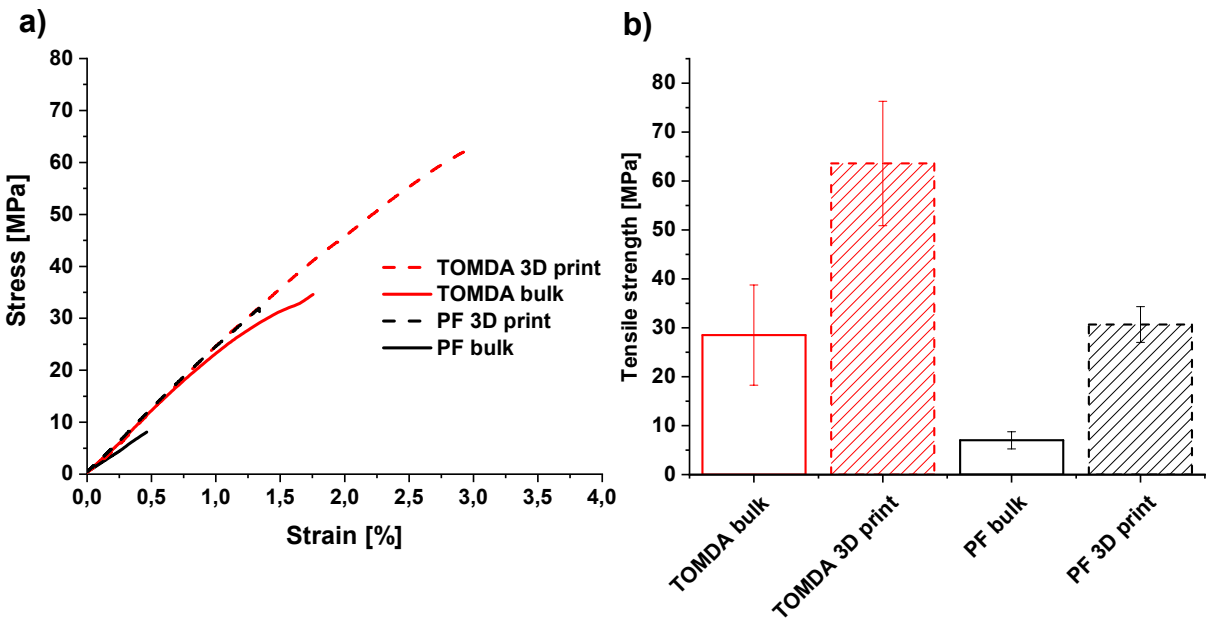

Figure 35: a) Stress–strain diagram of bulk cured and 3D printed parts. b) Tensile strength of bulk cured and 3D printed parts.

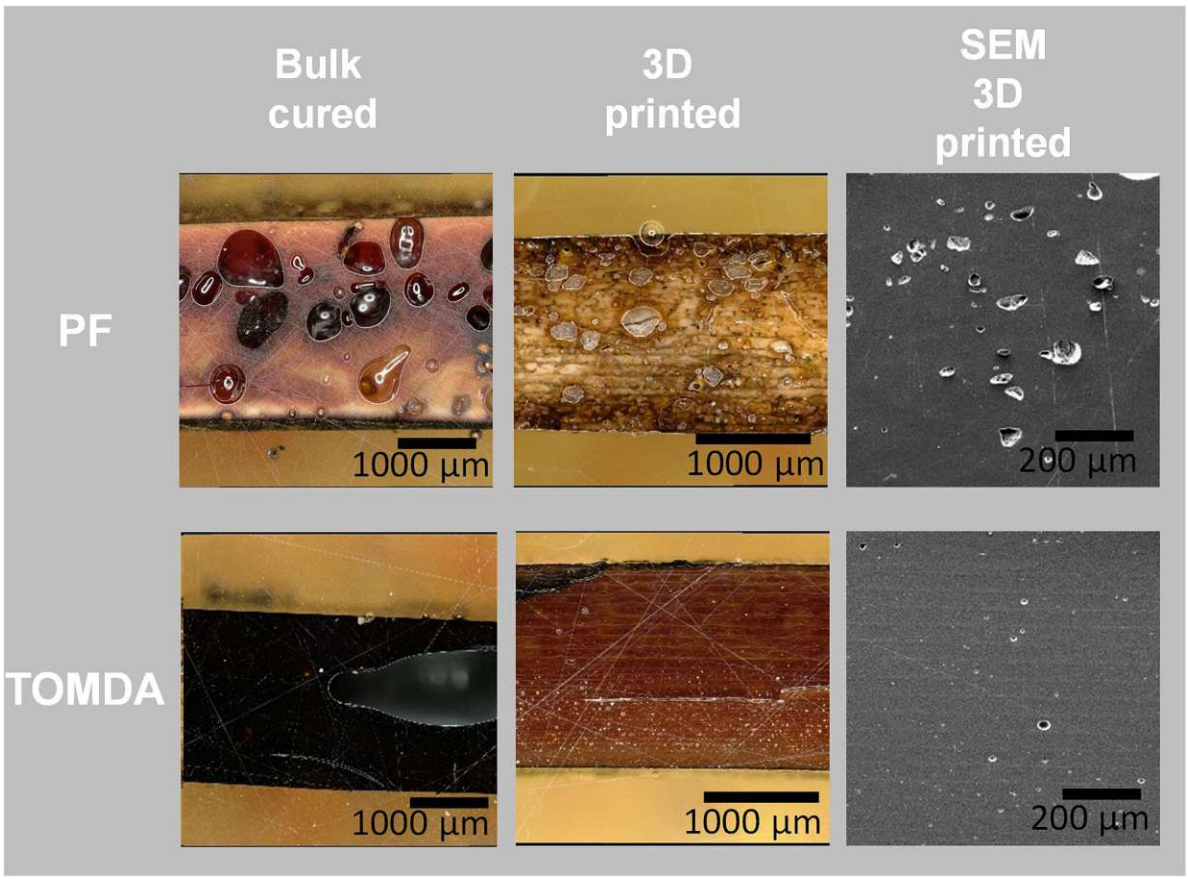

Figure 36: Microscopic images of the different produced specimen after post-curing.

Die approbierte gedruckte Originalversion dieser Dissertation ist an der TU Wien Bibliothek verfügbar.
The approved original version of this doctoral thesis is available in print at TU Wien Bibliothek.

The thermomechanical properties were assessed through DMTA. No significant difference was observed between the 3D printed and bulk-cured samples. However, a notable disparity emerged between the two different CAs. The sample composed of the homogeneous TOMDA mixture exhibited a T_g of approximately 95 °C, contrasting with the PF sample's T_g of about 140 °C (Figure 37a). Additionally, the PF sample displayed an elevated rubber plateau (Figure 37b), indicating, as per the literature, a higher network density.[118,119] This increased network density could account for the higher T_g, significantly influenced by network density.[120] Furthermore, alcohols and acetates are recognized as plasticizers for thermosets during the production process. Their presence disrupts hydrogen bonding interactions, contributing to the stability of phenoplasts, leading to a further reduction in T_g.[121–124] This reduction may be attributed to the residual acetate residues resulting from the CA's decomposition into acetic acid and formaldehyde.

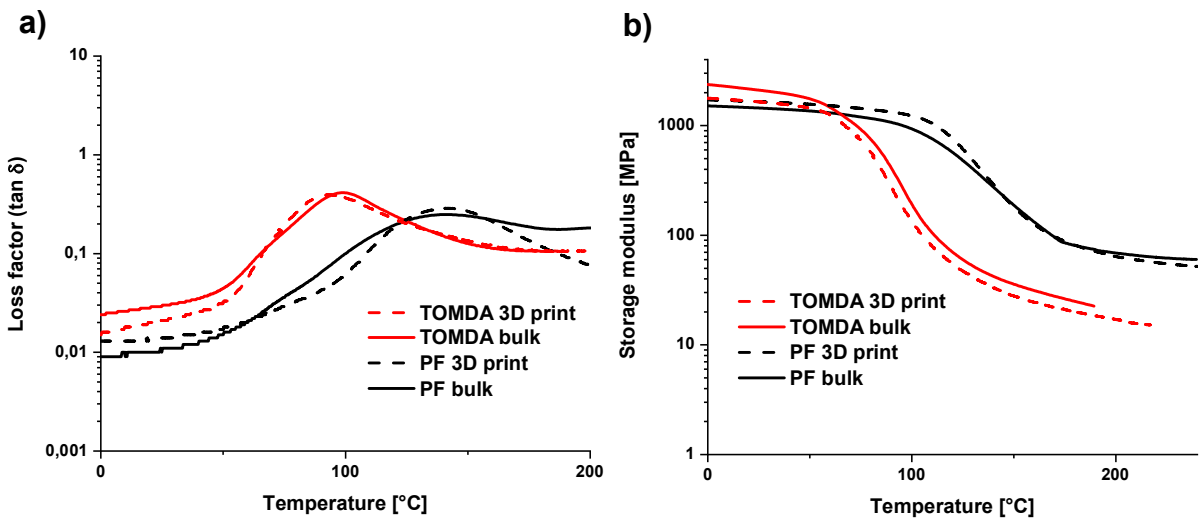

Figure 37: a) Loss factor of bulk cured and 3D printed parts. b) Storage modulus G′ curves of bulk cured and 3D printed parts.

The heightened network density of the PF samples seemingly contradicts the earlier findings regarding tensile strength. However, this discrepancy can be elucidated by considering the more homogeneous network in the TOMDA samples. The better regularity allows the TOMDA samples to compensate for the low network density compared to the heterogeneous PF sample. The PF formulation's heterogeneity might result in varying cross-linking densities across different parts of the samples, leading to both very high and very low cross-linking densities in different areas. This inhomogeneity is reflected in the broad peaks in the loss modulus and could account

Die approbierte gedruckte Originalversion dieser Dissertation ist an der TU Wien Bibliothek verfügbar.
The approved original version of this doctoral thesis is available in print at TU Wien Bibliothek.
TU WIEN Bibliothek Your knowledge hub

for the elevated T_g and higher rubber plateau, accompanied by reduced mechanical values.

1.5 Evaluation of additives to prevent bubble formation

As described above, the formation and evaporation of H_2O is a problem in the AM of phenolic resins. Therefore, the idea emerged to incorporate additives into the formulation that would chemically bind the H_2O before bubbles could form. There were two possible compounds considered. On the one hand, acetic anhydride (AA) was chosen, a substance that reacts quickly in combination with H_2O and releases two molecules of acetic acid (Scheme 8).

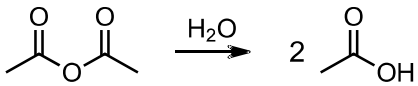

Scheme 8: Reaction of acetic anhydride (AA) with H_2O.

In addition to preventing the formation of bubbles, this would have a similar effect to that described in Chapter 1.2.3.4. The measured formulation consisted of 20 wt% TOMDA, 20 wt% AA with 5 wt% PAG. The energy values of the measurement at 120 °C resulted in 210 $J \cdot g^{-1}$ with a t_{max} of 25 s. These values are slightly lower than the standard TOMDA formulation, but the proportion of phenolic groups to be cured is reduced due to the amount of AA. The samples showed significantly less bubble formation than the samples without AA. Nevertheless, this formulation contains a large percentage that did not co-react in the end product. Another additive was therefore investigated in more detail.

Due to the similar properties with increased reactivity, epoxy resins are often used as co-resins in the curing of novolaks. These are more expensive but are still very interesting industrially due to the unique combination of properties. Furthermore, since they are cured via a cationic polymerization, they are able to absorb H_2O for a specific time. H_2O is considered a reversible inhibitor in cationic polymerization. Depending on the amount, the cationic polymerization stops, but can be resumed after removal. For

Die approbierte gedruckte Originalversion dieser Dissertation ist an der TU Wien Bibliothek verfügbar.
The approved original version of this doctoral thesis is available in print at TU Wien Bibliothek.
TU WIEN Bibliothek Your knowledge hub

this reason, different epoxy resins (37.5 wt%) were mixed with Novo (37.5 wt%), TOMDA (20 wt%) and PAG (5 wt%). The structures of the epoxy resin can be seen in (Figure 38). For comparison, a formulation without CA was also prepared. All of these formulations have been measured via photo-DSC (Table 9).

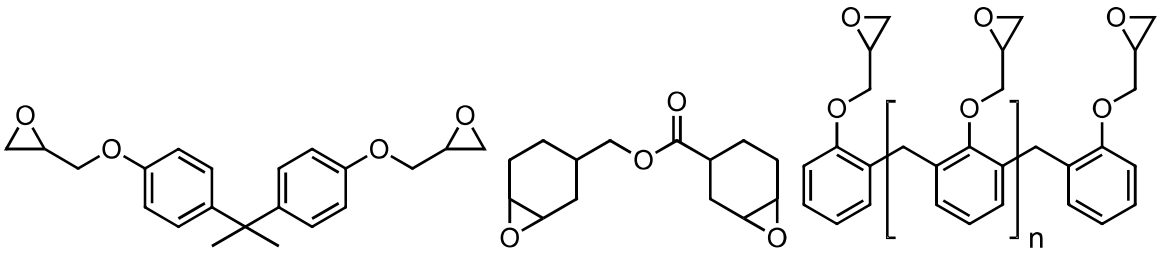

Figure 38: Structure of Bisphenol-A-diglycidylether (BADGE, left), 3,4-Epoxycyclohexylmethyl-3',4'-epoxycyclohexane carboxylate (middle, ECC) and epoxyphenol novolak (right, EpNovo).

Table 9: Photo-DSC results of the epoxy formulations at different temperatures, 2 × 900 s, 320-500 nm, 60 mW·cm^{-2}.

Temp. [°C]	POM	ΔH [J·g^{-1}]	t_{max} [s]
80	EpNovo without CA	280 ± 20	7 ± 1
	EpNovo	380 ± 20	10 ± 1
	ECC	340 ± 40	15 ± 2
	BADGE	380 ± 40	16 ± 2
90	EpNovo without CA	290 ± 10	7 ± 1
	EpNovo	440 ± 10	8 ± 1
	ECC	390 ± 20	13 ± 2
	BADGE	430 ± 10	14 ± 2
100	EpNovo without CA	290 ± 10	7 ± 1
	EpNovo	450 ± 20	7 ± 1
	ECC	410 ± 10	11 ± 1
	BADGE	440 ± 20	11 ± 1
120	EpNovo without CA	290 ± 10	5 ± 1
	EpNovo	460 ± 20	5 ± 1
	ECC	420 ± 20	8 ± 1
	BADGE	460 ± 10	8 ± 1

Die approbierte gedruckte Originalversion dieser Dissertation ist an der TU Wien Bibliothek verfügbar.
The approved original version of this doctoral thesis is available in print at TU Wien Bibliothek.
TU WIEN Bibliothek Your knowledge hub

If we first compare the formulations with versus without CA, we see a faster reaction with significantly lower exothermic energy. This indicates an exclusively cationic polymerization of the epoxy. In contrast, if CA is present in the formulation, the enthalpy is significantly increased. Together with the longer reaction time, an ongoing cationic polymerization as well as for the polycondensation of the novolak can be assumed.

Comparing the epoxides with each other shows lower energy values for the ECC. In addition to the pure reactivity of the resins, this may also be due to the chemical structure of the resin. In contrast to BADGE and EpNovo, ECC does not have an aromatic unit and thus cannot be part of the polycondensation reaction of novolak. EpNovo shows a slightly increased enthalpy and significantly faster reaction times compared to BADGE. This could be related to steric hindrance of BADGE on the aromatic in the para position.

The samples at 120 °C showed almost no bubble formation. Comparing this with the samples without epoxy, this formulation could also be printed faster at higher temperatures. Furthermore, the completeness of the reaction could be increased. To check this a sample of the EpNovo formulation cured at 90 °C and 120 °C was examined in the STA and compared with the sample of the pure TOMDA formulation cured at 90 °C.

Die approbierte gedruckte Originalversion dieser Dissertation ist an der TU Wien Bibliothek verfügbar.
The approved original version of this doctoral thesis is available in print at TU Wien Bibliothek.
TU WIEN Bibliothek Your knowledge hub

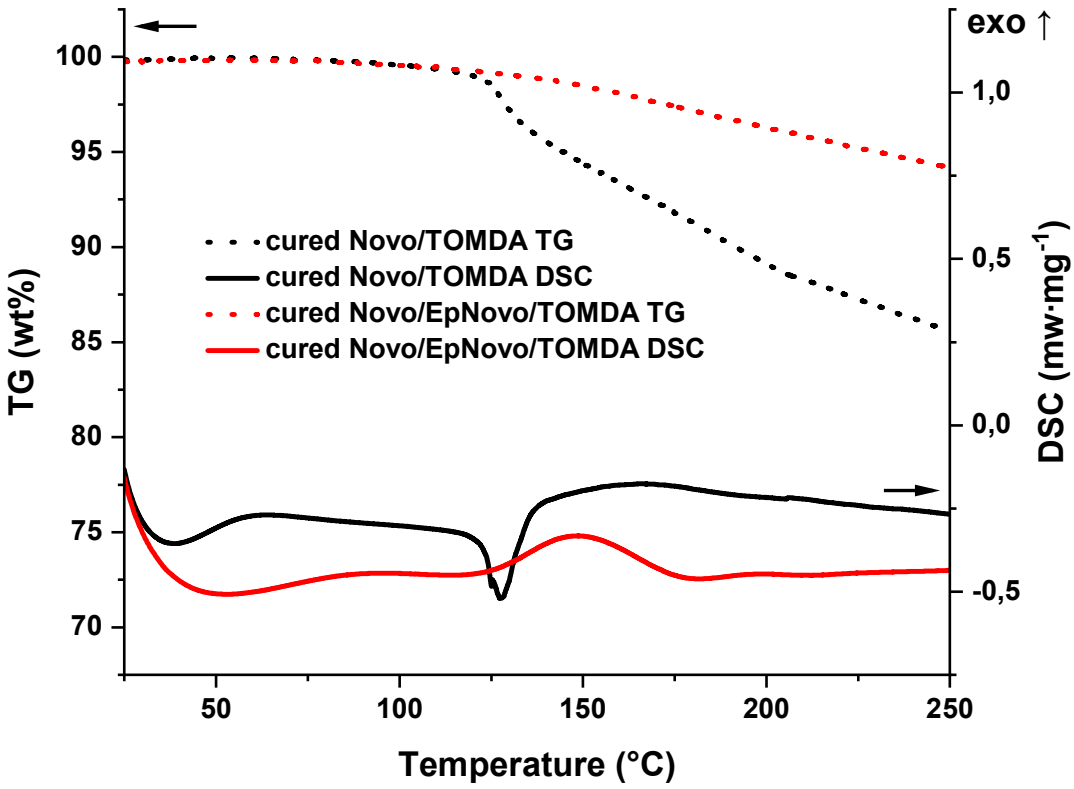

Figure 39: STA of the cured TOMDA sample (black; TG: dot; DSC: solid) and cured EpNovo with CA (red; TG: dot; DSC: solid) sample (both cured at 90 °C).

While the pure TOMDA formulation shows a clear weight loss due to the evaporation of water and acetic acid together with an endothermic energy flow, the EpNovo sample shows a slower weight loss and a slight exothermic peak. This could indicate remaining reactive material.

Since the formulation was very promising a print test was carried out (Figure 40). For this purpose the formulation was exposed to the laser at 100 °C (maximum of the printer). The sample showed slight overpolymerization, because of the slow speed of the laser and the high reaction rate of the cationic polymerization.

Die approbierte gedruckte Originalversion dieser Dissertation ist an der TU Wien Bibliothek verfügbar.
The approved original version of this doctoral thesis is available in print at TU Wien Bibliothek.
TU WIEN Bibliothek Your knowledge hub

Figure 40: Printing test of the EPNovo-Formulation with TOMDA as CA at 100 °C.

All in all, the additives used showed positive results in terms of preventing bubble formation and, depending on the application, could be a good addition in the field of AM of phenolic resins. However, this prevents in the end the pure curing of phenolic resins as you have always an additive present.

1.6 Further tested formaldehyde-based resins

In order to round off this study, all other commercially available formaldehyde-based resins were also tested for photopolymerizability.

1.6.1 Resole

In addition to novolaks, resoles (Figure 41) also belong to the phenol-based formaldehyde resins, as previously shown. Therefore, a self-curing resole was also tested to complete this work. Since no CA is necessary due to the terminal OH groups present, only a formulation with 5 wt% PAG was prepared and measured in the photo-DSC at 100 °C.

Die approbierte gedruckte Originalversion dieser Dissertation ist an der TU Wien Bibliothek verfügbar.
The approved original version of this doctoral thesis is available in print at TU Wien Bibliothek.
TU WIEN Bibliothek Your knowledge hub

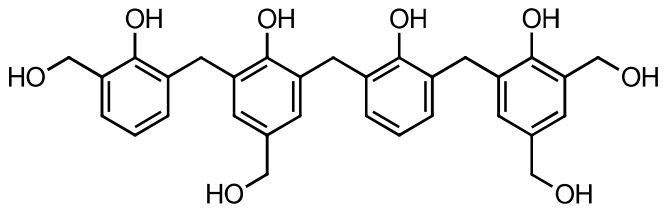

Figure 41: Example of a structure of a resole resin.

No exotherm or hardening was detected during the measurement. Consequently, no further tests were carried out.

1.6.2 Urea resin

The reaction of urea and formaldehyde produces the so-called urea formaldehyde resins (UF resins, Figure 42). This class of resin cures purely thermally at temperatures above 100 °C. The nitrogen-based resin also has a basic effect. It is therefore hardly surprising that a formulation with 5 wt% PAG and 15 wt% PF showed no reaction at all. Nevertheless, Novo formulations with up to 30 wt% UF resin were prepared, which showed a reduced enthalpy in the photo-DSC at 90 °C, but still became solid. Consequently, a UF resin can be included as a co-resin in the formulation.

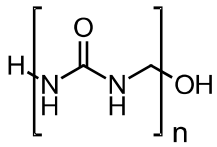

Figure 42: Example of a structure of a urea resin.

1.6.3 Melamine resin

The same applies to melamine formaldehyde resins (MF resins, Figure 43). These cure purely thermally in the same way as UF resins. Formulations without Novo showed no reaction at all, while formulations with Novo allowed a content of up to 30 wt% MF resin in the photo-DSC at 90 °C.

Die approbierte gedruckte Originalversion dieser Dissertation ist an der TU Wien Bibliothek verfügbar.
The approved original version of this doctoral thesis is available in print at TU Wien Bibliothek.
TU WIEN Bibliothek Your knowledge hub

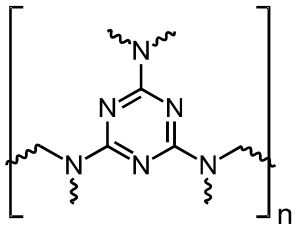

Figure 43: Structure of a melamine resin.

1.6.4 Furane resin

Polyfurane resins are considered a sustainable and biomass-derived alternative. The monomer FA can be obtained directly from biomass such as lignin or other natural waste products via furfural.[125] This monomer condenses to polyfufuryl alcohol (PFA) under acidic conditions in a similar way to resole but has the advantage that it does not undergo a self-condensation reaction as quickly. Nevertheless, the monomer is clearly more reactive under the mentioned conditions than, for example, resole.[126,127]

There is still some uncertainty about the mechanism of the condensation reaction. The first condensation step, in which the methylol group reacts with the C5 atom of another furfuryl alcohol to form methylene compounds with the addition of an electrophile, is assumed to be certain.[128,129] The resulting linear chain is proven to be the main product. However, acid-induced curing of furfuryl alcohol does not produce a thermoplastic but a dark thermoset network. How this network is formed is still an open question in research. One suggestion is the formation of γ-diketonic structures that enter into a Diels-Alder reaction with a linear chain in the subsequent step and thus form a network (Scheme 9).[130]

Die approbierte gedruckte Originalversion dieser Dissertation ist an der TU Wien Bibliothek verfügbar.
The approved original version of this doctoral thesis is available in print at TU Wien Bibliothek.
TU WIEN Bibliothek Your knowledge hub

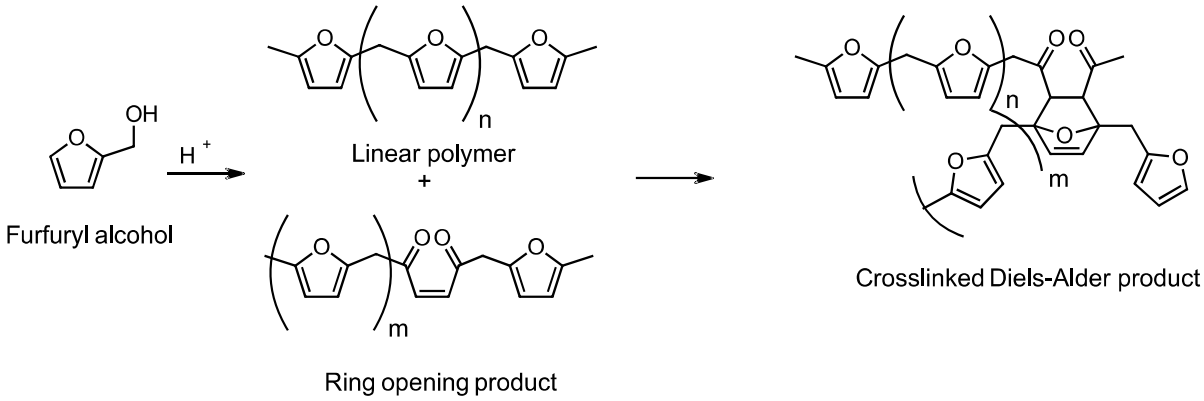

Scheme 9: Schematic example of curing of furfuryl alcohol to a furan-based thermoset.

First, pure FA was mixed with 5 wt% PAG, resulting in a homogeneous mixture at room temperature. This formulation was then irradiated at different temperatures in photo-DSC (Table 10).

Table 10: Photo-DSC results of the FA formulation at different temperatures, 2 × 900 s, 320-500 nm, 60 mW·cm^{-2}.

Temp. [°C]	ΔH [J·g^{-1}]	t_{max} [s]
60	160 ± 10	50 ± 10
80	200 ± 10	20 ± 3
90	190 ± 10	14 ± 2
100	140 ± 10	17 ± 3

At 60 °C, only incomplete and slow curing of the samples could be achieved. The energy values maximize at around 80 to 90 °C, after which the energy released is reduced by the evaporation of the H_2O produced by the condensation reaction. The t_{max} values are in an acceptable range for 3D printing (< 30 s), so that it can be concluded from the pure monomer that the system could be used for 3D printing.

Furthermore, there is a clear visual difference between the unirradiated and irradiated samples. After irradiation, a solid, insoluble, and non-meltable thermoset with a brownish black color is obtained (Figure 44).

Die approbierte gedruckte Originalversion dieser Dissertation ist an der TU Wien Bibliothek verfügbar.
The approved original version of this doctoral thesis is available in print at TU Wien Bibliothek.
TU WIEN Bibliothek Your knowledge hub

Figure 44: Photo-DSC samples of the FA formulation before (left) and after curing (right).

However, a slight evaporation of the formulation could already be detected during the sample preparation for the photo-DSC. Together with the carcinogenicity of furfuryl alcohol, this results in a system that is not suitable for commercial 3D printing. For this reason, higher molecular weight furan resins should be used as the base material. These are often used in industry as casting resins for binder jetting and are used according to viscosity. Therefore, a furan resin (FRA) with a viscosity of 200 mPa was ordered. According to the manufacturer's specifications, this higher-molecular resin should be pure as well as temperature stable up to 120 °C. The pure resin was stored overnight in a 100 °C oven and showed no weight loss. The viscosity was only slightly increased, nevertheless it was still a liquid material. The new resin was mixed with 5 wt% PAG and measured by means of photo-DSC (Table 11).

Table 11: Photo-DSC results of the FRA formulation at different temperatures, 2 × 900 s, 320-500 nm, 60 mW·cm^{-2}.

Temp. [°C]	ΔH [J·g^{-1}]	t_{max} [s]
80	120 ± 10	35 ± 3
90	130 ± 10	21 ± 2
100	130 ± 10	20 ± 2
120	160 ± 10	21 ± 2

Die approbierte gedruckte Originalversion dieser Dissertation ist an der TU Wien Bibliothek verfügbar.
The approved original version of this doctoral thesis is available in print at TU Wien Bibliothek.
TU WIEN Bibliothek Your knowledge hub

The data show that curing between 80 and 100 °C is only distinguished by the reaction speed. The energy values themselves are all in the same error range. At 120 °C, on the other hand, significantly increased energy values were recorded, but the reaction speed did not differ. All samples obtained were dimensionally stable after photo-DSC and were not soluble or meltable. For further analysis, the sample cured at 100 °C was examined in the STA and compared with the pure formulation (Figure 45).

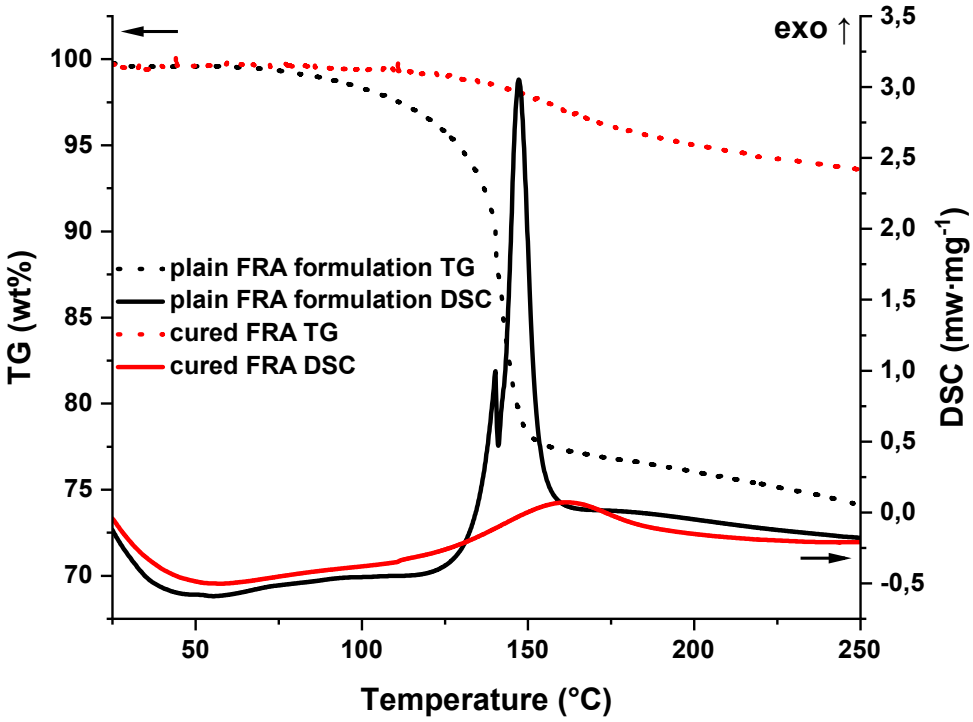

Figure 45: STA of the FRA formulation (black; TG: dot; DSC: solid) and the photo-DSC cured (red; TG: dot; DSC: solid) sample (100 °C).

The pure formulation has two adjacent peaks between 135 and 145 °C. This indicates the previously described reaction mechanism with first the pure condensation reaction and the subsequent uncertain part (e.g. Diels-Alder reaction). The weight loss due to the condensation reaction and the subsequent evaporation of H_2O in the area of the exothermic peaks is between 20 and 30 wt%. In comparison, the cured sample shows only a slight exothermic peak in the 160 °C range. The weight loss also starts much later and does not show any endothermic behavior. This indicates a complete reaction in the course of the photo-DSC measurements.

Die approbierte gedruckte Originalversion dieser Dissertation ist an der TU Wien Bibliothek verfügbar.
The approved original version of this doctoral thesis is available in print at TU Wien Bibliothek.
TU WIEN Bibliothek Your knowledge hub

The results from photo-DSC and STA indicated sufficient reaction and hardening. Therefore, first tests were made via Hot Lithography. There, the formulation showed insufficient reactivity at temperatures of 90 and 100 °C, respectively. Little to no solid material was obtained. It is assumed that the discoloration in the thermoset prevents the laser from penetrating into liquid resin and therefore only extremely thin layers can be cured. This is not sufficient for 3D printing, so no further attempts were made.

Die approbierte gedruckte Originalversion dieser Dissertation ist an der TU Wien Bibliothek verfügbar.
The approved original version of this doctoral thesis is available in print at TU Wien Bibliothek.
TU WIEN Bibliothek Your knowledge hub

2 Photo-induced catalytic poly-trimerization of cyanate ester to form high-performance polycyanurates for additive manufacturing

2.1 State of the art

In relation to high-performing polymers (HPPs), the temperature behavior is often used as the decisive material property as a criterion for classifying HPPs. However, these types of high-temperature polymers are still relatively limited in terms of choice, especially in the field of micrometer-precise additive manufacturing (AM), such as stereolithography (SLA). In order to achieve mechanical strength at elevated temperatures, epoxy resins[131] or complicated modified systems such as acrylated benzoxazines[132] or methacrylated bismaleimides[133] with a T_g between 150 and 260 °C are a few examples used as SLA resins in academia.

Cyanate ester (CE) resins are a well-known class of high-temperature thermosets. The resulting polycyanurates are formed by trimerization of the cyanate end group of the respective monomers (also often used in oligomeric form) creating triazine rings (cyanurates).[134] These were first synthesized in 1963 by Grigat using phenolic compounds with cyanogen chloride in the presence of an acid acceptor to produce CE monomers.[135] An alternative method involves using cyanogen bromide instead of cyanogen chloride, which, being a solid, is easier to handle safely.[134,136] This widely adopted approach, involving the low-temperature reaction of a cyanogen halide with bisphenol or polyphenol in the presence of a base, remains instrumental in the production of commercial CEs. The most well-known and industrially relevant CE monomers (Table 12) are based on bisphenol (A, E, F and M) and novolaks. The considerable hazards associated with handling and manufacturing cyanogen halides may contribute to the limited number of companies capable of producing CE resins on a commercial scale, thus explaining their relatively high cost.[134]

Die approbierte gedruckte Originalversion dieser Dissertation ist an der TU Wien Bibliothek verfügbar.
The approved original version of this doctoral thesis is available in print at TU Wien Bibliothek.
TU WIEN Bibliothek Your knowledge hub

Table 12: Industrially relevant CE resins.[134]

Name	Structure	Melting point (m.p.) [°C]	Glass transition Temperature (Tg) Polymer
Bisphenol A dicyanate	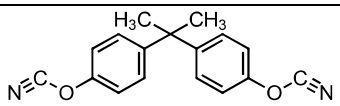	79	289
Bisphenol E dicyanate	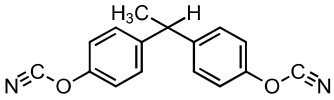	29	258
Bisphenol M dicyanate	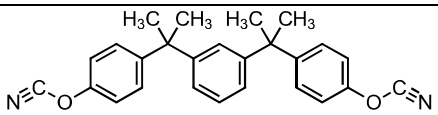	106	192
Novolac cyanate ester	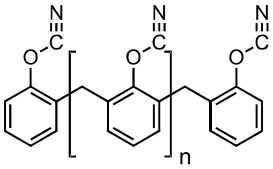	<0	300 to 400

Nevertheless, due to their low water absorption, high fracture toughness, high glass transition temperatures and low curing shrinkage, CE esters are preferred over conventional epoxy resins, despite the high cost, especially in aerospace applications.[134,137]

The polymerization process, as illustrated in Scheme 10, is characterized as a multi-step process. The polyaddition reaction is postulated to be an autocatalytic progression leading up to gel formation. Normally, the reaction proceeds slowly in the absence of a catalyst and only at elevated temperatures (170-200 °C).[134,138,139] Conversely, trimerization can be significantly accelerated and the reaction temperature reduced by employing a transition metal as a catalyst along with a hydrogen donor. Possible metal centers include copper, cobalt, zinc, manganese, iron and aluminum.[140] Typically, the

Die approbierte gedruckte Originalversion dieser Dissertation ist an der TU Wien Bibliothek verfügbar.
The approved original version of this doctoral thesis is available in print at TU Wien Bibliothek.
TU Bibliothek Your knowledge hub WIEN

hydrogen donor comprises of a high-boiling alkyl alcohol, predominantly nonylphenol (NP).[141]

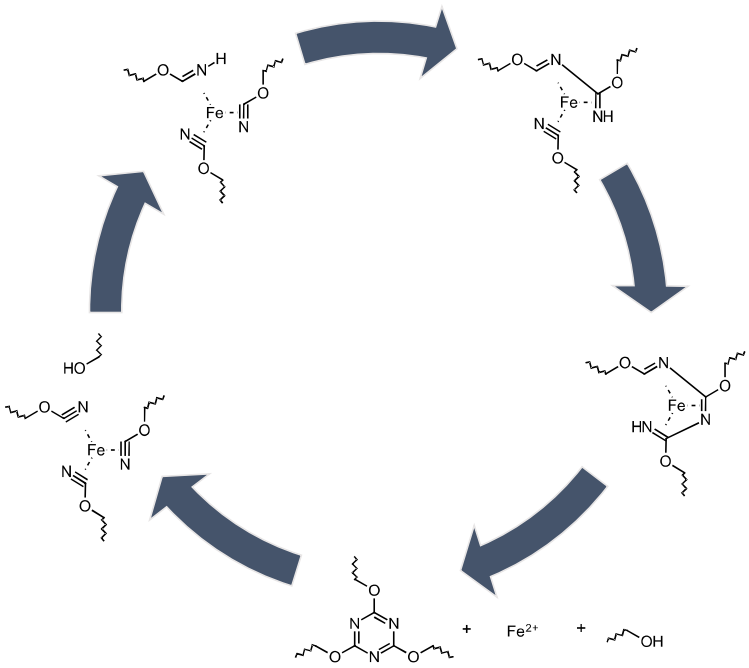

Scheme 10: Reaction mechanism of catalytic curing of cyanate esters to polycyanurates (adapted from [134]).

Polymerization is initiated by the acidic hydrogen donor and the formation of a carbonic ester imide structure. The metal center (including copper, zinc, iron or manganese) serves as a clustering agent that brings the three reactive cyanate (OCN) groups together. The previously formed structure reacts with the remaining OCN groups to form a triazine ring with the release of the hydrogen donor.[138] Gelation does not take place until about 60 % of the OCN groups have reacted, so commercial products are pre-cured and sold with a trimerization content of up to that 60 %.[134,142] Thus, the viscosity of the resins can be adjusted very well, apart from the choice of the basic building blocks, also by adjusting the molecular weight of the prepolymer.[143]

Classic curing, also catalytic, is purely thermal with a temperature program over several hours.[144] Kotch & Lees, on the other hand, describe the photocatalytic polymerization of CE resins. By using an iron-based photocatalyst and illuminating the resulting formulation, a reduction of the peak onset in the DSC by 130 °C could be achieved. These illuminated formulations showed a significantly shorter curing time during the subsequent thermal curing.[145] This demonstrates that, by employing a

Die approbierte gedruckte Originalversion dieser Dissertation ist an der TU Wien Bibliothek verfügbar.
The approved original version of this doctoral thesis is available in print at TU Wien Bibliothek.
TU Bibliothek Your knowledge hub WIEN

metal-based photocatalyst, photo-induced hardening of CE resins is possible in principle.

Metal-based photocatalysts are a very well-known photoactive component, especially in the field of polymer technology. However, these metal centers such as Pt, Ru, Ir, Cu and also Zn are often used in the field of redox-initiated polymerization (radical or cationic).[146] Yet, the coordination site at the metal center, which is important for curing CE resins, is not necessarily liberated during irradiation. In contrast, other photocatalysts, including commercially available ones, break the bond to the ligand under illumination with light and release the necessary coordination site. For example, Irgacure 261 (I261), an iron-based arene complex, cleaves off cumene as a ligand under illumination and is therefore able to coordinate other nucleophiles (Scheme 11). This is used in the course of the cationic photopolymerization of epoxides.[89,147] Another well-known example is cyclopentadienyl manganese tricarbonyl derivatives, which release carbon monoxide (CO) under illumination and thus also expose a coordination site. However, these compounds are often used for catalysis of small organic molecules and less in polymerization processes.[148,149] Nevertheless, radical polymerizations[150] and polyadditions with CE derivatives are also known for this type of catalyst.[151,152]

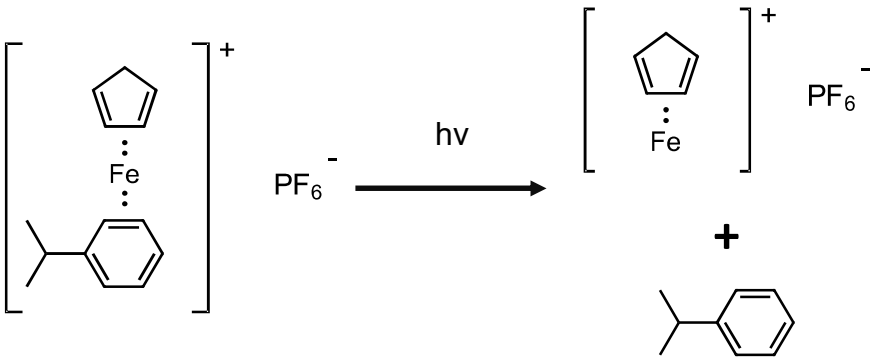

Scheme 11: Schematic decomposition of I261 during irradiation.[89]

A major advantage of metal-based photocatalysts is the high wavelength at which they absorb. I261, for example, has an absorption maximum at 241 nm, but the tail out range goes up to 500 nm (Figure 46).[89] Therefore, a photosensitizer with this type of photocatalyst is often not necessary.

Die approbierte gedruckte Originalversion dieser Dissertation ist an der TU Wien Bibliothek verfügbar.
The approved original version of this doctoral thesis is available in print at TU Wien Bibliothek.
TU Bibliothek Your knowledge hub WIEN

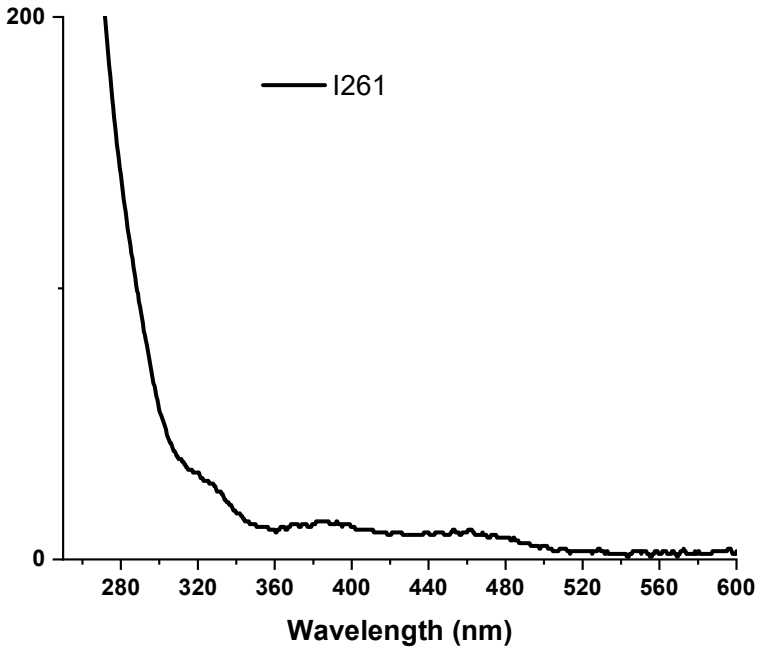

Figure 46: UV-Vis spectra of I261 in acetonitrile.

If these metal-based photocatalysts are used together with CE such as Kotch & Lees did,[145] the possibility of photochemical curing of polycyanurates and further AM of this class by means of Hot Lithography arises. McCormick et al. showed a further example, by using a variety of photocatalysts with metal transition centers, reducing the onset during curing of various cyanate ester monomers and thus facilitate curing to be used in an energy-polymerizable composition. Similar to Kotch & Lees, they do not use any co-catalyst.[153] Furthermore, Satoschi et al. describes the photoinduced hardening of CE esters with the aid of iron or ruthenium catalysts that have both an aryl group as a ligand and a non-nucleophilic anion from the group BF_4, PF_6, SbF_6 or AsF_6 as a counterpart, for the use in optical waveguides.[154]

In contrast, publications relating to CE and AM are very rare. One of the major disadvantages of these high-performance CE resins, the time-consuming processing with expensive molding tools, could be prevented using AM. For this reason, great efforts are being made to print CE resins in 3D using an AM process. Previous successes have been achieved with matrix polymers such as epoxies or acrylates, which are cured by UV radiation and either react with the CE resin or are degraded in a subsequent thermal step.[132,134,137] Chandrasekaran et al. were able to convert a formulation into a 3D printed object by direct writing with ink via thixotropic agents.[155]

Die approbierte gedruckte Originalversion dieser Dissertation ist an der TU Wien Bibliothek verfügbar.
The approved original version of this doctoral thesis is available in print at TU Wien Bibliothek.
TU Bibliothek Your knowledge hub WIEN

Nevertheless, despite various approaches, no one has yet succeeded in 3D printing a pure CE resin formulation.

2.2 Evaluation of photocatalysts

First, a suitable catalyst system was sought based on Kotch & Lee's work.[145] However, in addition to the photoactive component, the formulation was supplemented with the co-catalyst nonylphenol (NP, Figure 47) recommended in the literature.[138]

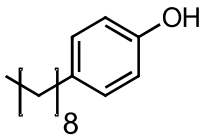

Figure 47: Structure of nonylphenol (NP).

As described above, there are several metal centers that can be used for the catalysis of cyanate esters to polycyanurates. Therefore, various metal-based (titanium,[153] zinc,[156] zirconium,[157] ruthenium,[153] manganese[158] and iron[153]) photocatalysts known from literature for photopolymerization processes have been tested. One of these was the commercially available iron-based photocatalyst I261, which is structurally very similar to the work of Kotch & Lees. In addition, $MeCpMn(CO)_3$, a catalyst known from literature for the production of polyisocyanurates, was used.[158] All tested photocatalysts are shown in the Figure 48.

Die approbierte gedruckte Originalversion dieser Dissertation ist an der TU Wien Bibliothek verfügbar.
The approved original version of this doctoral thesis is available in print at TU Wien Bibliothek.
TU WIEN Bibliothek Your knowledge hub

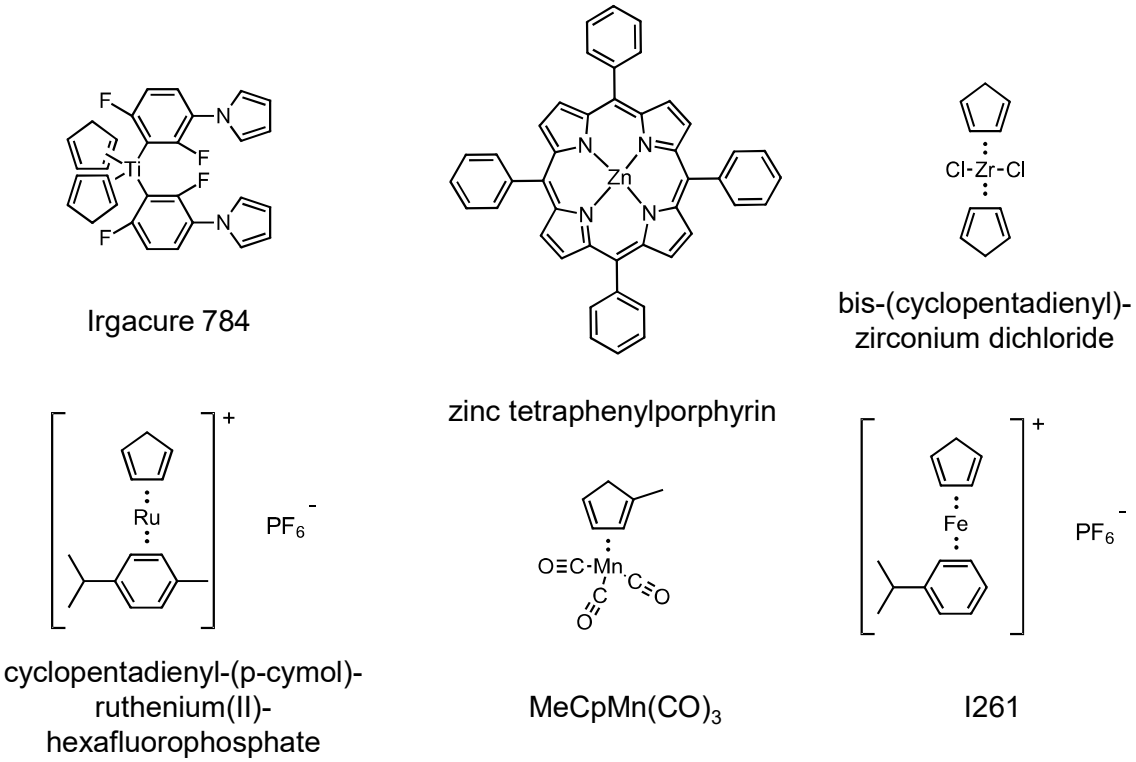

Figure 48: Tested photocatalysts.

The monomer used was PT-30 (Figure 49), a commercially available novolak-based cyanate ester from the company Arxada.[143]

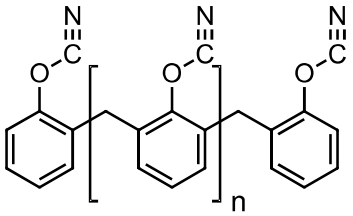

Figure 49: Structure of the novolak-based cyanate ester PT-30.

The 30 in PT-30 correspond to the molecular weight (320 to 420 g·mol^{-1}) controlled by the number of monomers (n = 1 or 2) used in the basic unit of the novolak.[134,159] This resin has a viscosity of 400 mPa·s and a gel time of 150 min at 200 °C according to the manufacturer. The final thermoset has a T_g of 401 °C, one of the highest of the commercially available products.[160] Since the exact molecular weight of the resin is unknown, weight percent (wt%) was used as the quantity.

PT-30 was mixed with 5 wt% NP and 1 wt% of the respective photocatalyst and analyzed using photo-DSC at 100 °C (2 x900 s, 320-500 nm, 60 mW·cm^{-2}). Of the six

Die approbierte gedruckte Originalversion dieser Dissertation ist an der TU Wien Bibliothek verfügbar.
The approved original version of this doctoral thesis is available in print at TU Wien Bibliothek.

catalysts tested, only I261 and $MeCpMn(CO)_3$ showed exothermicity and solidification of the sample after measurement. The exotherm and also the reaction rate was approximately in the same range between the two catalysts. Nevertheless, the $MeCpMn(CO)_3$ showed extreme bubble formation in the sample. This was probably caused by the release of CO during the photoactivation of the catalyst. Therefore, all further experiments were continued with the catalyst system I261 and NP.

2.3 Photopolymerization of a phenolic novolak cyanate ester

2.3.1 Theoretical investigation of cyanurates

For the theoretical exploration of cyanurates, an initial experiment employed a monofunctional reactant, phenyl cyanate (Scheme 12). Upon exposure to irradiation at 100 °C using photo-DSC (2 x900 s, 320-500 nm, 60 $mW \cdot cm^{-2}$), the formulation, comprising 1 wt% I261 and 5 wt% NP, exhibited an exothermic enthalpy of 610 $J \cdot g^{-1}$ (ΔH, tmax = 40 s). The structure of the photo product underwent analysis through ^1H and ^{13}C-NMR and comparisons made with literature values gave the expect result.[161] Additionally, the molecular weight was determined via UPLC-MS, revealing a weight of 357 $g \cdot mol^{-1}$, corresponding to the desired trimerization product.

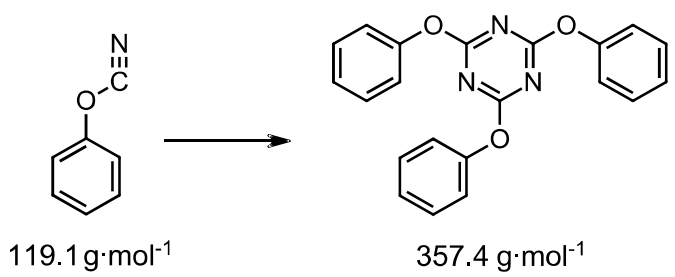

Scheme 12: Schematic reaction mechanism of the monofunctional phenyl cyanate.

Moreover, an 86 % conversion (α_{HPLC}) of phenyl cyanate was identified through HPLC. When considering the mass fractions of the resin ($m_{PhenylOCN}$) and the mass losses during polymerization (m_{loss} = 17.5 %) due to the evaporation of the volatile monomer, a calculated value of 74 $kJ \cdot mol^{-1}$ per equivalent cyanate group can be derived

Die approbierte gedruckte Originalversion dieser Dissertation ist an der TU Wien Bibliothek verfügbar.
The approved original version of this doctoral thesis is available in print at TU Wien Bibliothek.
TU Bibliothek Your knowledge hub WIEN

(Equation 2). This falls within the range of values reported in the literature (78 ± 3 kJ·mol^{-1}).[162]

$$\Delta H_0 = \left(\frac{\Delta H \times (1 - m_{Loss})}{\frac{m_{PhenylOC} \times M_{PhenylOC}}{1000}} \right) \times a_{HPLC}^{-1}$$

Equation 2: Calculation of the theoretical enthalpy per cyanate group.

Furthermore, is it possible to calculate (Equation 3) the rate of polymerization (Rp) from the height of the peak (h), using the density of the resin ρ = 1.27 g·ml^{-1}, resulting in 89.71 mmol·L^{-1}·s^{-1}.

$$Rp = \left(\frac{h \times \rho}{\Delta H_0} \right)$$

Equation 3: Calculation of the rate of polymerization Rp.

2.3.2 Determination of the conversion

2.3.2.1 Photo-DSC

Utilizing the photo-DSC values (ΔH) obtained from the measurements (Figure 50a & Table 13) of the PT-30 formulation, the conversion at different temperatures could be calculated (Equation 4), considering the monomer proportion ($m_{PT\text{-}30}$ = 94%) and assuming that the number of functional cyanate groups equals the repeating unit of the resin ($M_{PT\text{-}30}$ = 131 g·mol^{-1}). No loss of mass was observed in this analysis.

$$a_{PT-30} = \left(\frac{\Delta H \times M_{PT-3}}{m_{PT-3}} \right) \times 10^{-1} \times {\Delta H_0}^{-1}$$

Equation 4: Calculation of the conversion for the PT-30 formulation.

The photo-DSC analysis of the PT-30 with identical proportions of the PI and co-catalyst, revealed heat of trimerization values ranging from 240 to 300 J·g^{-1}, depending on the temperature. All irradiated samples exhibited solidity, non-melting behavior, and insolubility in various solvents, regardless of the irradiation temperature. The time until reaching the t_{max} ranged between 17 and 23 s (Table 13). Utilizing Equation 4, trimerization conversion values were determined to be 45 ± 2 % at 80 °C and 55 ± 3 %

Die approbierte gedruckte Originalversion dieser Dissertation ist an der TU Wien Bibliothek verfügbar.
The approved original version of this doctoral thesis is available in print at TU Wien Bibliothek.
TU Bibliothek Your knowledge hub WIEN

at 100 °C (Figure 50b & Table 13). Measurements without I261 showed no enthalpy, while those without NP released less than 100 J·g^{-1} of energy and did not solidify.

The reaction speeds, represented by both t_{max} and the Rp (density of the resin ρ = 1.2 g·ml^{-1})[163] notably improved with higher temperature, effectively demonstrating that elevated temperatures facilitate the 3D printing of pure cyanate ester resins.

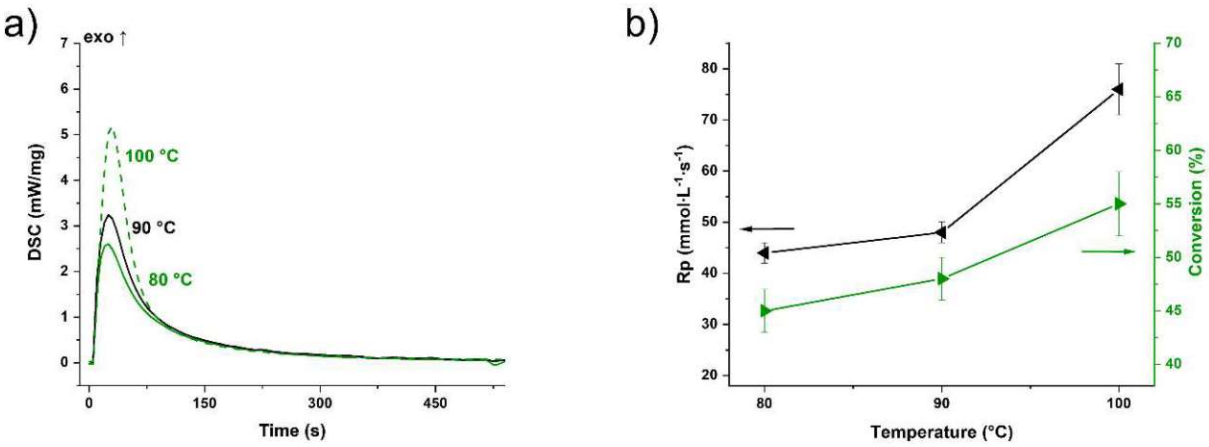

Figure 50: a) Photo-DSC of the PT-30 formulation at 80-100 °C, 2 x900 s, 320-500 nm, 60 mW·cm^{-2}. b) Temperature dependence of rate of polymerization (Rp black) and conversion of the cyanate ester groups (green).

Table 13: Photo-DSC values, calculated conversion and calculated Rp via Photo-DSC of the PT-30 formulation at different temperatures.

	PT-30 cured 80 °C*	PT-30 cured 90 °C*	PT-30 cured 100 °C*
ΔH [J·g^{-1}]	240 ± 10	260 ± 10	300 ± 20
Conversion [%] without post-curing	45 ± 2	48 ± 2	55 ± 3
t_{max} [s]	19 ± 2	20 ± 2	20 ± 3
Rp [mmol·L^{-1}·s^{-1}]	44 ± 2	49 ± 2	76 ± 5

* cured via photo-DSC at 80-100 °C, 2 x900 s, 320-500 nm, 60 mW·cm^{-2}

Die approbierte gedruckte Originalversion dieser Dissertation ist an der TU Wien Bibliothek verfügbar.
The approved original version of this doctoral thesis is available in print at TU Wien Bibliothek.
TU Bibliothek Your knowledge hub WIEN

2.3.2.2 IR

In the literature, infrared spectroscopy (IR) is frequently employed instead of DSC to monitor the conversion of the reaction for thermoset formation, given the varying theoretical enthalpy values of the OCN groups across different monomers.[164] To determine the latter, the C≡N stretching vibrations at 2270 and 2235 cm^{-1} are integrated and quantified, with reference to the methyl C–H stretching vibrations of the side chain at 2970 cm^{-1} (Figure 51).[138,140,164] Additionally, the qualitative observation of the triazine network formation via the triazine ring C=C stretching vibration at 1565 cm^{-1} is possible.[165] Consequently, conversions ranging from 50 ± 2 % at 80 °C to 58 ± 2 % at 100 °C were determined (Table 14). The consistency with the results from the photo-DSC can be considered satisfactory.

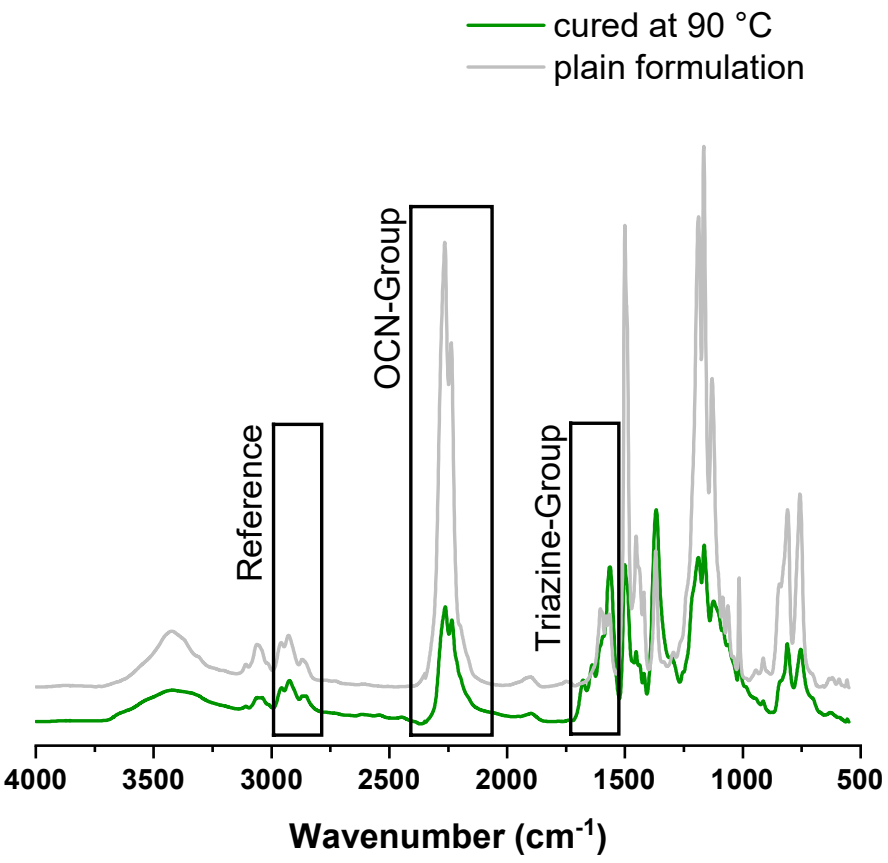

Figure 51: IR spectra of the plain formulation (grey) and the sample cured at 90 °C (green).

Moreover, the irradiated samples underwent a post-curing program recommended by the manufacturer (Figure 52).[163] In regard to conversion, this specimen solely could be measured via IR spectroscopy, resulting in elevated conversions up to a maximum

Die approbierte gedruckte Originalversion dieser Dissertation ist an der TU Wien Bibliothek verfügbar.
The approved original version of this doctoral thesis is available in print at TU Wien Bibliothek.
TU Bibliothek Your knowledge hub WIEN

of 86 ± 2 % (Table 14). Consequently, lower temperatures during the initial irradiation process resulted in lower final conversions. Furthermore, assessing the conversion through IR for the materials only cured thermally reveals a conversion approximately 5 % lower than that of the photochemically cured samples, even after post-curing.

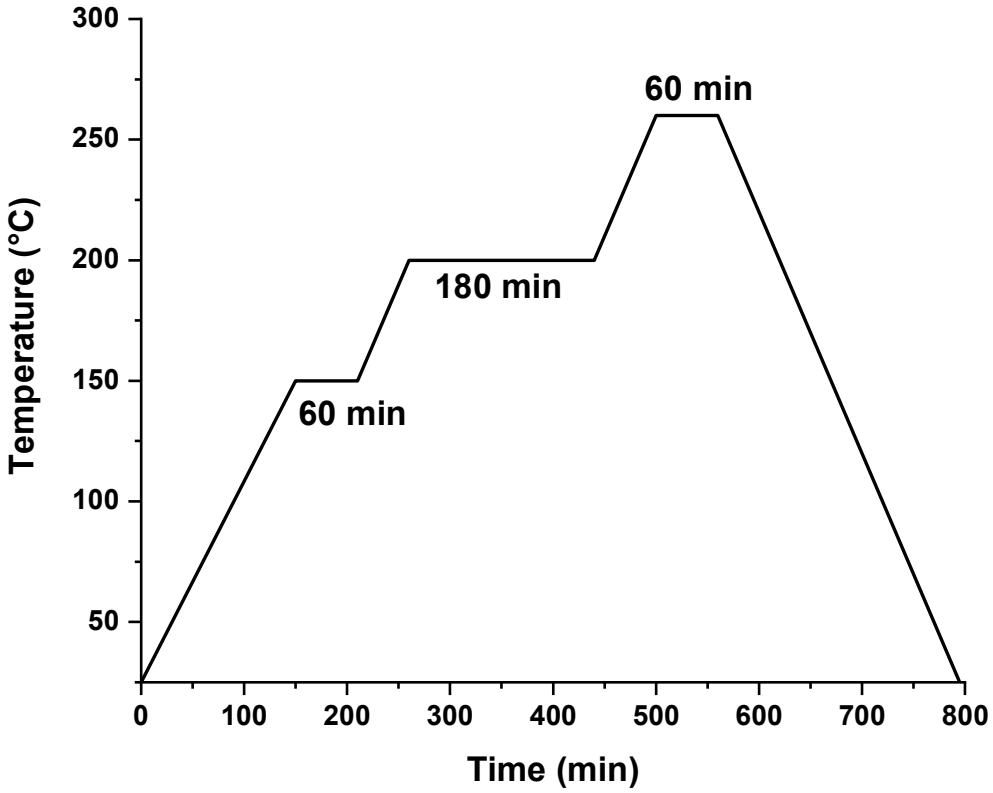

Figure 52: Post-processing program for the PT-30 specimen with a heating rate of 1 K·min^{-1}.

Die approbierte gedruckte Originalversion dieser Dissertation ist an der TU Wien Bibliothek verfügbar.
The approved original version of this doctoral thesis is available in print at TU Wien Bibliothek.

Table 14: Calculated conversion of the cyanate ester groups pf the PT-30 formulation via IR spectroscopy.

	PT-30 cured* 80 °C	PT-30 cured* 90 °C	PT-30 cured* 100 °C	PT-30 thermally cured at 120 °C⁺
Conversion [%] without post-curing	50 ± 2	53 ± 2	58 ± 2	51 ± 2
Conversion [%] with post-curing	83 ± 2	85 ± 2	86 ± 2	82 ± 2

* cured via photo-DSC at 80-100 °C, 2 x900 s, 320-500 nm, 60 mW·cm^{-2}

⁺ cured in a oven at 120 °C for 12 h

2.3.3 Thermal characterization

In simultaneous thermal analysis (STA), the observed trend in photo-DSC was verified. Analysing both the photo-cured samples and the pure formulation, it was evident that a higher initial irradiation temperature led to a greater conversion, resulting in a diminished remaining exotherm in the samples (Figure 53). Additionally, the findings by Kotch et al., demonstrating a reduced onset temperature for previously irradiated formulations with iron-arene complexes, were confirmed.[145] In comparison to the purely thermal curing of the resin, pre-irradiation of the samples at elevated temperatures lowered the onset of the exothermic peak from 160 °C to the range of 90–110 °C, depending on the irradiation temperature. Nevertheless, it's worth noting that I261 can also function as a pure thermal catalyst, as evidenced by comparing the onset of the pure formulation to temperatures typically used for curing without a catalyst (>240 °C).[166] Moreover, the material obtained through light-induced curing exhibited no difference in thermal degradation compared to the purely thermally cured material. The onset of degradation at 426 °C was slightly lower than that of conventionally cured PT-30 samples,[160] but comparable to the 3D printed samples via DIW by Chandrasekaran et al.[155]

Die approbierte gedruckte Originalversion dieser Dissertation ist an der TU Wien Bibliothek verfügbar.
The approved original version of this doctoral thesis is available in print at TU Wien Bibliothek.
TU WIEN Bibliothek Your knowledge hub

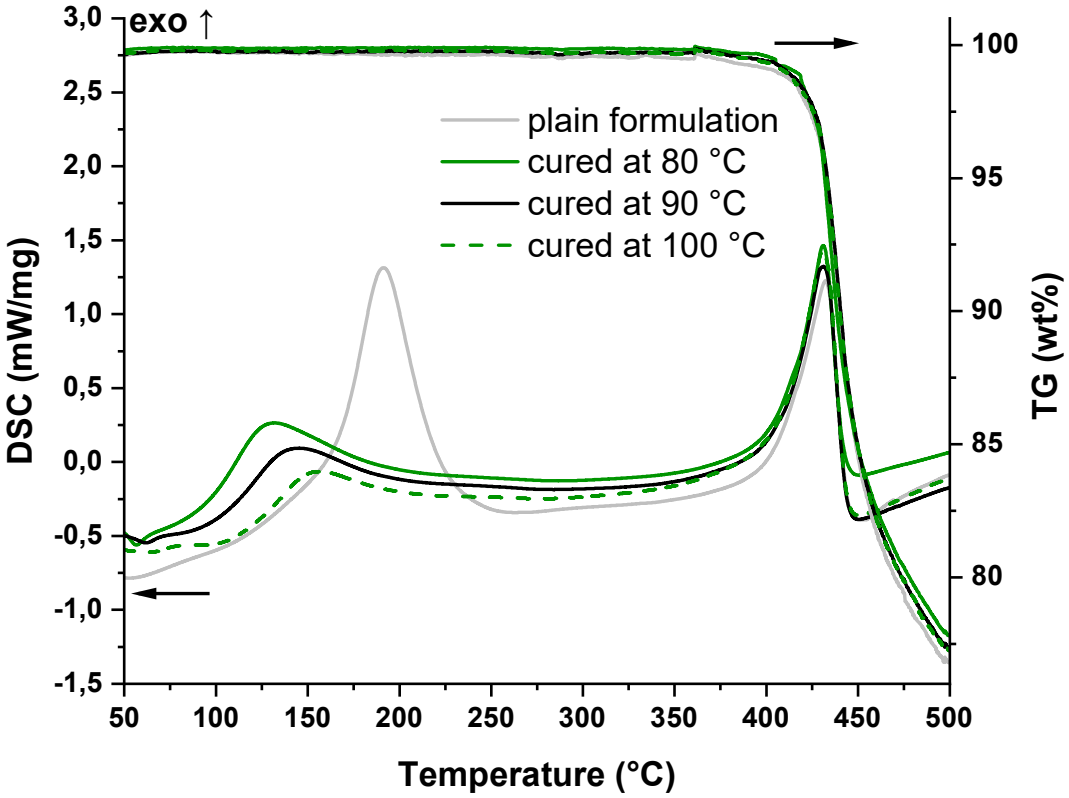

Figure 53: STA of the plain formulation (grey) and the photo-DSC cured samples at 80 °C (green solid), 90 °C (black solid) and 100 °C (green dot).

2.4 Photopolymerization of a bisphenol based cyanate ester

Since, as described above, the class of cyanate esters offers a large number of monomers for potential processing, further monomers and their mixtures should be tested for their suitability for light-induced curing. One of the most commonly used monomers of this class is bisphenol A dicyanate ester (BADCy, Figure 54).

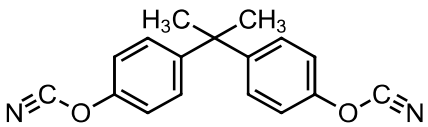

Figure 54: Structure of bisphenol A dicyanate ester (BADCy).

Die approbierte gedruckte Originalversion dieser Dissertation ist an der TU Wien Bibliothek verfügbar.
The approved original version of this doctoral thesis is available in print at TU Wien Bibliothek.
TU Bibliothek Your knowledge hub WIEN

The cured polycyanurates are characterized by a T_g of 289 °C at comparatively low cost for the monomer. Otherwise, the properties are similar to the other cyanate esters, such as low shrinkage during curing, high chemical resistance and a low dielectric constant.[134]

2.4.1 Photo-DSC & Conversion

Analogous to the PT-30 formulation, BADCy was mixed with 5 wt% NP as co-catalyst and 1 wt% I261 as photocatalyst and characterized by photo-DSC (Figure 55). The results are summarized in Table 15. Since the powder has a melting point of 79 °C, measurements were carried out from 80 °C.

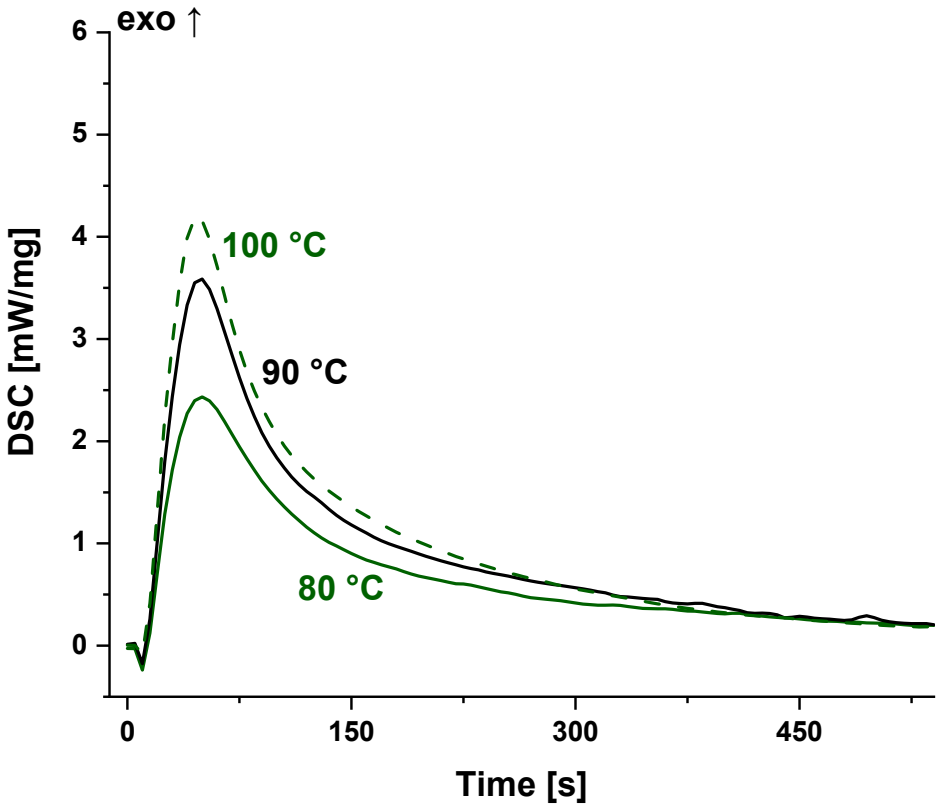

Figure 55: Photo-DSC of the BADCy formulation at 80-100 °C, 2 x900 s, 320-500 nm, 60 mW·cm^{-2}.

Die approbierte gedruckte Originalversion dieser Dissertation ist an der TU Wien Bibliothek verfügbar.
The approved original version of this doctoral thesis is available in print at TU Wien Bibliothek.
TU Bibliothek Your knowledge hub WIEN

Table 15: Results of the photo-DSC experiments of the BADCy formulations at different temperatures, 2 × 900 s, 320-500 nm, 60 mW·cm^{-2}.

Temp. [°C]	ΔH [J·g^{-1}]	t_{max} [s]	Conversion [%]	Rp [mmol·L^{-1}·s^{-1}]
80	350 ± 10	44 ± 2	70 ± 2	36 ± 2
90	430 ± 30	43 ± 5	86 ± 2	45 ± 2
100	500 ± 40	37 ± 5	99 ± 2	65 ± 2

The energy values here are significantly increased per unit of weight compared to the previous formulation. The 500 J·g^{-1} at 100 °C are comparable to the values from the literature (approx. 650 J·g^{-1} at full curing).[167] With the theoretical enthalpy from chapter 2.3.1 the conversion of this monomer system could be calculated. At 70 %, the conversion is already very good at 80 °C. Nevertheless, this reaction can be driven to almost full conversion at a temperature of 100 °C. The reaction time, on the other hand, is significantly slower with a t_{max} around 40 s (Rp = 65 mmol·L^{-1}·s^{-1}) then the one from PT-30. Unfortunately, these reaction kinetics do make 3D printing in this temperature range difficult. Higher temperatures could accelerate the reaction and thus make it 3D printable. However, this would reduce the stability of the formulation to such an extent that curing in the printer could not be ruled out.

Furthermore, the conversion of the reaction was analyzed using IR spectroscopy. Here, too, the samples were subjected to the same post-curing program and compared with the non-post-cured samples (Table 16).

Die approbierte gedruckte Originalversion dieser Dissertation ist an der TU Wien Bibliothek verfügbar.
The approved original version of this doctoral thesis is available in print at TU Wien Bibliothek.
TU WIEN Bibliothek Your knowledge hub

Table 16: Calculated conversion of the cyanate ester groups of the BADCy formulations via IR spectroscopy.

	BADCy cured 80 °C	BADCy cured 90 °C	BADCy cured 100 °C
Conversion [%] without post-curing	67 ± 2	82 ± 2	94 ± 2
Conversion [%] with post-curing	> 99	> 99	> 99

The values obtained reflect a conversion up to 94 % without any post-curing process and fit to the values obtained via photo-DSC. Generally the conversion is significantly higher than the values of the PT-30 formulation. This could be due to the reduced flexibility of the novolak chains compared to the pure BADCy monomer. Comparing the uncured with the cured and the post-cured formulation, a decrease in the band of the cyanate ester group is shown to extent, that it is nearly not detectable (Figure 56). This was already observed in the sample that was hardened at 80°C in the photo-DSC. Therefore, all post-cured samples were considered to have a conversion > 99 %.

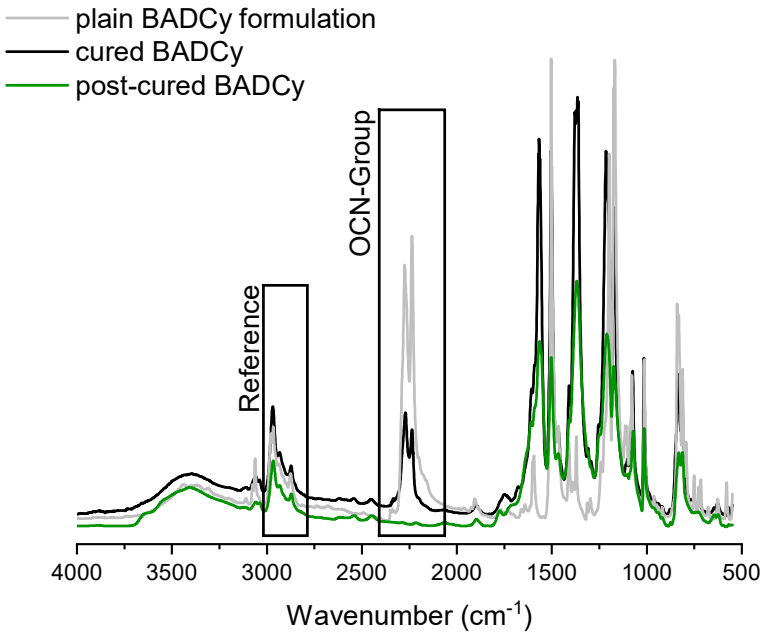

Figure 56: IR spectra of the plain BADCy formulation (grey), the sample cured at 90 °C (black) and the post-cured sample (green).

Die approbierte gedruckte Originalversion dieser Dissertation ist an der TU Wien Bibliothek verfügbar.
The approved original version of this doctoral thesis is available in print at TU Wien Bibliothek.
TU Bibliothek Your knowledge hub WIEN

2.4.2 Thermal characterization

In accordance with the previous chapter, the cured samples and the pure formulation were tested for complete curing using STA (Figure 57).

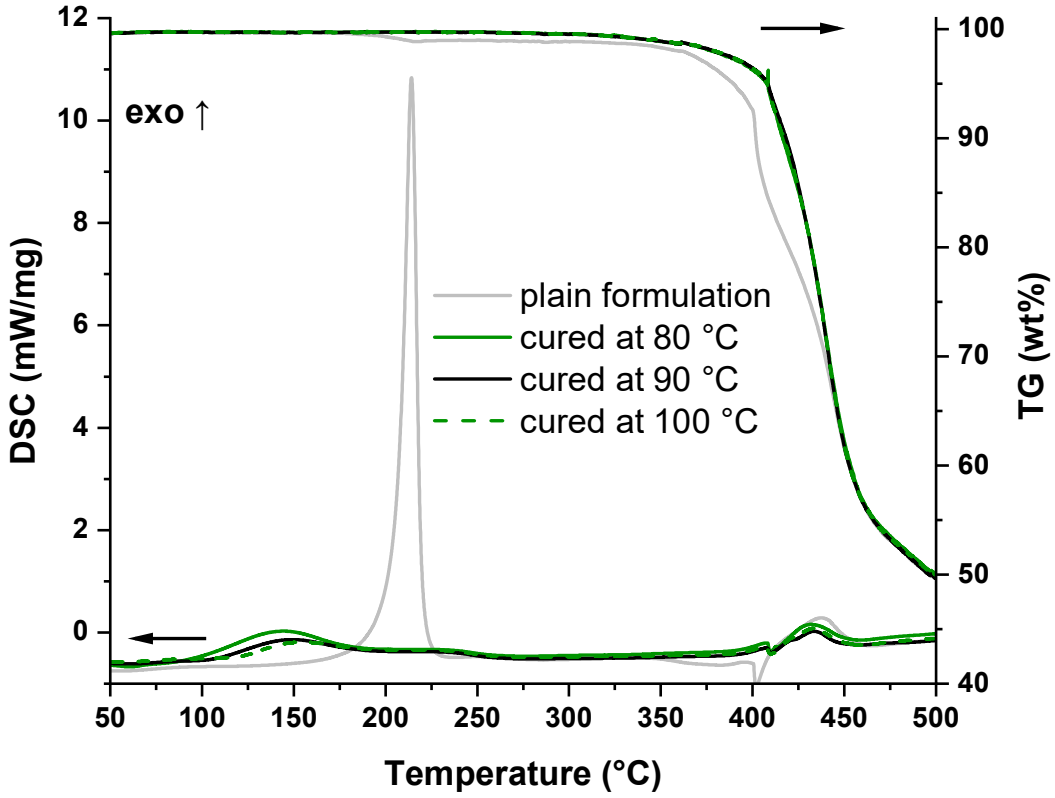

Figure 57: STA of the plain BADCy formulation (grey) and the photo-DSC cured samples at 80 °C (green solid), 90 °C (black solid) and 100 °C (green dot).

In the uncured formulations, the exothermic process due to thermal curing at about 210 °C can be observed. At 560 $J \cdot g^{-1}$, this is in the range of the photo-DSC measurements and in the range of the literature.[167] The hardened samples at 80, 90 °C, on the other hand, show nearly no exotherm. The degradation takes place at an onset temperature of about 410 °C, which is a little lower than that of the PT-30. As expected, no weight loss was observed in any of the cured samples.

Die approbierte gedruckte Originalversion dieser Dissertation ist an der TU Wien Bibliothek verfügbar.
The approved original version of this doctoral thesis is available in print at TU Wien Bibliothek.
TU WIEN Bibliothek Your knowledge hub

2.5 Photopolymerization of a mixture of PT-15 and BADCy

The two previous monomers differ mainly in their mechanical properties (T_g, tensile strength and elongation at break). By combining the two, the mechanical properties can be tailored to various applications. For this reason, a commercial product from Arxada was tested (LVT-50, Figure 58) in the further course of this work, which consists of a 50/50 w/w mixture of BADCy and PT-15. PT-15 is analogous to PT-30 except that in this case the underlying novolak has an n of 0 or 1.[143]

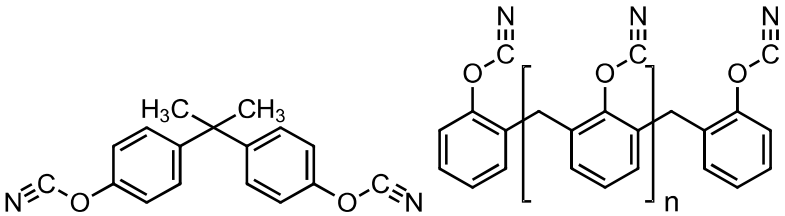

Figure 58: Mixture of LVT-50 (BADCy left, PT-15 right, n = 0 or 1)

2.5.1 Photo-DSC

As before, 5 wt% NP as co-catalyst and 1 wt% I261 as photocatalyst were added to the formulation and further analyzed by photo-DSC. The results are shown in Figure 59 and Table 10.

Die approbierte gedruckte Originalversion dieser Dissertation ist an der TU Wien Bibliothek verfügbar.
The approved original version of this doctoral thesis is available in print at TU Wien Bibliothek.
TU WIEN Bibliothek Your knowledge hub

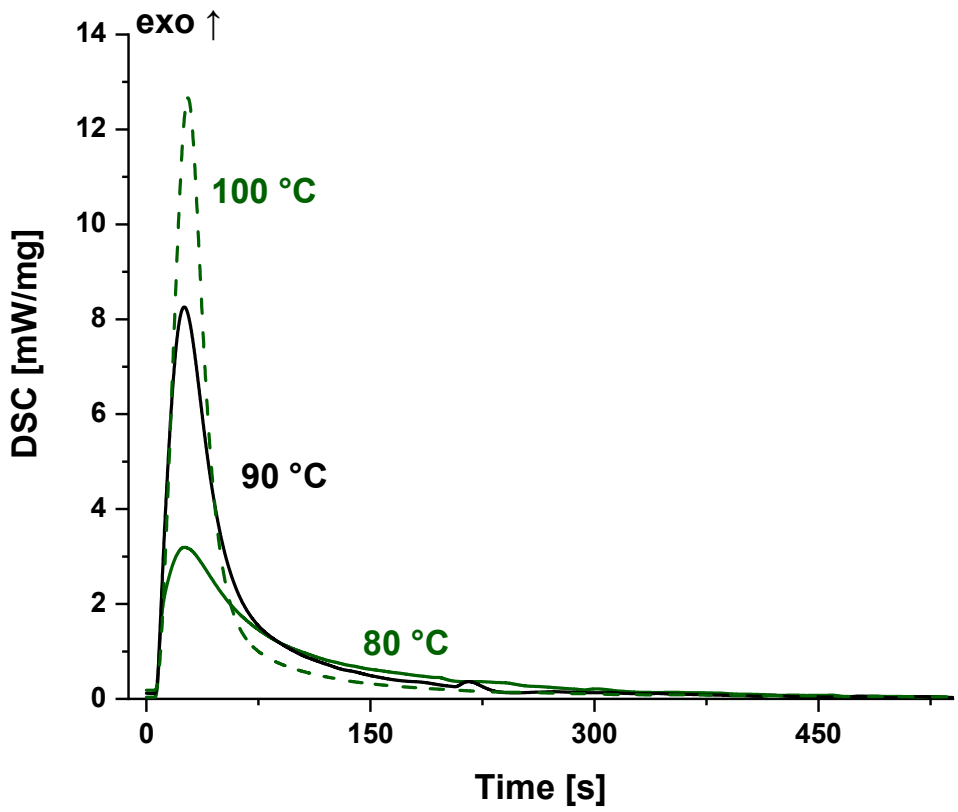

Figure 59: Photo-DSC of the LVT-50 formulation at 80-100 °C, 2 x900 s, 320-500 nm, 60 mW·cm^{-2}

Table 17: Results of the photo-DSC experiments of the LVT-50 formulations at different temperatures, 2 × 900 s, 320-500 nm, 60 mW·cm^{-2}.

Temp. [°C]	ΔH [J·g^{-1}]	t_{max} [s]	Conversion [%]	Rp [mmol·L^{-1}·s^{-1}]
80	350 ± 10	21 ± 2	69 ± 2	51 ± 2
90	390 ± 10	20 ± 2	76 ± 2	132 ± 2
100	410 ± 20	23 ± 3	84 ± 2	202 ± 2

The combination of the two monomers, which were characterized individually before, gives results concerning enthalpy, conversion and reaction speed (indicated by t_{max}) between the two. The speed with a t_{max} of about 20 s seems good enough for Hot

Die approbierte gedruckte Originalversion dieser Dissertation ist an der TU Wien Bibliothek verfügbar.
The approved original version of this doctoral thesis is available in print at TU Wien Bibliothek.
TU WIEN Bibliothek Your knowledge hub

Lithography, as well the conversion >70 %. Therefore, this formulation should be additive manufacturable, as long PT-30, with the faster reaction kinetics, is.

2.5.2 Thermal characterization

By means of STA, the completeness of the photo-induced reaction should be investigated (Figure 60).

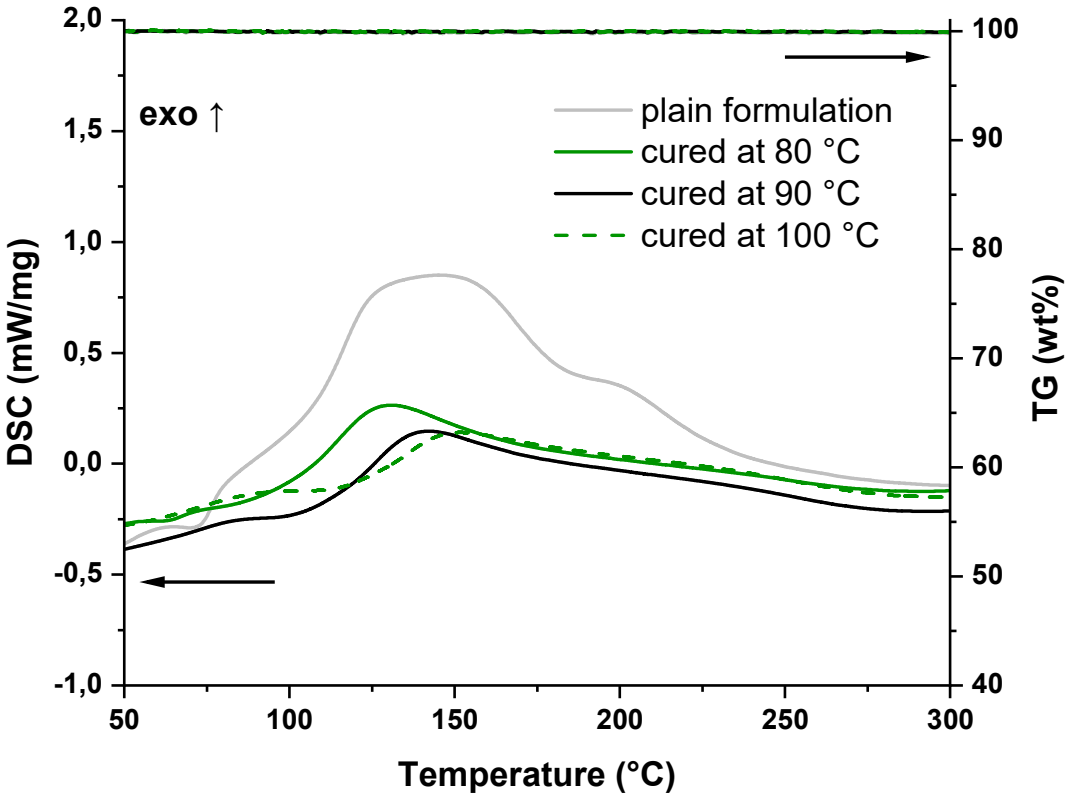

Figure 60: STA of the plain LVT-50 formulation (grey) and the photo-DSC cured samples at 80 °C (green solid), 90 °C (black solid) and 100 °C (green dot).

The uncured formulation shows the characteristics of the respective individual monomers. With an endothermic peak at approx. 80 °C (melting BADCy), a broad exothermic peak from 120 °C up to 220 °C, all specific peaks from before are shown. The cured samples show a residual exotherm between 130 and 140 °C. In this respect, complete curing has not been achieved, which can be compared with the PT-30 formulations. A post-curing process would also be here necessary.

Die approbierte gedruckte Originalversion dieser Dissertation ist an der TU Wien Bibliothek verfügbar.
The approved original version of this doctoral thesis is available in print at TU Wien Bibliothek.
TU WIEN Bibliothek Your knowledge hub

2.6 3D printing of the PT-30 formulation via Hot Lithography

Since only the PT-30 formulation showed sufficient reaction rates in the photo-DSC between the two monomers, only this formulation was used in the further course for characterization in additional tests and finally in 3D printing via Hot Lithography.

2.6.1 Stability of the formulation

To be suitable for the Hot Lithography printing process, the formulation must exhibit stability over an extended period at the designated printing temperature. To assess this, the formulation underwent monitoring for 2 hours at 100 °C in the STA to ascertain the volatility of its components. No weight loss was evident in this case (Figure 61).

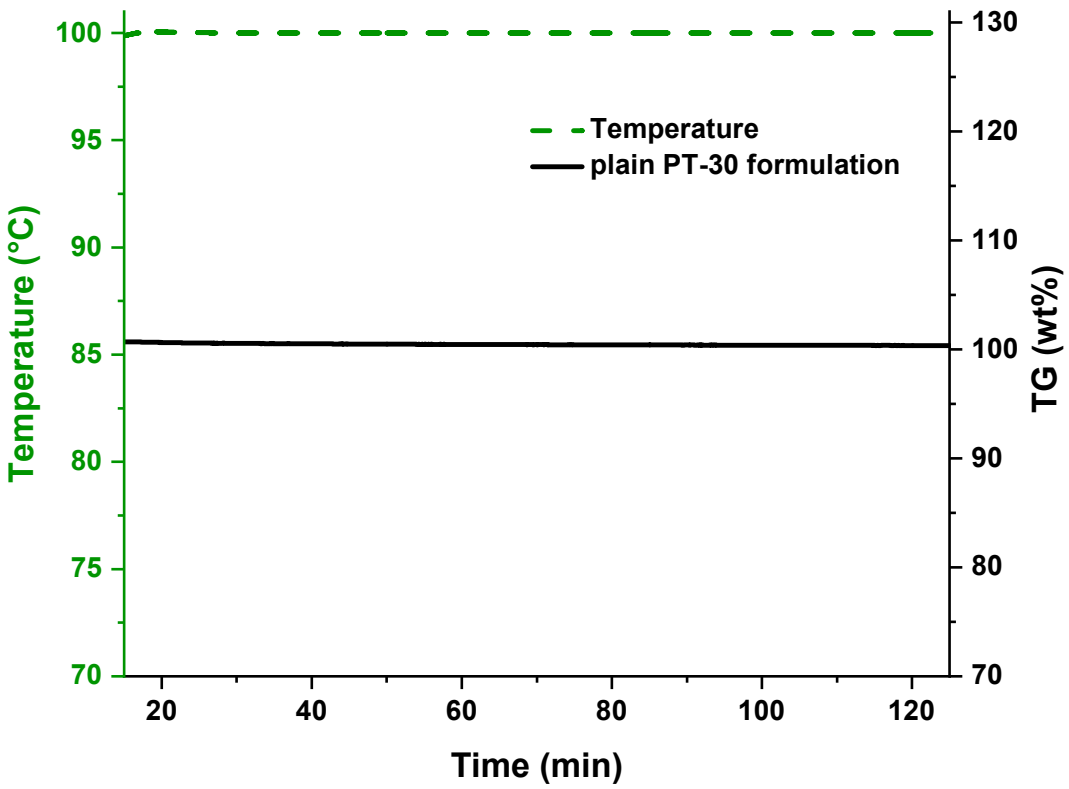

Figure 61: STA of the plain PT-30 formulation at 100 °C.

Additionally, a portion of the formulation was stored in an oven at 100 °C for several days, with its viscosity regularly measured to observe any progressive changes

Die approbierte gedruckte Originalversion dieser Dissertation ist an der TU Wien Bibliothek verfügbar.
The approved original version of this doctoral thesis is available in print at TU Wien Bibliothek.
TU WIEN Bibliothek Your knowledge hub

indicative of long-term stability. Starting from an initial viscosity of 0.1 Pa·s, well within the Hot Lithography processing range (<20 Pa·s)[56], the viscosity increased to 3.5 Pa·s within 72 hours. This suggests that the formulation remains adequately stable for the Hot Lithography process. In contrast, formulations lacking NP or I261 exhibited virtually no increase in viscosity over the tested period (Figure 62).

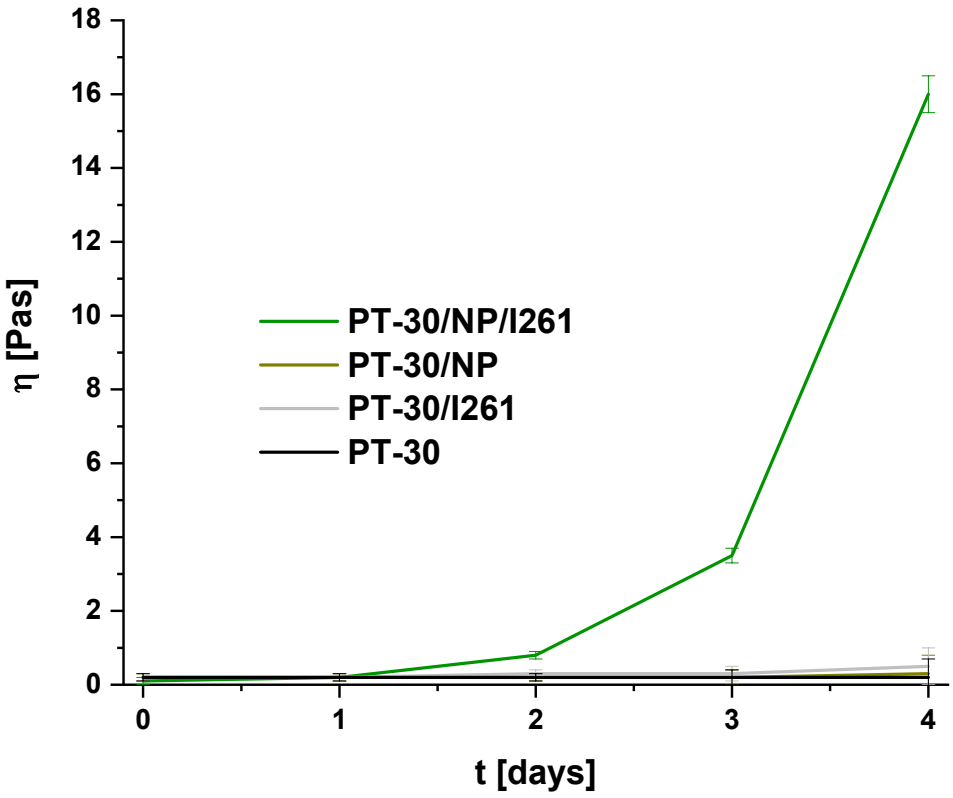

Figure 62: Stability Tests at 100 °C by means of viscosity measurements.

2.6.2 Printing & Overpolymerization

The demonstrated stability of the formulation, coupled with the potential for photoinduced catalytic poly-trimerization, positions this system as a promising candidate for application in Hot Lithography. A printing temperature of 90 °C, a printing speed of 1 m·s^{-1} with 10 repetitions, and a layer thickness of 50 µm were selected. Preliminary irradiation tests under identical conditions but without a building platform yielded a potential layer thickness of 203 µm (Figure 63).

Die approbierte gedruckte Originalversion dieser Dissertation ist an der TU Wien Bibliothek verfügbar.
The approved original version of this doctoral thesis is available in print at TU Wien Bibliothek.
TU Bibliothek Your knowledge hub WIEN

Figure 63: Printing test of PT-30 formulation at 90 °C.

In addition to dynamical mechanical analysis (DMA) test specimens, a computer aided design (CAD) model of a hollow cube was designed (Figure 64a) and 3D printed as a proof-of-concept for the system's functionality (Figure 64b). Both printed structures underwent the previously described post-curing program before imaging or further testing. As evident in the images, there is a slight overpolymerization during the printing process, which was subsequently polished off to refine the mechanical test specimen.

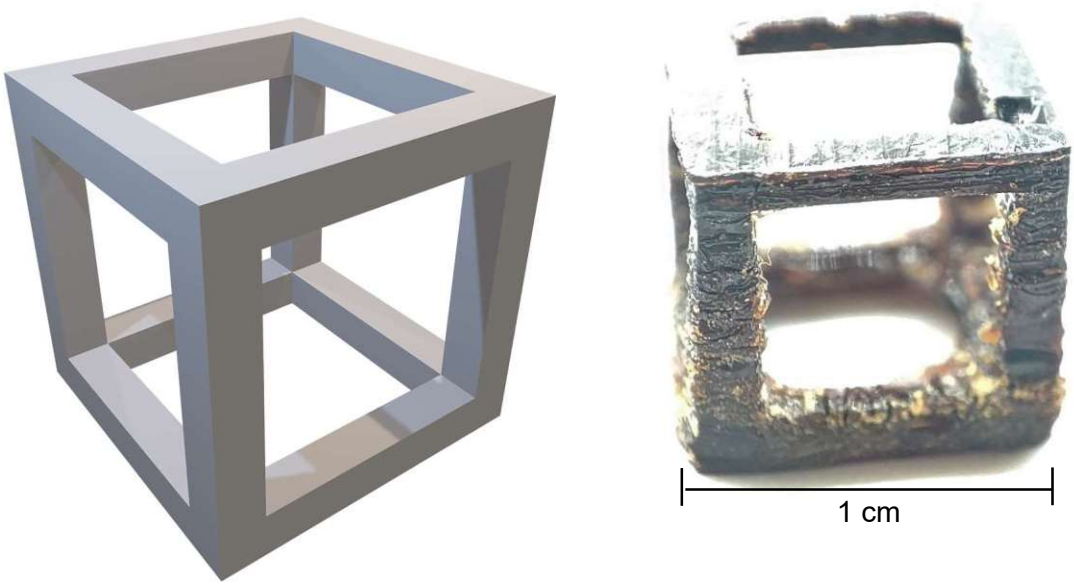

Figure 64: a) CAD model of the hollow cube. b) 3D printed and post-cured hollow cube.

Die approbierte gedruckte Originalversion dieser Dissertation ist an der TU Wien Bibliothek verfügbar.
The approved original version of this doctoral thesis is available in print at TU Wien Bibliothek.
TU WIEN Bibliothek Your knowledge hub

The overpolymerization can be attributed to the diffusion of the catalytic system. Scanning electron microscopy (SEM) images provide a detailed view of the structure, particularly the well-tuned layer thickness of 50 µm, despite the visible overpolymerization (Figure 65). Importantly, delamination between the printed layers induced by the post-processing program was not observed.

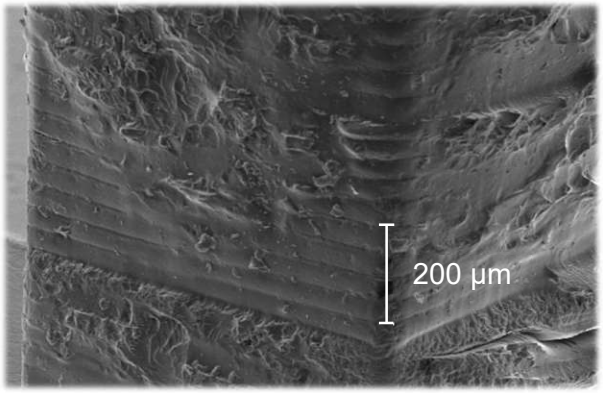

Figure 65: SEM image of the 3D printed structure.

To address the overpolymerization, various concepts to prevent dark polymerization were pursued and implemented. Since it was suspected that the iron atom was responsible for the dark polymerization, chelating agents were used to complex the iron. Oxidizing agents were also used to oxidize the Fe^{2+} to Fe^{3+} and thus prevent diffusion through the higher coordination of the iron. Furthermore, cumene was used to try to shift the equilibrium of the photocatalyst to the original substance, so that the catalyst would be created again by coordinating the cumene to the iron atom. Another attempt was to prevent dark polymerization via a cationic stabilizer, as I261 is originally a cationic initiator. Finally, it should be tried to remove the iron atom from the reaction by precipitation. The reactants and the structure/sum formula are shown in Table 18 according to the concept.

Die approbierte gedruckte Originalversion dieser Dissertation ist an der TU Wien Bibliothek verfügbar.
The approved original version of this doctoral thesis is available in print at TU Wien Bibliothek.
TU WIEN Bibliothek Your knowledge hub

Table 18: Overview of the concepts for the reduction of overpolymerization.

Concept	Name	Structure/sum formula
Chelating agents	Tartaric acid[168]	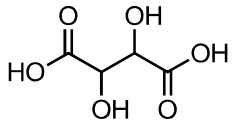
	Salicylic acid[169]	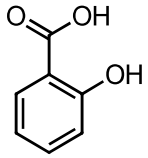
Oxidizing agents	Isopropylthioxanthone (ITX)[170]	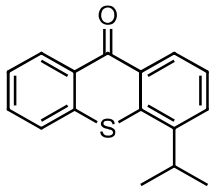
	Di-tert-butyl peroxide (DTBP)[171]	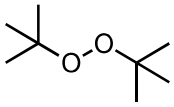
Equilibrium agent	Cumene[172]	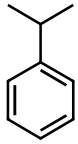
Cationic stabilizer	4-Hydroxyphenyldimethylsulfonium Methyl Sulfate (DMSMS)[173]	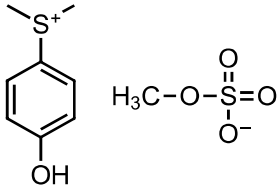
Precipitation	Potassium ferrocyanide[174]	$K_4[Fe(CN)_6]$
	Potassium thiocyanate[175]	KSCN

To the base formulation with 1 wt% I261 and 5 wt% NP, stabilizer was added according to the molar amount of I261 in a one-to-one molar ratio. For the experiments, the

Die approbierte gedruckte Originalversion dieser Dissertation ist an der TU Wien Bibliothek verfügbar.
The approved original version of this doctoral thesis is available in print at TU Wien Bibliothek.

respective samples were covered with a mask at 90 °C and irradiated with light (wavelength 320-500 nm, 60 mW·cm^{-2}) via a collimator for 20 s. The sample was then kept in a dark oven at 90 °C.

Overall, dark polymerization could not be prevented in any of the tests. The salts intended for precipitation were not soluble in the formulation. Additional tests, with reduced NP or I261 content did not circumvent overpolymerization. Therefore one last test, with a nitrogen-containing chelating agent (phen, Figure 66) was tested. This stabilizer is to be known to prevent cationic polymerization when I261 is used as a catalyst, since it forms a complex with the Fe center during radiation.[176]

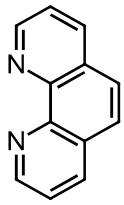

Figure 66: Structure of 1,10 phenanthroline (phen).

First, a one-to-one molar formulation was prepared analogous to the other stabilizers. In addition to the method described above, this was also tested using Hot Lithography. For this purpose, a disk with 10 layers was printed, similar to the printing tests but with a building platform (Figure 67).

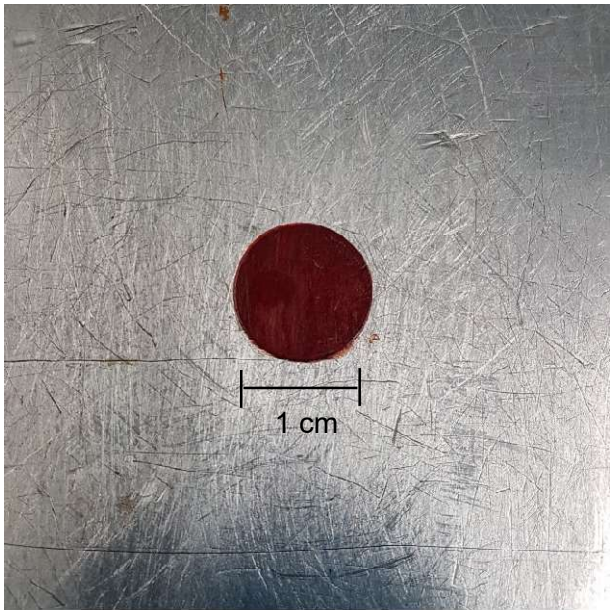

Figure 67: Printed disk with phen as stabilizer.

Die approbierte gedruckte Originalversion dieser Dissertation ist an der TU Wien Bibliothek verfügbar.
The approved original version of this doctoral thesis is available in print at TU Wien Bibliothek.
TU Bibliothek Your knowledge hub WIEN

The resulting disc shows hardly any overpolymerization. Despite the molar one-to-one ratio, phen does not prevent polymerization, presumably because several cyanate esters can coordinate per catalysis center. In comparison to the original printing test without phen, a clear red coloration can be detected, which is characteristic for the $Fe(phen)_3^{2+}$ complex.[176] Consequently, a first concept for the suppression of overpolymerization can be presented with this system and opens the possibility for further developments in this field.

2.7 Comparative mechanical testing of the 3D printed and bulk cured materials

In the final analysis, the DMA specimens manufactured through Hot Lithography underwent thermomechanical testing in 3-point bending mode and were compared with specimens thermally cured using the same formulation (Figure 68). All samples followed the same standard post-curing process. The storage modulus at 25 °C for both the purely thermally cured (4350 ± 200 MPa) and the 3D printed (3650 ± 100 MPa) samples falls within the literature-reported range or slightly higher (3580 MPa).[160] When assessing T_g, an increased T_g was observed for the 3D printed samples (336 ± 5 °C) compared to the thermally cured samples (305 ± 5 °C). Typically, this suggests that I261 is less active as a thermal catalyst than the combination of photo and thermal initiation, potentially leading to a lower crosslinking density and, consequently, a lower T_g. Generally, the height of the rubbery plateau serves as an indicator. However, since the samples start decomposition within the approximately 400 °C range, a confirmation of the lower crosslinking density becomes challenging. Still, this result also corresponds to those from the IR conversion determination, in which the purely thermally hardened materials had around 5 % less conversion than the photo-chemically cured samples, even in the post-cured stage. Nonetheless, the T_g of the 3D printed sample remains lower than values from the literature or by the manufacturer (up to 400 °C).[160,165] However, these references are based on curing pure PT-30 without a catalyst or co-catalyst, which can reduce the crosslinking density.

Die approbierte gedruckte Originalversion dieser Dissertation ist an der TU Wien Bibliothek verfügbar.
The approved original version of this doctoral thesis is available in print at TU Wien Bibliothek.
TU WIEN Bibliothek Your knowledge hub

Regardless, the T_g of 336 °C stands out as one of the highest reported for an unfilled photopolymerized material in the laser-based AM field.

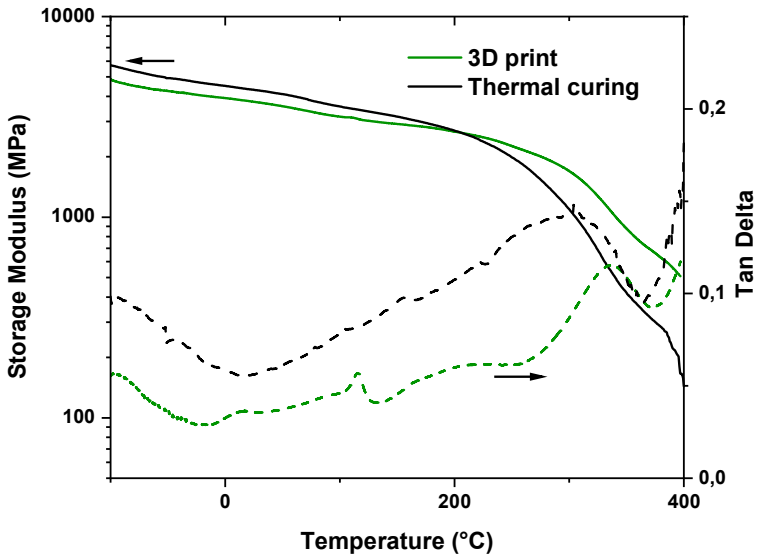

Figure 68: DMA tests in the 3-point bending mode: storage modulus (solid) and tan delta (dot) of the 3D printed (green) and thermally (black) cured samples.

Additionally, the advantages of post-curing could be observed through creep tests conducted on materials purely cured through thermal means (Figure 69a). The specimens subjected to post-curing initially exhibited reduced elongation under a 5 MPa load and, as the load increased, displayed significantly greater stability compared to specimens without post-curing. This effect is also noticeable in the creep modulus over time (Figure 69b).

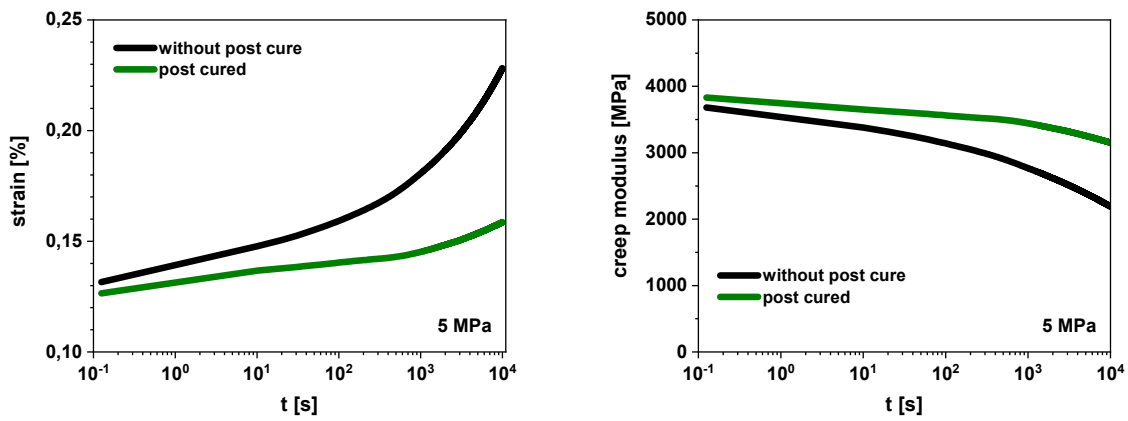

Figure 69: a) Stress-time behaviour for the materials with (green) and without post-curing (black). b) Creep modulus over time for the materials with (green) and without post-curing (black).

Die approbierte gedruckte Originalversion dieser Dissertation ist an der TU Wien Bibliothek verfügbar.
The approved original version of this doctoral thesis is available in print at TU Wien Bibliothek.
TU Bibliothek Your knowledge hub WIEN

3 Photo-induced catalytic poly-trimerization of isocyanates to form polyisocyanurates

3.1 State of the art

As positively convincing as the cyanate ester (CE) resins are as a material in the additive manufacturing (AM) area, the price component as a starting monomer is just as negative. Therefore, a cheaper alternative would be of great interest from an industrial point of view. Isocyanates and their multifunctional analogues are among the cheapest classes of monomers available on the market. This, together with their versatility, ensures that they are still used in endless applications despite their toxicity and environmental concerns.[177] Isocyanates, particularly polyisocyanates, are closely associated with polyurethane chemistry. Discovered by Wurtz in 1848, isocyanates unveiled their chemical properties through systematic exploration in the nineteenth century. The significant breakthrough in the discovery of polyurethanes occurred in 1937, credited to Bayer and his collaborators. This discovery involved the reaction of a polyester diol with a diisocyanate, establishing diisocyanates as one of the majorly produced chemicals globally, hence making them so cheap.[178]

Isocyanates are generally produced from the corresponding amine with phosgene. By splitting off hydrochloric acid, a carbamoyl chloride is formed, which results in an isocyanate through further heating releasing another molecule of hydrochloric acid.[177]

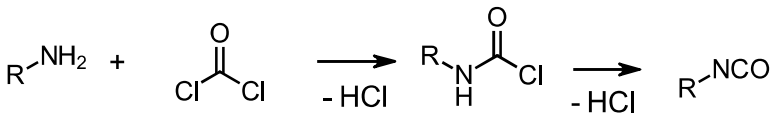

Scheme 13: Formation of a isocyanate.[177]

Polyurethanes can, depending on the choice of monomers, be used to produce virtually any type of material, from flexible to very hard and brittle. General areas of application are thermal insulation, building materials, as well as coatings for cars, buildings, metals, and sealants. Especially, when it comes to hard and resistant

Die approbierte gedruckte Originalversion dieser Dissertation ist an der TU Wien Bibliothek verfügbar.
The approved original version of this doctoral thesis is available in print at TU Wien Bibliothek.
TU Bibliothek Your knowledge hub WIEN

materials, not pure polyurethanes are used, but sometimes polymers with polyisocyanurates (PIR).[179–181] Initially, PIRs are found in application like thermal insulation, particularly as rigid foam boards. Through the combination of polyols and isocyanates, predominantly diphenylmethane diisocyanate (MDI), an excess of these components is employed to produce a polyurethane/polyisocyanurate blend. This process results in the formation of dimensionally stable, rigid, and thermally resistant foams.[182] PIRs, establishing a distinct material category with improved characteristics in terms of thermal and solvent stability, can be directly produced from isocyanates or polyisocyanates through poly-trimerization (Scheme 14).[183] The resulting dense network, featuring the isocyanurate core unit, can be theoretically tailored to exhibit properties ranging from hard and brittle to soft and flexible, or combinations thereof, depending on the chosen residue (R).[184–186]

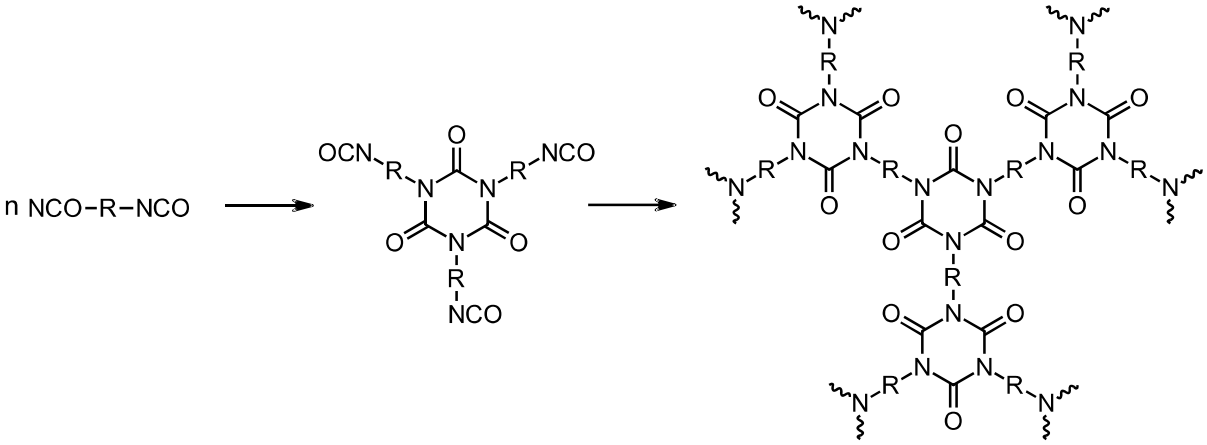

Scheme 14: Poly-trimerization of multifunctional isocyanates to polyisocyanurate.(adapted from [183])

Normally, trimerization catalysts encompass alkali metal salts derived from organic carboxylic acids, hydroxyalkyl trimethyl quaternary ammonium salts[186], select tertiary amines[179], and triazine compounds[187]. The trimerization process is initiated as a nucleophile targets the electrophilic carbon within the isocyanate group, leading to the trimerization toward the isocyanurate structure.[180,185] Additionally, it is known that transition metal complexes, including copper, nickel,[188] palladium,[189,190] iron, or manganese,[191] can serve as effective catalysts for isocyanate trimerization. The mechanism involving metal-based catalysts typically operates through the metal's role as a Lewis acid (Scheme 15). Coordination of the metal center with the isocyanate group generates a more electrophilic carbon, facilitating the trimerization progression through the attack of a nucleophilic nitrogen atom from another isocyanate. This

Die approbierte gedruckte Originalversion dieser Dissertation ist an der TU Wien Bibliothek verfügbar.
The approved original version of this doctoral thesis is available in print at TU Wien Bibliothek.
TU Bibliothek Your knowledge hub WIEN

cyclical process, involving the coordination of another isocyanate at the metal center, regenerates the catalyst and results in the formation of isocyanurate.[191]

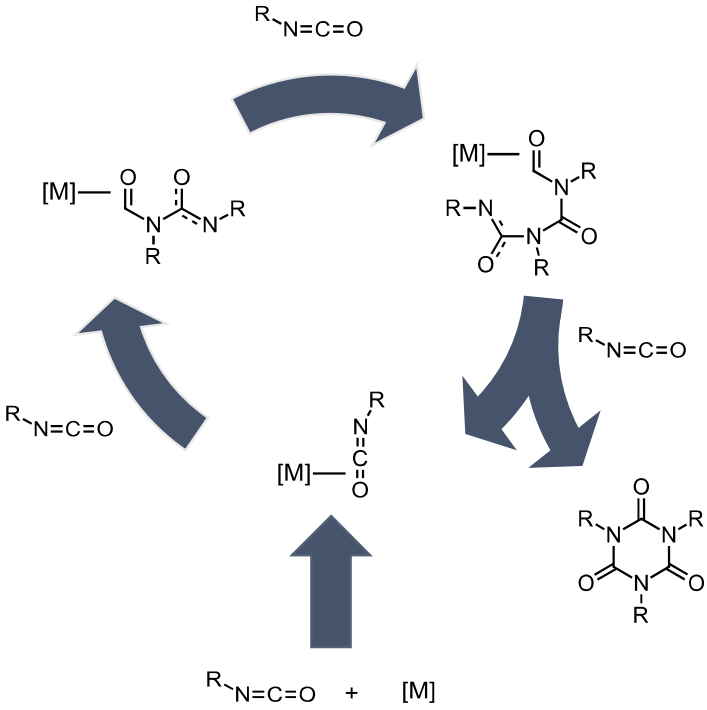

Scheme 15: Catalytic trimerization mechanism of isocyanates with a metal catalyst.(adapted from [191])

Contrarily, there is limited literature on photocatalysts in the area of pure polyisocyanurate trimerization. But as described in chapter 2.1, there are a number of photocatalysts that release metal centers for catalysis when exposed to light. Martelli et al. used this concept and demonstrated that subjecting a solution of phenyl isocyanate in tetrahydrofuran to five hours of UV irradiation at room temperature, with $MeCpMn(CO)_3$ as a photocatalyst, led to nearly complete conversion of the reactant into the trimerized product.[192] As described before $MeCpMn(CO)_3$ releases a carbon monoxide molecule under UV light irradiation. Subsequently, this molecule can bind to other nucleophiles at the vacated coordination position, making it available as a reactive center for catalytic reactions.[193,194] Consequently, the authors proposed the formation of a mono-adduct, which then evolves into the isocyanurate through the addition of two more isocyanates.[192]

Die approbierte gedruckte Originalversion dieser Dissertation ist an der TU Wien Bibliothek verfügbar.
The approved original version of this doctoral thesis is available in print at TU Wien Bibliothek.
TU Bibliothek Your knowledge hub WIEN

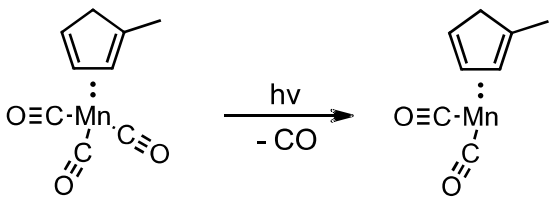

Figure 70: Decomposition of $MeCpMn(CO)_3$ under irradiation.

Further literature on photocatalytic curing of isocyanurates formation as well as on AM of PIRs is not available. However, the high thermal and chemical resistance of some of these materials would make them ideal for a wide range of applications such as electronics, aerospace and aeronautics. And not only in the course of AM, but also more generally like in the field of radiation-based coatings. For example, Golling et al. describe PIRs as one of the future trends in the coating industry.[183] And there, radiation curing for coatings stands out as one of the rapidly expanding sectors in the coatings industry.[195] This growth is primarily attributed to its energy-efficient and environmentally friendly advantages, swift curing capabilities, streamlined production processes, dependable chemical stability, and cost-effectiveness.[196] But there are also more elaborate processes such as light-based curing at elevated temperatures, with pre-bake or post-bake steps, as well as advanced light sources for any application.[197–199] These coatings are frequently employed to safeguard various materials, including wood, metal, glass, and plastic.[195] The diverse range of materials and their corresponding applications necessitate various properties in coatings. While conventional epoxy systems often yield coatings that are rigid and brittle, urethane-based systems tend to provide a degree of flexibility alongside reduced hardness.[12,200] Consequently, the search for adaptable materials and research into completely new classes of materials are therefore of continuing interest to both science and industry.

3.2 Basic studies

3.2.1 Screening of photocatalysts

Concluding from Martelli et al. research[192], an array of known photocatalysts featuring a transition metal core were initially mixed with an aromatic diisocyanate, toluene diisocyanate (TDI), or an aliphatic diisocyanate, hexamethylene diisocyanate (HMDI).

Die approbierte gedruckte Originalversion dieser Dissertation ist an der TU Wien Bibliothek verfügbar.
The approved original version of this doctoral thesis is available in print at TU Wien Bibliothek.
TU Bibliothek Your knowledge hub WIEN

These mixtures were then assessed for their use in photopolymerization. Beyond the previously mentioned manganese catalyst, experiments involved catalysts containing iron,[153] titanium,[153] zinc,[156] zirconium,[157] ruthenium,[153] various copper,[146] and an additional manganese center[201] (Figure 71).

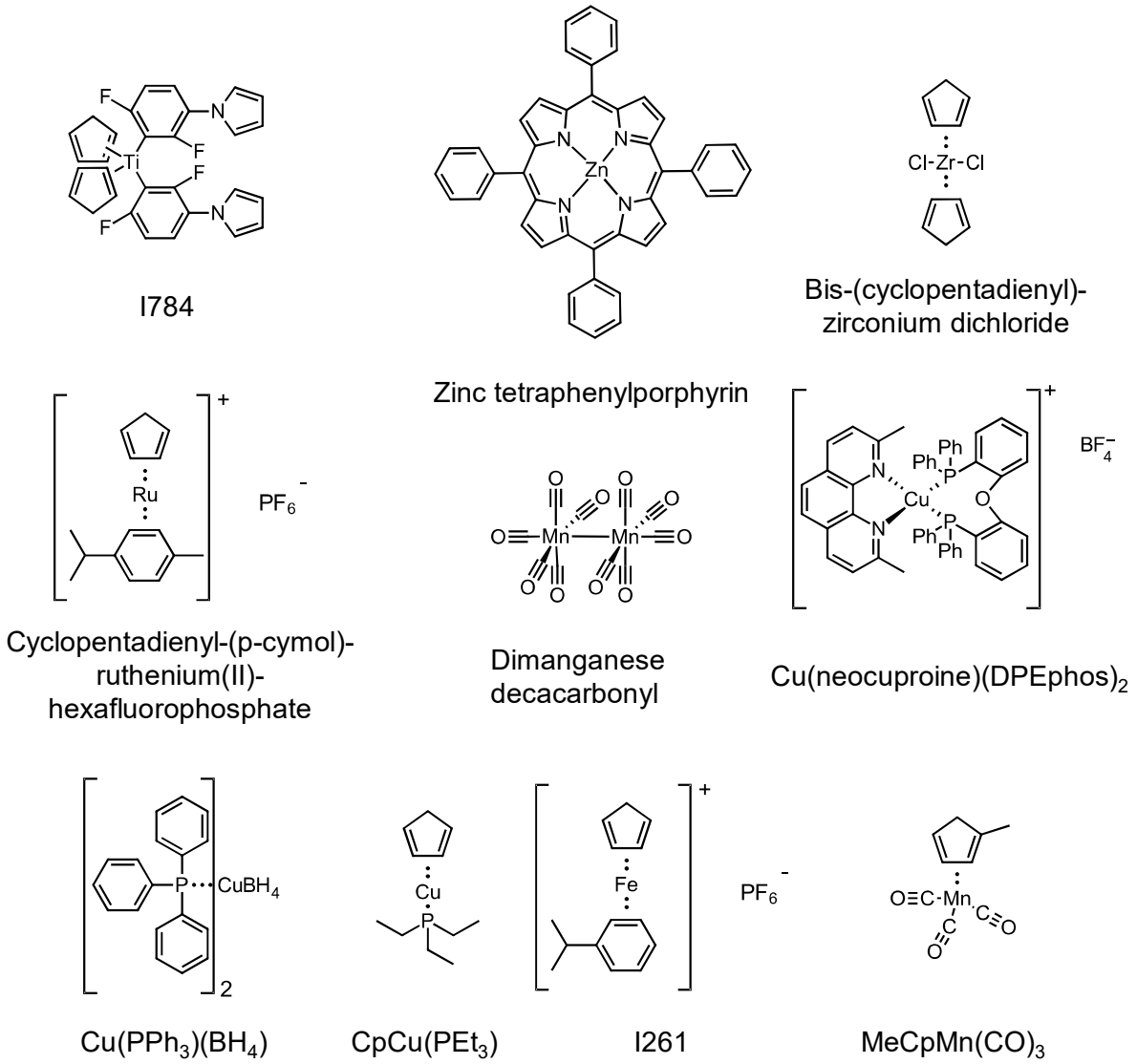

Figure 71: All tested catalysts.

5 mol% of each catalyst was combined with the corresponding monomer and examined through photo-DSC at 100 °C (2 x900 s, 320-500 nm, 60 mW·cm^{-2}). Out of all pairings, only MeCpMn(CO)$_3$ and I261 demonstrated the capability to undergo curing with the aliphatic HMDI. While I261 exhibited an enthalpy of <20 J·g^{-1} and a slow reaction rate, MeCpMn(CO)$_3$ exhibited an enthalpy of 690 J·g^{-1} (116 kJ·mol^{-1})

Die approbierte gedruckte Originalversion dieser Dissertation ist an der TU Wien Bibliothek verfügbar.
The approved original version of this doctoral thesis is available in print at TU Wien Bibliothek.

with a t_{max} of 68 s. Conversely, formulations with the aromatic diisocyanate exhibited no reactivity whatsoever. This aligns with the findings of Sharpe et al., where both manganese and iron catalysts were exclusively effective in the trimerization of primary isocyanates.[191]

The outcomes indicate that $MeCpMn(CO)_3$ exhibits satisfactory reactivity as a photocatalyst. For a comprehensive analysis, a UV-Vis spectrum was recorded (Figure 72). The photocatalyst displays a local peak in the area of 330 nm and an extended tail-out range up to 420 nm. This wavelength spectrum positions the photocatalyst as a viable candidate for utilization in radiation-based applications. Nevertheless, the reaction speed, with a t_{max} exceeding one minute, is relatively slow and may pose challenges in industrial processes, especially for AM. Hence, in the further course, efforts will be directed toward identifying co-catalysts to accelerate the trimerization process.

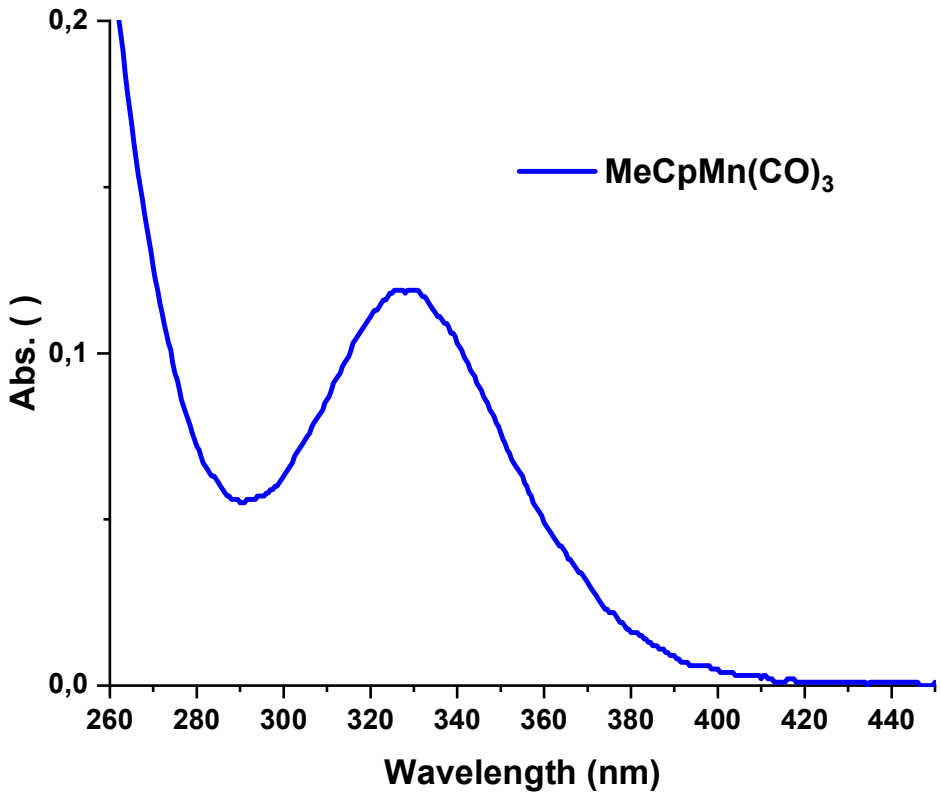

Figure 72: UV-Vis of the $MeCpMn(CO)_3$ photocatalyst.

Die approbierte gedruckte Originalversion dieser Dissertation ist an der TU Wien Bibliothek verfügbar.
The approved original version of this doctoral thesis is available in print at TU Wien Bibliothek.
TU WIEN Bibliothek Your knowledge hub

3.2.2 Screening of bases as co-catalyst

As indicated by literature, tertiary amines possess the ability to catalyze the trimerization process.[202,203] Consequently, research was conducted to find suitable bases as co-catalyst. In this context, non-nucleophilic bases, including 1,5-diazabicyclo(4.3.0)non-5-en (DBN) and 1,1,3,3-tetramethylguanidine (TMG), as well as the superbase P4-t-Bu, were evaluated (Figure 73). The aliphatic HMDI served once again as the monomer.

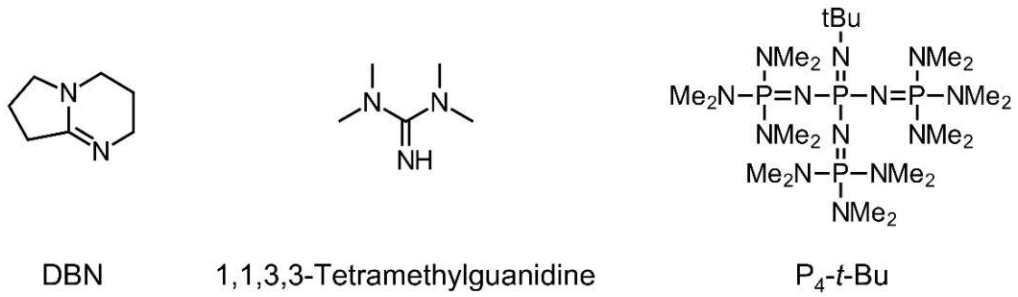

Figure 73: All tested bases.

Typically, 5 mol% of co-catalyst was introduced to HMDI, subjected to heating and ultrasonic bath treatment, and after cooling, 5 mol% of $MeCpMn(CO)_3$ was incorporated. Subsequently, the liquid formulations were analyzed by photo-DSC at 100 °C (2 x900 s, 320-500 nm, 60 mW·cm^{-2}). The superbase initiated an immediate reaction upon addition, whereas DBN engaged in the formation of an adduct with the isocyanate (Scheme 16)[204], which dissolved upon heating (80 °C) in the formulation. The TMG-containing formulation exhibited no enthalpy, whereas the DBN containing formulation displayed the same exotherm of 116 kJ·mol^{-1} as the formulation without DBN. However, the t_{max} shifted from 68 s to 33 s, effectively doubling the reaction speed. DBN is recognized for forming an adduct with HMDI, generating a stable cyclic adduct up to a temperature of 106 °C. Beyond this temperature, the adduct undergoes decomposition into its original reactants.[204] Presumably, the already initiated trimerization proves crucial for acceleration the reaction. Additionally, electronic effects may contribute to a more rapid coordination at the manganese center.

Die approbierte gedruckte Originalversion dieser Dissertation ist an der TU Wien Bibliothek verfügbar.
The approved original version of this doctoral thesis is available in print at TU Wien Bibliothek.
TU WIEN Bibliothek Your knowledge hub

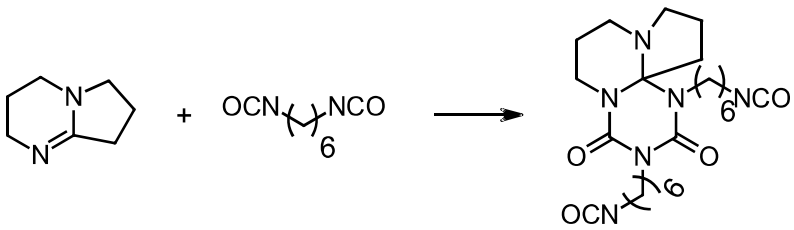

Scheme 16: Adduct formation of HMDI and DBN. (adapted from [204])

To examine the observed acceleration, all previously examined catalysts (Figure 71) were subjected to testing with DBN as a co-catalyst. Among them, only I261 demonstrated an enhancement, elevating from <3.4 kJ·mol⁻¹ enthalpy to 95.6 kJ·mol⁻¹ at a t_{max} of 56 s. This underscores the potential role of electronic effects in the adduct-bound isocyanate, transforming a reaction that previously had minimal enthalpy into one good enough to yield a solid product. In essence, it can be affirmed that the adduct formed between HMDI and DBN possesses the capability to facilitate trimerization at metal centers such as manganese or iron.

Other attempts to replace DBN with different photobases (Figure 74) were also unsuccessful even in combination with metal-based photocatalysts ($MeCpMn(CO)_3$).

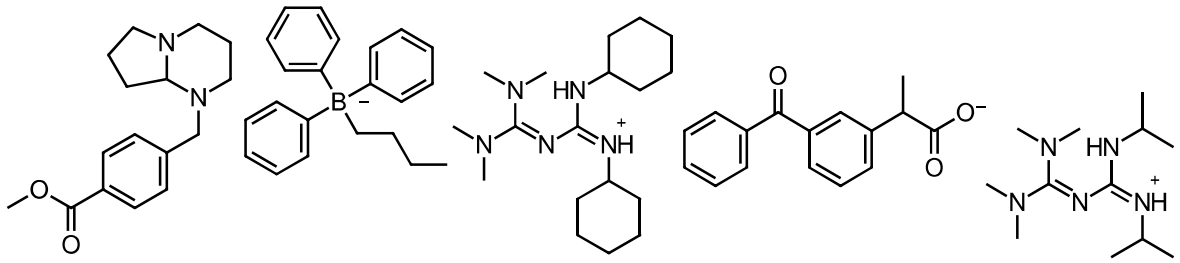

Figure 74: Structures of the used photobases.

3.2.3 Screening of monomers

The system involving DBN and $MeCpMn(CO)_3$, discovered through this approach, was applied similarly to other diisocyanates as monomers and subjected to analysis using photo-DSC. In addition to the previously examined HMDI, other diisocyanates, such as the structurally alike trimethyl hexamethylene diisocyanate (TMDI), as well as toluene diisocyanate (TDI) and methylene diphenyl diisocyanate (MDI) as aromatic options, isophorone diisocyanate (IPDI), and 4,4'-diisocyanatodicyclohexylmethane ($H_{12}MDI$) as aliphatic sterically demanding choices, were tested (Figure 75). Moreover,

Die approbierte gedruckte Originalversion dieser Dissertation ist an der TU Wien Bibliothek verfügbar.
The approved original version of this doctoral thesis is available in print at TU Wien Bibliothek.
TU WIEN Bibliothek Your knowledge hub

primary diisocyanates were included in the testing, featuring steric hindrance in the β-position (1,3-bis(isocyanatomethyl)cyclohexane, H_6XDI) or an aromatic system in that position (m-xylene diisocyanate, XDI).

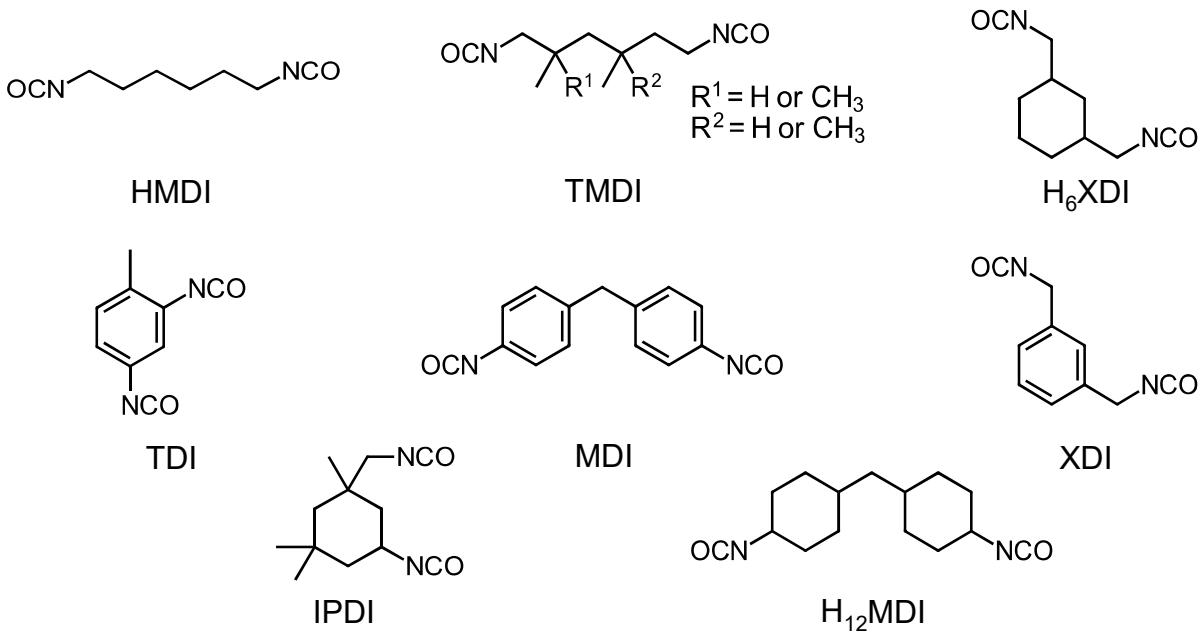

Figure 75: Tested monomers for the trimerization to polyisocyanurates.

Among the chosen monomers, only the primary diisocyanates, namely HMDI, TMDI, XDI, and H_6XDI, exhibited reactivity (Figure 76). At 100 °C, TMDI demonstrated an enthalpy of 67.9 $kJ \cdot mol^{-1}$ with a t_{max} of 64 s, XDI exhibited 91.6 $kJ \cdot mol^{-1}$ with a t_{max} of 49 s, and H_6XDI displayed 69.7 $kJ \cdot mol^{-1}$ with a t_{max} of 116 s. This aligns with the findings of Sharp et al., where trimerization was achievable only with primary aliphatic isocyanates.[191] Steric hindrance in the α-position prevents trimerization reactions, while hindrance in the β-position affects reactivity but does not impede it. Aromatic systems, alike to the thermal curing of polyisocyanurates, enhance trimerization, as evidenced by the comparison between XDI and H_6XDI in the photocatalytic reaction.

Die approbierte gedruckte Originalversion dieser Dissertation ist an der TU Wien Bibliothek verfügbar.
The approved original version of this doctoral thesis is available in print at TU Wien Bibliothek.
TU Bibliothek Your knowledge hub WIEN

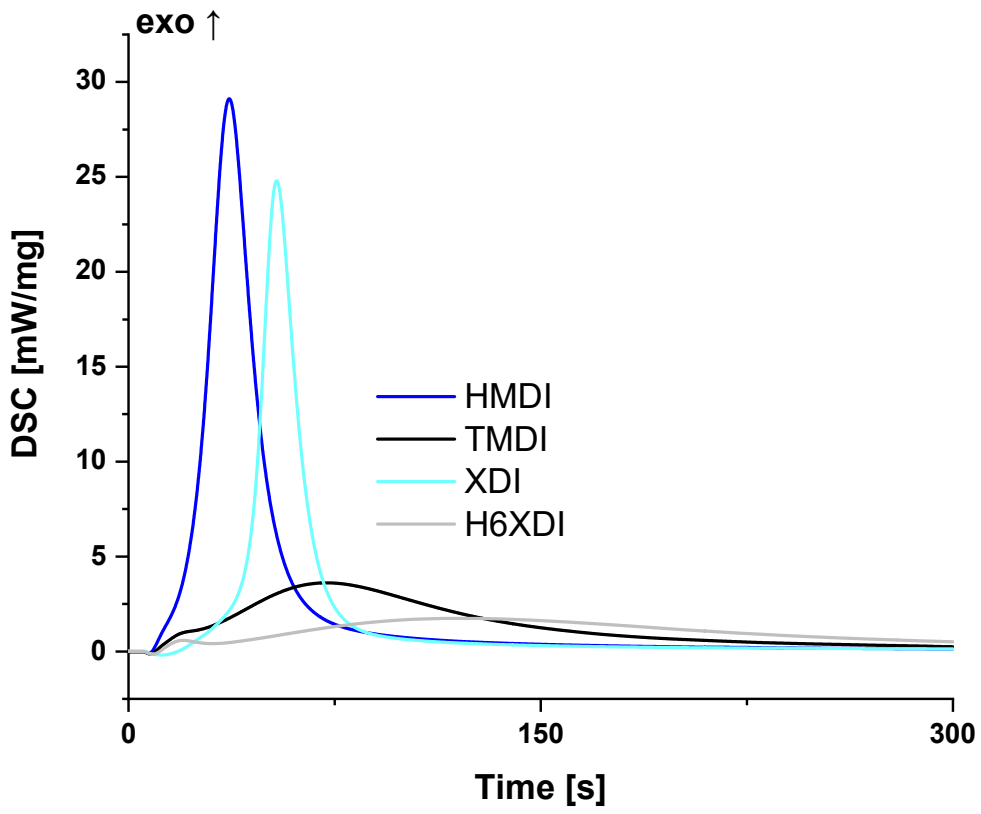

Figure 76: Photo-DSC of the different Isocyanate formulations at 80-100 °C, 2 x900 s, 320-500 nm, 60 mW·cm^{-2}.

3.2.4 Theoretical investigation of isocyanurates

For a deeper evaluation, a monofunctional isocyanate, hexylisocyanate (HMI), was employed to investigate the underlying principles of trimerization (Scheme 17). In line with the previously identified system, HMI was combined with 5 mol% DBN and subsequently with 1 mol% MeCpMn(CO)$_3$. Following measurement via photo-DSC at 100 °C, the resulting soluble product underwent analysis by ^{1}H-NMR. Comparisons with literature values revealed that, in addition to the mentioned adduct, only the intended trihexyl isocyanurate was generated.[204,205] Furthermore, UPLC-MS of the sample unveiled a molecular weight of 382 g·mol^{-1} for the isocyanurate.

Die approbierte gedruckte Originalversion dieser Dissertation ist an der TU Wien Bibliothek verfügbar.
The approved original version of this doctoral thesis is available in print at TU Wien Bibliothek.
TU WIEN Bibliothek Your knowledge hub

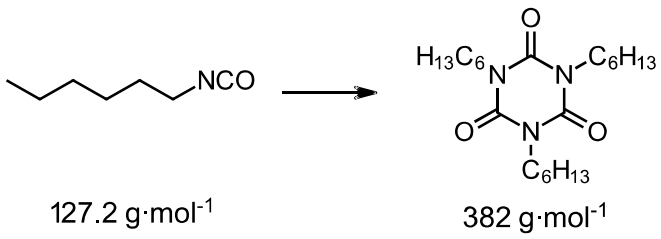

Scheme 17: Trimerization of HMI to trihexyl isocyanurate.

By utilizing the acquired enthalpy value of 54.7 kJ·mol^{-1} (ΔH = 430 J·g^{-1}, t_{max} = 78 s, Rp = 75.7 mmol·L^{-1}·s^{-1}), along with the molecular weight of the reactant (M_{HMI} = 172.2 g·mol^{-1}), the conversion assessed through ^{1}H-NMR ($a_{NMRconv}$ = 77 %), the mass fraction in the mixture (m_{HMI} = 94 %), the average weight loss during measurement due to evaporation (m_{Loss} = 22.8 %) as well as the monomer portion available for trimerization ($\alpha_{NMRavai}$ = 86 %), a theoretical enthalpy of 67.5 kJ·mol^{-1} per equivalent isocyanate group could be computed (Equation 5). This figure falls within the range established by Uchimaru et al. through computer-based calculations for the trimerization of hexyl isocyanate (66.4 kJ·mol^{-1}).[206]

$$\Delta H_0 = \left(\frac{\Delta H \times M_{HMI} \times a_{NMRconv}}{m_{HMI} \times (1 - m_{Loss}) \times a_{NMRavai} \times 100}\right)$$

Equation 5: Calculation of the theoretical enthalpy per isocyanate group.

3.3 Optimization of the system

To explore further applications, the parameters of the photoreaction and the impact of individual component concentrations on the reaction enthalpy were examined using Photo-DSC. To achieve this, the temperature (100 °C) and intensity (60 mW·cm^{-2}) were held constant, while the concentrations of $MeCpMn(CO)_3$ (chapter 3.3.1) and DBN (chapter 3.3.2) were systematically altered. In the subsequent phase, the temperature (chapter 3.3.3) and intensity (chapter 3.3.4) parameters were examined, maintaining the determined optimal concentration of the respective component. HMDI was once again employed as the monomer. The conversion was derived from the

Die approbierte gedruckte Originalversion dieser Dissertation ist an der TU Wien Bibliothek verfügbar.
The approved original version of this doctoral thesis is available in print at TU Wien Bibliothek.
TU Bibliothek Your knowledge hub WIEN

enthalpy in conjunction with the previously established theoretical enthalpy, taking into account the proportion of monomer ($m_{Isocyanate}$ between 89.5 and 98.5 %) as well as the molecular mass of the repeating unit ($M_{Isocyanate}$ = 168.2 g·mol^{-1} for HMDI and 210.3 g·mol^{-1} for TMDI) and the number of functional groups f (Equation 6). By considering the peak height, Rp can be computed together with ρ_{HMDI} = 1.05 and ρ_{TMDI} = 1.02 (Equation 7), serving as an indicator of the reaction's speed, along with t_{max}.

$$a_{Isocyanate} = \left(\frac{\Delta H \times M_{Isocyanate}}{m_{Isocyanate} \times f}\right) \times 10^{-1} \times \Delta H_0{}^{-1}$$

Equation 6: Calculation of the conversion for the isocyanate formulations.

$$Rp = \left(\frac{h \times \rho_{Isocyanate} \times 1000}{\Delta H_0}\right)$$

Equation 7: Calculation of the rate of polymerization.

3.3.1 Influence of the concentration of the photocatalyst

In the lower molar range, up to 1 mol% of $MeCpMn(CO)_3$, there is an increase in conversion, reaching approximately 92 % (Figure 77 left). However, higher concentrations (5 mol%) result in a decline in conversion due to an excess of the catalyst. The Rp demonstrates an increase up to 0.75 mol% of $MeCpMn(CO)_3$, after which it stabilizes at a constant level. This pattern is also mirrored by the t_{max} (Figure 77 right), indicating that further acceleration of the reaction by $MeCpMn(CO)_3$ alone is not attainable. All the data is available in Table 19.

Die approbierte gedruckte Originalversion dieser Dissertation ist an der TU Wien Bibliothek verfügbar.
The approved original version of this doctoral thesis is available in print at TU Wien Bibliothek.
TU WIEN Bibliothek Your knowledge hub

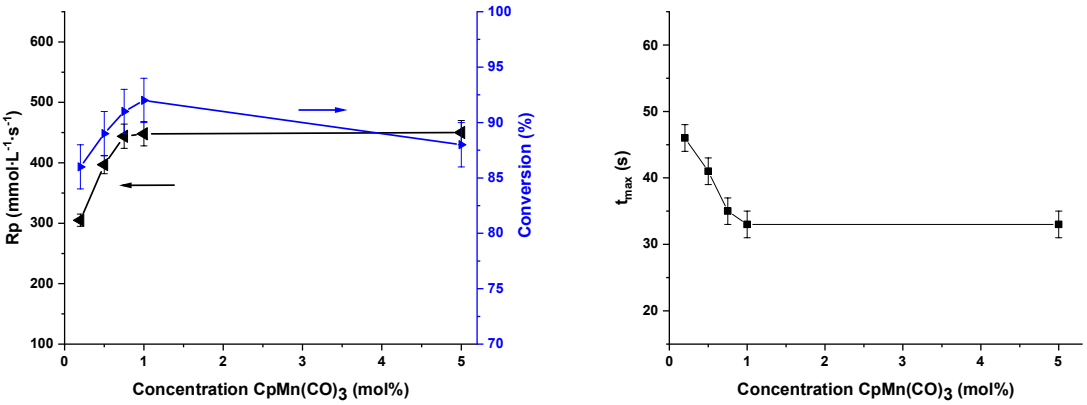

Figure 77: Photo-DSC (320-500 nm) results (left Rp in black, conversion in blue, right t_{max}) of HMDI formulation with 5 mol% DBN and varying concentration of $MeCpMn(CO)_3$ (0.2, 0.5, 0.75, 1 and 5 mol%) at 100 °C and 60 mW·cm^{-2}.

Table 19: Photo-DSC (320-500 nm) results) of HMDI formulation with 5 mol% DBN and varying concentration of $MeCpMn(CO)_3$ at 100 °C and 60 mW·cm^{-2}.

Conc. $MeCpMn(CO)_3$	ΔH [J·g^{-1}]	Conversion [%]	t_{max} [s]	Rp [mmol·L^{-1}·s^{-1}]
0.2	650 ± 20	86 ± 2	46 ± 2	300 ± 20
0.5	680 ± 20	89 ± 2	41 ± 2	400 ± 20
0.75	680 ± 20	91 ± 2	35 ± 2	440 ± 20
1	690 ± 20	92 ± 2	33 ± 2	450 ± 20
5	640 ± 20	88 ± 2	33 ± 2	450 ± 20

3.3.2 Influence of the concentration of the co-catalyst

As highlighted earlier, the introduction of DBN results in a notable acceleration of the reaction. Regarding Rp, it nearly doubles when comparing the formulation with 1 mol% DBN to that with 5 mol% (Figure 78 left). Simultaneously, there is an augmentation in

Die approbierte gedruckte Originalversion dieser Dissertation ist an der TU Wien Bibliothek verfügbar.
The approved original version of this doctoral thesis is available in print at TU Wien Bibliothek.
TU Bibliothek Your knowledge hub WIEN

conversion of almost 5 %. An even higher concentration (10 mol%) leads to a slight hastening of the reaction, but without an increase in conversion. The t_{max} already reaches a plateau at a concentration of 3 mol% (Figure 78 right), establishing a concentration of 5 mol% DBN along with 1 mol% $MeCpMn(CO)_3$ as the standard for subsequent experiments. All the data is available in Table 20.

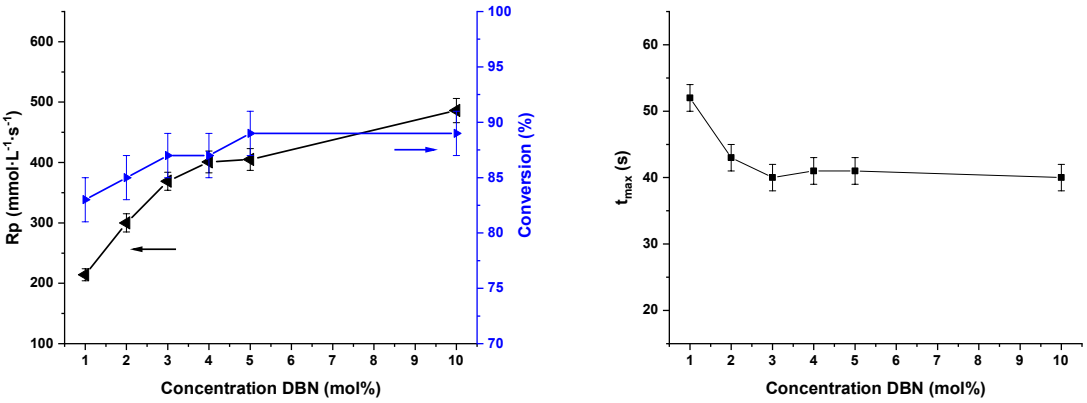

Figure 78: Photo-DSC (320-500 nm) results (left Rp in black, conversion in blue, right t_{max}) of HMDI formulation with 0.5 mol% $MeCpMn(CO)_3$ and varying concentration of DBN (1, 2, 3, 4, 5 and 10 mol%) at 100 °C and 60 mW·cm^{-2}.

Table 20: Photo-DSC (320-500 nm) results HMDI formulation with 0.5 mol% $MeCpMn(CO)_3$ and varying concentration of DBN at 100 °C and 60 mW·cm^{-2}.

Conc. DBN	ΔH [J·g^{-1}]	Conversion [%]	t_{max} [s]	Rp [mmol·L^{-1}·s^{-1}]
1	660 ± 20	83 ± 2	52 ± 2	210 ± 20
2	660 ± 20	85 ± 2	43 ± 2	300 ± 20
3	670 ± 20	87 ± 2	40 ± 2	370 ± 20
4	670 ± 20	87 ± 2	41 ± 2	400 ± 20
5	680 ± 20	89 ± 2	41 ± 2	400 ± 20
10	640 ± 20	89 ± 2	40 ± 2	490 ± 20

Die approbierte gedruckte Originalversion dieser Dissertation ist an der TU Wien Bibliothek verfügbar.
The approved original version of this doctoral thesis is available in print at TU Wien Bibliothek.
TU Bibliothek Your knowledge hub WIEN

3.3.3 Influence of the temperature

Subsequently, an investigation into the impact of temperature on the system was undertaken. The previously ascertained composition was measured at various temperatures to determine the temperature-dependent dynamics (Figure 79 left). The reaction rate (Rp and t_{max} progressing parallel, see Figure 79 right) is markedly influenced by the temperature. At 80 °C, a relatively sluggish reaction (t_{max} = 61 s) was observed, while at 100 °C, a reaction twice as rapid (t_{max} = 33 s) was determined. A further elevation of the temperature results in a continued increase in speed, albeit less swiftly. Concerning conversion, there is an augmentation of up to 95 % at 120 °C. The decline in conversion at 140 °C can be attributed to the monomer's volatility and the consequent evaporation, constituting an endothermic process. Again, all the data is available in Table 21.

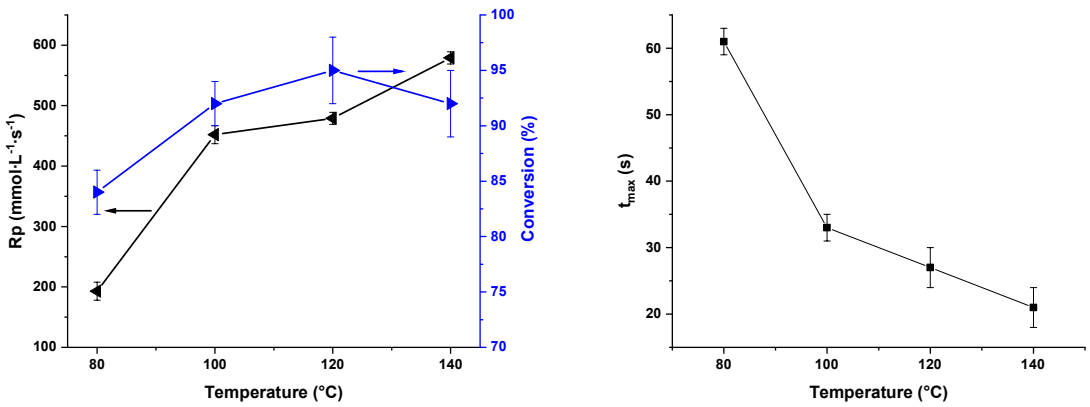

Figure 79: Photo-DSC (320-500 nm) results (left Rp in black, conversion in blue, right t_{max}) of HMDI formulation with 1 mol% $MeCpMn(CO)_3$ and 5 mol% DBN at different temperatures (80, 100, 120 and 140 °C) and 60 mW·cm^{-2}.

Die approbierte gedruckte Originalversion dieser Dissertation ist an der TU Wien Bibliothek verfügbar.
The approved original version of this doctoral thesis is available in print at TU Wien Bibliothek.
TU WIEN Bibliothek Your knowledge hub

Table 21: Photo-DSC (320-500 nm) results of HMDI formulation with 1 mol% $MeCpMn(CO)_3$ and 5 mol% DBN at different temperatures and 60 mW·cm^{-2}.

Temp.	ΔH [J·g^{-1}]	Conversion [%]	t_{max} [s]	Rp [mmol·L^{-1}·s^{-1}]
80	630 ± 20	84 ± 2	61 ± 2	190 ± 20
100	700 ± 20	92 ± 2	33 ± 3	450 ± 20
120	720 ± 20	95 ± 2	27 ± 3	480 ± 20
140	700 ± 20	93 ± 2	21 ± 3	570 ± 20

3.3.4 Influence of the intensity

Finally, an assessment of the light intensity dependency was undertaken (Figure 80 left). Both conversion and reaction rate exhibit a pronounced reliance on intensity. Once again, nearly a twofold acceleration of the reaction pace can be accomplished by elevating the intensity from 30 to 120 mW·cm^{-2}. Within this range, t_{max} diminishes from approximately 45 s to 25 s (Figure 80 right). The achieved conversion, surpassing 95 %, represents the highest in these optimization experiments at an intensity of 120 mW·cm^{-2}. All the data can be seen in Table 22.

Die approbierte gedruckte Originalversion dieser Dissertation ist an der TU Wien Bibliothek verfügbar.
The approved original version of this doctoral thesis is available in print at TU Wien Bibliothek.
TU WIEN Bibliothek Your knowledge hub

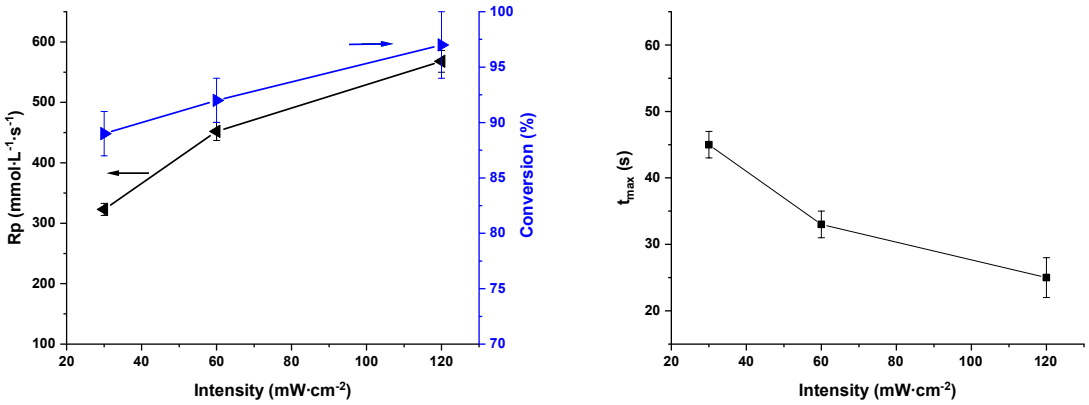

Figure 80: Photo-DSC (320-500 nm) results (left Rp in black, conversion in blue, right t_{max}) of HMDI formulation with 1 mol% $MeCpMn(CO)_3$ and 5 mol% DBN at 100 °C and different intensities (30, 60 and 120 mW·cm^{-2}).

Table 22: Photo-DSC (320-500 nm) results of HMDI formulation with 1 mol% $MeCpMn(CO)_3$ and 5 mol% DBN at 100 °C and different intensities.

Int.	ΔH [J·g^{-1}]	Conversion [%]	t_{max} [s]	Rp [mmol·L^{-1}·s^{-1}]
30	670 ± 20	65 ± 2	45 ± 2	320 ± 20
60	700 ± 20	92 ± 2	33 ± 2	450 ± 20
120	740 ± 20	97 ± 2	25 ± 3	570 ± 20

In summary, the reaction can be effectively manipulated through temperature and intensity, and, contingent upon the intended application, the concentration of catalysts or co-catalysts can also be subject to variation.

Die approbierte gedruckte Originalversion dieser Dissertation ist an der TU Wien Bibliothek verfügbar.
The approved original version of this doctoral thesis is available in print at TU Wien Bibliothek.
TU Bibliothek Your knowledge hub WIEN

3.4 Investigation HMDI vs. TMDI

3.4.1 Photo-DSC & Conversion

Ultimately, an examination and comparison were conducted on the monomers HMDI and TMDI, as well as a 50:50 blend of the two. To achieve this, the reaction rate of the corresponding formulations was analyzed via photo-DSC (Figure 81 left & right).

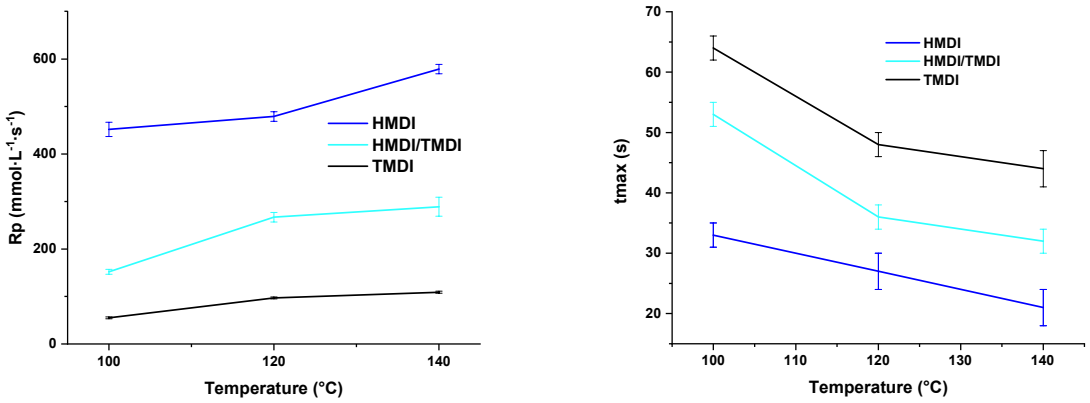

Figure 81: Rp (left) and t_{max} (right) from Photo-DSC (320-500 nm, 60 mW·cm^{-2}) for the HMDI (blue), HMDI/TMDI (turquoise) and TMDI (black) formulation for different temperatures (100, 120 and 140 °C).

The reaction kinetics, expressed in terms of Rp, exhibit an increase with higher temperatures across all three formulations. Nevertheless, the Rp of TMDI is only approximately one-fifth of that observed for HMDI. As anticipated, the Rp of the blend falls between the two pure formulations. Correspondingly, the t_{max} for TMDI at 140 °C is 44 s, while the mixture registers at 32 s (with HMDI at 21 s). It is plausible that steric hindrance in the beta position contributes to the slowing down of the reaction.

For the conversion, the samples were additionally analyzed using IR spectroscopy (Figure 82 left), to compare them (Figure 82 right) and validate the enthalpy-based method via photo-DSC.

Die approbierte gedruckte Originalversion dieser Dissertation ist an der TU Wien Bibliothek verfügbar.
The approved original version of this doctoral thesis is available in print at TU Wien Bibliothek.
TU WIEN Bibliothek Your knowledge hub

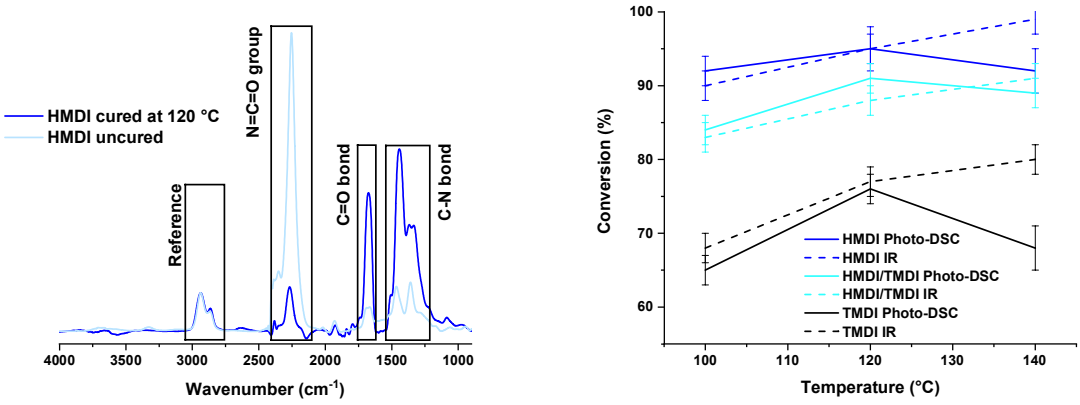

Figure 82: IR spectroscopy (left) of the uncured HMDI formulation (light blue) as well as the cured sample at 120 °C (blue). Conversion (right) from Photo-DSC (solid line, 320-500 nm, 60 mW·cm^{-2}) and IR spectroscopy (dashed line) for the HMDI (blue), HMDI/TMDI (turquoise) and TMDI (black) formulation for different temperatures (100, 120 and 140 °C).

The conversion of each formulation exhibits a parallel trend to the reaction kinetics. While HMDI attains a conversion ranging from 90 % to >95 % at all temperatures, TMDI falls within the 65 % to 80 % range. Interestingly, the blend of the two is not centered between them but slightly elevated, ranging between 80 % and 90 %. This can be explained by the less hindered access of HMDI to the catalyst, facilitating subsequent access for TMDI in the trimerization process. These values were also substantiated by the isocyanate band in the range from 2500 to 2000 cm^{-1}. However, unlike photo-DSC measurement at 140 °C, the actual conversion is documented as the sample had already solidified, eliminating the enthalpy of vaporization from the measurement. All the data from the measurements is available in Table 23.

Die approbierte gedruckte Originalversion dieser Dissertation ist an der TU Wien Bibliothek verfügbar.
The approved original version of this doctoral thesis is available in print at TU Wien Bibliothek.
TU WIEN Bibliothek Your knowledge hub

Table 23: Results from Photo-DSC (320-500 nm, 60 mW·cm^{-2}) for the HMDI (blue), HMDI/TMDI (turquoise) and TMDI (black) formulation for different temperatures (100, 120 and 140 °C)

	Temp.	ΔH [J·g^{-1}]	Conversion photo-DSC [%]	Conversion IR [%]	t_{max} [s]	Rp [mmol·L^{-1}·s^{-1}]
HMDI	100	700 ± 10	92 ± 2	90 ± 3	33 ± 3	450 ± 20
	120	720 ± 10	95 ± 2	95 ± 3	27 ± 3	480 ± 20
	140	700 ± 20	93 ± 2	99 ± 3	21 ± 3	570 ± 20
HMDI/TMDI	100	560 ± 20	84 ± 2	83 ± 3	53± 2	150 ± 5
	120	610 ± 20	91 ± 2	88 ± 3	36 ± 2	270 ± 10
	140	600 ± 20	90 ± 2	91 ± 3	32 ± 2	290 ± 20
TMDI	100	390 ± 20	65 ± 2	70 ± 3	64 ± 2	55 ± 2
	120	460 ± 20	76 ± 2	77 ± 3	48 ± 2	97 ± 2
	140	410 ± 20	68 ± 3	80 ± 3	44 ± 3	109 ± 2

3.4.2 Thermal characterization

Ultimately, in the thermal analysis of both the uncured formulation and the cured samples (Figure 83), an onset for the degradation of the samples above 400 °C is

Die approbierte gedruckte Originalversion dieser Dissertation ist an der TU Wien Bibliothek verfügbar.
The approved original version of this doctoral thesis is available in print at TU Wien Bibliothek.
TU WIEN Bibliothek Your knowledge hub

evident. This aligns well with the values reported in the literature.[184] Furthermore, the thermal stability of the pure HMDI sample is slightly enhanced compared to that of TMDI, possibly linked to the conversion rate. Additionally, it can be affirmed that under these measurement conditions, the photocatalyst $MeCpMn(CO)_3$ does not function as a thermal catalyst, as no exotherm was detected in the uncured formulations. Instead, only the evaporation of the respective monomer is observable.

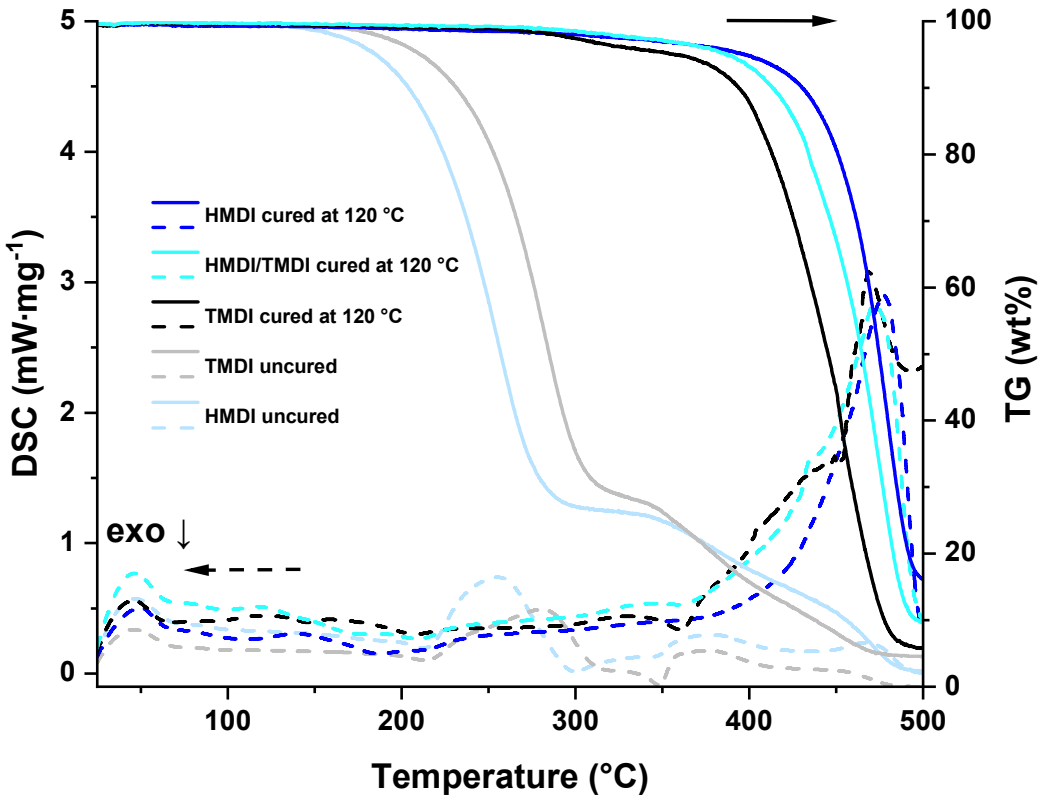

Figure 83: STA (TG solid line, DSC dashed line) of the uncured HMDI (light blue) and TMDI (grey) as well as the cured samples at 120 °C from HMDI (blue), HMDI/TMDI (turquoise) and TMDI (black).

3.4.3 Mechanical testing

Using the identical set of formulations, subsequent test specimens were prepared for dynamical mechanical thermal analysis (DMTA) and tensile tests. The DMTA measurements (Figure 84) reveal that HMDI exhibits a relatively broad peak in the loss modulus with a T_g around 70 °C. This, coupled with the high rubber plateau, suggests

Die approbierte gedruckte Originalversion dieser Dissertation ist an der TU Wien Bibliothek verfügbar.
The approved original version of this doctoral thesis is available in print at TU Wien Bibliothek.
TU WIEN Bibliothek Your knowledge hub

a highly crosslinked yet heterogeneous network. Conversely, TMDI has a T_g around 60 °C, a lower rubber plateau, but a narrow peak, indicating a more homogeneous network. Additionally, a shoulder around 120 °C is observed, potentially linked to the isomer composition (2,2,4 vs. 2,4,4-TMDI) of TMDI. As demonstrated earlier, steric hindrance in the β position hinders the reaction or makes this isocyanate group less accessible to the catalyst. This group in the 2,2,4-isomer could later trimerize, generating a higher T_g. In contrast, the mixture of the two shows a T_g at 75 °C with a high rubber plateau and a narrow peak, signifying a homogeneous and dense network, hence the high T_g. The shoulder that appears in TMDI is even more pronounced in the blend and is more of a peak at around 125 °C. A second cycle (after heating to 160 °C in the first cycle) of the same samples yields the expected T_g sequence of 80 °C for TMDI, 85 °C for the mixture, and 105 °C for pure HMDI (Figure 85). This demonstrates that a post-curing program can theoretically contribute to the enhancement of thermomechanical properties.

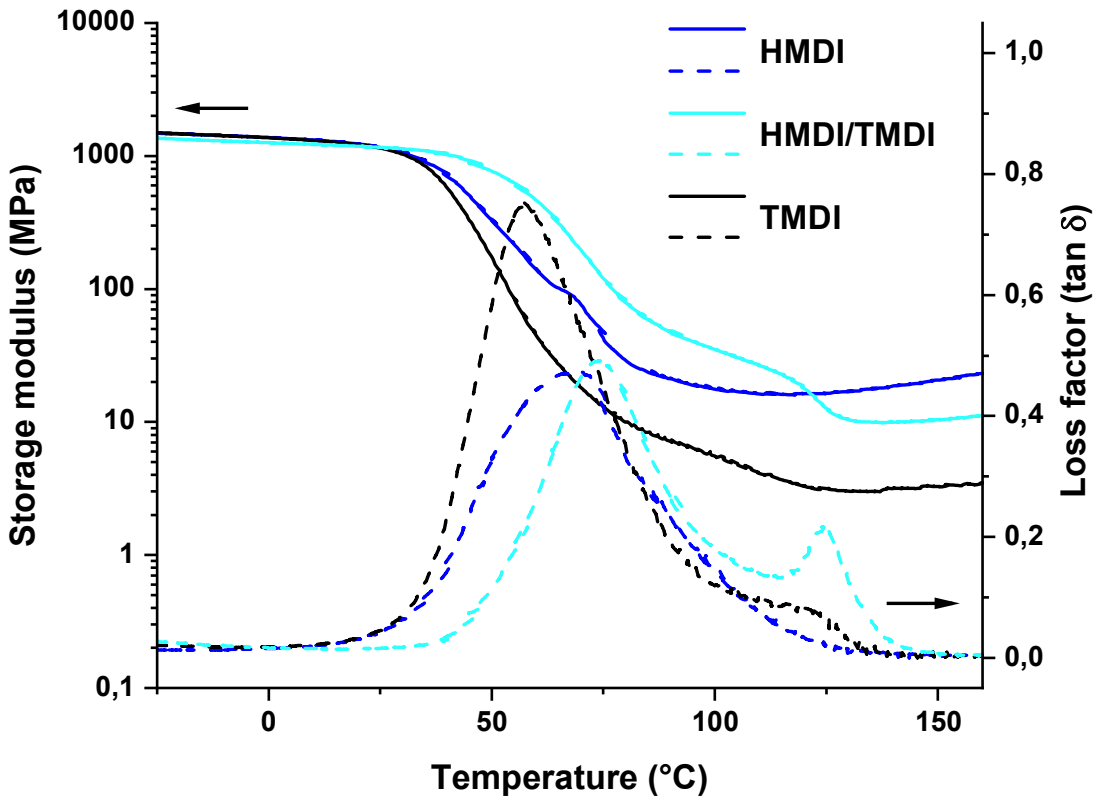

Figure 84: DMTA (storage modulus solid line, lass factor dashed line) measurements of the cured HMDI (blue), HMDI/TMDI (turquoise) and TMDI (black) specimen.

Die approbierte gedruckte Originalversion dieser Dissertation ist an der TU Wien Bibliothek verfügbar.
The approved original version of this doctoral thesis is available in print at TU Wien Bibliothek.
TU Bibliothek Your knowledge hub WIEN

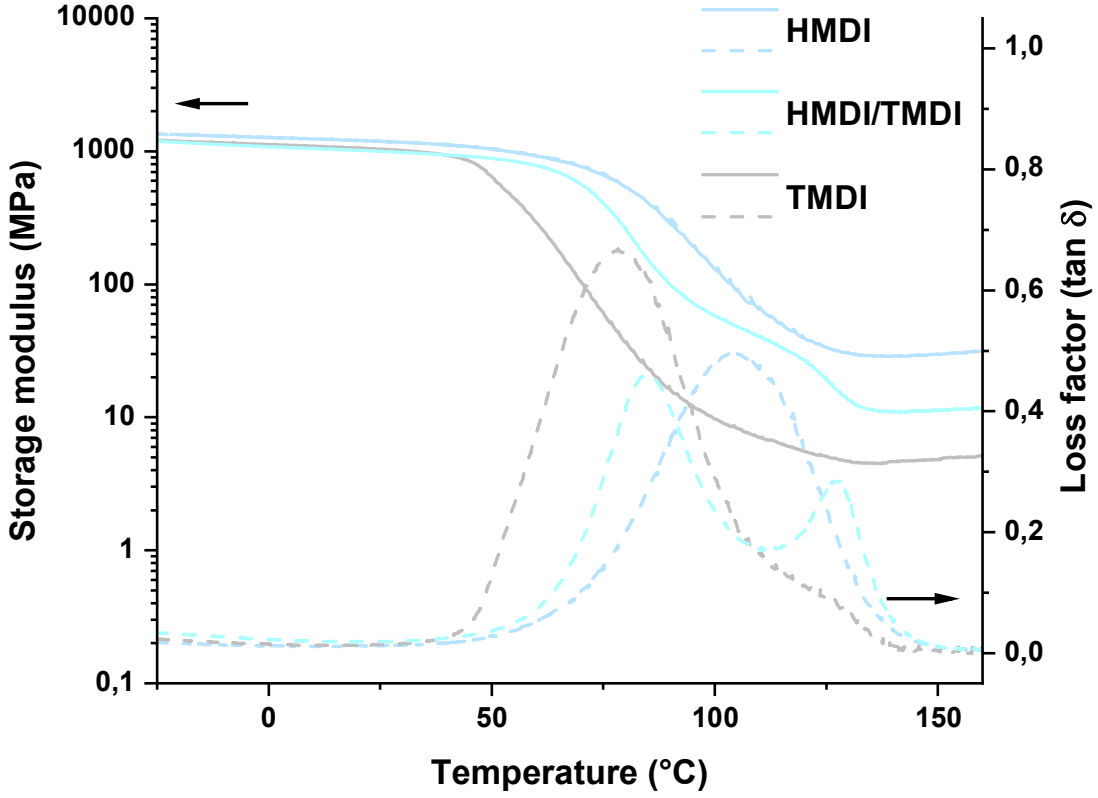

Figure 85: Second cycle of DMTA (storage modulus solid line, lass factor dashed line) measurements of the cured HMDI (light blue), HMDI/TMDI (light turquoise) and TMDI (grey) specimen.

The tensile tests (Figure 86) show an elevated tensile strength for TMDI. Despite TMDI having a lower network density and conversion, the steric demands of the methyl groups likely contribute to this enhancement. The elongation at break for the various samples falls within the error range of each other, thus approximately equal (Table 24). The blend of the two monomers falls within the range of TMDI in terms of tensile strength. Hence, a sufficient amount of TMDI is adequate to boost the tensile strength by just under 30 %.

Die approbierte gedruckte Originalversion dieser Dissertation ist an der TU Wien Bibliothek verfügbar.
The approved original version of this doctoral thesis is available in print at TU Wien Bibliothek.
TU WIEN Bibliothek Your knowledge hub

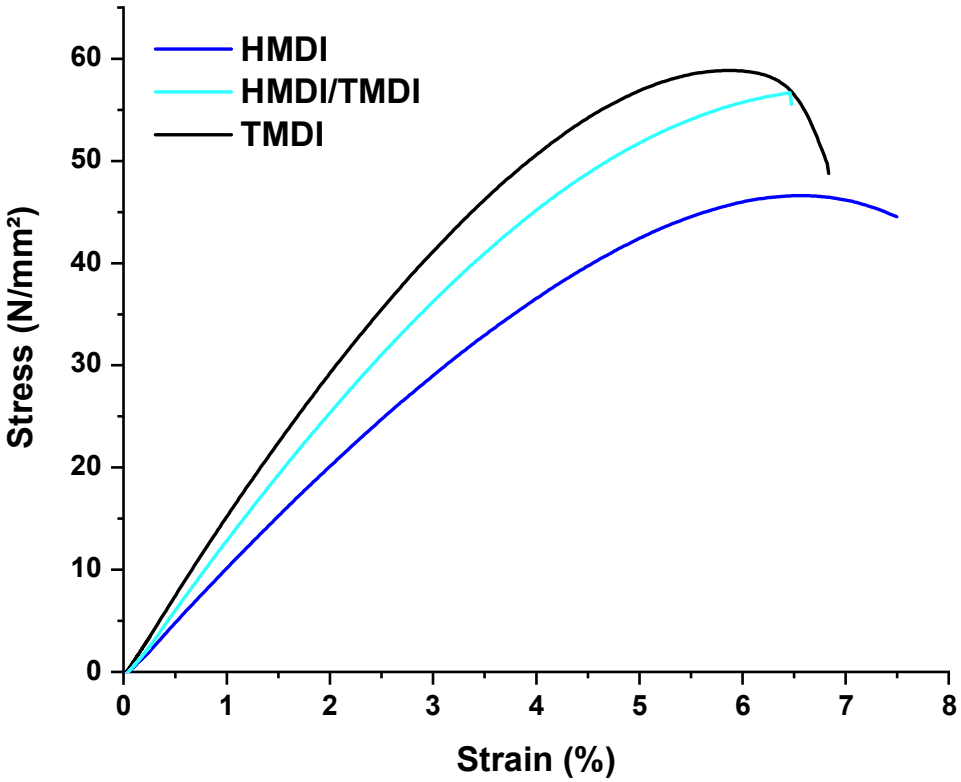

Figure 86: Tensile tests of the cured HMDI (blue), HMDI/TMDI (turquoise) and TMDI (black) specimen.

Table 24: Values of the tensile test of the cured HMDI, HMDI/TMDI and TMDI specimen.

	HMDI	HMDI/TMDI	TMDI
Tensile strength [MPa]	45 ± 2	59 ± 2	57 ± 4
Elongation at break [%]	7.9 ± 1.3	7.0 ± 1.0	7.5 ± 0.5

3.4.4 Printing & Coating

Unfortunately, the most reactive formulation, the HMDI formulation, did not show any polymerization in any kind during printing tests (even at lowest printing speed).

Die approbierte gedruckte Originalversion dieser Dissertation ist an der TU Wien Bibliothek verfügbar.
The approved original version of this doctoral thesis is available in print at TU Wien Bibliothek.
TU Bibliothek Your knowledge hub WIEN

Presumably, the reaction kinetics are not sufficient at the maximum printing temperature of 100 °C despite the high intensity of the laser. As described above, PIRs are regarded as one of the future innovations in the coating industry.[183] Light-induced curing is commercially interesting and feasible. Coatings were therefore considered as an reasonable alternative application option to the AM of PIRs.

Coating experiments were conducted using the formulations containing HMDI and TMDI on different substrates (glass and iron) with (Figure 87 left) and without doctor blade (Figure 87 right) were carried out. The tests conducted without a doctor blade were successful for both formulations, resulting in coating thicknesses ranging between 150-250 µm on metal and 350-500 µm on glass, with conversions falling within the range of the earlier findings from photo-DSC and IR spectroscopy (>90 % for HMDI, >75 % TMDI). However, when using a doctor blade, satisfactory results were achieved only with TMDI, owing to its slightly lower volatility. It is important to note that both HMDI and TMDI, as standalone substances, are unlikely to find significant industrial applications due to their volatility and toxicity. Nonetheless, this proof-of-concept lays the groundwork for future endeavors, such as exploring high molecular weight isocyanates, to facilitate the development of more practical coatings within the area of polyisocyanurates.

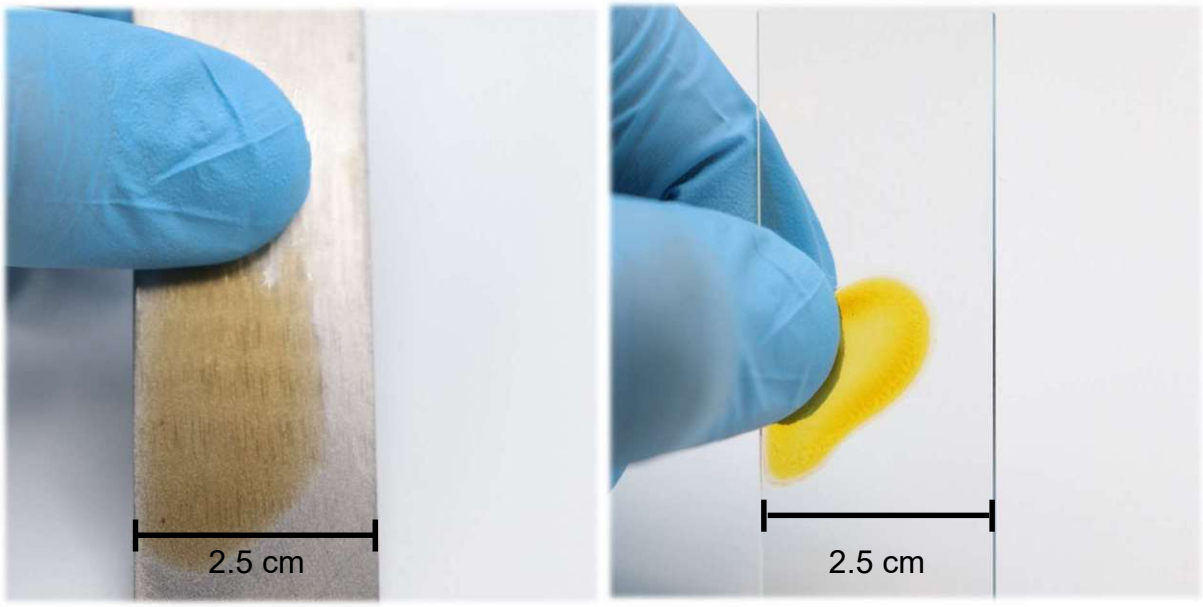

Figure 87: Coating of the cured TMDI formulation with doctor blade on metal (30 µm, left) and coating of the cured HMDI formulation without doctor blade on glass (right).

Die approbierte gedruckte Originalversion dieser Dissertation ist an der TU Wien Bibliothek verfügbar.
The approved original version of this doctoral thesis is available in print at TU Wien Bibliothek.
TU WIEN Bibliothek Your knowledge hub

SUMMARY

Liquid additive manufacturing technologies (L-AMTs) have brought significant advancements in the field of 3D printing of polymer materials, enabling exceptional precision and surface qualities. Stereolithography (SLA), in particular, has set a standard for accuracy in 3D printing, demanding rapid solidification of the liquid photopolymerizable formulation as the laser beam swiftly passes. Consequently, the progress made in recent decades has relied on the swift free-radical photopolymerization of acrylate and methacrylate monomers for effective layer-by-layer structuring.

As 3D printing has evolved from a rapid prototyping tool to a method for product manufacturing, challenges have emerged. The poor mechanical properties of photopolymer products have become increasingly problematic. Additionally, issues such as oxygen sensitivity and polymerization shrinkage in free radical photopolymerization have imposed limits on further enhancements in additive manufacturing processes. Therefore, the ongoing research has been focused on enabling SLA with a broader range of monomer classes, leveraging the advantageous polymerization chemistry offered by other materials.

However, the direct application of UV-induced curing of non-acrylic monomers in L-AMTs faced challenges due to limited reactivity at room temperature. Over the past decades, the workaround for the slow reactivity of other monomers often involved the addition of vinyl ether or (meth)acrylate monomers, resulting in dual-cure or hybrid systems as a compromise. Consequently, the actual direct 3D printing of other materials remained an elusive goal.

Recently, Hot Lithography, an innovative technique, has facilitated 3D printing through SLA at temperatures above 100 °C. This advancement not only addresses the challenge of high viscosity in methacrylate formulations, creating photopolymers with properties resembling thermoplastics, but also significantly reduces the activation energies associated with UV-induced polymerizations. The introduction of Hot Lithography has served as initiator for the research presented here, focusing on the photopolymerization of new monomers specifically for direct 3D printing. These monomers, previously unsuitable for additive manufacturing due to insufficient

Die approbierte gedruckte Originalversion dieser Dissertation ist an der TU Wien Bibliothek verfügbar.
The approved original version of this doctoral thesis is available in print at TU Wien Bibliothek.
TU Bibliothek Your knowledge hub WIEN

reactivity at room temperature, are now being explored under these elevated temperature conditions, to reach the additive manufacturing (AM) of high-performance polymers (HPPs).

In the first part of this work, phenolic resins and subsequently other formaldehyde-based resins were investigated for their suitability in photo-induced polycondensation for Hot Lithography. While most of these resins were not suitable for photo-induced curing, novolaks showed a promising performance in combination with p-octyloxyphenyl)phenyliodonium hexafluoroantimonate (I-Sb) as photoacidgenerator (PAG) and acid-labile curing agents (CAs) to produce a phenoplast (Scheme 18).

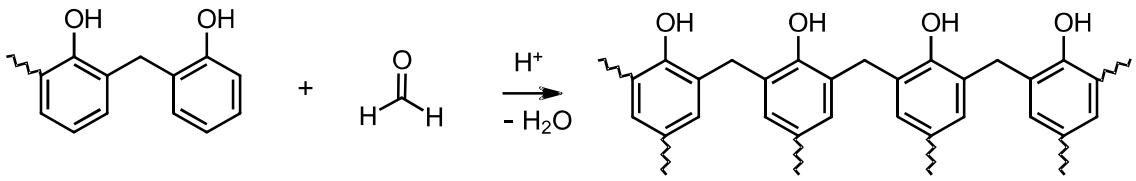

Scheme 18: Schematic curing of a novolak.

Several different substance classes could be analyzed as CA by means of photo-DSC at elevated temperatures. Further characterization using simultaneous thermal analysis (STA) showed that paraformaldehyde (PF), trioxymethylene diacetate (TOMDA) and, in a broader sense, 4-phenyl-1,3-dioxane (PD) and polyoxymethylene dimethyl ether ($PODE_5$) were possible sources of formaldehyde. These were also tested by means of printing tests in the Hot Lithography. Although the laser with its spectrum (375 nm) does not exactly match the absorption range of the initiator, it was still possible to work without a sensitizer. UV-Vis of the formulation showed a tail-out range up to 400 nm, making it presumably a self-sensitizing formulation. Due to long-term thermal stability and reaction temperature, the formulations with PF and TOMDA as CA (Figure 88) were printed into 3D objects.

Die approbierte gedruckte Originalversion dieser Dissertation ist an der TU Wien Bibliothek verfügbar.
The approved original version of this doctoral thesis is available in print at TU Wien Bibliothek.
TU WIEN Bibliothek Your knowledge hub

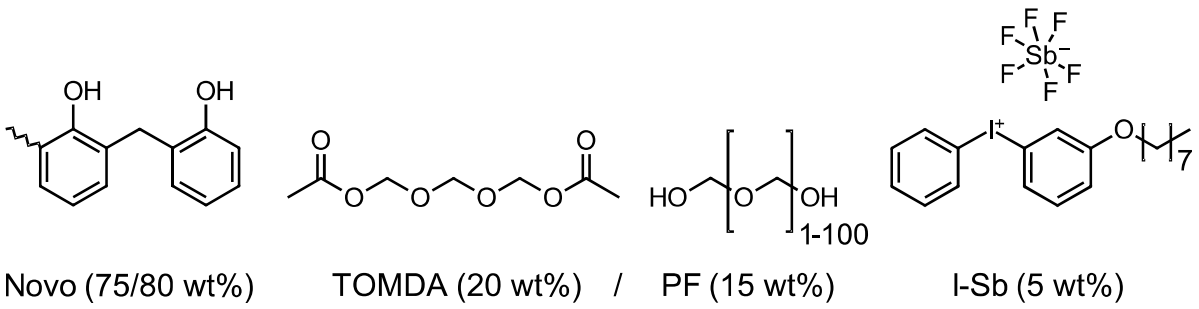

Figure 88: Composition of the end formulation for the curing of phenoplasts.

Post-curing of these objects showed no delamination, so that the (thermo-)mechanical properties of this material in this state could be investigated in the further course of the work. For comparison, mechanical test specimens of the same bulked-cured formulations were used. Tensile experiments generally show an increased strength for the added samples. In addition, TOMDA shows the significantly higher tensile strength of the two CAs. These trends can be explained primarily by the formation of voids in the mass-cured samples. Also, the PF samples showed significantly more voids due to evaporating water during the curing process from the polycondensation. The measurement using dynamic mechanical thermal analysis (DMTA) showed no difference in the course of the glass transition temperature (T_g) between the two manufacturing processes. However, the T_g of the PF sample (140 °C) was significantly higher than that of the TOMDA sample (95 °C). This results from the increased network density of the PF samples, which, however, fails due to the inhomogeneity of the network in the area of the tensile strength experiment. Consequently, additives were sought for the reduction of bubbles in the polymerization process. Two suitable candidates were found in the form of epoxides and anhydrides.

In conclusion, the custom-designed system introduced in this study, coupled with Hot Lithography, opens up the possibility to employ one of the earliest synthetic polymers with one of the most cutting-edge processing technologies.

In the second part of this work, the direct additive manufacturing of high-performing polycyanurates was investigated. These high-temperature materials undergo polyaddition by means of trimerization (Scheme 19) and offer T_g's of over 400 °C with perfect curing.

Die approbierte gedruckte Originalversion dieser Dissertation ist an der TU Wien Bibliothek verfügbar.
The approved original version of this doctoral thesis is available in print at TU Wien Bibliothek.
TU WIEN Bibliothek Your knowledge hub

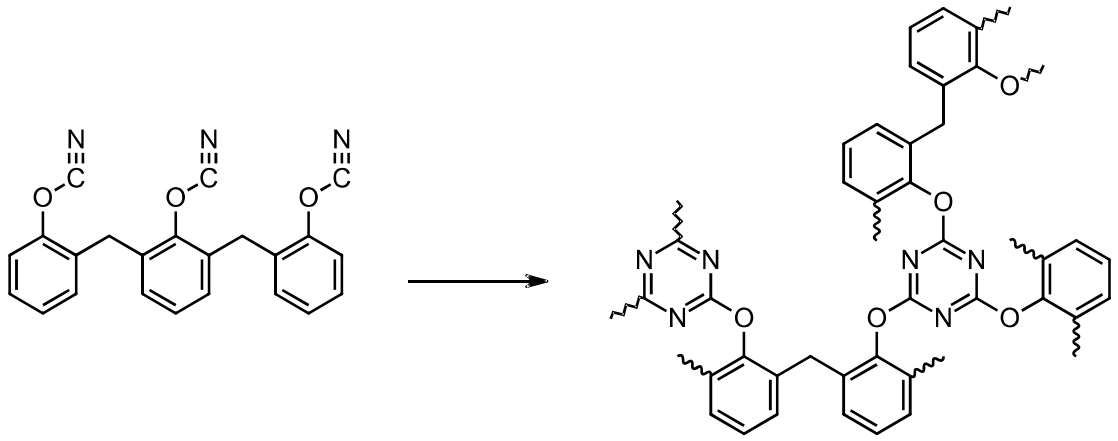

Scheme 19: Schematic curing of a cyanate ester.

Initially, a suitable photocatalyst was investigated, which cures the cyanate esters to a cyanurate network under irradiation with the co-catalyst nonylphenol (NP). Since metal transition catalysts are well-known substances in the curing of polycyanurates, it is not surprising that Irgacure 261 (I261), an iron-based photocatalyst, was the most suitable one.

With the help of Photo-DSC and subsequently IR and STA, the chemical background of the reaction was clarified and the reaction dynamics with regard to AM of the different monomers were analyzed. PT-30, a commercially available cyanate ester novolak with a conversion of just under 50 % after UV curing at 90 °C (85 % after post-curing) and a t_{max} of just under 20 s, was identified as a suitable base resin for the formulation (Figure 89) to be 3D printed.

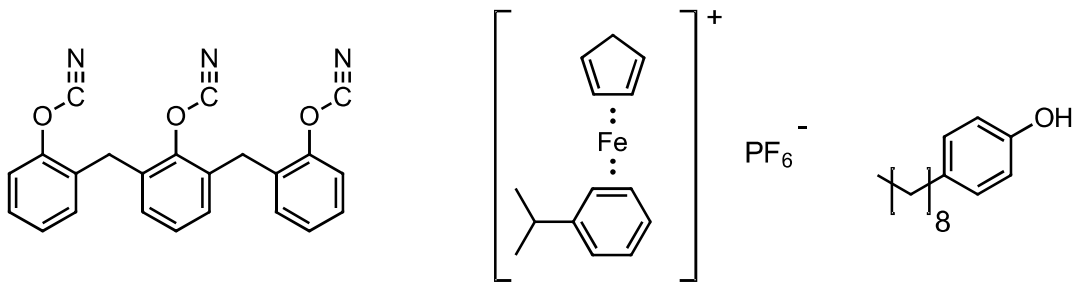

PT-30 (94 wt%) I261 (1 wt%) NP (5 wt%)

Figure 89: Composition of the end formulation for the curing of polycyanurates.

Die approbierte gedruckte Originalversion dieser Dissertation ist an der TU Wien Bibliothek verfügbar.
The approved original version of this doctoral thesis is available in print at TU Wien Bibliothek.
TU Bibliothek Your knowledge hub WIEN

Stability analyses using rheology and STA demonstrated sufficient temperature stability and completed the analysis of the formulation with regard to Hot Lithography. Despite significant overpolymerization, the 3D print produced a successful object and mechanical test specimens for further analysis. Post-curing showed no delamination and adequate layer thickness in microscopy. Various additive concepts were applied and analyzed to tackle overpolymerization. The complexation of the iron atom using 1,10-phenanthroline (phen) turned out to be the most effective approach.

The thermal-mechanical analysis showed not only that the post-curing program has a significant influence on the material properties, but also a T_g of almost 340 °C, resulting a material with thermal properties that hardly exist in the field of L-AMTs. Despite the significant deviation of the maximum achievable temperature in relation to the T_g, this material is an excellent HPP for AM.

In summary, a fundamental basis for the AM of polycyanurates was established. The analysis of the monomers shows that it is theoretically possible to tune the material properties exploiting photopolymerization techniques and consequently, 3D printing of polycyanurates is a valid option when using a suitable catalyst system and additives to prevent overpolymerization.

In the third and final part of this work, a favorable alternative to the polycyanurates was to be found by means of the poly-trimerization of isocyanates (Scheme 20). The resulting polyisocyanurates, known as a rigid component in e.g. construction foams and thermal insulation boards, are unknown as polymers in the literature on photochemistry.

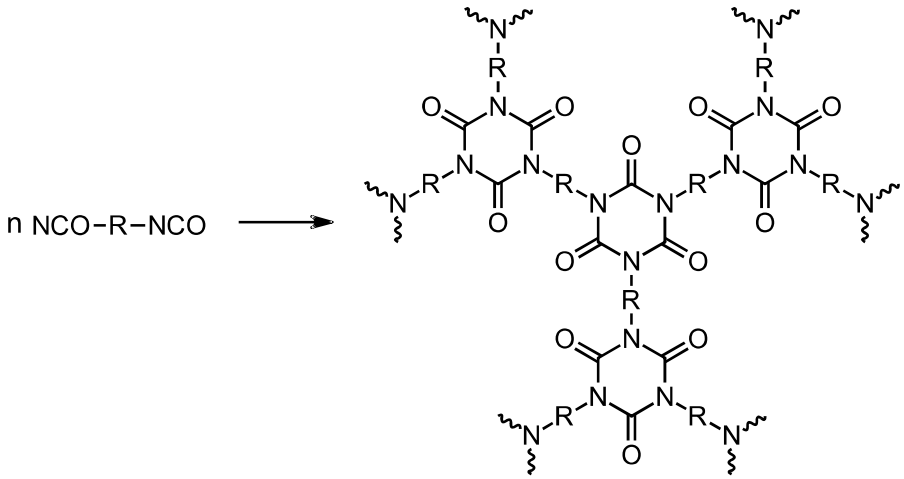

Scheme 20: Schematic curing of a isocyanate.

Die approbierte gedruckte Originalversion dieser Dissertation ist an der TU Wien Bibliothek verfügbar.
The approved original version of this doctoral thesis is available in print at TU Wien Bibliothek.
TU WIEN Bibliothek Your knowledge hub

Therefore, based on the photosynthesis of isocyanurates, a suitable photocatalyst was first found using photo-DSC. Due to the moderate performance of this photocatalyst, a suitable co-catalyst was required to accelerate the reaction kinetics. DBN, in the form of a previously formed adduct with hexamethylene diisocyanate (HMDI), acts as precisely this co-catalyst, accelerating the reaction from a t_{max} with 68 s to 33 s. Using this catalyst system in the end formulation (Figure 90), the photo-induced curing of primary isocyanates unhindered in the beta position to polyisocyanurates was achieved for the first time.

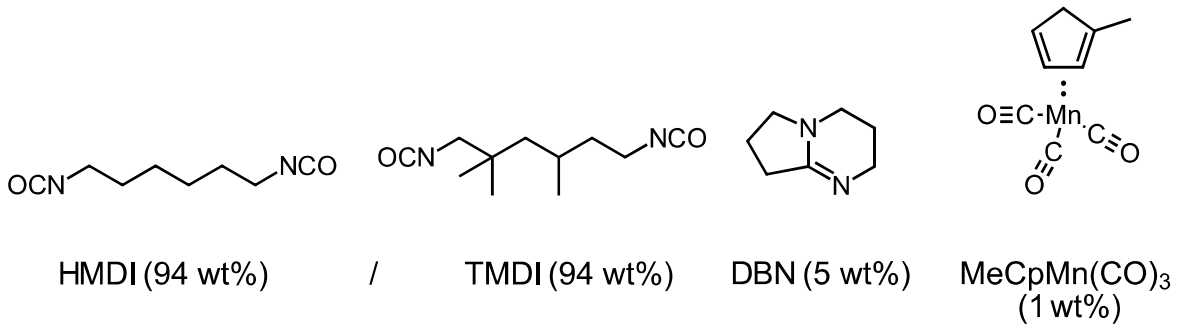

Figure 90: Composition of the end formulation for the curing of polyisocyanurates.

Following the previous chapter, photo-DSC was used to analyze the theoretical background of the reaction and the reaction kinetics as a function of the concentration of the reactants, temperature and intensity of the light source. A final evaluation by IR and STA of different monomers and their mixtures showed a conversion between 80-95 % at a moderate t_{max} >30 s. Despite the achieved acceleration, the reaction time was not sufficient to realize a successful 3D print. Consequently, the formulation was considered and tested as a valid option in the field of coating technology. Layer thicknesses of up to 500 µm make this system a proof-of-concept in the field of radiation-based coatings, with the disadvantage of the extreme volatility of isocyanates. However, the use of high molecular weight isocyanates with the right end groups could be used for a commercially successful concept.

Finally, the thermo-mechanical properties of the previously analyzed monomers were tested. With a T_g of 80-100 °C and tensile strength between 45 and 60 MPa at an elongation of almost 8 %, the polyisocyanurates offer very good properties for further research work.

Die approbierte gedruckte Originalversion dieser Dissertation ist an der TU Wien Bibliothek verfügbar.
The approved original version of this doctoral thesis is available in print at TU Wien Bibliothek.
TU WIEN Bibliothek Your knowledge hub

EXPERIMENTAL PART

1 Photo-chemically induced polycondensation of phenolic resins for additive manufacturing

1.2 Evaluation of curing agents

Novolak (Novo, from Süd-West Chemie) was mixed with p-(octyloxyphenyl)phenyliodonium hexafluoroantimonate (I-SB) as photoacid generator (PAG) (5 wt%). Before vigorously stirring, the formulation was heated to 80 °C to melt the Novo for better homogeneity. This formulation was then transferred in the heated stage to the crucible before measurement in simultaneous thermal analysis (STA) together with the pure Novo.

1.2.1 Hexamethylenetetraamine

Novo was mixed with I-SB as PAG (10 wt%) and hexamethylene tetraamine (Hexa) as curing agent (CA, 10 wt%). Before vigorously stirring, the formulation was heated to 80 °C to melt the Novo for better homogeneity. This formulation was then transferred in the heated stage to the crucible before measurement in Photo-DSC (320-500 nm, 80 °C, 60 mW·cm^{-2}).

1.2.2 Paraformaldehyde

Novo was mixed with I-SB as PAG (5 wt%) and paraformaldehyde (PF) as CA (15 wt%). Before vigorously stirring, the formulation was heated to 80 °C to melt the Novo for better homogeneity. This formulation was then transferred in the heated stage to the crucible before measurement in Photo-DSC (320-500 nm, 60-120 °C, 60 mW·cm^{-2}). Additionally, the at 90 °C cured sample was measured together with the plain formulation in STA.

Die approbierte gedruckte Originalversion dieser Dissertation ist an der TU Wien Bibliothek verfügbar.
The approved original version of this doctoral thesis is available in print at TU Wien Bibliothek.
TU WIEN Bibliothek Your knowledge hub

1.2.3 (Poly-)oxymethylene derivatives

1.2.3.1 n-Trioxane

Novo was mixed with I-SB as PAG (5-10 wt%) and trioxane as CA (10-20 wt%). Before vigorously stirring, the formulation was heated to 80 °C to melt the Novo for better homogeneity. This formulation was then transferred in the heated stage to the crucible before measurement in Photo-DSC (320-500 nm, 80 °C, 60 mW·cm^{-2}). Additionally, the cured sample with 20 wt% CA was measured together with the plain formulation in STA.

1.2.3.2 Polyoxymethylene

Novo was mixed with three different polyoxymethylenes (POMs, cryomilled before) as CA (15 wt%). Before vigorously stirring, the formulation was heated to 160 °C to melt the Novo and POM for better homogeneity. In a second step at 90 °C I-SB as PAG (5 wt%) was added. This formulation was then transferred in the heated stage to the crucible before measurement in Photo-DSC (320-500 nm, 80-100 °C, 60 mW·cm^{-2}).

1.2.3.3 Polyoxymethylene dimethyl ethers

Novo was mixed with I-SB as PAG (5 wt%) and polyoxymethylene diether (PODE$_5$) as CA (20 wt%). Before vigorously stirring, the formulation was heated to 80 °C to melt the Novo for better homogeneity. This formulation was then transferred in the heated stage to the crucible before measurement in Photo-DSC (320-500 nm, 70-90 °C, 60 mW·cm^{-2}).

1.2.3.4 Trioxymethylene diacetate

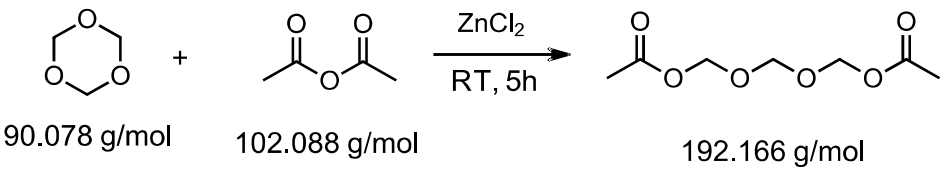

Scheme 21: Synthesis of TOMDA.

Die approbierte gedruckte Originalversion dieser Dissertation ist an der TU Wien Bibliothek verfügbar.
The approved original version of this doctoral thesis is available in print at TU Wien Bibliothek.

The synthesis of trioxymethylene diacetate (TOMDA, Scheme 21) was performed in accordance with the literature.[111] n-Trioxane (22.50 g, 250 mmol, 1 eq.) was mixed with freshly distilled acetic anhydride (25.55 g, 250 mmol, 1 eq.) and stirred with $ZnCl_2$ (1.02 g, 7.5 mmol) at 25 °C for 5 h. The mixture was washed with saturated $NaHCO_3$ solution followed by extraction with diethyl ether (3 x 200 mL). The organic phase was dried over Na_2CO_3. The solvent was evaporated and the crude product was purified by subsequent distillation to obtain the product as a clear liquid (40.12 g, 84 %).

^{1}H-NMR: (400 MHz, $CDCl_3$) δ (ppm): 5.36-5.33 (m, 4H, CH_2 oxymethylen-1); 4.93-4.87 (m, 2H,CH_2 oxymethylen-2); 2.10-2.09 (m, 6H, CH_3).

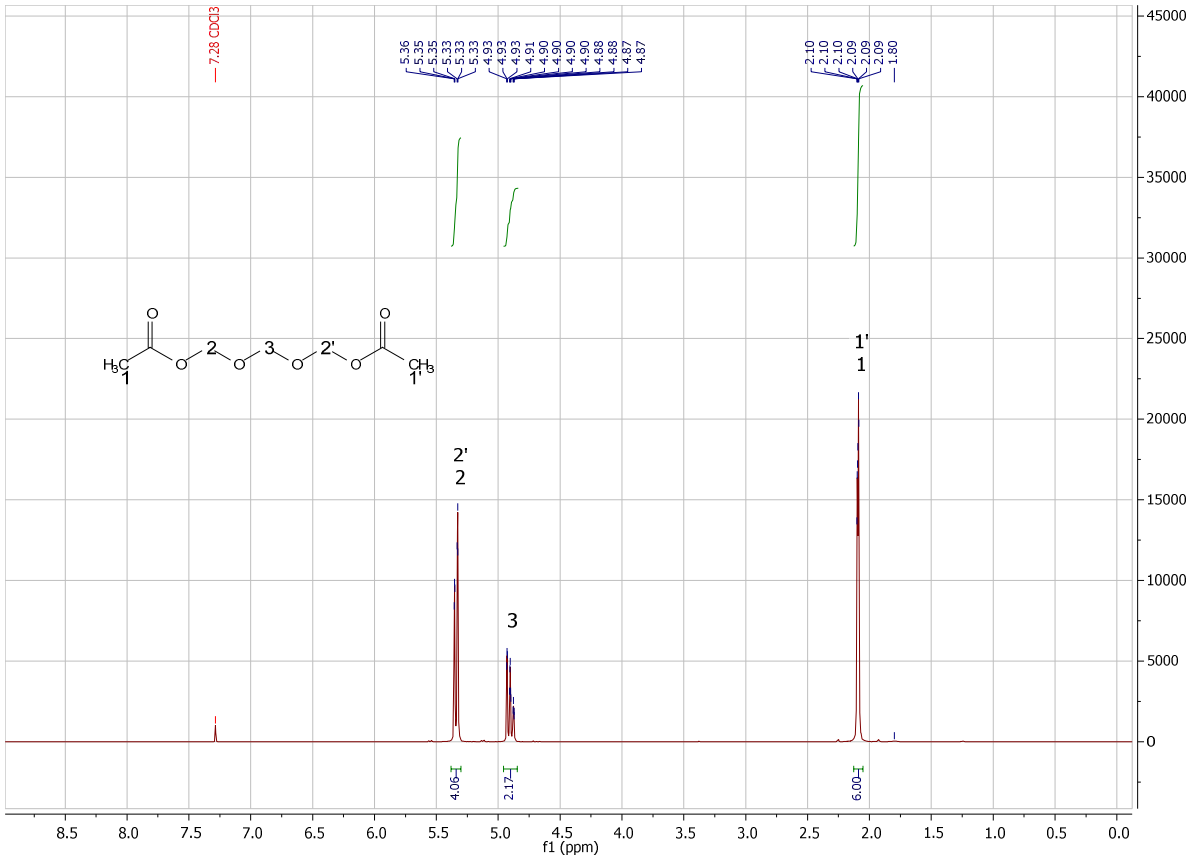

Figure 91: ^{1}H-NMR of TOMDA ($CDCl_3$, 400 MHz) δ (ppm): 5.36-5.33 (m, 4H, CH_2 oxymethylen-1); 4.93-4.87 (m, 2H,CH_2 oxymethylen-2); 2.10-2.09 (m, 6H, CH_3).

Novo was mixed with I-SB as PAG (5 wt%) and TOMDA as CA (20 wt%). Before vigorously stirring, the formulation was heated to 80 °C to melt the Novo for better homogeneity. This formulation was then transferred in the heated stage to the crucible before measurement in Photo-DSC (320-500 nm, 80-120 °C, 60 mW·cm^{-2}). Additionally, the at 90 °C cured sample was measured together with the plain formulation in STA.

Die approbierte gedruckte Originalversion dieser Dissertation ist an der TU Wien Bibliothek verfügbar.
The approved original version of this doctoral thesis is available in print at TU Wien Bibliothek.
TU Bibliothek Your knowledge hub WIEN

1.2.4 Formals

1.2.4.1 Glycerol formal

Novo was mixed with I-SB as PAG (5 wt%) and glycerol formal (GF) as CA (10-40 wt%). Before vigorously stirring, the formulation was heated to 80 °C to melt the Novo for better homogeneity. This formulation was then transferred in the heated stage to the crucible before measurement in Photo-DSC (320-500 nm, 100 °C, 60 mW·cm^{-2}). Additionally, the at 100 °C cured sample was measured together with the plain formulation in STA.

1.2.4.2 Cyclic Trimethylolpropane formal

Novo was mixed with I-SB as PAG (5 wt%) and cyclic trimethylolpropane formal (CMF) as CA (40 wt%). Before vigorously stirring, the formulation was heated to 80 °C to melt the Novo for better homogeneity. This formulation was then transferred in the heated stage to the crucible before measurement in Photo-DSC (320-500 nm, 100 °C, 60 mW·cm^{-2}).

1.2.4.3 4-Phenyl-1,3-dioxane

Novo was mixed with I-SB as PAG (10 wt%) and 4-phenyl-1,3-dioxane (PD) as CA (40 wt%). Before vigorously stirring, the formulation was heated to 80 °C to melt the Novo for better homogeneity. This formulation was then transferred in the heated stage to the crucible before measurement in Photo-DSC (320-500 nm, 60-120 °C, 60 mW·cm^{-2}). Additionally, the cured samples were measured together with the plain formulation in STA.

1.2.4.4 Pentaerythritol diformal

Pentaerythritol diformal (PDF) was prepared according to the literature.[116] Therefore pentaerythritol (40.8 g, 300 mmol, 1 eq.), paraformaldehyde (27.1 g, 900 mmol, 3 eq.) and sulfuric acid (conc., 0.23 g, 2.35 mmol) was heated in about 20 min to 145 °C and

Die approbierte gedruckte Originalversion dieser Dissertation ist an der TU Wien Bibliothek verfügbar.
The approved original version of this doctoral thesis is available in print at TU Wien Bibliothek.
TU WIEN Bibliothek Your knowledge hub

maintained at this temperature about 15 min. After cooling to room temperature the crystalline mass was extracted with hot petroleum (3 x 100 mL). Removing the solvent gave the diformal as a white solid (15.1 g, 35 %, m.p. 44-48 °C, Lit. 45-48 °C[116]). The H-NMR is displayed in Figure 92.

^{1}H-NMR: (400 MHz, $CDCl_3$) δ (ppm): 4.99-4.71 (m, 4H, 2xCH_2 oxymethylen); 3.69-3.57 (m, 8H, 4xCH_2).

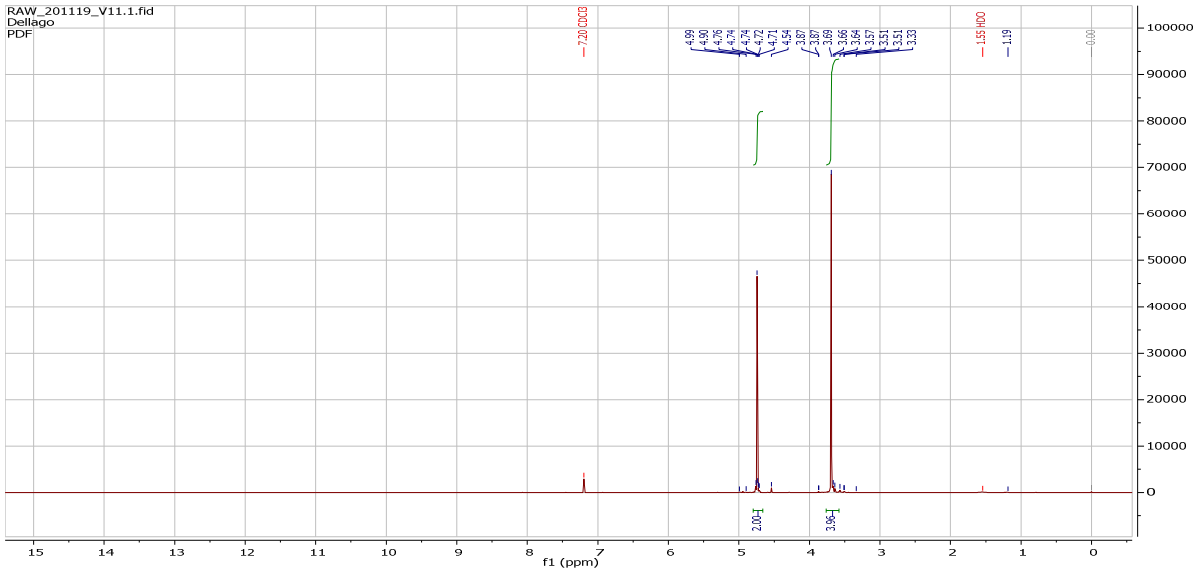

Figure 92: ^{1}H-NMR of PDF (400 MHz, $CDCl_3$) δ (ppm): 4.99-4.71 (m, 4H, 2xCH_2 oxymethylen); 3.69-3.57 (m, 8H, 4xCH_2).

Novo was mixed with I-SB as PAG (5 wt%) and PDF as CA (20 wt%). Before vigorously stirring, the formulation was heated to 80 °C to melt the Novo for better homogeneity. This formulation was then transferred in the heated stage to the crucible before measurement in Photo-DSC (320-500 nm, 80-120 °C, 60 mW·cm^{-2}).

1.2.5 Miscellaneous curing agents

1.2.5.1 Furfuryl alcohol

Novo was mixed with I-SB as PAG (5 wt%) and furfuryl alcohol (FA) as CA (40 wt%). Before vigorously stirring, the formulation was heated to 80 °C to melt the Novo for better homogeneity. This formulation was then transferred in the heated stage to the crucible before measurement in Photo-DSC (320-500 nm, 100 °C, 60 mW·cm^{-2}).

Die approbierte gedruckte Originalversion dieser Dissertation ist an der TU Wien Bibliothek verfügbar.
The approved original version of this doctoral thesis is available in print at TU Wien Bibliothek.
TU Bibliothek Your knowledge hub WIEN

1.2.5.2 Salicylaldehyde

Novo was mixed with I-SB as PAG (5 wt%) and salicylaldehyde (SA) as CA (40 wt%). Before vigorously stirring, the formulation was heated to 80 °C to melt the Novo for better homogeneity. This formulation was then transferred in the heated stage to the crucible before measurement in Photo-DSC (320-500 nm, 100 °C, 60 mW·cm^{-2}).

1.3 3D printing of the phenolic formulations via Hot Lithography

The general production of the formulations: Novo was mixed with I-SB as PAG (5 wt%) and the different CAs. Before vigorously stirring, the formulation was heated to 80 °C to melt the Novo for better homogeneity.

The hot formulation was subjected to the printer. The printing tests were completed at 70-80 °C with a laser speed of 100 mm·s^{-1}. Printing itself with a scan speed of 1 m·s^{-1}, a energy intensity of 2320 mJ·cm^{-1}, and a layer thickness of 50 µm.

1.4 Comparative mechanical testing of the 3D printed and bulk cured materials

For (thermo)mechanical tests, all formulations (prepared like 1.3) were poured into silicone molds (5 × 2 × 40 mm^3 for DMTA, ISO527 test specimens 5b dumbbell-shaped with a total length of 35 mm, and a parallel constriction region with dimensions of 2 × 2 × 12 mm^3 for tensile tests). The resins were cured with a UV-oven. The samples were irradiated at 80 °C for 15 min on each side and afterward polished with sandpaper to ensure uniform geometries.

1.5 Evaluation of additives to prevent bubble formation

Novo was mixed with I-SB as PAG (5 wt%), TOMDA as CA (20 wt%) and acetic anhydride (AA) as stabilizer (20 wt%). Before vigorously stirring, the formulation was

Die approbierte gedruckte Originalversion dieser Dissertation ist an der TU Wien Bibliothek verfügbar.
The approved original version of this doctoral thesis is available in print at TU Wien Bibliothek.
TU Bibliothek Your knowledge hub WIEN

heated to 80 °C to melt the Novo for better homogeneity. This formulation was then transferred in the heated stage to the crucible before measurement in Photo-DSC (320-500 nm, 120 °C, 60 mW·cm^{-2}).

For the epoxy formulations, Novo was mixed with I-SB as PAG (5 wt%), TOMDA as CA (20 wt%) and the different epoxy resins as co-resin (37.5 wt%). Before vigorously stirring, the formulation was heated to 80 °C to melt the Novo for better homogeneity. This formulation was then transferred in the heated stage to the crucible before measurement in Photo-DSC (320-500 nm, 80-120 °C, 60 mW·cm^{-2}). Additionally, the cured sample of epoxidized novolak (EpNovo) was measured in STA. The hot formulation was subjected to the printer. The printing tests were completed at 100 °C with a laser speed of 100 mm·s^{-1}.

1.6 Further tested formaldehyde-based resins

1.6.1 Resole

Resole (from Süd-West Chemie) was mixed with I-SB as PAG (5 wt%). After vigorously stirring the formulation was transferred to the crucible before measurement in Photo-DSC (320-500 nm, 100 °C, 60 mW·cm^{-2}).

1.6.2 Urea resin

The urea resin (from Deuteron) was mixed with I-SB as PAG (5 wt%) and PF as CA (15 wt%). After vigorously stirring the formulation was transferred to the crucible before measurement in Photo-DSC (320-500 nm, 100 °C, 60 mW·cm^{-2}).

For the co-resin formulations, Novo was mixed with I-SB as PAG (5 wt%), PF as CA (15 wt%) and the urea resin as co-resin (10-30 wt%). Before vigorously stirring, the formulation was heated to 80 °C to melt the Novo for better homogeneity. This formulation was then transferred in the heated stage to the crucible before measurement in Photo-DSC (320-500 nm, 80-120 °C, 60 mW·cm^{-2}).

Die approbierte gedruckte Originalversion dieser Dissertation ist an der TU Wien Bibliothek verfügbar.
The approved original version of this doctoral thesis is available in print at TU Wien Bibliothek.
TU WIEN Bibliothek Your knowledge hub

1.6.3 Melamine resin

The melamine resin (from Süd-West Chemie) was mixed with I-SB as PAG (5 wt%) and PF as CA (15 wt%). After vigorously stirring the formulation was transferred to the crucible before measurement in Photo-DSC (320-500 nm, 100 °C, 60 mW·cm^{-2}).

For the co-resin formulations, Novo was mixed with I-SB as PAG (5 wt%), PF as CA (15 wt%) and the melamine resin as co-resin (10-30 wt%). Before vigorously stirring, the formulation was heated to 80 °C to melt the Novo for better homogeneity. This formulation was then transferred in the heated stage to the crucible before measurement in Photo-DSC (320-500 nm, 80-120 °C, 60 mW·cm^{-2}).

1.6.4 Furane resin

FA was mixed with I-SB as PAG (5 wt%). After vigorously stirring the formulation was transferred to the crucible before measurement in Photo-DSC (320-500 nm, 60-100 °C, 60 mW·cm^{-2}).

For the furan resin (FRA, from Albert-Hüttens GmbH), FRA was mixed with I-SB as PAG (5 wt%). After vigorously stirring the formulation was transferred to the crucible before measurement in Photo-DSC (320-500 nm, 80-120 °C, 60 mW·cm^{-2}). Additionally, the at 100 °C cured sample was measured together with the plain formulation in STA. The hot formulation was subjected to the printer. The printing tests were completed at 100 °C with a laser speed of 100 mm·s^{-1}.

Die approbierte gedruckte Originalversion dieser Dissertation ist an der TU Wien Bibliothek verfügbar.
The approved original version of this doctoral thesis is available in print at TU Wien Bibliothek.
TU WIEN Bibliothek Your knowledge hub

2 Photo-induced catalytic poly-trimerization of cyanate ester to form high-performance polycyanurates for additive manufacturing

2.2 Evaluation of photocatalysts

Novolak cyanate ester (PT-30 from Arxada) was mixed with nonylphenol (NP) (5 wt%) as co-catalyst and 1 wt% of the respective photocatalyst. Before vigorously stirring, the formulation was heated to 80 °C to melt PT-30 for better homogeneity. This formulation was then transferred in the heated stage to the crucible before measurement in Photo-DSC (320-500 nm, 100 °C, 60 mW·cm^{-2}).

2.3 Photopolymerization of a phenolic novolak cyanate ester

2.3.1 Theoretical investigation of cyanurates

Phenyl cyanate was mixed with NP (5 wt%) as co-catalyst and 1 wt% Irgacure 261 (I261) as photocatalyst. After vigorously stirring the formulation was transferred to the crucible before measurement in Photo-DSC (320-500 nm, 100 °C, 60 mW·cm^{-2}). The plain formulation (Figure 93 & Figure 95) as well as the cured product (Figure 94 & Figure 96) have been analysed via NMR.

Phenyl cyanate:

^{1}H-NMR: (600 MHz, $CDCl_3$) δ (ppm): 7.45-7.20 (m, 5H, aromat. H).

^{13}C-NMR: (600 MHz, $CDCl_3$) δ (ppm): 109 (cyanate), 115, 126, 130, 153 (phenolic).

2,4,6-Triphenoxy-1,3,5-triazine:

^{1}H-NMR: (600 MHz, $CDCl_3$) δ (ppm): 7.40-7.05 (m, 5H, aromat. H).

^{13}C-NMR: (600 MHz, $CDCl_3$) δ (ppm): 121, 126, 129, 151 (phenolic), 174 (triazine).

Die approbierte gedruckte Originalversion dieser Dissertation ist an der TU Wien Bibliothek verfügbar.
The approved original version of this doctoral thesis is available in print at TU Wien Bibliothek.
TU WIEN Bibliothek Your knowledge hub

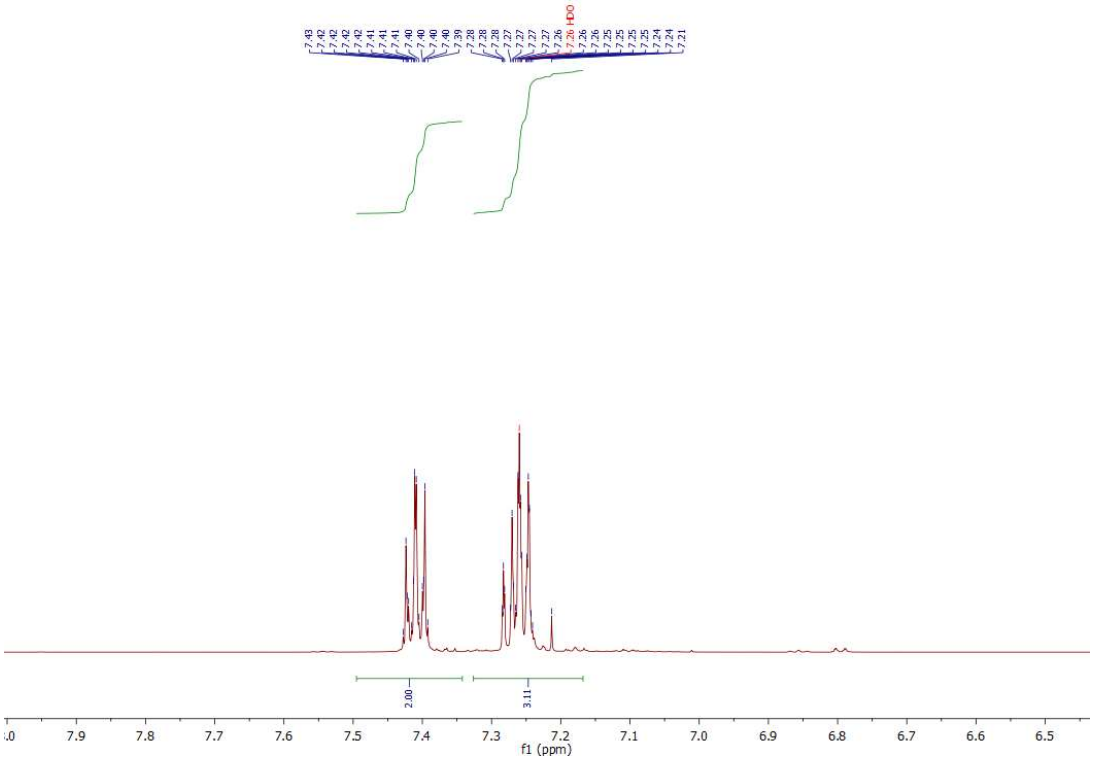

Figure 93: ^{1}H-NMR of phenyl cyanate ($CDCl_3$, 600 MHz) δ: 7.45-7.20 (m, 5H, aromat. H).

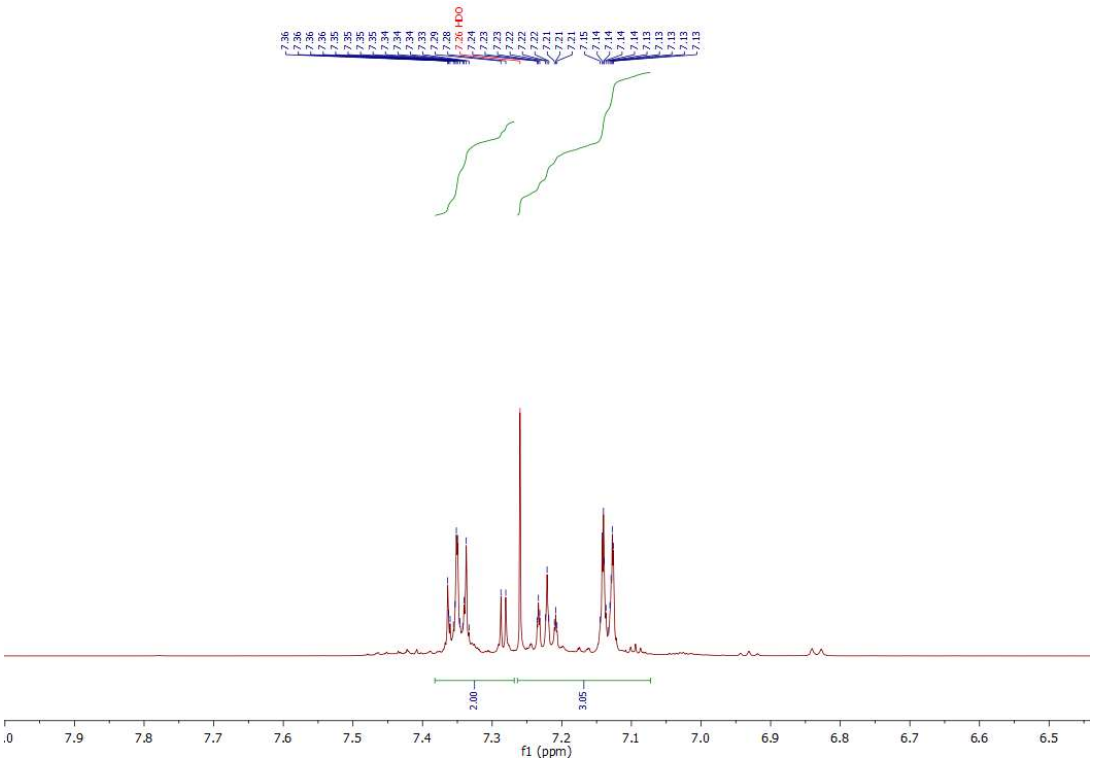

Figure 94: ^{1}H-NMR of 2,4,6-triphenoxy-1,3,5-triazine ($CDCl_3$, 600 MHz) δ: 7.40-7.05 (m, 5H, aromat. H).

Die approbierte gedruckte Originalversion dieser Dissertation ist an der TU Wien Bibliothek verfügbar.
The approved original version of this doctoral thesis is available in print at TU Wien Bibliothek.
TU WIEN Bibliothek Your knowledge hub

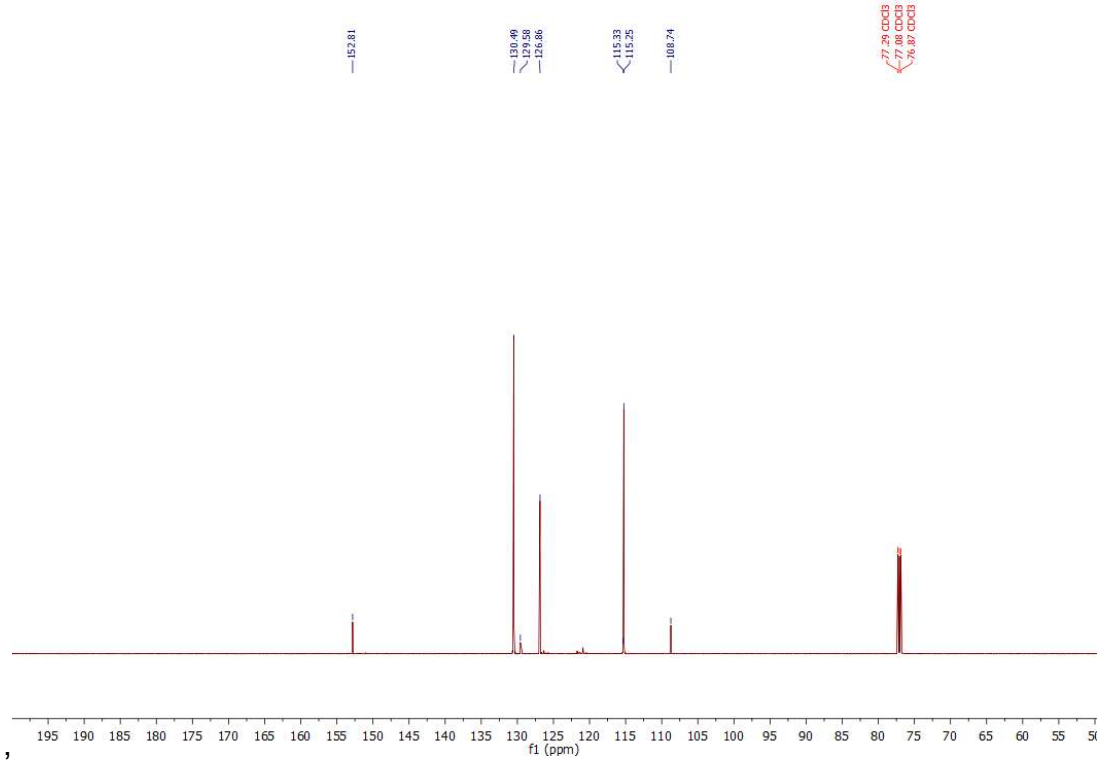

Figure 95: ^{13}C-NMR of phenyl cyanate ($CDCl_3$, 600 MHz) δ: 109 (cyanate), 115, 126, 130, 153 (phenolic).

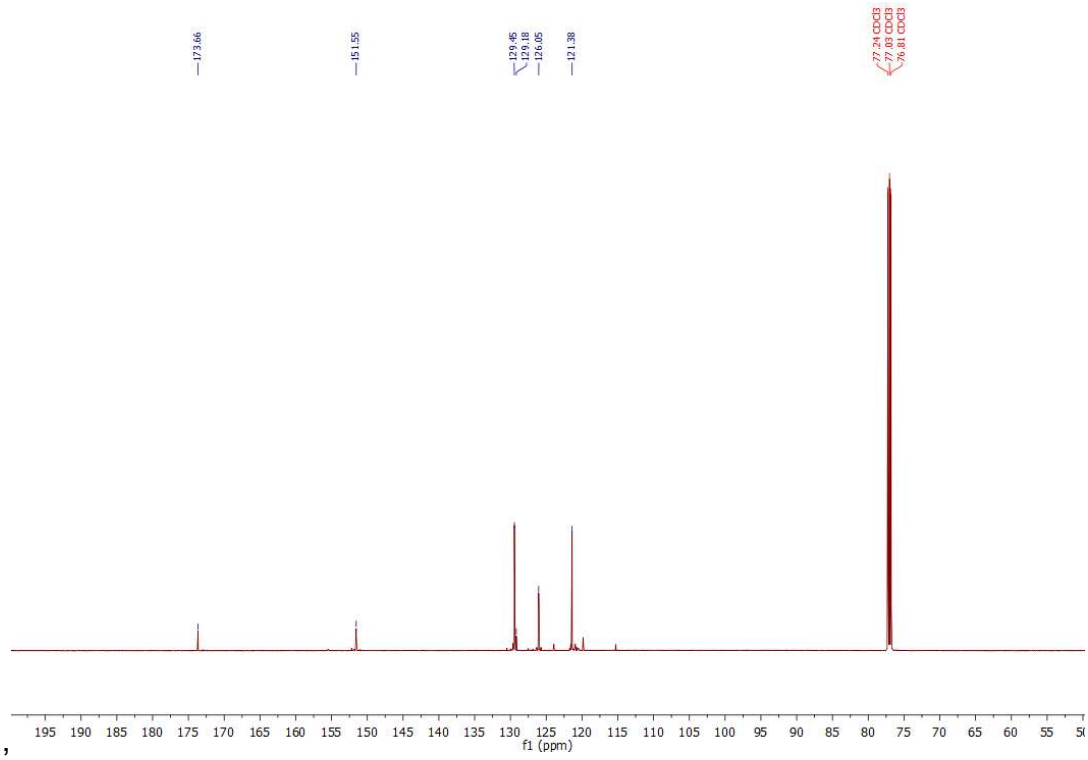

Figure 96: ^{13}C-NMR of 2,4,6-triphenoxy-1,3,5-triazine ($CDCl_3$, 600 MHz) δ: 121, 126, 129, 151 (phenolic), 174 (triazine).

Die approbierte gedruckte Originalversion dieser Dissertation ist an der TU Wien Bibliothek verfügbar.
The approved original version of this doctoral thesis is available in print at TU Wien Bibliothek.
TU Bibliothek Your knowledge hub WIEN

2.3.2 Determination of the conversion

2.3.2.1 Photo-DSC

PT-30 was mixed with NP (5 wt%) as co-catalyst and 1 wt% of the respective photocatalyst. Before vigorously stirring, the formulation was heated to 80 °C to melt PT-30 for better homogeneity. This formulation was then transferred in the heated stage to the crucible before measurement in Photo-DSC (320-500 nm, 80-120 °C, 60 mW·cm^{-2}).

2.3.2.2 IR

The in 2.3.2.1 produced formulation and samples, have been measured via transmission infrared spectroscopy. Before that, the cured samples have been milled via cryomill.

2.3.3 Thermal characterization

The in 2.3.2.1 produced formulation and samples, have been measured via STA.

2.4 Photopolymerization of a bisphenol based cyanate ester

2.4.1 Photo-DSC & Conversion

Bisphenol A dicyanate ester (BADCy from TCI) was mixed with NP (5 wt%) as co-catalyst and 1 wt% of the respective photocatalyst. Before vigorously stirring, the formulation was heated to 90 °C to melt BADCy for better homogeneity. This formulation was then transferred in the heated stage to the crucible before measurement in Photo-DSC (320-500 nm, 80-100 °C, 60 mW·cm^{-2}). The produced formulation and samples have been measured via transmission infrared spectroscopy. Before that, the cured samples have been milled via cryomill.

Die approbierte gedruckte Originalversion dieser Dissertation ist an der TU Wien Bibliothek verfügbar.
The approved original version of this doctoral thesis is available in print at TU Wien Bibliothek.
TU WIEN Bibliothek Your knowledge hub

2.4.2 Thermal characterization

The in 2.4.1 produced formulation and samples, have been measured via STA.

2.5 Photopolymerization of a mixture of PT-15 and BADCy

2.5.1 Photo-DSC

A mixture of novolak cyanate ester and bisphenol A dicyanate ester (LVT-50 from Arxada) was mixed with NP (5 wt%) as co-catalyst and 1 wt% of the respective photocatalyst. Before vigorously stirring, the formulation was heated to 90 °C to melt LVT-50 for better homogeneity. This formulation was then transferred in the heated stage to the crucible before measurement in Photo-DSC (320-500 nm, 80-100 °C, 60 mW·cm^{-2}).

2.5.2 Thermal characterization

The in 2.5.1 produced formulation and samples, have been measured via STA.

2.6 3D printing of the PT-30 formulation via Hot Lithography

2.6.1 Stability of the formulation

PT-30 was mixed with NP (5 wt%) as co-catalyst and 1 wt% of the respective photocatalyst. Before vigorously stirring, the formulation was heated to 80 °C to melt PT-30 for better homogeneity. The at 100 °C stored formulation was measured via STA and rheometer.

2.6.2 Printing & Overpolymerization

PT-30 was mixed with NP (5 wt%) as co-catalyst and 1 wt% of the respective photocatalyst. The formulation was homogenized by means of ultrasonic bath and kept

Die approbierte gedruckte Originalversion dieser Dissertation ist an der TU Wien Bibliothek verfügbar.
The approved original version of this doctoral thesis is available in print at TU Wien Bibliothek.
TU WIEN Bibliothek Your knowledge hub

at least 0.5 h at 80 °C in the vacuum oven. A printing temperature of 90 °C, a printing speed of 1 m·s^{-1} with 10 repetitions, and a layer thickness of 50 µm were selected.

For the overpolymerization experiments to the base formulation with 1 wt% I261 and 5 wt% NP, stabilizer was added according to the molar amount of I261 in a one-to-one molar ratio. For the experiments, the respective samples were covered with a mask at 90 °C and irradiated with light (wavelength 320-500 nm, 60 mW·cm^{-2}) via a collimator for 20 s. The sample was then kept in a dark oven at 90 °C for 3 h. The formulation with phen was printed as described before.

2.7 Comparative mechanical testing of the 3D printed and bulk cured materials

PT-30 was mixed with NP (5 wt%) as co-catalyst and 1 wt% of the respective photocatalyst. The formulation was homogenized by means of ultrasonic bath and kept at least 0.5 h at 80 °C in the vacuum oven. The specimens for mechanical testing were prepared by thermal curing of the formulations in silicon molds (for DMTA: 5 x 2 x 40 mm^3) The PT-30 formulation were preheated to 90 °C and filled into a preheated silicon-mold (90 °C) and put in the oven for 24 h at 120 °C. The preparation of the specimens was completed with a post-processing program in an oven.

Die approbierte gedruckte Originalversion dieser Dissertation ist an der TU Wien Bibliothek verfügbar.
The approved original version of this doctoral thesis is available in print at TU Wien Bibliothek.
TU WIEN Bibliothek Your knowledge hub

3 Photo-induced catalytic poly-trimerization of isocyanates to form polyisocyanurates

3.2 Basic studies

3.2.1 Screening of photocatalysts

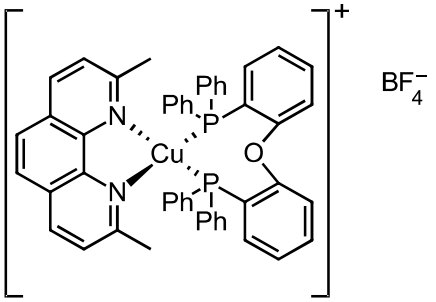

Figure 97: Cu(neocuproine)(DPEphos)

Cu(neocuproine)(DPEphos)$_2$ (Figure 97) was synthesized according to literature.[207] A mixture of [Cu(CH$_3$CN)4]BF$_4$ (310 mg, 1 mmol) and bis[2-(diphenylphosphino)phenyl] ether (540 mg, 1 mmol) in 200 mL of dichloromethane was stirred at 25 °C for 2 h and then treated with a solution of neocuproine (208 mg, 1 mmol) in 50 mL of dichloromethane. This reaction mixture was stirred at room temperature overnight and the solution was concentrated to ca. 15 mL. Addition of pentane precipitated the complex which was filtered off, washed several times with pentane and dried under vacuum. The title complex was isolated as a light yellow solid in 87% yield.

^{1}H-NMR (CDCl$_3$,400 MHz) δ(ppm): 2.45 (s, 6H), 6.94-7.05 (m, 18H), 7.17-7.22 (m, 8H), 7.34 (m, 2H), 7.63 (m, 2H), 7.86 (s, 2H), 8.40 (m, 2H);

Afterwards 5 mol% of each catalyst was mixed with the corresponding monomer. After vigorously stirring, the formulation was measured in Photo-DSC (320-500 nm, 80-100 °C, 60 mW·cm^{-2}).

Die approbierte gedruckte Originalversion dieser Dissertation ist an der TU Wien Bibliothek verfügbar.
The approved original version of this doctoral thesis is available in print at TU Wien Bibliothek.
TU WIEN Bibliothek Your knowledge hub

3.2.2 Screening of bases

5 mol% of co-catalyst (bases or photobases) was mixed with hexamethylene diisocyanate (HMDI) and subjected to heating and ultrasonic bath treatment. After cooling 5 mol% of $MeCpMn(CO)_3$ (or the other photocatalyst) was incorporated, the formulation was vigorously stirred and measured in Photo-DSC (320-500 nm, 80-100 °C, 60 mW·cm^{-2}).

3.2.3 Screening of monomers

5 mol% of 1,5-Diazabicyclo(4.3.0)non-5-en (DBN) was mixed with the respective monomer and subjected to heating and ultrasonic bath treatment. After cooling 5 mol% of $MeCpMn(CO)_3$ was incorporated, the formulation was vigorously stirred and measured in Photo-DSC (320-500 nm, 80-100 °C, 60 mW·cm^{-2}).

3.2.4 Theoretical investigation of isocyanurates

Hexamethylene isocyanate (HMI) was combined with 5 mol% DBN and subsequently with 1 mol% $MeCpMn(CO)_3$. The formulation was vigorously stirred and measured in Photo-DSC (320-500 nm, 80-100 °C, 60 mW·cm^{-2}). The plain formulation (Figure 98) as well as the cured product (Figure 99) have been analyzed via NMR.

HMI:

^{1}H-NMR: ($CDCl_3$, 400 MHz) δ (ppm): 3.28 (t, 2H, C**H$_2$**-NCO), 1.61 (m, 2H, C**H$_2$**-CH$_2$-NCO), 1.38-1.31 (m, 6H, 3xC**H$_2$**), 0.90 (m, 3H, C**H$_3$**).

Trihexyl isocyanurate:

^{1}H-NMR: ($CDCl_3$, 400 MHz) δ (ppm): 3.86 (m, 6H, 3xC**H$_2$**-triazine), 1.64-1.51 (m, 6H, 3xC**H$_2$**-CH$_2$-triazine), 1.38-1.25 (m, 18H, 9xC**H$_2$**), 0.88 (m, 9H, 3xC**H$_3$**).

Die approbierte gedruckte Originalversion dieser Dissertation ist an der TU Wien Bibliothek verfügbar.
The approved original version of this doctoral thesis is available in print at TU Wien Bibliothek.
TU WIEN Bibliothek Your knowledge hub

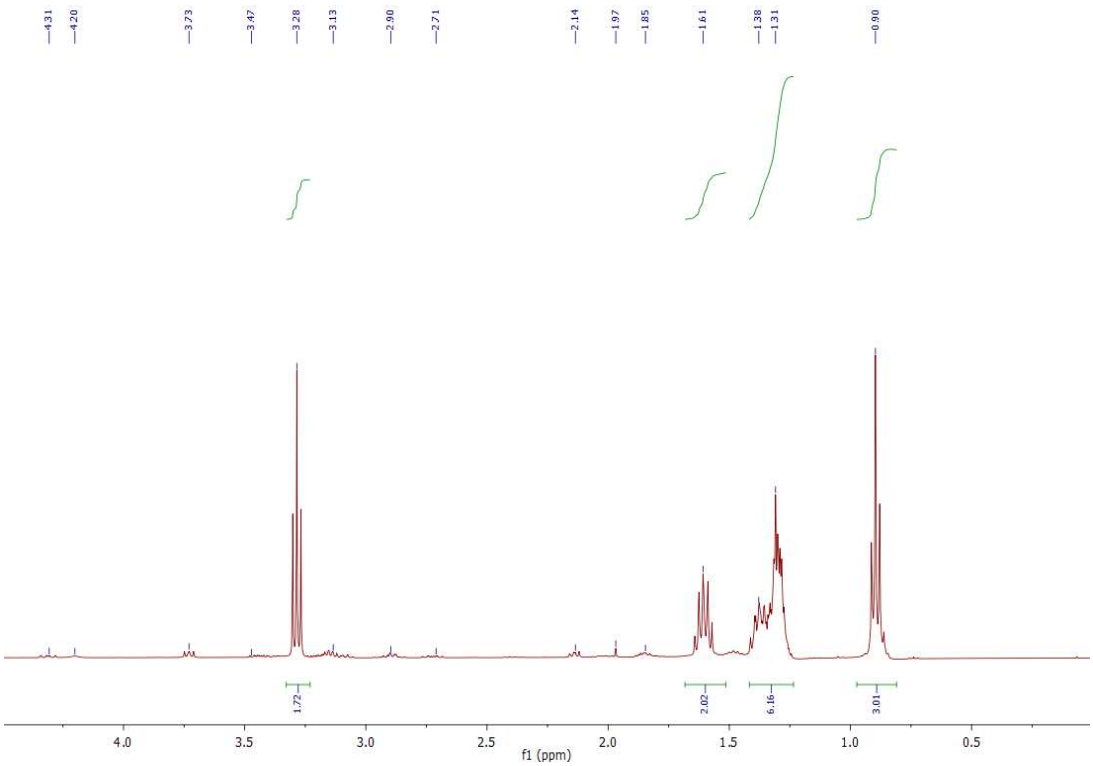

Figure 98: ^{1}H-NMR of the uncured HMI formulation ($CDCl_3$, 400 MHz) δ (ppm): 3.28 (t, 2H, C**H$_2$**-NCO), 1.61 (m, 2H, C**H$_2$**-CH_2-NCO), 1.38-1.31 (m, 6H, 3xC**H$_2$**), 0.90 (m, 3H, C**H$_3$**).

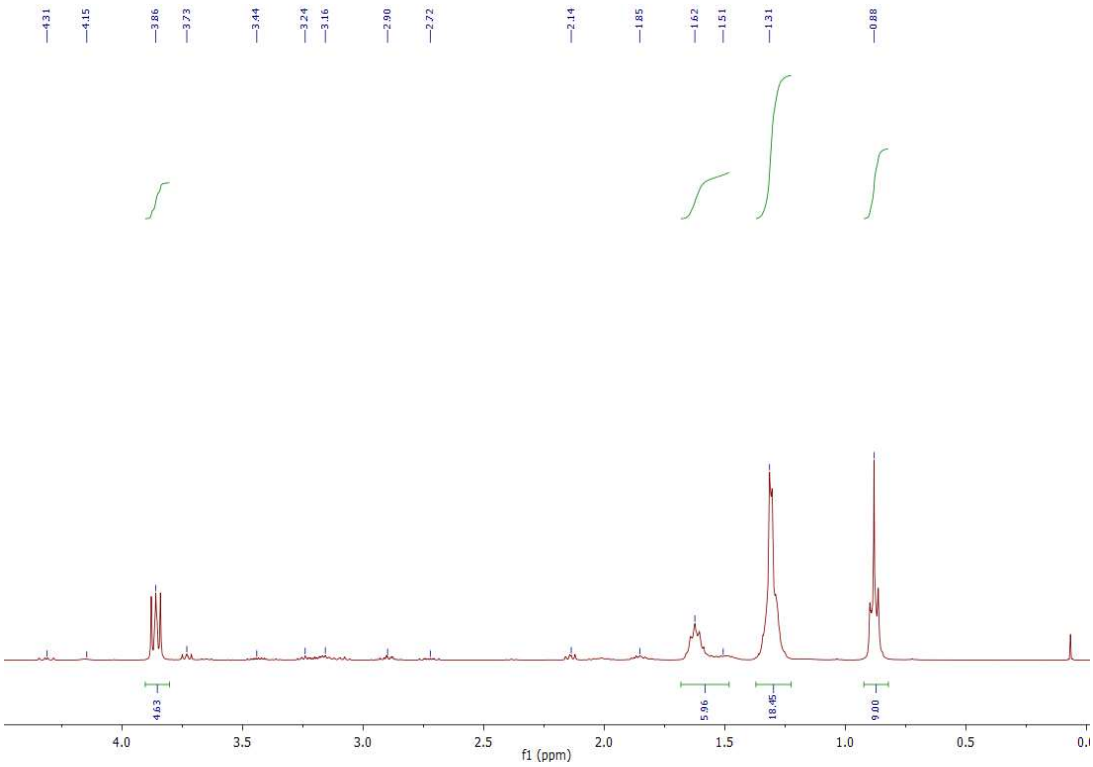

Figure 99: ^{1}H-NMR of the cured HMI formulation ($CDCl_3$, 400 MHz) δ (ppm): 3.86 (m, 6H, 3xC**H$_2$**-triazine), 1.64-1.51 (m, 6H, 3xC**H$_2$**-CH_2-triazine), 1.38-1.25 (m, 18H, 9xC**H$_2$**), 0.88 (m, 9H, 3xC**H$_3$**).

Die approbierte gedruckte Originalversion dieser Dissertation ist an der TU Wien Bibliothek verfügbar.
The approved original version of this doctoral thesis is available in print at TU Wien Bibliothek.
TU Bibliothek Your knowledge hub WIEN

3.3 Optimization of the system

3.3.1 Influence of the concentration of the photocatalyst

5 mol% of DBN was mixed with HMDI and subjected to heating and ultrasonic bath treatment. After cooling different mol% of $MeCpMn(CO)_3$ were incorporated, the formulation was vigorously stirred and measured in Photo-DSC (320-500 nm, 100 °C, 60 mW·cm^{-2}).

3.3.2 Influence of the concentration of the co-catalyst

Different mol% of DBN was mixed with HMDI and subjected to heating and ultrasonic bath treatment. After cooling 1 mol% of $MeCpMn(CO)_3$ were incorporated, the formulation was vigorously stirred and measured in Photo-DSC (320-500 nm, 100 °C, 60 mW·cm^{-2}).

3.3.3 Influence of the temperature

5 mol% of DBN was mixed with HMDI and subjected to heating and ultrasonic bath treatment. After cooling 1 mol% of $MeCpMn(CO)_3$ were incorporated, the formulation was vigorously stirred and measured in Photo-DSC (320-500 nm, 80-140 °C, 60 mW·cm^{-2}).

3.3.4 Influence of the intensity

5 mol% of DBN was mixed with HMDI and subjected to heating and ultrasonic bath treatment. After cooling 1 mol% of $MeCpMn(CO)_3$ were incorporated, the formulation was vigorously stirred and measured in Photo-DSC (320-500 nm, 100 °C, 30-120 mW·cm^{-2}).

Die approbierte gedruckte Originalversion dieser Dissertation ist an der TU Wien Bibliothek verfügbar.
The approved original version of this doctoral thesis is available in print at TU Wien Bibliothek.
TU WIEN Bibliothek Your knowledge hub

3.4 Investigation HMDI vs. TMDI

3.4.1 Photo-DSC & Conversion

5 mol% of DBN was mixed with HMDI, trimethyl hexamethylene diisocyanate (TMDI) or a 50:50 molar mixture of them and subjected to heating and ultrasonic bath treatment. After cooling 1 mol% of $MeCpMn(CO)_3$ were incorporated, the formulation was vigorously stirred and measured in Photo-DSC (320-500 nm, 100-140 °C, 60 mW·cm^{-2}). The produced formulation and samples have been measured via ATIR spectroscopy.

3.4.2 Thermal characterization

The in 3.4.1 produced formulation and samples, have been measured via STA.

3.4.3 Mechanical testing

5 mol% of DBN was mixed with HMDI, TMDI or a 50:50 molar mixture of them and subjected to heating and ultrasonic bath treatment. After cooling 1 mol% of $MeCpMn(CO)_3$ were incorporated and vigorously stirred. For (thermo)mechanical tests, all formulations were poured into silicone molds (5 × 2 × 40 mm^3 for DMTA, ISO527 test specimens 5b dumbbell-shaped with a total length of 35 mm, and a parallel constriction region with dimensions of 2 × 2 × 12 mm^3 for tensile tests). The formulations were cured with a UV-oven. The samples were irradiated at 100 °C for 50 s and then placed in oven at 120 °C for 12 h. Afterwards the specimen have been polished with sandpaper to ensure uniform geometries.

3.4.4 Printing & Coating

5 mol% of DBN was mixed with HMDI, TMDI or a 50:50 molar mixture of them and subjected to heating and ultrasonic bath treatment. After cooling 1 mol% of $MeCpMn(CO)_3$ were incorporated and vigorously stirred. For coating the formulations were subtracted to a metal or glass plate, coated with and without a doctor blade and finally cured with a UV-oven. The samples were irradiated at 120 °C for 200 s.

Die approbierte gedruckte Originalversion dieser Dissertation ist an der TU Wien Bibliothek verfügbar.
The approved original version of this doctoral thesis is available in print at TU Wien Bibliothek.
TU WIEN Bibliothek Your knowledge hub

Printing tests have been done at 100 °C with 50 mm·s^{-1}.

Die approbierte gedruckte Originalversion dieser Dissertation ist an der TU Wien Bibliothek verfügbar.
The approved original version of this doctoral thesis is available in print at TU Wien Bibliothek.
TU WIEN Bibliothek Your knowledge hub

MATERIALS AND METHODS

Chemicals	Distributor
Acetic anhydride	Merck
Acetonitrile	Merck
Bisphenol-A-dicyanate ester (BADCy)	TCI
Bisphenol-A-diglycidyl ether (BADGE)	Huntsman
Bis-(cyclopentadienyl)-zirconium dichloride	ABCR
Bis-(2-diphenylphosphinophenyl)-ether	Fisher Scientific
1,3-Bis(isocyanatomethyl)cyclohexane (H_6XDI)	TCI
Bis(triphenylphosphine)copper(I) borohydride	Merck
Chloroform-d	Eurisotop
Chloroform HPLC grade	Merck
Cumene	TCI
Cyanate ester novolak PT-30	Arxada
Cyclic trimethylolpropane formal (CMF)	Perstorp
Cyclopentadienyl-(p-cymol)-ruthenium(II)-hexafluorophosphate	ABCR
Cyclopentadienyl(triethylphosphine)copper(I)	ABCR
Delrin 500P	DuPont
Delrin 1700P	DuPont
1,5-Diazabicyclo(4.3.0)non-5-en (DBN)	Merck
Diethyl ether	Merck
4,4'-Diisocyanatodicyclohexylmethane ($H_{12}MDI$)	TCI
Dimanganese decacarbonyl	Merck
Diphenylmethane diisocyanate	MDI
Di-tert-butyl peroxide	Merck
DMSO-d_6	Eurisotop
3,4-Epoxycyclohexylmethyl 3,4-epoxycyclohexanecarboxylate (CE)	Sigma-Aldrich

Die approbierte gedruckte Originalversion dieser Dissertation ist an der TU Wien Bibliothek verfügbar.
The approved original version of this doctoral thesis is available in print at TU Wien Bibliothek.
TU Bibliothek Your knowledge hub WIEN

Epoxyphenol novolak (Epilok-60-838, EPNovo)	Bitrez
Furan resin (FRA)	Hüttenes-Albertus
Furfuryl alcohol (FA)	TCI
Glycerol formal (GF)	Sigma-Aldrich
Hexamethylene diisocyanate (HMDI)	TCI
Hexamethylene isocyanate (HMI)	TCI
Hexamethylenetetramine (Hexa)	Merck
4-Hydroxyphenyldimethylsulfonium methyl sulfate	TCI
Irgacure 261	Ciba Geigy
Irgacure 784	Ciba Geigy
Isophorone diisocyanate (IPDI)	TCI
Isopropylthioxanthone (ITX)	Sartomer
KBr FT-IR grade	Merck
LVT-50 (Mixture BADCy and PT-15)	Arxada
$MeCpMn(CO)_3$	ABCR
Melamine resin (MF resin)	Süd-West-Chemie
Methanol HPLC grade	Merck
Na_2CO_3	Merck
$NaHCO_3$	Merck
N‴-(1,1-dimethylethyl)-N,N′,N″-tris[tris(dimethylamino)phosphoranylidene]phosphorimidic triamide (P_4-*t*-Bu)	Merck
Neocuproin hemihydrat	Fisher Scientific
4-Nonylphenol	ABCR
Paraformaldehyde	Merck
Pentaerythritol	Sigma Aldrich

Die approbierte gedruckte Originalversion dieser Dissertation ist an der TU Wien Bibliothek verfügbar.
The approved original version of this doctoral thesis is available in print at TU Wien Bibliothek.
TU Bibliothek Your knowledge hub WIEN

Petroleum	Roth
1,10-Phenanthroline	Sigma-Aldrich
Phenyl cyanate	ABCR
4-Phenyl-1,3-dioxane	TCI
p-(Octyloxyphenyl)phenyliodonium hexafluoroantimonate (I-Sb)	ABCR
Polyoxymethylene dimethyl ether (PODE)	Albert-Ludwigs-Universität
Potassium ferrocyanide	Sigma-Aldirch
Potassium thiocyanate	Sigma-Aldrich
Resole resin	Süd-West-Chemie
Salicylaldehyde (SA)	TCI
Salicylic acid	TCI
Sulfuric acid	Merck
Supraplast 3616 (Novo)	Süd-West-Chemie
Tartaric acid	Sigma-Aldrich
Tetrakis-(acetonitril)-kupfer(I)-tetrafluorborat	Fisher Scientific
1,1,3,3-Tetramethylguanidine (TMG)	Merck
Toluene diisocyanate (TDI)	TCI
Trimethyl hexamethylene diisocyanate (2,2,4- and 2,4,4-mixture) (TMDI)	TCI
1,3,5-Trioxane	Merck
Ultraform S2320	DuPont
Urea resin (UF resin)	Deuteron
m-Xylylene diisocyanate (XDI)	TCI
Zinc chloride	Merck
Zinc tetraphenylporphyrin	Merck

Die approbierte gedruckte Originalversion dieser Dissertation ist an der TU Wien Bibliothek verfügbar.
The approved original version of this doctoral thesis is available in print at TU Wien Bibliothek.
TU WIEN Bibliothek Your knowledge hub

NMR spectra were recorded on a Bruker Avance at 400 MHz (600 Mhz) for ^{1}H and 100 MHz for ^{13}C. The signals are noted according to their shifts in comparison to tetramethylsilane (d = 0 ppm) and were always referenced on the used NMR-solvent:

^{1}H: $CDCl_3$: 7.26 ppm

^{13}C: $CDCl_3$: 77.16 ppm

The chemical shifts were reported in ppm. Analysis of the spectra was carried out with the program MestreNova.

ATR-FTIR was measured on a Spectrum 65 spectroscope from Perkin-Ellmer with a Specac golden gate diamond ATR. For the measurements, the pure formulation and cured samples from Photo-DSC were used. The spectra were collected in a range between 4000-500 cm^{-1} and 32 scans were made for each spectrum. For the transmission infrared spectra measurements, the samples were ground and pressed with 50 times the amount of KBr. The spectra were collected in a range between 4000-500 cm^{-1} and 16 scans were made for each spectrum. For the analysis of the results the software Spectrum from Perkin-Ellmer in version 10.03.07.0112 was used.

Simultaneous thermal analysis was performed using a STA 449 F1 Jupiter from Netzsch. Nitrogen was used as protection and purge gas. Calibration was done in Nitrogen with the elements bismuth, indium, tin and zinc. Proteus - Thermal Analysis in version 5.2.1 from Netzsch Geraetebau was used for the data analysis.

For all **photo-DSC and STA** measurements 25 µ aluminium pans (DSC-crucible Order-No: 6.239.2-64.5.01) were used.

The preparation of photoreactive formulations and substances was carried out in a **orange light laboratory**. The laboratory had adhesive foils of the company IFOHA attached to all windows and the fluorescent lamps were type Osram lumilux with chip control light colour 62 (wavelengths below 480 nm are filtered).

Photo-DSC measurements were performed using Omnicure 2000 from Lumen Dynamics with glass fibre light wave guides. The UV source was calibrated at least once a day with an Omnicure R2000 radiometer.

Die approbierte gedruckte Originalversion dieser Dissertation ist an der TU Wien Bibliothek verfügbar.
The approved original version of this doctoral thesis is available in print at TU Wien Bibliothek.
TU WIEN Bibliothek Your knowledge hub

Photo-DSC studies were conducted on a Photo-DSC 204 F1 from Netzsch. As light source an Omnicure 2000 was used in combination with a glassfiber filled double-core lightguide (3 mm fiber diameter). The formulations (11 ± 1 mg) were irradiated twice with filtered UV-light (320−500 nm) via an Exfo OmniCureTM series 2000 broadband Hg lamp under constant N2 flow (20 mL·min^{-1}). The light intensity was set to 1.5 W·cm^{-2} at the tip of the light guide corresponding to ~60 mW·cm^{-2} on the surface of the sample. The heat flow of the polymerization reaction was recorded as a function of time. The times when the maximum of heat evolution was reached (t_{max}) was used as indicator for the reactivity of a formulation. All measurements were performed in triplicates. Proteus - Thermal Analysis in version 5.2.1 from Netzsch Geraetebau was used for the data analysis.

Polymer specimen were cured using a Uvitron UV 1080 Flood Curing System with Uvitron Intelliray 600 halide lamps (600 W, 120 mW cm^{-2}, 320-580 nm).

Coating. The respective formulation was cured with a Intelli-Ray 600 UV-oven with a broadband Hg lamp (600 W; UV-A: 125 mW·cm^{-2}; Vis: 125 mW·cm^{-2}; ~280−550 nm). The samples were irradiated at 120 °C for 200 s.

DMTA measurements of molded photopolymers were performed with an Anton Paar MCR 301 with a CTD 450 oven and an SRF 12 measuring system. The prepared DMTA samples were tested in torsion mode with a frequency of 1 Hz and a strain of 0.1 %. The temperature was increased from −50 to 300 °C with a heating rate of 2 K·min^{-1}. The glass transition temperature (T_g) was defined as the temperature at the maximum loss factor (tan δ).

Tensile tests were performed by means of a Zwick Z050 with Zwick Z050 with a maximum test force of 50 kN. TestXpert II software was used to process and evaluate the recorded

Hot Lithography 3D printing was conducted on a heated SLA prototype by TU Wien and a Caligma 200 UV developed by the company Cubicure GmbH. The Hot Lithography printer setup uses a 375 nm diode laser source. This beam is scanned over a 2-dimensional plane using a galvanometer scanning system. The laser spot on the surface of the material vat has a diameter of 18 µm.

Die approbierte gedruckte Originalversion dieser Dissertation ist an der TU Wien Bibliothek verfügbar.
The approved original version of this doctoral thesis is available in print at TU Wien Bibliothek.
TU WIEN Bibliothek Your knowledge hub

Rheology measurements were performed with a Physica Anton Paar MCR 300 with a CP25 measuring system. A distance of 100 µm between Peltier plate and stamp plate was set. Measurements were conducted in rotation mode with a constant shear rate of 100 s^{-1}.

Void Content. The overview to observe macroscopic voids was recorded by a Keyence VHX 6000 optical microscope in panorama mode, the detailed views of the morphology to observe microscopic voids were imaged with a Phillips XL-30 scanning electron microscope or Zeiss AxioImager light microscope.

SEM. To determine layer quality, the 3D printed parts were characterized via scanning electron microscopy (SEM). The sample morphology was imaged with a Phillips XL-30 after sputtering with a thin gold layer.

HPLC was measured on was measured on a Hewlett-Packard Agilent 1100 Series HPLC Value System using a normal phase LiChrosorb CN-5µ, 4.6 x 150 mm column. A UV detector was used for signal recording. The solvent mixture used was chloroform-methanol. Quantitative evaluation was performed by integration based on a calibration line of the monomer used.

Short-time creep tests were done at a TA Instruments DMA 850 in bending mode at a bending stress of 5 MPa. Support span was 10 mm, the specimens had a thickness of 0.8 mm and a width of 5 mm.

UV-Vis absorption. UV-Vis absorption spectra were recorded in quartz cuvettes using a Thermo Scientific NanoDrop One/OneC Microvolume UV-Vis Spectrophotometer in a range between 250-500 nm.

Die approbierte gedruckte Originalversion dieser Dissertation ist an der TU Wien Bibliothek verfügbar.
The approved original version of this doctoral thesis is available in print at TU Wien Bibliothek.
TU WIEN Bibliothek Your knowledge hub

ABBREVIATIONS

A	Absorption
AA	Acetic anhydride
α	Conversion
abs.	absolute
AM	Additive manufacturing
AMT	Additive manufacturing technology
ATR-IR	Attenuated total reflection infrared spectroscopy
BADCy	Bisphenol A dicyanate ester
BADGE	Bisphenol-A-diglycidyl ether
b.p.	boiling point
CA	Curing agent
CAD	Computer-aided design
CE	Cyanate ester
CMF	Cyclic trimethylolpropane formal
conc.	concentration
DBN	1,5-diazabicyclo(4.3.0)non-5-en
ΔH	Enthalpy
DIW	Direct ink writing
DLP	Digital light processing
DMA	Dynamic mechanical analysis
DMD	Digital micromirror device

Die approbierte gedruckte Originalversion dieser Dissertation ist an der TU Wien Bibliothek verfügbar.
The approved original version of this doctoral thesis is available in print at TU Wien Bibliothek.
TU WIEN Bibliothek Your knowledge hub

DMTA	Dynamic-mechanical thermal analysis
DSC	Differential scanning calorimetry
ECC	3,4-epoxycyclohexylmethyl 3,4-epoxycyclohexanecarboxylate
eq	equivalents
EpNovo	Epoxyphenol novolak
f	Functional groups
FA	Furfuryl alcohol
FDM	Fused deposition modeling
FRA	Furan resin
GF	Glycerol formal
h	Height of the peak
$H_{12}MDI$	4,4'-diisocyanatodicyclohexylmethane
H_6XDI	1,3-bis(isocyanatomethyl)cyclohexane
Hexa	Hexamethylenetetramine
HMDI	Hexamethylene diisocyanate
HPLC	High-performance liquid chromatography
HPP	High-performance polymer
I261	Irgacure 261
IPDI	Isophorone diisocyanate
IR	Infrared spectroscopy
I-Sb	p-(Octyloxyphenyl)phenyliodonium hexafluoroantimonate

Die approbierte gedruckte Originalversion dieser Dissertation ist an der TU Wien Bibliothek verfügbar.
The approved original version of this doctoral thesis is available in print at TU Wien Bibliothek.
TU WIEN Bibliothek Your knowledge hub

L-AMT	Lithography-based additive manufacturing technology
m	Mass
M	molecular weight
MDI	Diphenylmethane diisocyanate
MF	Melamine formaldehyde
mol%	Molar percent
m.p.	Melting point
NMR	Nuclear magnetic resonance
Novo	Novolak resin
NP	Nonylphenol
PAG	Photoacid generator
PAI	Polyamideimides
PBI	Polybenzimidazoles
PD	4-Phenyl-1,3-dioxane
PDF	Pentaerythritol diformal
PEEK	Polyetheretherketone
PEI	Polyetherimides
PEKK	Polyetherketoneketone
PES	Polyethersulfones
PF	Paraformaldehyde
PFA	Polyfurfuryl alcohol
Phen	1,10-phenanthroline
photo-DSC	photo differential scanning calorimetry

Die approbierte gedruckte Originalversion dieser Dissertation ist an der TU Wien Bibliothek verfügbar.
The approved original version of this doctoral thesis is available in print at TU Wien Bibliothek.
TU Bibliothek Your knowledge hub WIEN

PI	Photoinitiator
PIR	Polyisocyanurate
PIS	Polyimides
P_n	Degree of polymerization
PODE	Polyoxymethylene dimethyl ether
POM	Polyoxymethylene
POMDA	Polyoxymethylene diacetate
POM-H	Homo-polyoxymethylene
PPS	Polyphenylene sulphide
PPSU	Polyphenylenesulphones
PSU	Polysulphones
PTFE	Polytetrafluoroethylene
PVDF	Polyvinylidene difluoride
R_P	Rate of polymerization
SA	Salicylaldehyde
SEM	Scanning electron microscopy
SLA	Stereolithography (apparatus)
SLS	Selective laser sintering
STA	Simultaneous thermal analysis
STL	Standard transformation language
TDI	Toluene diisocyanate

Die approbierte gedruckte Originalversion dieser Dissertation ist an der TU Wien Bibliothek verfügbar.
The approved original version of this doctoral thesis is available in print at TU Wien Bibliothek.
TU WIEN Bibliothek Your knowledge hub

T_g	Glass transition temperature
TGA	Thermogravimetric analysis
t_{max}	Time of polymerization maximum
TMDI	Trimethyl hexamethylne diisocyanate
TMG	1,1,3,3-tetramethylguanidine
TOMDA	Trioxymethylene diacetate
UF	Urea formaldehyde
UPLC-MS	Ultra-performance liquid chromatography-mass spectrometry
UV	Ultraviolet
wt%	Weight percent
XDI	m-xylene diisocyanate
3D	3-dimensional

Die approbierte gedruckte Originalversion dieser Dissertation ist an der TU Wien Bibliothek verfügbar.
The approved original version of this doctoral thesis is available in print at TU Wien Bibliothek.
TU WIEN Bibliothek Your knowledge hub

BIBLIOGRAPHY

[1] T. S. Srivatsan, T. S. Sudarshan, *Additive Manufacturing : Innovations, Advances, and Applications*, Taylor & Francis, Abingdon-on-Thames, **2015**.

[2] A. Gebhardt, J.-S. Hötter, *Additive Manufacturing*, Carl Hanser Verlag GmbH & Co. KG, München, **2016**.

[3] S. C. Ligon, R. Liska, J. Stampfl, M. Gurr, R. Mülhaupt, *Chem. Rev.* **2017**, *117*, 10212–10290, DOI: 10.1021/acs.chemrev.7b00074.

[4] R. H. Awad, S. A. Habash, C. J. Hansen, *3D Print. Appl. Cardiovasc. Med.* **2018**, 11–32, DOI: 10.1016/B978-0-12-803917-5.00002-X.

[5] M. Burns, *Automated Fabrication : Improving Productivity in Manufacturing*, Prentice Hall, Upper Saddle River, **1993**.

[6] Wohlers Associates, *Wohlers Report 2023. Analysis. Trends. Forecasts. 3D Printing and Additive Manufacturing State of the Industry.*, USA, **2023**.

[7] Wohlers Associates, *Wohlers Report 2022. Analysis. Trends. Forecasts. 3D Printing and Additive Manufacturing State of the Industry.*, USA, **2022**.

[8] IDTechEx, *3D Printing and Additive Manufacturing 2023-2033 : Technology and Market Outlook*, United Kingdom, **2023**.

[9] Align Technology Inc., *Q4 and Fiscal 2022 Financial Results*, USA, **2023**.

[10] Adidas Group, "4DFWD: DATA-DRIVEN 3D PRINTED PERFORMANCE TECHNOLOGY DESIGNED TO MOVE YOU FORWARD," can be found under https://news.adidas.com/running/4dfwd--data-driven-3d-printed-performance-technology-designed-to-move-you-forward/s/514baddb-1029-4686-abd5-5ee3985a304a (accessed 04/26/2023), **2021**.

[11] T. Hoffman, "The Best 3D Printers for 2021," can be found under https://uk.pcmag.com/3d-printers/36506/the-best-3d-printers (accessed

Die approbierte gedruckte Originalversion dieser Dissertation ist an der TU Wien Bibliothek verfügbar.
The approved original version of this doctoral thesis is available in print at TU Wien Bibliothek.
TU WIEN Bibliothek Your knowledge hub

04/26/2023), **2021**.

[12] S. C. Ligon-Auer, M. Schwentenwein, C. Gorsche, J. Stampfl, R. Liska, *Polym. Chem.* **2016**, *7*, 257–286, DOI: 10.1039/c5py01631b.

[13] S. Theresa, S. Jürgen, G. Kempf, R.-M. Hucke, *RTejournal - Forum für Rapid Technol.* **2014**, 1–10.

[14] B. Husar, M. Hatzenbichler, V. Mironov, R. Liska, J. Stampfl, A. Ovsianikov, in *Biomater. Bone Regen. Nov. Tech. Appl.*, Woodhead Publishing, **2014**, pp. 149–201.

[15] J. P. Fouassier, X. Allonas, D. Burget, *Prog. Org. Coatings* **2003**, *47*, 16–36, DOI: 10.1016/S0300-9440(03)00011-0.

[16] J. P. Fouassier, J. Lalevée, *Photoinitiators for Polymer Synthesis: Scope, Reactivity and Efficiency*, Wiley-VCH, Weinheim, Germany, **2012**.

[17] R. Kirchmayr, G. Berner, G. Rist, *Farbe Lack* **1980**, *86*, 224–230.

[18] P. Gauss, Advanced Additives for Radical Photopolymerization, Wien, **2019**.

[19] A. Mautner, Development of Low Cytotoxic Photopolymers, **2012**.

[20] B. Husár, C. Heller, M. Schwentenwein, A. Mautner, F. Varga, T. Koch, J. Stampfl, R. Liska, *J. Polym. Sci. Part A Polym. Chem.* **2011**, *49*, 4927–4934, DOI: 10.1002/pola.24933.

[21] G. Peer, P. Dorfinger, T. Koch, J. Stampfl, C. Gorsche, R. Liska, *Macromolecules* **2018**, *51*, 9344–9353, DOI: 10.1021/ACS.MACROMOL.8B01991.

[22] C. Hull, *Apparatus for Production of Three Dimensional Objects by Stereolithography*, **1986**, US4575330A.

[23] P. J. Bartolo, *Stereolithography - Materials, Processes and Applications*, Springer US, Boston, MA, **2011**.

[24] Formlabs, “Guide to Stereolithography (SLA) 3D Printing,” can be found under https://formlabs.com/blog/ultimate-guide-to-stereolithography-sla-3d-printing/ (accessed 05/03/2023), **2021**.

[25] D. W. Hutmacher, in *Adv. Manuf. Technol. Med. Appl. Reverse Eng. Softw.*

Die approbierte gedruckte Originalversion dieser Dissertation ist an der TU Wien Bibliothek verfügbar.
The approved original version of this doctoral thesis is available in print at TU Wien Bibliothek.
TU Bibliothek Your knowledge hub WIEN

Convers. Rapid Prototyp., John Wiley & Sons, Ltd, **2006**, pp. 163–189.

[26] T. D. Ngo, A. Kashani, G. Imbalzano, K. T. Q. Nguyen, D. Hui, *Compos. Part B Eng.* **2018**, *143*, 172–196, DOI: 10.1016/j.compositesb.2018.02.012.

[27] J. Stampfl, S. Baudis, C. Heller, R. Liska, A. Neumeister, R. Kling, A. Ostendorf, M. Spitzbart, *J. Micromechanics Microengineering* **2008**, *18*, 125014, DOI: 10.1088/0960-1317/18/12/125014.

[28] Scott Frey, "Laser SLA vs DLP vs Masked SLA 3D Printing Technology - The Ortho Cosmos," can be found under https://theorthocosmos.com/laser-sla-vs-dlp-vs-masked-sla-3d-printing-technology-compared/ (accessed 05/03/2023), **2017**.

[29] J. Homa, M. Schwentenwein, in *Adv. Process. Manuf. Technol. Nanostructured Multifunct. Mater.*, Wiley, **2015**, pp. 33–40.

[30] E. Zanchetta, M. Cattaldo, G. Franchin, M. Schwentenwein, J. Homa, G. Brusatin, P. Colombo, *Adv. Mater.* **2016**, *28*, 370–376, DOI: 10.1002/adma.201503470.

[31] P. M. Hergenrother, *High Performance Polymers*, Springer Berlin Heidelberg, Berlin, Heidelberg, **1994**.

[32] P. M. Hergenrother, *High Perform. Polym.* **2003**, *15*, 3–45, DOI: 10.1177/095400830301500101.

[33] J. K. Fink, *High Performance Polymers*, Springer Berlin Heidelberg, Berlin, Heidelberg, **2008**.

[34] A. C. C. de Leon, Í. G. M. da Silva, K. D. Pangilinan, Q. Chen, E. B. Caldona, R. C. Advincula, *React. Funct. Polym.* **2021**, *162*, 104878, DOI: 10.1016/j.reactfunctpolym.2021.104878.

[35] T. L. Cottrell, *The Strengths of Chemical Bonds*, Butterworth, London, **1958**.

[36] M. Wagner, *Thermal Analysis in Practice*, Carl Hanser Verlag GmbH & Co. KG, München, **2017**.

Die approbierte gedruckte Originalversion dieser Dissertation ist an der TU Wien Bibliothek verfügbar.
The approved original version of this doctoral thesis is available in print at TU Wien Bibliothek.
TU WIEN Bibliothek Your knowledge hub

[37] D. J. Liaw, K. L. Wang, Y. C. Huang, K. R. Lee, J. Y. Lai, C. S. Ha, *Prog. Polym. Sci.* **2012**, *37*, 907–974, DOI: 10.1016/j.progpolymsci.2012.02.005.

[38] A. Sezer Hicyilmaz, A. Celik Bedeloglu, *SN Appl. Sci.* **2021**, *3*, 1–22, DOI: 10.1007/s42452-021-04362-5.

[39] Plenco, "Phenolic Novolac And Resol Resins - Phenolic thermosetting resin," can be found under https://www.plenco.com/phenolic-novolac-resol-resins.htm (accessed 08/24/2023), **2022**.

[40] M. Asim, N. Saba, M. Jawaid, M. Nasir, M. Pervaiz, O. Y. Alothman, *Curr. Anal. Chem.* **2018**, *14*, 1–13, DOI: 10.2174/1573411013666171003154410.

[41] H.-G. Elias, *Makromoleküle*, Wiley-VCH, Weinheim, **1999**.

[42] T. A. Saleh, in *Polym. Hybrid Mater. Nanocomposites*, William Andrew Publishing, **2021**, pp. 59–103.

[43] W. H. Carothers, *Trans. Faraday Soc.* **1936**, *32*, 39–49, DOI: 10.1039/TF9363200039.

[44] D. Stoye, W. Freitag, *Lackharze Chemie, Eigenschaften Und Anwendungen*, Carl Hanser Verlag GmbH & Co. KG, München, **1996**.

[45] BMAS, *TRGS 430*, **2009**.

[46] W. Kaiser, *Kunststoffchemie Für Ingenieure*, Carl Hanser Verlag GmbH & Co. KG, München, **2015**.

[47] S. Koltzenburg, M. Maskos, O. Nuyken, *Polymere: Synthese, Eigenschaften Und Anwendungen*, Springer, Berlin, Heidelberg, **2014**.

[48] H. Kricheldorf, in *Polycondensation*, Springer, Berlin, Heidelberg, **2014**, pp. 69–91.

[49] A. A. Caraculacu, S. Coseri, *Prog. Polym. Sci.* **2001**, *26*, 799–851, DOI: 10.1016/S0079-6700(00)00033-2.

[50] L. U. Kim, J. W. Kim, C. K. Kim, *Biomacromolecules* **2006**, *7*, 2680–2687, DOI: 10.1021/bm060453h.

[51] J.-P. Fouassier, *Photochemistry and UV Curing : New Trends 2006*, Research

Die approbierte gedruckte Originalversion dieser Dissertation ist an der TU Wien Bibliothek verfügbar.
The approved original version of this doctoral thesis is available in print at TU Wien Bibliothek.
TU Bibliothek Your knowledge hub WIEN

Signpost, **2006**.

[52] R. R. Moraes, J. W. Garcia, M. D. Barros, S. H. Lewis, C. S. Pfeifer, J. Liu, J. W. Stansbury, *Dent. Mater.* **2011**, *27*, 509–519, DOI: 10.1016/j.dental.2011.01.006.

[53] R. Gmeiner, *Method and Device for Lithography-Based Additive Production of Three-Dimensional Shaped Bodies.*, **2018**, WO2018032022A1.

[54] B. Steyrer, B. Busetti, G. Harakály, R. Liska, J. Stampfl, *Addit. Manuf.* **2018**, *21*, 209–214, DOI: 10.1016/J.ADDMA.2018.03.013.

[55] H. Bayer, *Photo-Curable Resin with Low Shrinkage and Its Use in a Stereolithography Process.*, **1995**, DE19541075C1.

[56] M. Pfaffinger, *Laser Tech. J.* **2018**, *15*, 45–47, DOI: 10.1002/LATJ.201800024.

[57] B. Steyrer, R. Liska, J. Stampfl, **2017**.

[58] N. Klikovits, L. Sinawehl, P. Knaack, T. Koch, J. Stampfl, C. Gorsche, R. Liska, *ACS Macro Lett.* **2020**, *9*, 546–551, DOI: 10.1021/ACSMACROLETT.0C00055.

[59] Y. Mete, P. Knaack, R. Liska, *Polym. Int.* **2022**, *71*, 797–803, DOI: 10.1002/pi.6326.

[60] L. Pezzana, R. Wolff, G. Melilli, N. Guigo, N. Sbirrazzuoli, J. Stampfl, R. Liska, M. Sangermano, *Polymer (Guildf).* **2022**, *254*, 125097, DOI: 10.1016/j.polymer.2022.125097.

[61] A. Knop, W. Scheib, *Chemistry and Application of Phenolic Resins*, Springer-Verlag, Berlin, **1979**.

[62] American Chemical Society National Historic Chemical Landmarks, “Bakelite: First Synthetic Plastic,” can be found under https://www.acs.org/content/acs/en/education/whatischemistry/landmarks/bakelite.html (accessed 09/17/2021), **1993**.

[63] L. Pilato, *Phenolic Resins: A Century of Progress*, Springer Berlin Heidelberg, **2010**.

Die approbierte gedruckte Originalversion dieser Dissertation ist an der TU Wien Bibliothek verfügbar.
The approved original version of this doctoral thesis is available in print at TU Wien Bibliothek.
TU WIEN Bibliothek Your knowledge hub

[64] M. Asim, N. Saba, M. Jawaid, M. Nasir, M. Pervaiz, O. Y. Alothman, *Curr. Anal. Chem.* **2017**, *13*, DOI: 10.2174/1573411013666171003154410, DOI: 10.2174/1573411013666171003154410.

[65] A. Böttcher, *Kunststoffe* **1995**, *8*, 1142–1144.

[66] K. Hirano, M. Asami, in *React. Funct. Polym.*, Elsevier, **2013**, pp. 256–269.

[67] C. Nita, M. Bensafia, C. Vaulot, L. Delmotte, C. Matei Ghimbeu, *Carbon N. Y.* **2016**, *109*, 227–238, DOI: 10.1016/j.carbon.2016.08.011.

[68] H. Bensalah, M. Raji, H. Abdellaoui, H. Essabir, R. Bouhfid, A. el kacem Qaiss, *Int. J. Adv. Manuf. Technol.* **2021**, *112*, 1917–1930, DOI: 10.1007/s00170-020-06535-9.

[69] G. Özbay, N. Ayrilmis, M. S. Ahmad, *Environ. Sci. Eur.* **2023**, *35*, 1–7, DOI: 10.1186/s12302-023-00719-2.

[70] M. S. Celiktas, M. Yaglikci, F. Khosravi Maleki, *Polym. Test.* **2019**, *77*, 105918, DOI: 10.1016/j.polymertesting.2019.105918.

[71] B. Jadhav, R. Roy, M. S. Rahman, T. A. Amit, S. Subedi, M. Hummel, Z. Gu, D. E. Raynie, *Biomass* **2022**, *2*, 178–187, DOI: 10.3390/biomass2030011.

[72] J. Li, Z. Liu, Y. Liu, Y. Zhao, M. Wang, H. Wang, X. Chen, *Int. J. Press. Vessel. Pip.* **2023**, *206*, 105017, DOI: 10.1016/j.ijpvp.2023.105017.

[73] J. V. Anguita, C. T. G. Smith, T. Stute, M. Funke, M. Delkowski, S. R. P. Silva, *Nat. Mater.* **2020**, *19*, 317–322, DOI: 10.1038/s41563-019-0565-3.

[74] L. Paglia, J. Tirillò, F. Marra, C. Bartuli, A. Simone, T. Valente, G. Pulci, *Mater. Des.* **2016**, *90*, 1170–1180, DOI: 10.1016/j.matdes.2015.11.066.

[75] R. Hsissou, R. Seghiri, Z. Benzekri, M. Hilali, M. Rafik, A. Elharfi, *Compos. Struct.* **2021**, *262*, DOI: 10.1016/j.compstruct.2021.113640, DOI: 10.1016/j.compstruct.2021.113640.

[76] Y. D. Dong, H. Zhang, G. J. Zhong, G. Yao, B. Lai, *Chem. Eng. J.* **2021**, *405*, DOI: 10.1016/j.cej.2020.126980, DOI: 10.1016/j.cej.2020.126980.

[77] Y. Yang, Y. Xu, Y. Ji, Y. Wei, *Prog. Mater. Sci.* **2021**, *120*, DOI:

Die approbierte gedruckte Originalversion dieser Dissertation ist an der TU Wien Bibliothek verfügbar.
The approved original version of this doctoral thesis is available in print at TU Wien Bibliothek.
TU WIEN Bibliothek Your knowledge hub

10.1016/j.pmatsci.2020.100710, DOI: 10.1016/j.pmatsci.2020.100710.

[78] Y. Ma, Y. Yang, C. Lu, X. Wen, X. Liu, S. Wu, K. Lu, J. Yin, *Compos. Sci. Technol.* **2019**, *180*, 60–70, DOI: 10.1016/j.compscitech.2019.05.005.

[79] G. Yang, G. Yang, W. Wang, S. Peng, Z. Huang, *Mater. Res. Express* **2020**, *7*, DOI: 10.1088/2053-1591/ab9856, DOI: 10.1088/2053-1591/ab9856.

[80] J. K. Park, D. Cho, T. J. Kang, *Carbon N. Y.* **2004**, *42*, 795–804, DOI: 10.1016/j.carbon.2004.01.046.

[81] Z. Huang, W. Ma, C. Jia, X. Lei, Z. Zhang, Z. Ma, *Int. J. Press. Vessel. Pip.* **2021**, *192*, DOI: 10.1016/j.ijpvp.2021.104398, DOI: 10.1016/j.ijpvp.2021.104398.

[82] M. Basso, L. Pupure, M. Simonato, R. Furlanetto, L. De Nardo, R. Joffe, *Compos. Part B Eng.* **2019**, *163*, 702–709, DOI: 10.1016/j.compositesb.2019.01.052.

[83] Y. Y. Zhang, Z. Sun, Y. Q. Li, P. Huang, Q. Chen, S. Y. Fu, *Compos. Part B Eng.* **2021**, *212*, DOI: 10.1016/j.compositesb.2021.108717, DOI: 10.1016/j.compositesb.2021.108717.

[84] W. Hesse, J. Lang, in *Ullmann's Encycl. Ind. Chem.*, Wiley-VCH Verlag GmbH & Co. KGaA, Weinheim, Germany, **2011**.

[85] H. E. Adabbo, R. J. J. Williams, *J. Appl. Polym. Sci.* **1982**, *27*, 893–901, DOI: 10.1002/app.1982.070270309.

[86] M. I. Aranguren, J. Borrajo, R. J. J. Williams, *J. Polym. Sci. Polym. Chem. Ed.* **1982**, *20*, 311–318, DOI: 10.1002/POL.1982.170200205.

[87] Y. Saito, katsuhisa Mizoguchi, M. Ueda, *J. Photopolym. Sci. Technol.* **2008**, *21*, 161–164, DOI: 10.2494/PHOTOPOLYMER.21.161.

[88] E. Reichmanis, *Polym. Mater. Sci. Eng. Proc. ACS Div. Polym. Mater. Sci. Eng.* **1992**, *66*, 36–37, DOI: 10.1021/BK-1994-0537.CH001.

[89] W. A. Green, *Industrial Photoinitiators: A Technical Guide*, CRC Press, **2011**.

Die approbierte gedruckte Originalversion dieser Dissertation ist an der TU Wien Bibliothek verfügbar.
The approved original version of this doctoral thesis is available in print at TU Wien Bibliothek.
TU WIEN Bibliothek Your knowledge hub

[90] J. V. Crivello, in *Initiat. — Poly-Reactions — Opt. Act.*, Springer, Berlin, Heidelberg, **2005**, pp. 1–48.

[91] S. Dadashi-Silab, S. Doran, Y. Yagci, *Chem. Rev.* **2016**, *116*, 10212–10275, DOI: 10.1021/acs.chemrev.5b00586.

[92] K. Crivello, J. V. & Dietliker, *Photoinitiators for Free Radical, Cationic & Anionic Photopolymerization*, Wiley, Weinheim, **1998**.

[93] J. V Crivello, *J. Polym. Sci. Part A Polym. Chem.* **1999**, *37*, 4241–4254, DOI: 10.1002/(SICI)1099-0518(19991201)37:23<4241::AID-POLA1>3.0.CO;2-R.

[94] A. Ovsianikov, A. Ostendorf, B. N. Chichkov, *Appl. Surf. Sci.* **2007**, *253*, 6599–6602, DOI: 10.1016/J.APSUSC.2007.01.058.

[95] S. Gaidukovs, A. Medvids, P. Onufrijevs, L. Grase, *Express Polym. Lett.* **2018**, *12*, 918–929, DOI: 10.3144/EXPRESSPOLYMLETT.2018.78.

[96] A. del Campo, C. Greiner, *J. Micromechanics Microengineering* **2007**, *17*, R81, DOI: 10.1088/0960-1317/17/6/R01.

[97] S. S. Nechausov, M. Y. Yablokova, V. V Avdeev, B. A. Bulgakov, D. I. Kalugin, *Photocurable Polymer Composition for UV Photopolymerization and Method of Making a Hardened Product Therefrom*, **2019**, RU2699556.

[98] D. R. McKean, S. A. MacDonald, N. J. Clecak, C. G. Willson, *Adv. Resist Technol. Process. V* **1988**, *0920*, 60, DOI: 10.1117/12.968302.

[99] W. Dong, C. Bao, W. Lu, R. Liu, H. Ma, S. Li, K. Sun, *Compos. Commun.* **2023**, *38*, 101497, DOI: 10.1016/j.coco.2023.101497.

[100] A. P. Cooney, M. R. Crampton, P. Golding, *J. Chem. Soc. Perkin Trans. 2* **1986**, 835–839, DOI: 10.1039/P29860000835.

[101] E. Gipstein, A. C. Ouano, T. Tompkins, *J. Electrochem. Soc.* **1982**, *129*, 201–205, DOI: 10.1149/1.2123757.

[102] J. F. Walker, A. F. Chadwick, *Ind. Eng. Chem.* **1947**, *39*, 974–977, DOI: 10.1021/ie50452a011.

[103] J. F. Walker, A. F. Chadwick, *Ind. Eng. Chem.* **1947**, *39*, 974–977, DOI:

Die approbierte gedruckte Originalversion dieser Dissertation ist an der TU Wien Bibliothek verfügbar.
The approved original version of this doctoral thesis is available in print at TU Wien Bibliothek.
TU Bibliothek Your knowledge hub WIEN

10.1021/ie50452a011.

[104] W. Kern, V. Jaacks, *J. Polym. Sci.* **1960**, *48*, 399–404, DOI: 10.1002/pol.1960.1204815040.

[105] S. Lüftl, V. M. Archodoulaki, S. Seidler, *Polym. Degrad. Stab.* **2006**, *91*, 464–471, DOI: 10.1016/J.POLYMDEGRADSTAB.2005.01.029.

[106] V. M. Archodoulaki, S. Lüftl, S. Seidler, *Polym. Degrad. Stab.* **2004**, *86*, 75–83, DOI: 10.1016/j.polymdegradstab.2004.03.011.

[107] G. Reuss, W. Disteldorf, A. O. Gamer, A. Hilt, in *Ullmann's Encycl. Ind. Chem.*, John Wiley & Sons, Ltd, Weinheim, Germany, **2000**, pp. 735–763.

[108] H. Wang, S. JY, *Catal. Today* **2017**, *298*, 263–268, DOI: 10.1016/j.cattod.2017.01.041.

[109] H. Staudinger, R. Singer, H. Johner, M. Lüthy, W. K. D. Russidis, O. Schweitzer, *Justus Liebigs Ann. Chem.* **1929**, *474*, 145–275, DOI: 10.1002/JLAC.19294740105.

[110] M. Hoffmann, C. Bizzarri, W. Leitner, T. E. Müller, *Catal. Sci. Technol.* **2018**, *8*, 5594–5603, DOI: 10.1039/C8CY01691G.

[111] J. Tomiška, E. Spousta, *Angew. Chemie Int. Ed. English* **1962**, *1*, 211–211, DOI: 10.1002/anie.196202112.

[112] T. Ito, F. Yoshida, *J. Chem. Eng. Data* **1963**, *8*, 315–320, DOI: 10.1021/je60018a012.

[113] A. W. Franz, H. Kronemayer, D. Pfeiffer, R. D. Pilz, G. Reuss, W. Disteldorf, A. O. Gamer, A. Hilt, *Ullmann's Encycl. Ind. Chem.* **2016**, 1–34, DOI: https://doi.org/10.1002/14356007.a11_619.pub2.

[114] M. Matsuzaki, J. N. Masamoto, K. Kazuhiko, *Polym. Plast. Technol. Eng.* **1994**, *33*, 221–232, DOI: 10.1080/03602559408015297.

[115] A. Heslinga, A. Schors, *J. Appl. Polym. Sci.* **1964**, *8*, 1921, DOI: 10.1002/app.1964.070080501.

Die approbierte gedruckte Originalversion dieser Dissertation ist an der TU Wien Bibliothek verfügbar.
The approved original version of this doctoral thesis is available in print at TU Wien Bibliothek.
TU WIEN Bibliothek Your knowledge hub

[116] A. C. Poshkus, *J. Heterocycl. Chem.* **1979**, *16*, 1075–1076, DOI: 10.1002/jhet.5570160550.

[117] N. Klikovits, P. Knaack, D. Bomze, I. Krossing, R. Liska, *Polym. Chem.* **2017**, *8*, 4414–4421, DOI: 10.1039/C7PY00855D.

[118] I. M. Ward, J. Sweeney, *Mechanical Properties of Solid Polymers: Third Edition*, John Wiley And Sons, Chichester, **2012**.

[119] K. S. Santhosh Kumar, C. P. Reghunadhan Nair, T. S. Radhakrishnan, K. N. Ninan, *Eur. Polym. J.* **2007**, *43*, 2504–2514, DOI: 10.1016/j.eurpolymj.2007.03.028.

[120] J. D. Monk, J. B. Haskins, C. W. Bauschlicher, J. W. Lawson, *Polymer (Guildf).* **2015**, *62*, 39–49, DOI: 10.1016/j.polymer.2015.02.003.

[121] J. P. Patel, C. X. Zhao, S. Deshmukh, G. X. Zou, O. Wamuo, S. L. Hsu, A. B. Schoch, S. A. Carleen, D. Matsumoto, *Polymer (Guildf).* **2016**, *107*, 12–18, DOI: 10.1016/J.POLYMER.2016.11.005.

[122] J. P. Patel, S. Deshmukh, C. Zhao, O. Wamuo, S. L. Hsu, A. B. Schoch, S. A. Carleen, D. Matsumoto, *J. Polym. Sci. Part B Polym. Phys.* **2017**, *55*, 206–213, DOI: 10.1002/POLB.24261.

[123] Sears J. K., Darby J. R., *The Technology of Plasticizers*, John Wiley And Sons, New York, **1982**.

[124] T. Cairns, G. Eglinton, *Nat. 1962 1964854* **1962**, *196*, 535–537, DOI: 10.1038/196535a0.

[125] X. Li, P. Jia, T. Wang, *ACS Catal.* **2016**, *6*, 7621–7640, DOI: 10.1021/ACSCATAL.6B01838.

[126] R. González, R. Martínez, P. Ortíz, *Die Makromol. Chemie, Rapid Commun.* **1992**, *13*, 517–523, DOI: 10.1002/MARC.1992.030131107.

[127] M. Chanda, S. R. Dinesh, *Die Angew. Makromol. Chemie* **1978**, *69*, 85–98, DOI: 10.1002/APMC.1978.050690107.

[128] B. K. Kandola, J. R. Ebdon, K. P. Chowdhury, *Polym. 2015, Vol. 7, Pages 298-315* **2015**, *7*, 298–315, DOI: 10.3390/POLYM7020298.

Die approbierte gedruckte Originalversion dieser Dissertation ist an der TU Wien Bibliothek verfügbar.
The approved original version of this doctoral thesis is available in print at TU Wien Bibliothek.
TU Bibliothek Your knowledge hub WIEN

[129] A. P. Dunlop, F. N. Peters, in *A.C.S Monogr. Ser.*, American Association For The Advancement Of Science, New York, **1953**, p. 867.

[130] G. Tondi, N. Cefarin, T. Sepperer, F. D'Amico, R. J. F. Berger, M. Musso, G. Birarda, A. Reyer, T. Schnabel, L. Vaccari, *Polym. 2019, Vol. 11, Page 2126* **2019**, *11*, 2126, DOI: 10.3390/POLYM11122126.

[131] C. Dall'Argine, A. Hochwallner, N. Klikovits, R. Liska, J. Stampf, M. Sangermano, *Macromol. Mater. Eng.* **2020**, *305*, 2000325, DOI: 10.1002/MAME.202000325.

[132] Y. Lu, K. W. J. Ng, H. Chen, X. Chen, S. K. J. Lim, W. Yan, X. Hu, *Chem. Commun.* **2021**, *57*, 3375–3378, DOI: 10.1039/d0cc07801h.

[133] W. Hua, Q. Lin, B. Qu, Y. Zheng, X. Liu, W. Li, X. Zhao, S. Chen, D. Zhuo, *Materials (Basel).* **2021**, *14*, 1708, DOI: 10.3390/ma14071708.

[134] M. R. Kessler, in *Wiley Encycl. Compos.*, John Wiley & Sons, Inc., Hoboken, NJ, USA, **2012**, pp. 1–15.

[135] E. Grigat, R. Pütter, *Angew. Chemie Int. Ed. English* **1967**, *6*, 206–218, DOI: 10.1002/anie.196702061.

[136] A. W. Snow, in *Chem. Technol. Cyanate Ester Resins*, Springer, Dordrecht, **1994**, pp. 7–57.

[137] W. Kern, R. Schröder, K. Hummel, C. Mayer, M. Hofstötter, *Eur. Polym. J.* **1998**, *34*, 987–995, DOI: 10.1016/S0014-3057(97)00209-7.

[138] J. Bauer, M. Bauer, *Acta Polym.* **1988**, *39*, 548–551, DOI: 10.1002/actp.1988.010391004.

[139] C.-C. Chen, T.-M. Don, T.-H. Lin, L.-P. Cheng, *J. Appl. Polym. Sci.* **2004**, *92*, 3067–3079, DOI: 10.1002/app.20314.

[140] D. A. Shimp, W. M. Craig, in *Int. SAMPE Symp. Exhib.*, Publ By SAMPE, **1989**, pp. 1336–1346.

[141] T. Fang, D. A. Shimp, *Prog. Polym. Sci.* **1995**, *20*, 61–118, DOI: 10.1016/0079-6700(94)E0006-M.

Die approbierte gedruckte Originalversion dieser Dissertation ist an der TU Wien Bibliothek verfügbar.
The approved original version of this doctoral thesis is available in print at TU Wien Bibliothek.
TU WIEN Bibliothek Your knowledge hub

[142] M. Bauer, J. Bauer, in *Chem. Technol. Cyanate Ester Resins*, Springer Netherlands, **1994**, pp. 58–86.

[143] Arxada, *Primaset ™ Cyanate Ester Resins Leading Edge High Performance Thermoset Resins Product Manual*, **2022**.

[144] A. Osei-Owusu, G. C. Martin, J. T. Gotro, *Polym. Eng. Sci.* **1992**, *32*, 535–541, DOI: 10.1002/pen.760320805.

[145] T. G. Kotch, A. J. Lees, S. J. Fuerniss, K. I. Papathomas, *Chem. Mater.* **1995**, *7*, 801–805, DOI: 10.1021/cm00052a028.

[146] F. Dumur, *Catalysts* **2019**, *9*, 736, DOI: 10.3390/catal9090736.

[147] R. Bowser, R. Stephen Davidson, *J. Photochem. Photobiol. A Chem.* **1994**, *77*, 269–276, DOI: 10.1016/1010-6030(94)80053-7.

[148] F. Calderazzo, R. Ercoli, G. Natta, **1967**, 1–272.

[149] D. Kang, M. S. Wrighton, *Langmuir* **1991**, *7*, 2169–2174, DOI: 10.1021/la00058a033.

[150] C. H. Bamford, C. A. Finch, *Trans. Faraday Soc.* **1963**, *59*, 540–547, DOI: 10.1039/tf9635900540.

[151] H. Liu, G. A. George, *Polymer (Guildf).* **1996**, *37*, 3675–3682, DOI: 10.1016/0032-3861(96)00185-1.

[152] H. Liu, G. A. George, *Polym. Int.* **2000**, *49*, 1505–1512, DOI: 10.1002/1097-0126(200011)49:11<1505::AID-PI546>3.0.CO;2-H.

[153] F. Mccormick, K. Brown-Wensley, R. Devoe, *Energy-Curable Cyanate Compositions*, **1993**, EP0364073B1.

[154] Y. K. Satoschi, F. Y. Imahashi, Y. Yosuke;, K. Kazunori;, *Dry Film for Forming Optical Waveguide and Optical Waveguide Formed by Using the Same*, **2009**, JP2010191156A.

[155] S. Chandrasekaran, E. B. Duoss, M. A. Worsley, J. P. Lewicki, *J. Mater. Chem. A* **2018**, *6*, 853–858, DOI: 10.1039/c7ta09466c.

[156] A. Al Mousawi, C. Poriel, F. Dumur, J. Toufaily, T. Hamieh, J. P. Fouassier, J.

Die approbierte gedruckte Originalversion dieser Dissertation ist an der TU Wien Bibliothek verfügbar.
The approved original version of this doctoral thesis is available in print at TU Wien Bibliothek.
TU WIEN Bibliothek Your knowledge hub

Lalevée, *Macromolecules* **2017**, *50*, 746–753, DOI: 10.1021/acs.macromol.6b02596.

[157] D. L. Versace, F. Dalmas, J. P. Fouassier, J. Lalevee, *ACS Macro Lett.* **2013**, *2*, 341–345, DOI: 10.1021/mz400081p.

[158] H. Liu, G. A. George, *Polymer (Guildf).* **1996**, *37*, 3675–3682, DOI: 10.1016/0032-3861(96)00185-1.

[159] I. Hamerton, *Chemistry and Technology of Cyanate Ester Resins*, Springer Netherlands, Dordrecht, **1994**.

[160] A. Toldy, P. Niedermann, G. Szebényi, B. Szolnoki, *Express Polym. Lett.* **2016**, *10*, 1016–1025, DOI: 10.3144/expresspolymlett.2016.94.

[161] H. Namazi, M. Adeli, *J. Polym. Sci. Part A Polym. Chem.* **2005**, *43*, 28–41, DOI: 10.1002/POLA.20471.

[162] M. R. Pallaka, S. L. Simon, in *43rd North Am. Therm. Anal. Soc. Conf.*, Montreal, **2015**.

[163] Arxada, *Primaset ™ PT-30 A Multifunctional Cyanate Ester Delivering High Tg and Inherent Flame Retardancy*, **2017**.

[164] S. L. Simon, J. K. Gillham, *J. Appl. Polym. Sci.* **1993**, *47*, 461–485, DOI: 10.1002/app.1993.070470308.

[165] W. A. Heckle, H. A. Ory, J. M. Talbert, *Spectrochim. Acta* **1961**, *17*, 600–606, DOI: 10.1016/0371-1951(61)80120-3.

[166] M. L. Ramirez, R. Walters, R. E. Lyon, E. P. Savitski, *Polym. Degrad. Stab.* **2002**, *78*, 73–82, DOI: 10.1016/S0141-3910(02)00121-0.

[167] C. Zhai, E. L. Quitevis, S. L. Simon, *J. Polym. Sci. Part B Polym. Phys.* **2019**, *57*, 1315–1324, DOI: 10.1002/POLB.24874.

[168] S. Tang, Z. Wang, D. Yuan, C. Zhang, Y. Rao, Z. Wang, K. Yin, *J. Clean. Prod.* **2020**, *268*, 122253, DOI: 10.1016/j.jclepro.2020.122253.

Die approbierte gedruckte Originalversion dieser Dissertation ist an der TU Wien Bibliothek verfügbar.
The approved original version of this doctoral thesis is available in print at TU Wien Bibliothek.
TU WIEN Bibliothek Your knowledge hub

[169] F. An, B. Gao, X. Dai, M. Wang, X. Wang, *J. Hazard. Mater.* **2011**, *192*, 956–962, DOI: 10.1016/j.jhazmat.2011.05.050.

[170] P. Garra, C. Dietlin, F. Morlet-Savary, F. Dumur, D. Gigmes, J. P. Fouassier, J. Lalevée, *Polym. Chem.* **2017**, *8*, 7088–7101, DOI: 10.1039/c7py01778b.

[171] D. H. R. Barton, V. N. Le Gloahec, H. Patin, *New J. Chem.* **1998**, *22*, 565–568, DOI: 10.1039/a800562a.

[172] W. A. Green, *Industrial Photoinitators a Technical Guide*, CRC Press, Boca Raton, FL, USA, **2010**.

[173] F. Hamazu, S. Akashi, T. Koizumi, T. Takata, T. Endo, *J. Polym. Sci. Part A Polym. Chem.* **1993**, *31*, 1023–1028, DOI: 10.1002/pola.1993.080310424.

[174] R. S. Ghosh, D. A. Dzombak, R. G. Luthy, *Environ. Eng. Sci.* **1999**, *16*, 293–313, DOI: 10.1089/ees.1999.16.293.

[175] C. A. Peters, C. L. French, *Ind. Eng. Chem. - Anal. Ed.* **1941**, *13*, 604–607, DOI: 10.1021/i560097a008.

[176] J. F. Rabek, J. Lucki, M. Zuber, B. J. Qu, W. F. Shi, *Polymer (Guildf).* **1992**, *33*, 4838–4844, DOI: 10.1016/0032-3861(92)90700-7.

[177] M. F. Sonnenschein, *Polyurethanes : Science, Technology, Markets, and Trends*, Wiley-VCH, Hoboken, NJ, USA, **2015**.

[178] E. Delebecq, J. P. Pascault, B. Boutevin, F. Ganachaud, *Chem. Rev.* **2013**, *113*, 80–118, DOI: 10.1021/cr300195n.

[179] R. H. Pit Lehmann, Peter Malotki, Gianpaolo Tomasi, Gillian Peden, *Verfahren Zur Herstellung von Polyisocyanurat Hartschaum*, **2006**, WO 2007/025888.

[180] A. L. Silva, J. C. Bordado, *Catal. Rev. - Sci. Eng.* **2004**, *46*, 31–51, DOI: 10.1081/CR-120027049.

[181] J. E. E. da Silva, R. T. Alarcon, C. Gaglieri, A. G. Magdalena, L. C. da Silva-Filho, G. Bannach, *J. Therm. Anal. Calorim. 2018 1333* **2018**, *133*, 1455–1462, DOI: 10.1007/S10973-018-7211-1.

[182] S. Okuzono, K. Tokumoto, Y. Tamano, D. W. Lowe, *J. Cell. Plast.* **2001**, *37*, 72–

Die approbierte gedruckte Originalversion dieser Dissertation ist an der TU Wien Bibliothek verfügbar.
The approved original version of this doctoral thesis is available in print at TU Wien Bibliothek.
TU Bibliothek Your knowledge hub WIEN

89, DOI: 10.1106/DWGD-PX79-WR0G-9GBW.

[183] F. E. Golling, R. Pires, A. Hecking, J. Weikard, F. Richter, K. Danielmeier, D. Dijkstra, *Polym. Int.* **2019**, *68*, 848–855, DOI: 10.1002/PI.5665.

[184] P. J. Driest, V. Lenzi, L. S. A. Marques, M. M. D. Ramos, D. J. Dijkstra, F. U. Richter, D. Stamatialis, D. W. Grijpma, *Polym. Adv. Technol.* **2017**, *28*, 1299–1304, DOI: 10.1002/pat.3891.

[185] K. H. Hsieh, J. E. Kresta, in *ACS Symp. Ser.*, ACS, **1982**, pp. 311–324.

[186] J. Hu, X. Zhang, *J. Mater. Sci.* **2017**, *52*, 12524–12539, DOI: 10.1007/s10853-017-1372-3.

[187] A. L. Silva, J. C. Bordado, *Catal. Rev. - Sci. Eng.* **2004**, *46*, 31–51, DOI: 10.1081/CR-120027049.

[188] J. F. Villa, H. B. Powell, *Synth. React. Inorg. Met. Chem.* **1976**, *6*, 59–63, DOI: 10.1080/00945717608057340.

[189] F. Paul, S. Moulin, O. Piechaczyk, P. Le Floch, J. A. Osborn, *J. Am. Chem. Soc.* **2007**, *129*, 7294–7304, DOI: 10.1021/ja068291k.

[190] S. G. Lee, K. Y. Choi, Y. J. Kim, S. Park, S. W. Lee, *Dalt. Trans.* **2015**, *44*, 6537–6545, DOI: 10.1039/c5dt00534e.

[191] H. R. Sharpe, A. M. Geer, H. E. L. Williams, T. J. Blundell, W. Lewis, A. J. Blake, D. L. Kays, *Chem. Commun.* **2017**, *53*, 937–940, DOI: 10.1039/C6CC07243G.

[192] E. Martelli, C. Pelizzi, G. Predieri, *J. Mol. Catal.* **1983**, *22*, 89–91, DOI: 10.1016/0304-5102(83)80090-X.

[193] C. R. Kemnitz, E. S. Ball, R. J. McMahon, *Organometallics* **2012**, *31*, 70–84, DOI: 10.1021/om200555e.

[194] P. J. Giordano, M. S. Wrighton, *Inorg. Chem.* **1977**, *16*, 160–166, DOI: 10.1021/ic50167a034.

[195] R. Schwalm, *UV Coatings: Basics, Recent Developments and New Applications*,

Die approbierte gedruckte Originalversion dieser Dissertation ist an der TU Wien Bibliothek verfügbar.
The approved original version of this doctoral thesis is available in print at TU Wien Bibliothek.
TU WIEN Bibliothek Your knowledge hub

Oxford, **2006**.

[196] L. Li, Z. Zhang, M. Wang, Y. Zhang, X. Lu, *Prog. Org. Coatings* **2023**, *182*, 107649, DOI: 10.1016/j.porgcoat.2023.107649.

[197] H. T. Chua, A. Tay, Y. Wang, X. Wu, *Appl. Therm. Eng.* **2009**, *29*, 985–997, DOI: 10.1016/j.applthermaleng.2008.05.024.

[198] J. O'Brien, P. J. Hughes, M. Brunet, B. O'Neill, J. Alderman, B. Lane, A. O'Riordan, C. O'Driscoll, *J. Micromechanics Microengineering* **2001**, *11*, 353–358, DOI: 10.1088/0960-1317/11/4/312.

[199] R. L. Clough, *Nucl. Instruments Methods Phys. Res. Sect. B Beam Interact. with Mater. Atoms* **2001**, *185*, 8–33, DOI: 10.1016/S0168-583X(01)00966-1.

[200] R. Schwalm, L. Häußling, W. Reich, E. Beck, P. Enenkel, K. Menzel, *Prog. Org. Coatings* **1997**, *32*, 191–196, DOI: 10.1016/S0300-9440(97)00060-X.

[201] F. Lohse, H. Zweifel, *PHOTOCROSSLINKING OF EPOXY RESINS.*, Springer-Verlag, **1986**.

[202] K. Schwetlick, R. Noack, *J. Chem. Soc. Perkin Trans. 2* **1995**, 395–402, DOI: 10.1039/P29950000395.

[203] A. F. A. Wallis, R. H. Wearne, *Eur. Polym. J.* **1990**, *26*, 1217–1220, DOI: 10.1016/0014-3057(90)90031-X.

[204] I. Polenz, A. Laue, T. Uhrin, T. Rüffer, H. Lang, F. G. Schmidt, S. Spange, *Polym. Chem.* **2014**, *5*, 6678–6686, DOI: 10.1039/c4py01002g.

[205] J. Helberg, Y. Oe, H. Zipse, *Chem. - A Eur. J.* **2018**, *24*, 14387–14391, DOI: 10.1002/chem.201804016.

[206] T. Uchimaru, S. Yamane, J. Mizukado, S. Tsuzuki, *RSC Adv.* **2020**, *10*, 15955–15965, DOI: 10.1039/d0ra02463e.

[207] P. Xiao, F. Dumur, J. Zhang, J. P. Fouassier, D. Gigmes, J. Lalevée, *Macromolecules* **2014**, *47*, 3837–3844, DOI: 10.1021/ma5006793.

Die approbierte gedruckte Originalversion dieser Dissertation ist an der TU Wien Bibliothek verfügbar.
The approved original version of this doctoral thesis is available in print at TU Wien Bibliothek.
TU WIEN Bibliothek Your knowledge hub